ISTA - School of Technology and Arquitecture

A STOCHASTIC MODEL OF MALARIA TRANSMISSION

João Fernando Araújo Sequeira

PhD in Complexity Sciences

Supervisors:
PhD Jorge Louçã, ISCTE-IUL, Lisboa
PhD Pedro G. Lind, Oslo Metropolitan University, Oslo
PhD António M. Mendes, IMM, Lisboa

June, 2022

ISTA - School of Technology and Arquitecture

A STOCHASTIC MODEL OF MALARIA TRANSMISSION

João Fernando Araújo Sequeira

PhD in Complexity Sciences

Supervisors:
PhD Jorge Louçã, ISCTE-IUL, Lisboa
PhD Pedro G. Lind, Oslo Metropolitan University, Oslo
PhD António M. Mendes, IMM, Lisboa

June, 2022

ISTA - School of Technology and Arquitecture

A STOCHASTIC MODEL OF MALARIA TRANSMISSION

João Fernando Araújo Sequeira

PhD in Complexity Sciences

Jury:

PhD Rui Calado Lopes (President), ISCTE-IUL, Lisboa

PhD Rui Martins Travasso, Universidade de Coimbra

PhD José Ferreira Mendes, Universidade de Aveiro

PhD Sérgio Carneiro Moro, ISCTE-IUL, Lisboa

PhD Pedro G. Lind, Oslo Metropolitan University, Oslo

PhD Maurício Breternitz Jr., ISCTE-IUL, Lisboa

June, 2022

Abstract

Malaria models have evolved since Ross and Macdonald. By using an agent-based stochastic model we have looked into different aspects of disease transmission:

1. Gametocytemia phase transition between epidemic stability and disease elimination, and the potential benefit of combining gametocidal agents and ivermectin. 2. Heterogeneity promotes disease spreading. 3. Disease supression from the combined use of ivermectin and primaquine. 4. Utility of Hurst exponent and Shannon entropy in malaria forecasting.

Results and conclusion:

Malaria transmission was simulated with a computational agent-based model assuming a small African village. We have confirmed gametocytemia as a critical factor in disease transmission, revealing an abrupt phase transition between epidemic stability and disease elimination [326]. We have also found that synergism between gametocidal agents (primaquine) and ivermectin (a selective Anophelocide drug affecting parasite maturation after mosquito infection) could effectively suppress human-to-mosquito disease transmission [326]. We have found that heterogeneity amplifies disease transmission (roughly three times in our model). Different aspects of heterogeneity were analyzed such as human migration, mosquito density, and rainfall [327]. We have confirmed the potential benefit of suppressing heterogeneity-induced disease transmission with the use of gametocidal agents and ivermectin. Hurst exponent has been used in hydrology and in the stock market. No previous evidence of its application to infectious theory has been found. Yet, our data suggests that Hurst exponent and information entropy could be useful in malaria forecasting [328]. Our results support the combined use of gametocidal agents (primaquine or methylene blue) and ivermectin as part of an integrated approach to malaria.

Keywords— *Gametocytemia, Agent-based model, Heterogeneity, Primaquine, Ivermectin, Hurst exponent.*

Resumo

Os modelos de malária são úteis desde Ross e Macdonald. Através de um modelo estocástico de agente, foram analisados vários aspectos da transmissão da malária:

1. A existência de uma transição de fase entre estabilidade e eliminação da doença em função da gametocitemia. 2. O uso combinado de fármacos gametocidas e ivermectina na redução da transmissão. 3. O papel da heterogeneidade na propagação da malária. 4. A utilidade do expoente de Hurst e da entropia de Shannon na previsão da malária.

Resultados e conclusões:

Foi utilizado um modelo computacional de agente com simulação da transmissão de malária numa pequena aldeia africana. Confirmámos a gametocitemia como um factor crítico na propagação da malária demonstrando uma transição abrupta de fase entre estabilidade epidémica e eliminação da doença. No nosso modelo foi demonstrado que na presença de heterogeneidade a transmissão de malária pode sofrer uma amplificação significativa, de aproximadamente três vezes. Foram analisados diferentes aspectos da heterogeneidade tais como a migração humana, a densidade vectorial e a precipitação sazonal. Foi confirmado o potencial benefício de supressão da transmissão da malária na presença de heterogeneidade com a utilização de fármacos gametocidas (primaquina) e ivermectina. O expoente de Hurst tem sido aplicado com sucesso nas áreas da hidrologia e do mercado bolsista. Não houve até agora evidência da sua aplicação à área da infecciologia. No entanto, os dados apresentados sugerem a sua utilidade, a par da entropia de Shannon, na previsão da incidência da malária. Foi demonstrado que o uso combinado de agentes gametocidas (primaquina ou azul de metileno) e ivermectina pode constituir uma abordagem eficaz na prevenção da malária.

Palavras-chave—*Gametocitemia, Modelo-de-agente, Heterogeneidade, Primaquina, Ivermectina, Expoente de Hurst.*

Dedication

To my wife Raquel, and to my three children, Inês, Leonor and Miguel.

Declaration

I am aware of and understand the university's policy on plagiarism and I certify that this thesis was based on my research work, has been written by me except where indicated by referencing, and has not be submitted for any other degree or professional qualification.

Some of the work presented here has been previously published in **Journal of Theoretical Biology** and **Applied Sciences**, with the kind collaboration of my thesis advisors.

My personal contribution and those of the other authors to the published work is presented in detail in the following references [326–328].

Contents

List of Tables

List of Figures

Acknowledgments

I wish to thank Professor Miguel Prudêncio (IMM – Lisbon) for his help in defining the model parameters, and for his crucial remarks in discussing the model design.

Glossary

λ Force of infection. 302

$G = ZX$ Sporozoite-Parasite combined rate. 106, 190, 196, 197

H_{36} Hurst exponent of a 36-months length time series. 152, 153, 154, 155, 158

H_t Herd immunity threshold. 28

I_{36} Malaria incidence of a 36-months length time series. 152, 153, 154, 155

I_C Vectorial capacity. 30

R_0 Basic reproductive number. xv, 24, 32, 36, 42, 47, 51, 80, 94, 102, 110, 191, 302

S Stability index. 30

S_{36} Shannon entropy of a 36-months length time series. 153, 154, 155

X Parasite rate. 109, 188, 190

Z Sporozoite rate. 31, 53, 94, 106, 188, 190

phm Monthly cases per 100 human inhabitants. 168, 171

phy Annual cases per 100 human inhabitants. 5, 6, 107, 142, 143, 153, 165, 168, 171

AC Asymptomatic carriers. 40

ACF Autocorrelation function. 284, 286, 287

ACT Artemisinin combined therapy. 6, 7, 17, 38, 121, 194

AICc Akaike corrected information criterion. 289

AL Artemether-Lumefantrine. 16, 40

ARIMA Auto-regressive integrated moving average. 42, 283, 284, 287, 289, 290, 291, 295, 296, 299, 300

ARMA Auto-regressive moving average. 283, 284

AS-AQ Artesunate-amodiaquine. 17

ATSB Outdoor attractive toxic sugar bait. 42

BN Bayesian network. 46

CDC Centers for Disease Control and Prevention. xix, 13

CDF Cumulative distribution function. xx, 92, 163, 166, 169, 171, 175

CSC Community screening campaign. 39

DDT Dichlorodiphenyltrichloroethane. 80, 125, 194

DHA-PPQ Dihydroartemisinin-piperaquine. 16, 17

EIR Annual entomological inoculation rate. 31, 36, 41, 51, 81, 93, 106, 110, 115, 163, 180, 182, 191

ETS Exponential smoothing model. 284

FPE Fokker-Planck equation. 76, 255

G6PD Glucose-6-phosphate dehydrogenase. 20

GARCH Generalized auto-regressive conditionally heteroscedastic. 42, 282

HW Holt-Winters forecasting. 284

IRS Insecticide residual spraying. 6, 7, 15, 16, 39, 42, 44, 46, 47, 68, 70, 71, 88, 194, 195, 197, 298, 303

ITN Insecticide-treated bed nets. 6, 15, 16, 41, 42, 46, 52, 68, 70, 71, 80, 88, 140, 298, 303

KPSS Kwiatkowski-Phillips-Schmidt-Shin. 289

LLIN Long-lasting insecticide-treated bed nets. 6, 15, 38, 42, 44, 68, 70, 71, 88

LOD Level of detection. 15, 302

LRD Long range dependence. 146, 147, 158

LRS Low-resource settings. 15

MAE Mean absolute error. 93, 163, 168, 169, 172, 175, 177

MAPE Mean absolute percentage error. 93, 163, 168, 169, 172, 175, 177

MDA Mass drug administration. 16, 17, 18, 20, 33, 42

MEWS Malaria early warning system. 42

MI Malaria incidence. 171

MmT Minimum temperature of the coldest quarter. 19

MMT Maximum temperature of the warmer quarter. 19

MSAT Mass screening and treatment. 16, 40

MTP Mean total annual precipitation. 20

NDVI Normalized difference vegetation index. 18, 19, 38, 121

Pc *P.cynomolgi*. 12

PDF Probability density function. xxi, xxii, 113, 114

PEV Pre-erythrocytic vaccine. 41

Pf *P.falciparum*. 12, 66, 67, 104, 122, 125

PfHRP2 *P.falciparum* histidine-rich protein 2. 15

PfpLDH *P.falciparum* lactate dehydrogenase. 15

Pk *P.knowlesi*. 12

Pm *P.malariae*. 12

Po *P.ovale*. 12

Ps *P.simium*. 12

Pv *P.vivax*. 12

PW Pareto-Woolhouse rule. xxi, 100, 101, 102, 107, 108, 111

RDT Rapid diagnostic testing. 6, 15, 106, 121, 190, 194, 198

RF Reed-Frost model. 26, 27

RM Ross-Macdonald model. 23

RMSE Root mean square error. 163, 168, 169, 172, 175, 177

SARIMA Seasonal auto-regressive integrated moving average. 287, 289, 295

SEIR Susceptible-exposed-infectious-recovered model. 34

SEIRS Susceptible-exposed-infectious-recovered-susceptible model. 25, 26, 41, 44, 55

SEIS Susceptible-exposed-infectious-susceptible model. 25

SIS Susceptible-infectious-susceptible model. 25, 38, 55, 57

Part I

BACKGROUND

Chapter 1

Introduction

1.1 Preamble

In Babylon, during the year 323 BC, Alexander the Great fell ill after returning from Persia, and died shortly after at the age of 32. The reason of his death was most probably a disease now known to be caused by an infection with the parasite *P.falciparum* [316].

Throughout the ages, malaria has persisted in the history of mankind as one of the most recurrent and life-threatening infectious diseases worldwide. In particular, it stands as a disease globally epidemic in tropical regions, having stronger impact in sub-Saharan Africa and Southeast Asia.

Malaria cases have declined globally from 238 million cases, in 2000, to 227 million, in 2019 [288, 289]. However, in 2020, malaria cases have increased again to 241 million, mainly related to disruption of health services as a result of COVID-19 pandemic [289].

During the XXI century, malaria incidence decreased all over the world from 8.1 in the year 2000, to 5.6 annual malaria cases per 100 human inhabitants-year (*phy*) in the year 2019, before increasing again in 2020 to 5.9 cases *phy* [288, 289].

However, this last result has not changed significantly in recent years, maintaining similar levels in 2020 in relation to 2015 (5.9 cases *phy*) [288]. Global malaria incidence declined 27% between 2000 and 2015, but only 2% from 2015 to 2019, rising again in 2020 to similar results of 2015 due to the COVID-19 pandemic [288, 289].

Malaria mortality also decreased worldwide from around 896 000 in 2000 to 562 000 in 2015, and to 558 000 malaria deaths in 2019 [288, 289]. However, in 2020, the number of malaria deaths stepped up again to 627 000, corresponding to an increase in fatal cases by 12%, when compared to 2019 [289].

Globally, the malaria mortality rate decreased by half from about 30 deaths

per 100 000 population at risk in 2000, to 15 in 2015 [289] while decreasing more slowly until 2019, to 13 deaths per 100 000 population at risk. However, in 2020, malaria mortality risk increased again to 15 deaths per 100 000 population at risk [289]. And as a result of lower immunity protection, children under 5 years old were still a highly vulnerable group, accounting for 77% of all global fatal cases in 2020 [289].

Twenty-nine countries were responsible for 96% of all malaria cases worldwide. And only six African countries notified 55% of all malaria cases globally: Nigeria (27%), the Democratic Republic of the Congo (12%), Uganda (5%), Mozambique (4%), Angola (3.4%) and Burkina Faso (3.4%). The World Health Organization (WHO) African Region alone was responsible for 95% of all cases globally with an estimated 228 million cases in 2020 [289]. Although the total of malaria cases in Africa was higher in 2019 with an estimated 215 million cases, malaria incidence in that region actually declined from 36.8 to 22.2 cases *phy* from 2000 to 2019, due to the significant increase in African population from about 665 million in 2000 to 1.1 billion in 2019. However, in 2020, malaria incidence stepped up again to 23.2 cases *phy* as a result of health services disruption from COVID-19 pandemic [288, 289].

This significant improvement was the result of a more effective public health policy concerning preventive actions such as adequate vector control, implementation of rapid diagnostic testing (RDT), drug administration of artemisinin-combined therapy (ACT), and the widespread use of barrier protection measures such as insecticide-treated nets (ITN), long-lasting insecticide-treated bed nets (LLIN) or insecticide residual spraying (IRS).

The protozoan parasite *P.falciparum* (*Pf*) was the cause of the most prevalent form of malaria in the African continent during 2018 (99.7% of all estimated cases in Africa [287]), and has been implicated in the vast majority of fatal cases assuming severe clinical presentations such as cerebral malaria, renal failure or hemolytic anemia, amongst others. *Pf* genetic diversity is a critical issue to be addressed in future vaccination programs. However, two other *Plasmodium* species may also be responsible for severe forms of the disease – *P.vivax* (*Pv*) and *P.knowlesi* (rare, and mostly restricted to a small region in Asia).

In 2018, the prevalence of *Pf* was lower in the WHO Eastern Mediterranean region (71% of all malaria cases), WHO Western Pacific region (65% of all cases) and WHO South-East Asia region (50% of all cases) ([287]). The second most important clinical form of *Plasmodium* infection consisted in *P.vivax* infection, being responsible for 75% of all malaria cases in WHO Americas region and 53% of all cases in the WHO South-East Asia region, (the majority of which in India with 47% of all cases), but resulting in milder clinical forms of the disease with much lower mortality than the *Pf* infection. However, globally, the proportion of cases resulting from *P.vivax* infection decreased from around 8% in 2000 to 2% in 2020 [288, 289].

Concerning malaria mortality, the WHO African region alone was responsible for 93% of all malaria deaths in the year of 2017. And the following six African countries accounted for nearly half of all global malaria deaths during 2017: Nigeria (19%), Democratic Republic of the Congo (11%), Burkina Faso (6%), United Republic of Tanzania (5%), Sierra Leone (4%) and Niger (4%) [286].

Yet, malaria mortality decreased 63% in the World Health Organization (WHO) African Region, from a total of 840 000 malaria deaths reported in 2000, to 534 000 malaria deaths in 2019 (corresponding to 96% of all malaria deaths worldwide, in 2019). The African mortality rate reduced by 67% over the same time period from 121 to 40 deaths per 100 000 population at risk [288, 289].

This data seems to indicate that despite all recent efforts in improving disease control in tropical Africa, effective malaria prevention is still unsatisfactory. The risk of an epidemic resurgence remains a persistent threat to regions where the disease was assumed to have been eliminated. A recent malaria outbreak in Burundi highlights the need for better and more consistent anti-malaria interventions [338].

Lack of consistency in implementing region-wide programs for preventive protection with IRS or effective barrier protection with ITN/LLIN, failure in early diagnosis from lack of RDT, irregular use of ACT leading to a higher *Pf* drug resistance, and growing *Anopheles* resilience as a result of the widespread use of insecticides are altogether responsible for the recent lack of progress in the fight against malaria. Children under 5 years of age have been particularly vulnerable to the disease, with an increased fatality rate.

Disease transmission depends on several geophysical factors such as humidity, rainfall, vegetation density and atmospheric temperature. These factors play a critical role in the vector (*Anopheles* mosquito) life cycle, with a decisive impact on vector density. Global warming stands as a potential threat as it may promote disease transmission in nontropical latitudes, where the disease had previously been considered eliminated.

Seasonality resulting from extreme weather conditions amplified by climate change, and disease resurgence due to human migration and imported disease cases have been severely implicated in sustained and delayed disease transmission. *Anopheles* mosquito subsists as the critical vector in transmission of the most dangerous form of the parasite – *P.falciparum*.

Although disease elimination may become a realistic possibility in some parts of the world, induced drug resistance from massive administration of quinine and artemisinin derivative therapy still remains a threat to an effective fight against malaria.

1.2 Research questions

Deterministic models have been classically employed in defining more effective strategies for malaria transmission suppression. Stochastic models have been used with moderate success in infectious epidemiology. However, few agent-based models have tried to reproduce the full scale multi-variable dimension of the mosquito-human system involved in malaria transmission dynamics.

Here, we present the essential research questions derived from our present work:

1. Is it possible to create a single stochastic computational model that can capture the full range of complex interactions between all relevant variables in malaria transmission?

2. How important is to adequately suppress gametocytemia during human disease?

3. Is ivermectin a reliable drug in suppressing disease transmission by early mosquito killing after gametocyte transmission from an infected human?

4. Could there be any benefits from combining the gametocytemia suppression effect resulting from gametocidal agents (like primaquine or methylene blue) with the administration of ivermectin?

5. How relevant is heterogeneity in malaria spreading, especially in the presence of high transmission hot-spots?

6. In the presence of heterogeneity how effective is the combined use of a gametocidal agent (like primaquine) and ivermectin?

7. In malaria time series, how useful can it be the application of Hurst exponent and Shannon information entropy to the Box-Jenkins theory in disease forecasting?

1.3 Objectives

In this PhD dissertation it was the author intention to:

1. Answer the research questions previously defined in section 1.2., by using a stochastic computational agent-based model in different disease transmission scenarios.

2. Prove the existence of a gametocytemia phase transition between epidemic stability and disease elimination.

3. Prove the effectiveness of a combined preventive strategy using a gametocidal agent like primaquine along with ivermectin.

4. Prove heterogeneity enhancement of malaria transmission.

5. Prove that the combined use of a gametocidal agent and invermectin could effectively suppress disease transmission in the presence of high heterogeneity.

6. Prove that the combined use of a gametocidal agent and invermectin could effectively suppress disease transmission in the presence of other forms of heterogeneity like human migration, rainfall seasonality, a wide variation in mosquito density and transmission hot-spots.

7. Prove that the use of Hurst exponent and Shannon entropy in malaria time series could be useful in disease forecasting.

1.4 Dissertation structure

The present dissertation will be divided in three parts, with four Appendices:

Background:

A brief introduction to the dissertation theme, along with the main research questions, will be displayed in chapter 1. The impact of malaria will be presented along with a simple description of malaria biology in chapter 2. State-of-the-art on the subject will be described in relation to a chronological timeline of all the relevant references concerning malaria modeling in chapter 3. The mathematical background of malaria theory will be presented in chapter 4.

Contributions:

Our model design will be described in detail in chapter 5, including the mathematical background in support of the agent-based model of malaria transmission. The influence of vector control in our malaria transmission model will be presented in chapter 6. In chapter 7 we will prove the existence of a gametocytemia phase transition between epidemic stability and disease elimination. The importance of combining a gametocidal agent with ivermectin will also be determined in chapter 7. The impact of heterogeneity in malaria transmission and the interaction between gametocytemia and heterogeneity will be determined and quantified in chapter 8. The importance of human migration will be presented in chapter 9. Seasonal malaria transmission will be discussed in chapter 10. The importance of the Hurst exponent and Shannon entropy in forecasting malaria incidence will be established in chapter 11.

Model validation procedures will be presented in chapter 12.

Discussion:

Discussion and conclusions will be presented in chapter 13.

Appendices:

The appendices will cover a mathematical supplement on Markov transition processes in Appendix A, the mathematical formalism of the master equation in one- and two-dimensions with Taylor approximation, as well as the Itô master equation formulation in Appendix B, the importance of initial conditions and final outcome in Appendix C, and malaria time series in the perspective of Box-Jenkins theory in Appendix D.

Chapter 2

The impact of malaria

2.1 Historical perspective

The malaria parasite *Plasmodium* was first described in a blood sample by Alphonse Laveran in 1880 [86, 118, 382]. A few years later (1883) Albert King, an American doctor, assumed the suspicion that mosquitoes could somehow be related to malaria transmission. That suspicion was confirmed by Sir Ronald Ross in 1899, in Sierra Leone, in partnership with Patrick Manson since 1894 [86]. In India, during the early years of the XX century, Ross conducted a remarkable epidemiological work on malaria prevention [86, 237, 317, 343]. He was the author of the first reliable mathematical model of malaria transmission. During the 1950s, Macdonald improved on Ross original theory, introducing the concept of mosquito mortality and disease latency; more recent models added human mortality as an important model parameter. However, deterministic mathematical models have revealed limitations in the analysis of subtle problems resulting from stochastic computational disease simulations. More recently, the results of stochastic modeling in malaria based in current views on the dynamics and biology of the parasite *Plasmodium*, the vector *Anopheles* mosquito, and the disease behavior of the human individual, have proven useful in the search for more effective strategies of disease control [232, 237, 317, 343]. Unraveling the mathematical complexity of the malaria epidemic has become a decisive step in developing more powerful models for disease prevention in the long term. Yet, malaria elimination remains a major challenge for health services all around the world.

2.2 Malaria biology

2.2.1 Disease dynamics

P.falciparum is the agent responsible for most of the fatal cases of malaria. The disease vector is the *Anopheles* mosquito. When an infected mosquito with *Plas-*

modium sporozoites inside the salivary glands bites a healthy human individual, these forms of the parasite travel rapidly through the human blood stream into the liver. There, they invade and replicate inside liver cells, differentiating into merozoites. Infected liver hepatocytes may harbor a large number of merozoites (as close as 30 000 in a single cell). The liver cycle is completed after 1 to 2 weeks. After rupture of infected liver cells, it follows a blood stage with merozoite invasion of red blood cells. Inside red blood cells (erythrocytes), merozoite differentiation proceeds to trophozoite and schizont forms, during a period of 48-72 hours. After this time, schizont forms may rupture releasing 10-30 merozoites in the blood stream. These will re-infect new erythrocytes. Inside the red blood cell, some merozoites will differentiate to sexual forms called gametocytes. These sexual forms may be of male or female gender. When a mosquito bites an infectious human host, it ingests $1.0 - 2.5$ μl of human blood with infected red blood cells. Already inside the mosquito gut, gametocytes will emerge from the aspirated erythrocytes, and cross-fertilize to form diploid zygotes. These will further differentiate into ookinetes, and later to oocysts. Each oocyst may contain up to 1 000 sporozoites that will later migrate through the mosquito hemolymph and invade its salivary glands. These sporozoites will then be able to infect human individuals during the next mosquito feeding, thus perpetuating the parasite life cycle. When a healthy mosquito feeds on an infected human individual carrying gametocytes in his blood circulation, it will become infected. After that event, it follows an incubation period of 7-14 days before that mosquito will become infectious. Likewise, on healthy human individuals, after an infectious mosquito bite, a long incubation time may also occur from the initial infectious bite to gametocyte development inside red blood cells. This time period, corresponds to the liver cell/red blood cell cycle and is usually in the range from 10 to 21 days [118, 382] – see figure 2.1.

2.2.2 The parasite: *Plasmodium*

In nature, we may find five *Plasmodium* species responsible for malaria: *P.falciparum (Pf)*, *P.vivax (Pv)*, *P.ovale (Po)* (with two different forms), *P.malariae (Pm)*, and *P.knowlesi (Pk)*. Rarer species like *P.cynomolgi (Pc)* and *P.simium (Ps)* have been related to documented animal infection, but rarely affecting humans, and if so, only in specific geographic locations [118, 228, 382].

Among the four different species of the parasite *Plasmodium* that usually promote human infection (*P.falciparum*, *P.vivax*, *P.ovale* and *P.malariae*), *P.falciparum*, stands as the most prevalent malaria parasite in Africa, being responsible for more than 99% of all malaria cases during 2017 [286]. However, in the Americas, *P.vivax* is the most prevalent malaria parasite, representing almost three quarters of all malaria cases [286].

From the study of genetic evolution and specific mutations in human hemoglobin, it is possible to track down how the parasite evolved in time in human populations. Apparently, *P.falciparum* infection was transmitted to man, from the

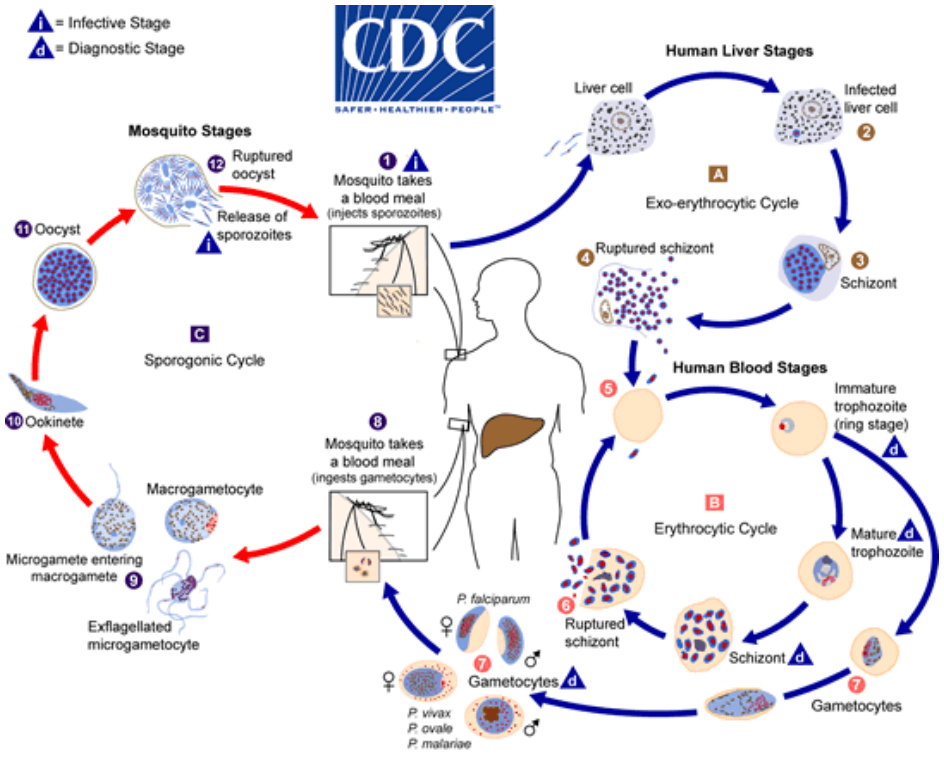

Figure 2.1: Malaria biology: Human-mosquito cycle (obtained from Centers for Disease Control and Prevention – CDC [60]).

gorilla, around 10 000 years ago [223, 354]. This form of malaria corresponds to the malignant tertiary form of the disease (also denominated *sledgehammer* presentation) in the form of fever and malaise resurgence every 48 hours, by the third day of disease manifestations.

P.vivax, also clinically known as benign tertiary malaria (also presenting with symptoms every 48 hours like *Pf*) probably migrated with the first human populations out of Africa, around 100,000 years ago, spreading thereafter to all parts of the globe. However, the more recent occurrence in the African population of a particular mutation in red blood cells leading to an absent expression of a specific red blood receptor essential for the erythrocyte uptake of *P.vivax* merozoites – the *Duffy* antigen – turned *P.vivax* infection into a rare event in Africa [226]. *P.ovale* is geographically limited to tropical West Africa and is responsible for a benign form of the disease symptoms every 48 hours (benign tertiary form). *P.malariae* is responsible for the quartan form of the disease (symptoms recurring every 72 hours). The different periodicities of the *sledgehammer* disease symptoms in malaria – with either a 48 or 72 interval between fever peaks – are responsible for these different clinical patterns of fever [378].

2.2.3 The vector: *Anopheles* mosquito

Of over 3 000 mosquito species, around 400 belong to the *Anopheles* genus (*Diptera* and *Culicidae*).

The female *Anopheles* mosquito is the malaria vector. The male *Anopheles* mosquito does not transmit malaria, and its main biological purpose resides in being able to mate with a female mosquito and secure species reproduction. Different species of *Anopheles* mosquito have been involved in disease transmission to humans. Although close to 70 *Anopheles* species may have the potential for malaria transmission, there are significant differences in that ability between different subspecies. Less than half of those *Anopheles* species are important in disease transmission. The wide presence in antiquity of an *Anopheles* species – *An.atroparvus* – with lower capacity for sporozoite transmission to human hosts may explain why malaria was probably a rarer event in Ancient Rome and Greece. However, at the time of the fall of the Roman Empire of the West, more effective *Anopheles* mosquito vectors were quite abundant in northern Africa (*An.labranchiae*) and Asia (*An.sacharovi*). Henceforth, *Pf* malaria became a widespread disease with harmful consequences to human demography [90].

The main mosquito species responsible for malaria transmission in Africa is *An.gambiae*. Its survival depends on two critical weather factors: heat and rain precipitation. In tropical countries, around two weeks after the beginning of the rainy season, mosquitoes will evolve into the last of four stages of development (egg-larva-pupa-mosquito). After emerging from this cycle, the female mosquito will need to have a blood feed, mate with a male mosquito, and be able to lay eggs completing the oviposition cycle (usually lasting 2 to 3 days). The life expectancy of mosquitoes is usually short. Some of them will eventually die before reaching the end of the latency time, necessary for the presence of sporozoites in mosquito salivary glands after feeding on human hosts with gametocytes, and therefore will never be able to transmit malaria. The small proportion of mosquitoes surviving the incubation period, will be responsible for disease transmission. These mosquitoes will eventually repeat the process of oviposition-biting, more than once during their lifetime [17, 244, 344]

2.3 Disease prevention

2.3.1 Vector control

The capacity of flying longer distances in search of a blood meal depends on proper mosquito feeding, and oviposition is not possible without it. Thus, mosquito survival beyond incubation time (time needed between ingestion of gametocytes and the presence of sporozoites in mosquito saliva) seems to be a crucial parameter for effective disease transmission. A significant reduction in this time could possibly, and decisively, reduce the potential for human infection.
Mosquito survival is also essential for an effective disease transmission. Daily mosquito mortality is usually high, depending on climate conditions and host-

feeding availability.

2.3.2 Barrier protection (LLIN/ITN/IRS)

For several years now, the effect of barrier protection induced by insecticide treated bed-nets (ITN), long-lasting insecticide-treated nets (LLIN) and active indoor residual insecticide spraying (IRS), has played a decisive role in malaria prevention [320, 381]. Its widespread implementation has significantly improved the efforts to reduce malaria transmission, as has been shown, for example, in the island of *S. Tomé e Príncipe* [217].

2.3.3 Rapid diagnostic testing (RDT)

The use of highly-sensitive rapid diagnostic tests (RDT) is crucial for early identification of a large proportion of all malaria patients. Detection of asymptomatic patients has become a necessary goal for an effective malaria prevention strategy. Yet, low antigen concentration is a common problem in diagnostic immunoassays [91, 303].

The use of point-of-care (POC) effective diagnostic tools is divided in two well-defined strategies: case management and laboratory-based surveillance methods. The use of microscopy-based direct identification of the parasite and of medium to high sensitivity RDT (results usually obtained in less than 20 minutes) stands as the standard approach to case management of symptomatic patients. Ultra-highly sensitive rapid diagnostic tests, molecular diagnostic testing with polymerase chain reaction (PCR) and loop mediated isothermal amplification (LAMP) are laboratory-based tools, and may also become essential in surveillance for the purpose of early detection of asymptomatic patients [303].

Conventional RDT are usually based in the detection of histidine-rich protein 2 (PfHRP2) and *P.falciparum* lactate dehydrogenase (PfpLDH) identification. They are low cost and easy to use, while allowing for faster results. The desired level of detection (LOD) is defined in the average range between 50 to 200 parasites/μL, but may be lower, in the range between 4 and 20 parasites/μL, in the case of well-trained medical lab experts. Microscopy and fast RDT are particularly effective methods in low-resource settings (LRS). While implementing an adequate surveillance strategy, ultra-sensitive RDT will usually define an acceptable LOD at close to 5 parasites/μL or less. When using the detection of PfHRP2, the concentration range may stand between 6 and 12 ng/mL [303]. In the case of PCR testing the LOD may be defined as lower as 0.5 to 5.0 parasites/μL. The use of LAMP may also allow a lower value for the LOD, usually below 2 parasites/μL [82, 366]. Detection of placental malaria during pregnancy is usually based on the detection of circulating antigen. In this setting, the use of methods like PCR or microscopy may prove less useful in the diagnosis of malaria during pregnancy.

2.3.4 Human immunity

Plasmodium extreme antigenic diversity presents a problem in achieving adequate acquired immunity in human population [106, 118, 142, 158, 325, 380, 382]. This diversity is responsible for less effective immunity protection induced by specific malaria vaccination programs. Acquired immunity protects human individuals from more severe forms of malaria, and to some extent may also reduce the probability of disease transmission, while not assuring full protection against the disease. The parasite spends an important part of its life inside the erythrocyte, assuring it partial protection against cell-mediated immune recognition. This fact may partially explain the shortcomings of malaria vaccination, so far. However, the parasite liver stage may become an alternative and reliable target in the development of an effective vaccine capable of long-term immunity protection [219, 251, 311].

2.3.5 Antimalarial drugs

In 2015, the WHO defined three strategic pillars in malaria prevention (universal access to prevention, drugs and diagnosis, elimination and surveillance) [285]. From the failure of some of the initial strategies involving vector control, to the incapability of specific vaccination in inducing mass immunity in the population at risk, we can draw the conclusion that only with proper and aggressive antimalarial strategy will it be possible to significantly reduce malaria transmission risk [30, 65, 217, 315, 320, 381]. Antimalarial drugs like quinine derivatives and artemisinin, alone or in combination such as in artemether-lumefantrine (AL) or dihydroartemisinin-piperaquine (DHA-PPQ), have been extensively used worldwide in malaria prevention and treatment [63, 279, 300]. However, the importance of selectively eliminating gametocytemia with gametocidal drugs could also be critical in the control of parasite transmission to mosquitoes [1, 42, 44, 187, 201]. Different strategies have been implemented in order to increase the effectiveness of antimalarial drugs, while reducing the risk of drug resistance. In mass drug administration (*MDA*), an entire population will be under treatment with antimalarial drugs. However, MDA in preventive campaigns should be used cautiously as it may contribute to an undesirable boost in antimalarial drug resistance. Other promising strategies are currently under scrutiny [187]. The mass screening and treatment approach (*MSAT*), has been tested in Burkina Faso [80]. A similar strategy with *focal screening and treatment* was used against artemisinin-resistant *P.falciparum* malaria in western Cambodia [105]. *MSAT* could still be more effective if combined with an active policy favoring the mass use of insecticide treated bed-nets (ITN), and indoor residual insecticide spraying (IRS) [134].

2.3.6 *Plasmodium* drug resistance

Antimalarial drug resistance is well documented in *P.falciparum* and *P.vivax*. In recent years, its occurrence has become more severe in several parts of the world

[114]. Chloroquine and sulfadoxine–pyrimethamine resistance in *P.falciparum* were first described in South-East Asia during the late 1950s. During the 1960s those forms of drug resistance spread across Asia, and later on Africa, with dramatic consequences in malaria mortality [105]. Chloroquine resistance is most frequently related to excessive and sub-therapeutical drug usage in certain parts of the world such as South-East Asia and sub-Saharan Africa.

Drug resistance to artemisinin-combined therapy (ACT) has become a critical problem in malaria prevention with new cases being reported every year [105, 288, 362]. However, a strong adaptive and innate population immunity may slow the spread of that form of drug resistance [198].

During 2002-2003 a new mutation (associated with the S769N mutation in the PfSERCA gene) concerning artemether resistance was described in *P.falciparum*. Some mutations have been identified as molecular markers of partial artemisinin resistance. The *PfKelch13* mutations have been found in the WHO African Region [288]. In this region, the first approach to treatment directed to *P.falciparum* includes different ACT protocols such as artemether-lumefantrine (AL), artesunate-amodiaquine (AS-AQ) and dihydroartemisinin-piperaquine (DHA-PPQ). Their overall efficacy rates for *P.falciparum* are consistently above 98.0% in all cases [288].

Yet, a high level of clinical immunity may interfere in drug-resistance depending on the disease transmission setting. Drug-resistance is relatively easier to spread in a low or unstable transmission setting when compared to a high transmission one [194]. In high transmission intensity settings, the influence of ACT on drug resistance may become quite limited due to the presence of stronger immunity in a large fraction of the population. As many infections become asymptomatic, a smaller proportion of the infections will ultimately receive drug treatment [309].

In areas with low disease transmission, parasitemia can be residual in the general population. In these settings, drug resistance may spread more slowly by using therapeutic combination of two or more effective drugs, which do not share resistance mechanisms. In this case, effective and swift treatment of symptomatic individuals with ACT-primaquine combinations, or seasonal chemoprophylaxis, may assume an important role in reducing malaria incidence, with better results than those from MDA campaigns with the treatment of a small minority of infected individuals.

MDA with DHA-PPQ has been combined with primaquine with promising results in gametocytemia reduction and disease transmission suppression. Other ACT schemes such as AL have also been shown to be effective in MDA campaigns [176].

While the widespread use of antimalarial drugs may result in the selection of surviving resistant parasites, implementing the use of MDA is still quite controversial as it may promote this effect and is the reason why it is currently being

used with caution by the World Health Organization.

MDA can quickly reduce or eliminate parasite reservoirs. It is usually effective in settings based upon solid health structures with easy access to diagnosis and treatment, and an effective surveillance system with a strong community adherence [208, 298].

2.3.7 Climate conditions and seasonality

Malaria is significantly influenced by climate and topography. Warmer temperatures, higher water precipitation, proximity to water surfaces and living at lower altitudes, may increase malaria incidence [79].

Rainfall, temperature and humidity are the most relevant weather factors affecting the intensity of malaria transmission. Environmental conditions such as altitude, the presence and distribution of vegetation, the nearness of human populations to water reservoirs and topography may also all play a decisive role in malaria transmission.

High volumes of waterfall provide for significant water surfaces, and adequate sheltering to mosquito breeding sites, leading to enhanced malaria transmission with a short delay in time. However, in the case of excessive water precipitation, mosquito eggs may also be flushed away, compromising global mosquito survival and maturation. Higher atmospheric temperatures also facilitate malaria transmission by shortening the duration of *Plasmodium* development inside the mosquito [277].

Temperature may affect mosquito biology influencing *Anopheles* mosquito biting rate, reproduction and survival conditions [191]. Malaria transmission is apparently facilitated at moderate temperatures in the range between 23°C and 24°C, in a weekly average within a 2 weeks lag. At lower (12°C) or higher temperatures (27.9°C), the risk of malaria transmission is lower. At higher temperatures, mosquito survival could be significantly reduced, affecting the population size of susceptible mosquitoes [191]. Malaria transmission seems to be stronger at a temperature range between 16°C and 34°C, with a peak at 25°C [257].

However, minimum daily temperature may also have a strong influence in mosquito survival. In a study from China, Zhang [395] showed that a small increase of 1°C in the minimum daily temperature could result in a substantial increase in malaria incidence (by 12 to 16%). This study also suggests that minimum daily temperature may even be more decisive than maximum daily temperatures in mosquito survival, by facilitating *Plasmodium* and *Anopheles* survival during the colder winter months, while resulting in more effective disease transmission during the warmer rainy seasons [102]

Other climatic factors such as the relative humidity and the normalized difference vegetation index (NDVI) have also been used in weather malaria prediction models [16, 134, 358].

Several studies point to the fact that the observed value of NDVI correlates well with predictions of parasitemia incidence [134]. NDVI is obtained from satellite imagery and defined to be lower than 0.350 in drier regions with less vegetated areas. More vegetated and less dry areas correspond to values of NDVI equal or above 0.350 [358].

2.3.8 Risk of disease resurgence

There are several examples of successful malaria elimination worldwide. However, the risk of malaria resurgence may endure indefinitely in regions where *Anopheles* mosquitoes persist in the absence of malaria cases [319]. Facilitating conditions for *Anopheles* mosquito breeding are supposed to increase the risk of local disease transmission in the presence of asymptomatic hosts with silent and chronic forms of submicroscopic gametocytemia, who do not usually seek treatment [179]. Age patterns of clinical malaria are known to influence local parasite prevalence and malaria incidence [153]. And human migration has also been strongly linked to malaria resurgence [101].

Southern Europe is one of the world regions with potential for malaria outbreaks. A warmer climate, with seasonal rainfall, the existence of widespread biological pockets of *Anopheles* mosquito along the Mediterranean countries, the proximity to migration routes from Northern Africa as well as from poor countries with increasing population, the presence of increasing malaria incidence, and the anthropogenic environmental modifications facilitating local mosquito breeding are all of them important risk conditions that may facilitate malaria outbreaks in regions where malaria had been previously eliminated [319].

Different subspecies of *Anopheles* predominate in several European regions in relation to subtle climate differences affecting temperature and rainfall during the warmer and coldest months of the year. These climate changes may explain why *An.atroparvus* predominate over *An.maculipennis* in Portugal and Spain, while *An.hyrcanus* is most frequent in France, and *An.labranchiae* is typically found in Italy [145, 319].

Also, the vulnerability of *An.atroparvus* toward different *P.falciparum* strains may be heterogeneous, being higher in European strains in relation to afro-tropical strains. However, *An.atroparvus* may be more susceptible to infection by *P.vivax* strains imported from African countries, with a greater risk of resurgence of this form of malaria in Mediterranean countries such as Portugal, Spain, France and Greece [145, 319].

Several climate aspects should be considered in terms of the potential risk of malaria outbreaks. The mean maximum temperature of the warmer quarter (MMT) plays a harmful role to *Anopheles* breeding, facilitating the death of mosquito larvae from desiccation at higher temperatures. Also, the mean minimum temperature of the coldest quarter (MmT) could be harmful to mosquito

survival and parasite sporogony in lower winter temperatures. Both the mean total annual precipitation (MTP), as well as the presence of higher altitude wetland and agricultural density, are critical to the level of suitability index in vector control, allowing for greater availability of mosquito breeding sites [145].

The presence of widespread *Anopheles* insecticide resistance was probably responsible for reduced vector control effectiveness and the occurrence of severe malaria outbreaks in several regions of Rwanda and Zambia. Also, the reduced effectiveness of insecticide-treated nets in the past may have significantly increased the risk of malaria resurgence in countries like Kenya and Senegal [78].

Disease resurgence risk may be higher in the presence of *Plasmodium* drug resistance. Malaria outbreaks such as the one described in Sri Lanka between 1963 and 1968 may be explained by the occurrence of massive chloroquine resistance from drug overuse [159].

Most importantly, disease resurgence risk appears to be strongly connected to the massive reduction in financial support of local malaria preventive campaigns, following significant success in reducing malaria incidence. This "out of sight, out of mind" negligent approach may be, most likely, the cause of several malaria outbreaks connected to an increased mortality from long lost population immunity [179].

2.3.9 Primaquine and gametocytemia suppression

The suppression of *Pf* gametocytes by mass drug administration (MDA) of primaquine is quite effective in reducing the risk of disease transmission, even in the setting of the potential risk of hemolysis in glucose-6-phosphate dehydrogenase (G6PD) deficient individuals. Primaquine base in the dosage of 0.25 mg/Kg is apparently a safe and effective dosage against *Pf* gametocytes, with a minimal risk of inducing non-fatal hemolytic anemia. Even lower dosages of primaquine may still be quite effective in terms of gametocyte reduction. Just by using a smaller dosage of 0.15 mg/Kg it was possible to obtain a reduction in the percentual presence of gametocytes from 13 % to 0.8 % [179]. While this drug is usually part of the main treatment of *P.vivax*, its role in malaria prevention of *P.falciparum* infection by generalized gametocyte suppression in the human population, as a result of MDA, could become a reliable alternative in reducing malaria resurgence risk [268]. In South America, malaria is usually caused by *P.vivax* in the face of decreasing importance of *P.falciparum*. Also, the dominant *Anopheles darlingi* species is clearly related to heavy rainfall incidents, such as in the 2017 malaria outbreak in the French Guianese and Brazilian border areas [258].

2.3.10 Ivermectin and malaria prevention

Ivermectin in the form of mass drug administration (MDA) is a drug known to be useful in some African countries as a cheap and effective anti-parasitic agent in

the control of onchocerciasis and lymphatic filariasis [195, 357]. When ivermectin is ingested by *An.gambiae* s.s. during feeding on a human individual under treatment it is known to significantly reduce mosquito survival affecting sporogony of *P.falciparum* inside the mosquito [63, 196, 357]. The recommended effective dosage is in the range between 150 and 400 μg/Kg [357]. Its use could be particularly useful in synergism with gametocidal agents such as primaquine or methylene blue.

2.3.11 Insight from malaria modeling

Constant malaria prevention is necessary to reduce malaria incidence in high risk areas like sub-Saharan regions. Several procedures have been adopted for that matter, sometimes less successful than expected. Modeling malaria is not a very straightforward task. It involves a subtle and complete knowledge of several variables with influence on disease transmission.

However, most malaria models have given critical information on the effectiveness of certain preventive measures, if implemented. Better models lead to more effective decisions in disease prevention and more reliable information in disease forecasting.

Chapter 3

Malaria modeling: State-of-the-art

Malaria models may be classified according to the type of object in analysis. From deterministic and mathematical models to stochastic agent-based models, several methods have been used in malaria modeling. These models may be directed to transmission dynamics involving the parasite (*Plasmodium*), the vector population (*Anopheles*), or the existence of parasite drug resistance and vector insecticide refractoriness. It may also concern to different environment variables, such as climatic conditions (temperature, precipitation, or other weather parameters), or to territorial topographic characteristics such as the type and intensity of local vegetation as well as the nearness to mosquito breeding sites. Models are mainly applied to incidence prediction or estimation of disease transmission risk. Different technical procedures may be used such as computational simulations, imaging spatial models based on satellite imaging, or pure theoretical models such as the original Ross-Macdonald model (RM).

In this chapter we will present a summary of malaria modeling history, with a detailed timeline explaining the rationale of modern views on the subject. All presented models are listed from tables 3.5 to 3.8. A selection of the most important models will be discussed in the text, with further detail.

Since early preliminary work by Sir Ronald Ross, published from 1911 to 1915 [317], the quest for an adequate model explaining malaria epidemics has been persistent. This model was further extended during the 1920s, based upon the use of compartments in epidemic models by Kermack and McKendrick [186], and the theory of predator-prey dynamical systems, by Lotka and Volterra [370]. Further innovation in thinking had to wait for the duration of two world wars until 1952 when George Macdonald was able to further improve Ross initial theory [231]. At the time, the Ross-Macdonald model explained reasonably well the evolution of both human and mosquito infection dynamics, while defining the epidemic in a sound mathematical and deterministic frame. It included modern concepts based on what was then known, concerning the biological cycles of the parasite, *Plas-*

modium, as well as the vector, *Anopheles* mosquito. This theory will be presented with further detail in section 3.4 and chapter 4, according to well accepted concepts such as those defined by Smith, 2004 [343]. It has been, since then, properly named as the *Malaria standard model*, supporting some of the most important improvements in the field.

3.1 Early disease models

Most of the early malaria models used a deterministic and mathematical approach [185, 317, 371]. Some of these mathematical models have uncovered specific disease aspects such as the role of human gametocytemia in mosquito infection and disease transmission [181]. The importance of different critical state variables involved in malaria transmission highlights the complexity of the epidemic dynamics. Human and mosquito population size will usually amplify the magnitude of stochastic noise in multiple dimensions, with unpredictable impact in conditional variance. Some mathematical problems resulting from stochastic handling of the transmission model are still a challenge in infectious disease modeling [371]. Several physical computational models inspired by the Monte Carlo methodology and the Metropolis algorithm have also been used with variable enthusiasm in biology [59, 104, 348]. Stochastic agent-based models have produced consistent results [73, 95, 157, 171, 234, 348, 349], while generating more realistic model simulations.

In 1957, MacDonald established the significance of several important parameters in malaria modeling and disease prevention (Table 3.5), such as the basic reproductive number R_0 and the transmission coefficient β. A decade later (1968) he consistently described an improved approach to malaria dynamics [232]. His model included stochastic modeling of malaria transmission supported on a probabilistic Monte Carlo computational procedure, while requiring four epidemiological parameters: mosquito man-biting habit, mosquito daily survival, human disease recovery rate and the mosquito reproduction rate [232].

In 1974, Najera published a critical review of the application of MacDonald model based upon collected field data obtained from disease transmission statistics in Nigeria from 1966 to 1969 [269]. That same year, Dietz emphasized the role of immunity in disease transmission, supported by solid empirical work in the African savannah, in northern Nigeria [103].

A decade later, Verma (1983) published a refinement of the original malaria models describing a solid stochastic approach with good fit to realistic field data [369].

From 1972 to 1991, Anderson and May published several improvements on Ross-MacDonald malaria model theory [17]. These models included important demographical aspects such as human migration, human population age distribution and mortality.

Effective disease models are supposed to rely firmly on three important aspects: 1) accuracy (reproduction of the observed data and reliable prediction of epidemic disease outcome); 2) transparency (good definition of the dynamical role played by all model components) and 3) flexibility (flexible model adaptation to different environments) [185].

For several decades, malaria transmission has been thoroughly evaluated with the help of different disease models. The complex interaction between climate variables, vector dynamics, superinfection prevalence, children immunity, microscopic gametocytemia, and human heterogeneity, is responsible for different epidemiological patterns of disease transmission, frequently unpredictable. Network theory has also been applied to infection dynamics with promising results [95, 222, 225]. However, it has been difficult to determine some of its implications in designing a more effective disease prevention planning.

The role of spatial heterogeneity in epidemic models was described by Lloyd in 1996 [224]. The fact that human heterogeneity may influence disease transmission has been the focus of recent research on the subject. Somehow, human heterogeneity may have been systematically underrated as in the case of children with lower immunity against *P.falciparum* and less protection against the vector *Anopheles*. These so-called higher transmission hot-spots may act as important human-mosquito reinfection reservoirs.

In recent years we have witnessed an exponential growth in malaria modeling and forecasting procedures (tables 3.5 to 3.8). Stochastic models have improved previous malaria predictive models. Recent research on the subject has focused on a diversity of stochastic and computational methods to explore disease dynamics, including perturbation theory, time-series approach, numeric computation, agent-based modeling, mechanistic within-host modeling, and individual-based simulations, all of them with considerable relevance to malaria modeling [12, 25, 53, 109, 110, 141, 143, 152, 157, 158, 177, 180, 228, 272, 290].

3.2 The Kermack-McKendrick SIR model

Several issues should be taken into consideration when building an infectious disease model: The natural history of the disease, the time frame of the infectious process, and the phase transition between disease states. The basic *susceptible-infective* (SI) and *susceptible-infective-susceptible* (SIS) compartment models stand as the standard structures in infection modeling. More detailed models are available including a latency phase (*exposed* agents – SEIS), and a recovery phase, when individuals acquire partial or full immunity protection (*recovered* agents – SEIRS) following complete disease recovery [92, 186, 371].

Assuming the absence of fully protected recovered individuals, the SIS model could be used for the sake of simplicity as the standard malaria mathematical

model. During the 1950s, Macdonald improved the initial model by using a third epidemiological compartment of exposed mosquitoes [232]. Later in 1991, Anderson and May defined the compartment of exposed human individuals, including it in the model. The need for a recovered group as a consequence of acquired immunity and induced resistance to reinfection was solved by including a recovered compartment [237, 343].

In the present theory, the SEIRS model assumes humans and mosquitoes to be in one of four different compartments: susceptible (S), exposed (E), infective (I), and recovered (R) agents [17, 185, 371].

3.3 Stochastic models

In stochastic dynamics, disease transmission may behave like a Wiener (gaussian) process, including a noise factor applied to mosquito and human host compartments, with null average and stable variance. Several types of noise, with multiple sources, may add to the complexity of the stochastic equations. Different population mixing patterns, with relevance to heterogeneity in human vulnerability to mosquito biting behavior, may also strongly influence disease transmission.

3.3.1 Reed-Frost and Greenwood models

One may define three different settings for stochastic models:

a) Individual agent-based model, when the system keeps track of what happens to each individual in the population during a predefined time frame. However, it assumes a computer intensive methodology while requiring more equations.

b) Discrete-time compartmental model, where the susceptible and infective populations are viewed as single compartments in the epidemic process.

c) Continuous time (or "time to next event") compartmental model.

The Reed-Frost (RF) equation (1928) defines the risk of infection at each time step in the algorithm [371]. It is supported by a Markov chain process applied to a random variable with a binomial distribution. An alternative and very similar method was also defined by Greenwood in 1931. Both classical models use a discrete time algorithm to define the outcome of a stochastic event supported by a Markov transition probability between two potential states of a random state variable. Both are defined as chain binomial models.

Equation $\lambda_t = \beta I_t$ defines the *force-of-infection* (where λ_t represents the proportion of susceptible individuals that become infective in each time step of the algorithm, and β is equivalent to the rate of effective contact between two specific individuals during an unit time interval), and will probably overestimate the real infection risk in small populations. In such a case, one may use the Reed-Frost (RF) equation for evaluation of λ_t, where p stands for the probability of an effective

infective contact between individuals, and I_t represents the numbers of infectives at time t – equation 3.1.

$$\lambda_t = 1–(1–p)^{I_t} \tag{3.1}$$

In the simplified Greenwood model, the infection dynamics is not related to the size of the infective compartment, and the probabilities are usually slightly different from those of the Reed-Frost RF model.

If the time step is small, we will then have $p \sim \beta$ [371].

3.3.2 Gillispie algorithm

Stochastic processes applied to biological and demographic parameters will implicate randomness at the individual level of disease transmission. The *Gillispie's direct algorithm* may be used in stochastic modeling as an event-driven approach [185]. The algorithm estimates the time between events based on the cumulative rates of all possible events. Then, by using event rates in the form of probabilities, it will randomly select one of the events. This process will be iterated in time. As an alternative, one may use the *Gillispie's first reaction method* as a simpler but slower algorithm. The amount of used computer time will depend on the size of the population, and will assume an important limitation to the algorithm [185].

3.3.3 Stochastic algorithms and Ross-Macdonald theory

These similar algorithms have been applied with reasonable success in stochastic computational models. They have become crucial in defining relevant aspects of malaria transmission to be replicated within formal mathematical algorithms relating different SEIRS compartment models. These procedures should express standard computational relations equivalent to similar concepts within Ross-Macdonald theory. This will be explained with further detail in the following section (3.4).

3.4 Ross-Macdonald theory

Ross-Macdonald theory is a fundamental framework in malaria modeling. In the next subsection, its fundamental concepts will be presented. Later on, they will also be useful in model validation procedures – chapter 12.

3.4.1 The Ross-Macdonald model

In malaria research, much relevance has been given to R_0, the basic reproductive number. It represents the average number of human infections resulting from a single contact between one infective person with a healthy individual within a

susceptible human population. In malaria, the transmission mechanism is more complex as it involves both human-to-mosquito and mosquito-to-human transmission in a coupled interaction cycle of human and mosquito infectiousness. In epidemic disease expansion, R_0 is expected to be higher than 1. On the other hand, in the long term, disease elimination will likely result from a value of R_0 lower than 1. From the estimation of R_0 it is also possible to infer the concept of *Herd Immunity Threshold (H_t)* which stands as a golden landmark in large population immunization planning:

$$H_t = 1 - \frac{1}{R_0} \tag{3.2}$$

In neoclassical models, idealized populations may present with different levels of risk resulting from mosquito feeding in the presence of heterogeneous transmission. Differences in human spatial mixing and mosquito biting preferences in relation to biochemical odors, human self-defense ability, human population proximity to larval breeding sites, and human age distribution, among other human host properties, have been shown to promote disease transmission. This transmission heterogeneity risk may partially explain some of the differences found in R_0 values between stochastic models and empirical data [177, 344, 347].

3.4.2 Classic model assumptions

The initial theory assumed human individuals and mosquitoes as the model agents to be in one of two compartments: susceptible and infective. During the 1950s, Macdonald improved the old model by adding a third epidemiological compartment for exposed mosquitoes. Anderson and May (1991) further added the compartment of exposed humans to the original model [17, 237].

In these classical models, several assumptions were accepted, called the classical assumptions – see table 3.1. These assumptions are of axiomatic nature, and have been used time and again in malaria modeling.

However, recent evidence points out that some of these assumptions may not be realistic enough in representing malaria transmission, population dynamics and mosquito ecology [344]. Geographic variation and spatial effects must be also accounted for. Also, vector transmission models should address the problem that human populations are biologically diverse, and therefore heterogeneous.

3.4.3 The role of biological parameters and secondary indices

Mathematical models have become crucial in malaria epidemiology, improving the knowledge of non-linear systems in terms of equilibrium stability. Multiple indices [1] have been useful in defining disease dynamics with a wider scope [177, 343, 347].

[1] Smith,2004 [343]

Classical assumptions of malaria models
Mosquito populations are homogeneous
Mosquito senescence is ignored
Adult mosquito population is of constant size
Mosquito biting is random
Human biting is homogeneous
After infection, infected mosquitoes will remain so, indefinitely

Table 3.1: Classical assumptions of malaria mathematical of models [343]

From P_Q – see table 3.2 – we will obtain the proportion of mosquito bites occurring in human individuals (anthropophilic feeding behavior). And from P_Q and f, one may also obtain the human feeding rate a, corresponding to the expected number of bites on human hosts, per mosquito, per day, as in equation 3.3:

$$a = fP_Q \tag{3.3}$$

Here, we will assume X as the proportion of infected human hosts, and Y as the proportion of infected mosquitoes, whether infective or during latency in the latter case. In the event of adopting a straightforward static approach, X will be held constant – see table 3.3.

	Parameter
a	Human feeding rate
b	Mosquito-to-human infectiousness
c	Human-to-mosquito infectiousness
$\Delta_m = \frac{M}{H}$	Mosquito density
f	Mosquito feeding rate
q_m	Mosquito daily mortality rate
$\tau_s = \frac{1}{f}$	Gonotrophic cycle duration (days)
$\frac{1}{q_m}$	Expected lifespan of one mosquito
ϵ	Mosquito daily emergence rate
τ_{lm}	Mosquito disease incubation period
P_Q	Mosquito feeding fraction on human host
τ_c	Average human infectious period
τ_{lh}	Human disease incubation period
$q_h = \frac{1}{\tau_c}$	Human disease daily recovery
μ_h	Human yearly mortality rate

Table 3.2: Ross-Macdonald primary biological parameters [237, 343, 344]

Waiting time to biological events

It will also be possible to define some waiting times to biological events [343]:

a) The waiting time τ_μ to either the first human bite or mosquito death can be obtained from

$$\tau_\mu = \frac{1}{a + q_m}. \tag{3.4}$$

b) The waiting time τ_χ to the first human bite of surviving mosquitoes may be obtained from

$$\tau_\chi = \frac{1}{a} \tag{3.5}$$

c) The waiting time to infection of the daily surviving mosquitoes – τ_ζ can be obtained from

$$\tau_\zeta = \frac{1}{acX} \tag{3.6}$$

d) The waiting time τ_ξ to one of two events – mosquito death or infection – may be obtained from

$$\tau_\xi = \frac{1}{q_m + acX} \tag{3.7}$$

From these results it will be possible to define Y, as the proportion of infected mosquitoes (wether or not they are already infective), as in equation 3.8.

$$Y = \frac{acX}{q_m + acX} = \frac{\tau_\xi}{\tau_\zeta} \tag{3.8}$$

	Indices
X	Parasite rate (infected human hosts)
Y	Mosquito infection rate (infected mosquitoes)
Z	Sporozoite rate (infective mosquitoes)
$HBR = \Delta_m\ a$	Human biting rate
$EIR = \Delta_m\ a\ Z$	Entomological inoculation rate
$S = \frac{a}{q_m}$	Stability index (S)
$HBI = \frac{a}{a+q_m}$	Human blood index
R_0	Basic reproductive number
$\lambda = b\ EIR$	Force of infection

Table 3.3: Ross-Macdonald secondary biological indices [343]

Derived results

It will also be possible to derive other important results:

a) The individual vectorial capacity I_C, which is the expected number of infectious bites from a single vector after feeding on an infectious host, as defined in equation 3.9

$$I_C = \frac{ac}{q_m} e^{-q_m \tau_{lm}} \tag{3.9}$$

b) The vectorial capacity V_C, representing the disease transmission potential of a mosquito population in the absence of *Plasmodium*, as in equation 3.10:

$$V_C = \frac{\Delta_m \ a^2}{q_m} e^{-q_m \tau_{lm}} \tag{3.10}$$

c) The lifetime disease transmission potential τ_β, equivalent to transmission potential of a mosquito population in the absence of *Plasmodium*, as in equation 3.11:

$$\tau_\beta = \frac{a^2 bcX}{q_m(q_m + acX)} e^{-q_m \tau_{lm}} \tag{3.11}$$

d) The rate χ at which mosquitoes become infected is represented in equation 3.12:

$$\chi = acX \tag{3.12}$$

e) The mosquito emergence parameter ϵ – defining the vector birth rate – is obtained from equation 3.13:

$$\epsilon = \Delta_m \ q_m \tag{3.13}$$

Finally, we consider the fundamental sporozoite rate Z, defined as the proportion of infective mosquitoes, as in equation 3.14:

$$Z = Y e^{-q_m \tau_{lm}} \tag{3.14}$$

By using Z, one may then obtain the critical entomological inoculation rate EIR from equation 3.15:

$$EIR = \Delta_m \ a \ Z \tag{3.15}$$

These parameters have been considered critical tools in defining the epidemiological equations of malaria analysis, covering different aspects of malaria transmission. EIR and Z are of utmost importance in grasping the full dynamical aspects of vector behavior.

However, in a global picture of malaria transmission, the basic reproductive number (R_0) has been used as the main benchmark in evaluating the dynamical impact of malaria, and it will be presented with more detail in the next section (3.5).

3.5 The basic reproductive number – R_0

From the initial Ross classical formula [2] we may define the earlier and most consistent expression for R_0 (without a term ϵ for mosquito emergence) [237, 317]:

$$R_0 = \frac{\Delta_m \ a^2 bc}{q_m q_h} \tag{3.16}$$

This expression was reformulated by Macdonald in 1957 [231, 237] with the introduction of an exponential factor for the mosquito disease incubation time, τ_{lm}:

$$R_0 = \frac{\Delta_m \ a^2 bc}{q_m q_h} e^{-q_m \tau_{lm}} \tag{3.17}$$

Minor improvements in the initial model were later included by Anderson and May (1991), with respect to the residual impact of human mortality on the global outcome in the original Ross-Macdonald equations [17, 237].

$$R_0 = \frac{\Delta_m \ a^2 bc}{q_m q_h} e^{-q_m \tau_{lm}} e^{-\mu_h \tau_{lh}} \tag{3.18}$$

Several of the mentioned parameters above assume critical importance in defining more robust malaria models. In the previous sections we have presented different mathematical aspects of malaria transmission derived from Ross-Macdonald theory.

In the following section (3.6) a detailed chronological perspective of malaria modeling will be presented.

3.6 Malaria modeling – Historical perspective

Models are supposed to experimentally reproduce what happens in a system while simulating its dynamics as realistically as possible. Different types of classification may create a problem, as some of the models share operational characteristics belonging to more than one of the functional groups. In this case, we could have chosen to classify each model according to its main operational characteristic – see table 3.4.

A wide diversity of malaria models have been in use since the early model created by Sir Ronald Ross in the beginning of the XX century [317]. Different types of models have evolved since then (tables 3.5 to 3.8).

[2] Here, we will use q_m and q_h, instead of the symbols for the mosquito mortality symbol g and the human disease recovery rate r, respectively, as were used by Smith in 2004 [343]; we will also use Δ_m for mosquito density definition, instead of m originally used by Smith

Model operational characteristic
Mathematical models (SEIRS models; Ross-Macdonald theory)
Infection dynamical models (human host/vector)
Drug administration and drug-induced resistance models
Models including immunity
Climate models
Geospatial models
Agent-based models
Stochastic models
Time series models (Box-Jenkins theory)
Other unclassifiable models

Table 3.4: Malaria models – Operational classification

Here, we have used a more tedious, but less confusing, chronological approach in describing all malaria models considered relevant to modeling theory. However, it would also be possible to classify these models according to its structural properties and dynamical behavior.

3.6.1 Early years – From the XIX century to 1995

Inspired by the Ross-Macdonald model, a new malaria model was presented by Dietz in 1974 [103], including the effect of human immunity against the parasite. This work was based on empirical field results collected in the African savannah of Kano state, in northern Nigeria, from 1970 to 1976, under the support of the World Health Organization (WHO). In Nigeria and also under the support of WHO, from 1969 to 1976, the Garki project model for malaria control was implemented, parts of it being presented by Najera in 1974 [269], and later on in the full project by Molineaux and Gramiccia in 1980 [255]. This mathematical model evaluated the effectiveness of insecticide house spraying campaigns and the use of mass antimalarial drug administration (MDA) in malaria epidemiological control.

In 1983, Verma presented an interesting model, involving the use of stochastic processes with the assessment of transition probabilities for prediction of daily malaria incidence. It was based on longitudinal data, including several biological parameters, and showed reasonable good fit against observed data [369].

Roy Anderson and Robert May published in 1991 their seminal textbook in infectious diseases [17], containing a thorough and detailed explanation of mathematical malaria models at the time, including the effect of human latency and the role of gametocytemia in malaria transmission.

3.6.2 From 1995 to 1999

Martens (1995) used an integrated mathematical model assessing the impact of climatic factors such as temperature and precipitation in mosquito development and malaria risk [242].

The effect of spatial heterogeneity was included as a general SEIR model in a paper by Lloyd, in 1996 [224]. Although this model did not apply to malaria, it laid down the ideas for its future application to the epidemic.

Heterogeneity was included for the first time in a malaria epidemic model by Woolhouse in 1997 [386]. That same year, two quite different papers on malaria models were published. The first paper concerned the use of genetic algorithms in the control of vector modeling and vector and parasite resistance to insecticides and to drug administration, respectively (Janssen [171]), and was based on a previous work by Martens in 1995 [242]. The second paper focused on the role of human migration in the risk of a malaria outbreak (Torres-Sorando [360]).

The impact of climate factors in the disease risk was also included as a simple numerical approach defining disease transmission distribution of a malaria model in Africa, published by Craig in 1999 [87].

3.6.3 From 2000 to 2009

In 2000, Ngwa presented a mathematical model for malaria transmission with endemic behavior in variable human and mosquito populations [273]. It involved a deterministic approach and used a dynamical system model of differential equations, where equilibrium points were established by computer simulations in endemic malaria. In that same year, Killeen defined a pure mathematical model of entomological inoculation rate prediction in malaria at different sites in Papua New Guinea, Tanzania, and Nigeria, based upon several entomological and parasitological parameters (human population size and infectiousness, vector emergence rate, longevity, feeding cycle length and human blood index, and the sporogony incubation time of the parasite) [188].

From the year 2000 onwards, malaria modeling research steadily gained momentum, with new and fresh perspectives. Hay (2002) presented a climate model for evaluation of the risk of malaria resurgence in East African highlands. Long-term meteorological trends were investigated in four high-altitude sites in East Africa (Kenya, Uganda, Rwanda and Burundi) [162].

In 2003, Koella described an epidemiological mathematical model based upon Ross-Macdonald theory to investigate the spread of anti-malarial resistance in a fraction of treated individuals, taking into account acquired human immunity dependent on human exposure to infectious vectors [198]. Still in 2003, Gu established an individual-based model of *Pf* transmission based upon the dynamics of human-mosquito interaction. It also included human immunity as a result of human history of exposure to the parasite [156].

Hoshen (2004) presented a weather-driven mathematical-biological malaria model based on parasite dynamics, comprising both the weather-dependent within-vector stages and the weather-independent within-host stages. Infection prevalence was estimated based on numerical evaluations of the model in both

Model specification	**Author,Year**
Primordial malaria mathematical model	Ross,1915 [317]
Model with human/mosquito latency	Macdonald, 1968 [232]
Ross-Macdonald model application in Nigeria	Najera,1974 [269]
Model improvement including immunity	Dietz,1974 [103]
The Garki project in Western Africa	Molineaux,1980 [255]
Stochastic model predicting malaria incidence	Verma,1983 [369]
Improved version of Ross-Macdonald model	Anderson,1991 [17]
Climatic factors in malaria risk model	Martens,1995 [242]
Spatial heterogeneity in epidemic models	Lloyd,1996 [224]
Genetic algorithms in vector control modeling	Janssen,1997 [171]
Population migration models	Torres-Sorando,1997 [360]
The role of heterogeneity in disease transmission	Woolhouse,1997 [386]
Climate model of malaria transmission in Africa	Craig,1999 [87]
Entomological inoculation rate (EIR) modeling	Killeen,2000 [188]
SEIRS mathematical modeling	Hethcote,2000 [164]
Mathematical model of endemic malaria	Ngwa,2000 [273]
Climate model and the risk of malaria resurgence	Hay,2002 [162]
Model of *Pf* transmission in Kenya	Gu,2003 [156]
Models for spreading of antimalarial resistance	Koella,2003 [198]
Upgrade in previous model of endemic malaria	Ngwa,2004 [272]
A weather-driven model of malaria transmission	Hoshen,2004 [167]
Mosquito availability and malaria transmission	Killeen,2004 [189]
Multi-agent malaria modeling	Rateb,2005 [313]
Oviposition in disease transmission	LeMenach,2005 [216]
Model with within-host dynamics and immunity	McKenzie,2005 [249]
A geospatial model of malaria risk in East Africa	Omumbo,2005 [282]
Bifurcation analysis in a malaria model	Chitnis,2006[69]
Malaria immunity acquisition models	Filipe,2007 [126]
Oscillatory model with temporary immunity	Tumwiine,2007 [363]
Model of immune-modulated malaria in children	Gurarie,2007 [157]
Malaria short-term prediction in Sri Lanka	Briët,2008 [52]
Malaria spatio-seasonal modeling in Mozambique	Abellana,2008 [3]
Heterogeneity in stochastic models	Smith,2008 [349]
Delayed Ross–Macdonald malaria model	Ruan,2008 [318]
A model of malaria pathogenesis	Mideo,2008 [252]
Role of prophylaxis model in malaria prevention	Nyabadza,2008 [275]
Anti-malarial drug resistance mathematical model	Pongtavornpinyo,2008 [309]
Artemisinin therapy in disease transmission	Okell,2008 [279]

Table 3.5: Malaria modeling – Historical perspective (1911 to 2008)

time and space [167]. In 2005, Rateb used a multi-agent malaria model for evaluation of the impact of education on malaria healthcare in Haiti [313]. A differential equation model of malaria was used by McKenzie (2005) supported by within-host dynamics and including acquired immunity from involvement of different parasite genotypes [249].

A geospatial approach to modeling of malaria risk in East Africa was presented by Omumbo, in 2005. Statistical techniques were used in predicting the intensity of malaria transmission in terms of the childhood parasite rate (X) in a high-resolution spatial map, according to human settlement and land-use in East Africa [282]. In 2006, Chitnis investigated the spread of malaria in human and mosquito populations with endemic stability equilibrium points for $R_0 > 1$. An ordinary differential equation mathematical model for malaria transmission was used, based on bifurcation analysis [69].

Tumwiine (2007) presented a malaria model with oscillatory malaria dynamics in a population with temporary immunity after disease recovery [363]. In 2008, Abellana presented a malaria model for malaria incidence prediction based on hierarchical Bayesian models, incorporating a seasonal effect on malaria incidence spatial distribution in children under 10 years old in Manhiça district, Mozambique [3]. Briët (2008) presented different malaria models (ARIMA, SARIMA and exponentially weighted moving average models) based in the covariation of rainfall affecting malaria incidence prediction in Sri Lanka, from one to four months ahead in time [52].

Still in 2008, Thomas Smith presented a method for heterogeneity quantification in malaria models. Entomological inoculation rate (EIR) in relation to malaria incidence was analyzed using published data cohorts of children in Saradidi, in Western Kenya. Infection risk was treated assuming a binomial distribution, and measurement-error (Poisson and negative binomial) models were considered for EIR determination. Models were fitted using Bayesian Markov chain Monte Carlo algorithms, and model fit was compared for different model assumptions [349]. In the same year, Pogtavornpinyo described a model for the prediction of the spread of drug resistance in different malaria transmissions settings, incorporating several important human and mosquito factors. This model pretended to evaluate different anti-malarial strategies focusing on artemisinin-based combination therapy (ACT) [309].

Mideo (2008) published a thorough review paper detailing the conceptual development of epidemiological and biological malaria models [252].

Still in the same year, Ruan presented a delayed Ross–Macdonald Model of malaria transmission including parasite incubation times in mosquitoes and human hosts, and the effect of time delays on the basic reproduction number R_0 result [318].

Finally, in 2008, Okell described a basic parasite model of malaria transmission

Model specification	**Author,Year**
Multi-step polynomial regression model	Chatterjee,2009 [65]
Larval reduction and insecticide treated nets	Yakob,2009 [389]
Insecticide-treated nets and malaria transmission	Gu,2009 [155]
Environmental dependency in Mali	Gaudart,2009 [134]
Mathematical models in malaria strategy	White,2009 [381]
Mathematical model for estimation of malaria risk	Massad,2009 [245]
Model of village scale malaria transmission	Bomblies,2009 [39]
Multi-variable transmission model in Africa	Griffin,2010 [152]
Climate model and malaria transmission	Parham,2010 [297]
Temporal modeling with time-series analysis	Wangdi,2010 [376]
Model for prediction of transmission hot-spots	Bousema,2010 [43]
A spatio-temporal vector distribution model	Kashiwada,2010 [183]
Disease transmission model of vector life cycle	Bellan,2010 [36]
malERA agenda for modeling malaria eradication	malERA,2011 [236]
Artemisinin combined therapy model	Kern,2011 [187]
Malaria mathematical models review	Mandal,2011 [237]
Ecology model of vector life cycle	Eckhoff,2011 [110]
Model with sub-microscopic gametocyte reservoir	Karl,2011 [181]
Distribution model of infection duration	Bretscher,2011 [49]
Malaria immunity agent-based model	Gurarie,2012 [158]
Epidemiology of malaria transmission in Kenya	Stuckey,2012 [353]
Ecohydrological model of malaria resurgence	Montosi,2012 [256]
Asexual parasitemia model of disease transmission	Johnston,2013 [177]
Vector dynamic model and malaria transmission	Lunde,2013 [228]
A model of vector exposure risk in west Africa	Moiroux,2013 [254]
Cost-effectiveness of mass screening and treatment	Crowell,2013 [88]
VECTRI model of malaria transmission dynamics	Tompkins,2013 [359]
Model of malaria elimination in South Africa	Silal,2014 [335]
Agent-based model of vector dynamics	Arifin,2014 [25]
Stochastic simulation analysis in disease modeling	Klein,2014 [193]
Comparison of five malaria transmission models	Wallace,2014 [373]
Mathematical model of malaria transmission	Muhammed,2014 [260]
Challenges for modeling indirect transmission	Hollingsworth,2014 [165]
Seasonal forecasting model of malaria in India	Lauderdale,2014 [210]
Ivermectin prevention model	Slater,2014 [339]
SARIMA model of malaria mortality in Nigeria	Dan,2014 [94]

Table 3.6: Malaria modeling – Historical perspective (2009 to 2014)

in human and mosquito populations, directed at the consequences of artemisinin-based combination therapy on malaria endemicity [279].

In 2009, Gaudart described a deterministic SIRS-type model of malaria transmission including a stochastic environmental factor where the seasonal pattern of *Pf* incidence was reasonably explained by a vegetation density index (*NDVI*) issued from satellite imagery series, with a time delay of 15 days. This SIRS-model of malaria incidence with environmental dependency, was based in data from Bancoumana locality, in Mali [134].

Lisa White (2009) described a simple deterministic compartmental model including key parameters of malaria transmission and integrated control obtained from data sets of areas with different transmission intensities. It included a clinically immune state that could be maintained through repeated infection boosting immunity or lost in the absence of parasite exposure [381].

Still in 2009, Dangerfield described an interesting SIS-model deterministic-stochastic approach to malaria modeling. This model combined a diffusion Ornstein–Uhlenbeck approximation for stochastic populations with a pair-wise approximation of a deterministic malaria SIS-model infection spreading through a network, highlighting the interaction between local spatial structure and stochasticity [95].

Massad (2009) presented a mathematical model of malaria risk in non-immune individuals acquiring *P.falciparum* malaria when traveling to the Amazonas region of Brazil. The risk of malaria infection was dependent on the duration of human exposure to the parasite and the season of traveler arrival to the region [245].

Also in 2009, Bomblies presented a mechanistic model that coupled a distributed hydrology scheme and an entomological model with environmental conditions and associated entomological activity in high spatial- and temporal-resolution, for accurate simulation of village scale malaria transmission. Model results were compared to regular field observations of *An.gambiae* s.s. (*sensu lato*) mosquito populations and local hydrology [39].

3.6.4 From 2010 to 2015

In 2010, Griffin presented an individual-based simulation model of the effect of artemisinin-combined therapy (ACT) with wide coverage of long-lasting insecticide treated nets (LLIN) in *Pf* transmission in Africa, concerning three important vector species (*An.gambiae* s.s., *An.arabiensis*, and *An.funestus*) [152]. In that same year, Parham developed a simple model dealing with the importance of rainfall and temperature on mosquito population dynamics, disease persistence and seasonal transmission in Tanzania [297]. Also in 2010, Kashiwada described a model of vector spatial and temporal distribution based in the life history of the *Anopheles* mosquito, by using an ecophysiological approach with the availability and temperature of surface water in Monsoon Asia (China, Japan, South Korea,

Thailand and India) [183].

Wangdi (2010) used an ARIMA malaria model for prediction of malaria incidence built from a data set from 1994 to 2006 in seven malaria endemic districts in Bhutan. This model was developed taking into account the trend of malaria cases over the years with assumed stability of all other conditions (climate factors, preventive measures, and human migration) [376].

Still in 2010, Bellan designed a model on how age-dependent mosquito mortality could affect the effectiveness of anti-vectorial interventions in reducing disease transmission [36]. In that same year, Bousema designed a spatial methodology for identification of malaria transmission hot-spots. Environmental, household factors and serological markers of malaria exposure were used to develop a model for prediction of malaria transmission hot-spot areas [43].

In 2011, the malERA group proposed an important agenda for malaria model research and development, with a broader eradication research agenda. It detailed modeling objectives and data management methods, pointing to further aspects of model development such as models concerning within-host dynamics of *Plasmodium* infections, as well as the importance of human infectious reservoir, bionomics and ecology of the vectors. It included genetically modified mosquitoes, parasite dynamics, host and vector movements, and drug dynamics. Also of concern were how could human immunity and the use of vaccines be able to interrupt malaria transmission in the presence of host and vector heterogeneity [236].

Mandal (2011) published an important and detailed review on the evolution in time of mathematical malaria models with the most critical features of host-vector-parasite interactions. Models were presented, evolving from the original Ross equations to a hierarchical structure of deterministic models with different levels of complexity [237].

Eckhoff, in 2011, presented a reliable model for mosquito population dynamics including mosquito feeding behavior, weather conditions and the impact of vector control interventions such as bed nets, indoor residual spraying (IRS), larval control and space spraying, both alone and in combination, for a single-location simulation with seasonality typical of central Tanzania [110]. Still in 2011, Karl presented an important model focused on the presence of low-level gametocytemia and its consequences in disease transmission. This model was a refinement of the classical Ross-Macdonald model of malaria transmission, and incorporated multiple infectious compartments with potential impact on low-level gametocytemia reservoirs in the population [181].

Bretscher (2011) presented an infection dynamic model focused on the probability distribution curves of human disease duration with several parameter settings, with validation by empirical data from the region of Navrongo, in Northern Ghana [49]. Finally, in 2011, Kern presented a computer simulation model directed at the impact of community screening campaigns (CSC) followed by sys-

tematic treatment of *P.falciparum* asymptomatic carriers (AC) with artemether-lumefantrine (AL), incorporating a seasonality effect. This model was based on a basic parasite model of malaria transmission in human and mosquito populations published by Okell in 2008 [279], and directed at the consequences of artemisinin-based combination therapy on malaria endemicity [187].

In 2012, Stuckey described an individual-based stochastic simulation model of malaria in humans coupled with a deterministic model of malaria for mosquitoes while reproducing the seasonal pattern of the entomological rate. The transmission model was supported by a periodically-forced difference equation for mosquito feeding and human and mosquito infectiousness, in a heterogeneous human population background [353]. In that same year, Gurarie described a new in-host agent-based model combining deterministic and stochastic components of in-host dynamics with several features of the parasite replication cycle and parasite-host interaction, such as antigenic variation of *P.falciparum*, human immunity and parasite clearance [158]. Also in 2012, Montosi described a full eco-hydrological model of malaria transmission dynamics coupled with a hydrological model of soil water content in relation to climatic factors such as the minimum monthly temperature and the presence of precipitation anomalies [256].

In 2013, Johnston described a mechanistic within-host model of *P.falciparum* infection in humans and pathogen transmission to *Anopheles* mosquitoes during the entire parasite life-cycle, from intra-erythrocytic asexual forms, to mature transmissible gametocytes with high human-to-mosquito infectiousness [177]. During that same year, Moiroux described a spatio-temporal malaria risk model based on human-vector interaction concerning two *Anopheles* species (*An.funestus* and molecular forms M and S of *An.gambiae* s.s.) in an area of Benin with strong vector control intervention [254]. Also in 2013, Crowell presented a dynamic, individual-based, stochastic model of malaria biology and epidemiology intending to evaluate effectiveness of mass screening and treatment (MSAT) strategy for *P.falciparum* disease-burden reduction [88]. Lunde (2013) presented a detailed biophysical model with spatial distribution and time-dependent vector density of two competing species (*An.gambiae* s.s. and *An.arabiensis*), and where vector survival is dependent on mosquito size and climate factors such as temperature and relative humidity [228].

The first published version of the VECTRI malaria dynamics model originated in Trieste and was presented in 2013 by Tompkins. This model analyzed the importance of rainfall, and water and air temperature on the *P.falciparum* parasite and the *An.gambiae* vector life cycles, in close interaction with the human host population. Larval life cycle and larval mortality along with *Anopheles* mosquito gonotrophic and sporogony cycles were considered in mathematical detail. Human host population density and surface hydrology were also included in the transmission model [359].

In 2014, Arifin presented an agent-based entomological model of vector popula-

tion dynamics, with analysis of the impact of vector control interventions in specific phases of the mosquito life cycle [25]. In that same year, Klein, among other models, presented an individual malaria simulation model based in a detailed computer simulation using the Separatrix Algorithm. This algorithm combined binomial regression, based on specific kernel methods, with an experimental design procedure for optimized information gain. This model focused on the goal of local malaria elimination by the use of insecticide treated bed nets (ITN) and pre-erythrocytic vaccination (PEV) [193]. Still in 2014, Wallace published a comparative analysis of five malaria models concerning several aspects of disease transmission dynamics at equilibrium such as malaria incidence in human and mosquito populations, human-biting rate, and entomological inoculation rate (EIR) [373].

Muhammed (2014) presented a malaria mathematical model based on a previously published SEIRS/SEI model for human/mosquito populations by Shu and Ngwa [273]. It included drug effectiveness evaluation, but excluded direct human recovery from the infection to the susceptible compartment [260].

Also in 2014, Silal presented a deterministic non-linear compartmental model of malaria transmission dynamics in the human population of Mpumalanga, South Africa, including seasonality and elimination-focused interventions such as vector control and mass drug administration [335]. Dan (2014) used a seasonal ARIMA (SARIMA) model for analysis and forecasting of malaria mortality rate in Nigeria, adopting the reliable Box and Jenkins methodology [94].

In 2015, Kamgang presented a mathematical compartmental model of malaria transmission including several aspects of malaria dynamics like intrinsic vector behavior variables, parasite biological parameters and specific human factors such as immunity and immigration [180]. Meanwhile, in 2015, Sharma presented a machine-learning model for prediction of malaria incidence by using two popular data mining classification algorithms (Support Vector Machine and Artificial Neural Network) based upon a large data set from Maharashtra state [331]. Also in 2015, Gebremeskel published a mathematical model describing the dynamics of malaria in different human population compartments. This model was supported by a system of ordinary differential equations (ODEs) applying dimensional analysis, scaling, perturbation techniques and stability theory of ODE systems in defining the stability of all equilibrium points in the model [135].

3.6.5 From 2016 to 2022

In 2016, Yamana presented a mechanistic modeling tool to investigate the effects of hysteresis in malaria transmission in Banizoumbou, a small village in Niger. A process-based model was used to simulate the dynamics of malaria transmission including vector and parasite variables and intrinsic factors such as human immunity and prior population infection status [390]. Also in 2016, Anwar presented an autoregressive integrated moving average (ARIMA) model with environmental and climate data, for malaria incidence prediction in Afghanistan [22].

The year of 2017 was an important one for innovation in new malaria models. Alam presented a spatial agent-based model of *An.vagus* biological attributes and life-cycle, concerning the role of climatic factors such as daily temperature and rainfall, and the impact of combined vector control interventions in Bandarbaran, Bangladesh [10]. That same year, Ferreira presented an agent-based stochastic model simulating the impact of insecticide-treated bed nets (ITN) and indoor residual spraying (IRS) on mosquito survival and biting rate, allowing for the possibility of genetic natural selection of insecticide-resistant mosquitoes under the pressure of adopted control strategies [124]. Slater (2017) published a comprehensive review of the role of mathematical models in antimalarial drug research, focusing on drug properties and effectiveness in malaria control, and mechanisms of parasite drug resistance [341]. Still in 2017, Winskill presented a mathematical model of control intervention cost-effectiveness in Sub-Saharan Africa with RTS,S malaria vaccine, long-lasting insecticide net (LLIN), indoor residual spraying (IRS) and seasonal malaria chemoprevention (SMC) over a 10-year period [383]. Gerardin (2017) described a dynamical model of malaria transmission with spatially-connected household local variation in vectorial capacity and intervention coverage according to empirical data from Gwembe District, Gambia [138]. Belay (2017) presented a model relating mosquito abundance and time to malaria incidence in a Bayesian joint framework [35]. Zhu (2017) described a spatial individual-based model of malaria transmission in a hypothetical isolated African village setting with the use of LLIN and outdoor attractive toxic sugar bait (ATSB) stations as vector control measures [396].

Also in 2017, Girond presented a SARIMA model for malaria outbreak forecasting based in an automated web-based sentinel malaria early warning system (MEWS) [143]. Getnet (2017) developed GARCH and seasonal ARIMA models aimed at forecasting malaria incidence in Addis Zemen, Ethiopia [141].

In 2017, concerning models on MDA, Brady studied its effects in the presence of low malaria transmission [48], while Pemberton-Ross, with the help of probability generating functions, presented a compartmental model for analysis of the probability of malaria stochastic extinction in different scenarios of MDA coverage, population size, and in terms of its effect on the reproduction number, R_0 [301].

In 2018, Bakary presented a mathematical model of malaria transmission dynamics considering vector age, vector periodic biting rate, and human immunity status. Equilibrium points in the dynamical system were analyzed with detail. Numerical simulations were used to illustrate the system evolution in time [29]. In that same year, Smith presented a systematic review of 90 agent-based models of malaria transmission published between 1998 and 2018, that were considered the most relevant at the time [346]. Meanwhile, Coalson (2018) developed a mathematical model to estimate the proportion of new mosquito infections according to the age and gametocyte density of infectious human hosts, and the type of season in terms of rainfall [76]. Still in 2018, Koutou presented a SIR-SI malaria

Model specification	**Author**
A model of malaria transmission dynamics	Kamgang,2015 [180]
Times series analysis of malaria cases in Ghana	Appiah,2015 [23]
Vector model with non-linear forces of infection	Avila-Vales,2015 [27]
Infection duration model and acquired immunity	Bretscher,2015 [50]
Stochastic epidemic models review	Britton,2015 [53]
Disease ecology models in multi-agent systems	Buhnerkempe,2015 [54]
Pre-erythrocytic vaccine in intra-host malaria	McCarthy,2015 [248]
Malaria diagnosis model in african children	Phillips,2015 [304]
Insect sterilization and vector control model	Gentile,2015 [136]
Machine learning malaria prediction model	Sharma,2015 [331]
Mathematical model of malaria dynamics	Gebremeskel,2015 [135]
ARIMA models in malaria time series	Anwar,2016 [22]
Malaria and weather time series analysis in Iran	Ostovar,2016 [290]
Malaria prevention efficiency model	Walker,2016 [372]
Bistable equilibrium and malaria elimination	Griffin,2016 [151]
Artemisinin and drug resistance model in Africa	Slater,2016 [340]
Climate conditions in malaria transmission	Yamana,2016 [390]
Spatial effects in *Pf* multiple infections	Karl,2016 [182]
Cost-effectiveness modeling of a malaria vaccine	Winskill,2017 [383]
Reactive case detection and malaria elimination	Gerardin,2017 [138]
Bayesian weather model of malaria incidence	Belay,2017 [35]
Individual-based model of outdoor vector control	Zhu,2017 [396]
Malaria forecasting model in Madagascar	Girond,2017 [143]
Stochastic model for time series in Ethiopia	Getnet,2017 [141]
Time series malaria analysis in Ghana	Alhassan,2017 [12]
Time series malaria control model in South Africa	Ebhuoma,2017 [109]
Diagnostic testing and *Pf* selection	Watson,2017 [377]
Long-acting/transmission blocking drugs model	Bretscher,2017 [51]
Malaria prevention in HIV+ pregnant women	Choi,2017 [72]
Diagnostic testing and *Pf* selection	Gatton,2017 [133]
Impact of ITN use in *Anopheles* biting time	Ferreira,2017 [124]
Agent-based model of *An.vagus* epidemiology	Alam2017 [10]
Drug development model for malaria elimination	Slater,2017 [341]
MDA model in low malaria transmission areas	Brady,2017 [48]
MDA model and disease extinction probability	Pemberton-Ross,2017 [301]
Pf sexual stage immunity in infection dynamics	Ouédraogo,2018 [292]
Wind and water proximity in disease transmission	Endo,2018 [111]
Mass drug use and disease transmission	Gerardin,2018 [139]
Human movement and disease transmission model	Pizzitutti,2018 [307]
Host-seeking vector behavior and LLIN model	Shcherbacheva,2018 [332]
ARIMA model of malaria incidence in Ghana	Anokye,2018 [21]
Mathematical model of malaria transmission	Bakary,2018 [29]
Role of children in disease transmission in Malawi	Coalson,2018 [76]
Systematic review of malaria agent-based models	Smith,2018 [346]
A mathematical model of malaria transmission	Koutou,2018 [200]
Threshold conditions in dynamic malaria models	Wanduku,2018 [374]
A stochastic model of malaria transmission	Mbogo,2018 [247]

Table 3.7: Malaria modeling – Historical perspective (2015 to 2018)

transmission model to analyze the effects of infection incubation time in disease transmission, considering a variable human immunity status [200]. Anokye (2018) analyzed the use of ARIMA models in malaria incidence forecasting, in Kumasi, Ghana [21].

Also in 2018, Wanduku presented a family of deterministic SEIRS epidemic dynamic malaria models in terms of the time to acquisition of immunity and the time of disease incubation in human hosts and mosquitoes [374]. During that same year, Mbogo presented a stochastic model for malaria transmission dynamics, deriving relations between the basic reproductive number for malaria and extinction thresholds of corresponding continuous-time Markov chain models, under certain assumptions. The model was formulated by using the continuous-time discrete state Galton-Watson branching process [247]. Still in 2018, Pizzitutti described a spatial agent-based model of human behavior and mobility in local-scale malaria transmission, and its relation to seasonal flooding of Amazon river, in Peru [307]. Finally, in 2018, Shcherbacheva presented a malaria transmission agent-based model concerning the protective efficiency of LLIN and IRS against different species of *Anopheles* mosquito [332].

In 2019, Abiodun described a dynamical zero-inflated negative binomial regression model in Limpopo Province, South Africa. The predictive power of climate variables such as the daily rainfall and average temperature in malaria incidence was determined as a function of the number of daily cases, at different time lags [4]. In that same year, Weiss described a Bayesian space-time geospatial model of parasite rate, malaria incidence and disease mortality in a cartographic approach concerning 36 countries with high-burden endemic malaria in sub-Saharan Africa, while comparing its results with those of other 70 countries where data was collected using the surveillance approach [379]. Still in 2019, Le presented a stochastic lattice-based malaria model with the ability to make predictions of disease dynamics, vector burden and parasite life cycle, in relation to climate changes in one of Kenya sub-regions. Climate-driven hydrological changes under global warming were considered critical for defining vector habitat distribution [215]. Also, in 2019, Onah described a mathematical epidemiological model of malaria transmission dynamics and stability analysis of endemic equilibrium points concerning the impact of several disease control measures [284].

With the purpose of defining better strategies for vaccine protective efficacy enhancement, Atcheson (2019) described a mathematical probabilistic model of protective efficacy obtained by the combination of different pre-erythrocytic malaria vaccine subunits in mice [26].

In 2020, Sequeira (author of the current dissertation) described a multi-variable agent-based model of disease transmission with a computational demonstration of the potential utility of combining ivermectin with gametocidal agents such as primaquine or methylene blue in reducing malaria transmission, with no further need for additional anti-malarial drug intervention [326]. Also in 2020, Sequeira used

Model specification	**Author**
Malaria regression model in South Africa	Abiodun,2019 [4]
Global prevalence of *Pf* malaria	Weiss,2019 [379]
Malaria and climate change impact in Kenya	Le,2019 [215]
Mathematical model of malaria prevention	Onah,2019 [284]
Model of malaria vaccine combination in mice	Atcheson,2019 [26]
Reactive case detection and *Pf* transmission	Reiker,2019 [314]
Impact of falsified anti-malarial drugs in Uganda	Ozawa,2019 [293]
Ivermectin and gametocidal drugs model	Sequeira,2020 [326]
Model of heterogeneity in malaria transmission	Sequeira,2020 [327]
Epidemiological model of malaria transmission	Aguilar,2020 [7]
Neural network malaria prediction model	Verma,2020 [368]
Mathematical model of malaria transmission	Traoré,2020 [361]
Modeling malaria dynamics	Olaniyi,2020 [280]
Age of infection in a vector-borne disease model	Wang,2020 [375]
Quarantine in the Ross-Macdonald model	Jin,2020 [174]
Dynamical model of malaria transmission in India	Chaturvedi,2020 [66]
Fourier residual ARIMA model in malaria	Eze,2020 [116]
Malaria model with climate variables in India	Kumar,2020 [203]
A fuzzy logic based model for malaria prediction	Chekol,2020 [67]
A weather-based deterministic model	Yiga,2020 [391]
Probabilistic model of malaria recognition	Parveen,2021 [299]
Model of malaria population dynamics	Witbooi,2021 [384]
Malaria agent-based complex model	Amadi,2021 [15]
SIS-SI stochastic model of malaria spreading	Syams,2021 [356]
Bayesian decision model for malaria prediction	Clearly,2021 [75]
Modeling Anopheles distribution in arid regions	Valderrama,2021 [365]
Risk model of mosquito-borne diseases	Colón-González,2021 [81]
Malaria temporal variation in a time series model	Ferrão,202 [125]
Agent-based model of mosquito aquatic habitats	Layie,2021 [214]
Malaria forecasting – Hurst exponent and entropy	Sequeira,2022 [328]
Nonlinear differential equations model	Sinan,2022 [336]
Time-dependent social deterministic model	Olaniyi,2022 [281]
Fractional-order delayed Ross–Macdonald model	Cui,2022 [89]
Mathematical model using the Jacobian matrix	Ahmed,2022 [8]
Relative humidity dynamical model based in India	Santos-Vega,2022 [323]

Table 3.8: Malaria modeling – Historical perspective (2019 to 2022)

the previous malaria model in establishing the importance of heterogeneity in increasing malaria transmission more than three-fold, as well as the potential benefit of the combination ivermectin-gametocidal agents in reducing that transmission amplifying effect [327].

In that same year, Aguilar presented an epidemiological malaria model with evaluation of the influence of asymptomatic carriers in disease transmission [7].

Meanwhile, Verma described a back-propagation neural network malaria model defining disease risk in terms of regional climate data [368]. Still in 2020, Traoré used a global mathematical model of malaria transmission which was based on a structured mosquito population in Burkina Faso, and included the seasonal variation of monthly mean temperature [361].

In 2020, Olaniyi presented a mathematical model of malaria dynamics with partial immunity and the presence of protected travelers. It included different scenarios of preventive strategy with the use of IRS and ITN, and a cost-effectiveness analysis [280]. And in that same year, Wang described a vector-borne disease model with quantification of human and mosquito age of infection, and its influence in disease transmission dynamics [375]. Meanwhile, Jin presented a model based on the Ross-Macdonald theory that included the influence of quarantine in disease transmission [174].

Chaturvedi (2020) described a climatic dynamical model for estimation of malaria incidence in India in a setting of a warming environment [66]. Meanwhile, Eze described an ARIMA model with Fourier residual modification for determination of malaria incidence rates among pregnant women in Thailand [116]. In 2020, Kumar presented a time series regression model for malaria prediction based on climate variables and data collected in the Odish district in India [203].

Yiga (2020) presented a weather-based human host-mosquito vector deterministic model by looking into how temperature and rainfall may influence transmission dynamics. He found a unique endemic equilibrium that was locally and globally asymptotically stable whenever $R_0 > 1$. The model was analyzed for steady states and their stability. Temperature was more important than rainfall in malaria transmission [391].

Finally, Chekol (2020) presented an unconventional recent model capable of malaria epidemic prediction based in an innovative mathematical method described as type 2-fuzzy logic system, optimized according to Big Bang-Big Crunch theory. This original method could predict with reasonable accuracy a new malaria epidemic spike, up to 3 months ahead of its occurrence [67].

Parveen, in 2021, proposed a Bayesian network (BN) probabilistic-based model in the prediction of malaria. The proposed model was based on patient's symptoms and environmental data. The model had an accuracy of 81% when evaluated on the collected data set [299].

In 2021, Witbooi described a compartmental model based upon ordinary dif-

ferential equations of malaria disease transmission. It included the effect of IRS on the vector population, while allowing for the influx of infected immigrants into the host population, as well as for the outflow of cured emigrants [384]. In a paper published by Amadi (2021), an agent-based stochastic model was used as a tool for regression analysis with the help of simulation results compared to experimental field data, while allowing for the calibration of important classical model parameters such as biting rates and vector mortality [15]. Meanwhile, Syams used a continuous time Markov chain stochastic model adapted in the form of a modified mathematical model to describe the dynamics of malaria transmission. It focused on the basic reproduction number R_0, the probability of disease outbreak, and the time to reach disease-free equilibrium [356].

Still in 2021, in Papua New Guinea, Clearly presented a predictive model to analyze *P.falciparum* and *P.vivax* malaria prevalence maps by using Bayesian decision networks and multilevel logistic regression models in terms of disease spatial risk prediction accuracy [75].

Also in 2021, Valderrama presented a model of the potential distribution of the malaria vector *An.pseudopunctipennus* in subtropical regions in northern Chile. With the help of a minimum number of variables, a logistic regression model was created defining the spatial distribution of the vector presence probability in the northern regions of Chile [365].

Colón-González (2021) used a multi-model multi-scenario framework, for estimation of the length of the transmission season and global population at risk of malaria in different altitude settings during an extended time period between 1951 and 1999, according to regional climatic suitability [81].

A Box-Jenkins model was used by Ferrão in 2021, while analyzing the leading causes of malaria morbidity and mortality in Mozambique. Temporal modeling with autoregressive integrated moving average (ARIMA) was implemented, based upon empirical malaria incidence data collected from 2015 to 2019 [125]. Layie (2021), used an agent-based model aiming at controlling malaria transmission by focusing on mosquito aquatic habitats management and larval control around houses through population sensitizing campaigns in a traditional sub-Sahara region.[214].

In 2022, Sequeira used a previous malaria model [326, 327] in establishing the importance of the Hurst exponent and information entropy in malaria time series forecasting, by defining its application to long memory stochastic processes in the presence of long-range dependence [328].

Also in 2022, Sinan analyzed the dynamics of malaria among human individuals and vectors with the help of a mathematical model applying non-linear ordinary differential equations generalized by the Atangana–Baleanu fractional derivative. This model was found to be globally asymptomatically stable as the solution converged to its equilibrium [336].

Cui (2022) proposed a novel fractional-order delayed Ross–Macdonald model for malaria transmission, by using different mathematical approaches such as inequality techniques, contraction mapping theory, fractional linear stability theorem, and bifurcation theory in local stability analysis [89].

In 2022, Olaniyi presented a time-dependent socially structured deterministic model based upon an eight-dimensional system of differential equations aiming at the prevention and control of the effects of social differences on the transmission dynamics of malaria [281].

Meanwhile, in 2022, Ahmed investigated the local stability of critical equilibrium points in a mathematical model by applying the Jacobian matrix technique [8]. The general stochastic fractional Euler method, the Runge–Kutta method, and a proposed numerical method were used in defining all model solutions [8].

Finally, in 2022, Santos-Vega analyzed the role of relative humidity in the interannual variability of epidemic malaria in two semi-arid cities of India by using a process-based dynamical model supported by almost two decades of monthly surveillance of geophysical data. He found relative humidity to be a critical factor in the spread of urban malaria and potentially other vector-borne epidemics [323].

3.6.6 Synopsis

With all malaria models here presented we have witnessed an evolution in time, from the initial mathematical deterministic models [69, 188, 198, 232, 273, 317, 318, 383] based upon SEIRS compartments and the system of differential equations that supports them, to the more recently used computer-dependent stochastic [124, 247, 369] and agent-based malaria models [10, 25, 158, 214, 307, 326, 332, 346, 396].

A different type of malaria model currently in use has been based upon geospatial maps of disease prevalence, sometimes supported by satellite imaging [3, 138, 282, 379].

Models dedicated to disease dynamics in relation to the presence of gametocytemia in human hosts [49, 181] or to special characteristics of vector behavior [29, 36, 39, 110, 183, 249] are fundamental in our historical review of malaria modeling.

Finally, models including malaria immunity [26, 156, 236, 363], climate seasonality [87, 162, 167, 242, 256, 297, 359], and drug-induced resistance or mass drug administration [48, 187, 279, 309] were also taken into consideration in the construction of our computational and stochastic agent-based model.

In the last decade, malaria models have been used with far more consistency in malaria prevention by using stronger computer power, more detailed satellite imaging and new and promising mathematical approaches like neural network prediction models [368], machine learning models [331] and Bayesian weather models [35]. Although not directly related to the computational approach used in our stochastic model, some of these unclassifiable, conceptually interesting, and most

recent models were also listed for the sake of completeness [4, 35, 193, 331, 368].

Our malaria model [326] was created as a detailed, multi-variable, stochastic, agent-based model reproducing several realistic aspects of malaria transmission in a typical African village with high malaria incidence.

Chapter 4

Mathematical background

4.1 Model adaptation to Ross-Macdonald theory

In the current chapter, expected results from classical Ross-Macdonald parameters to be used in our model will be presented. Some of these parameters will be correlated with our own model parameters later described in chapter 5 – tables 5.1 and 5.2. We will follow the methodology for EIR and R_0 calculation, based upon the mathematical formalism of D.L. Smith,2004 and 2007, and Mandal,2011 [237, 343, 344]. This theory was previously described in section 3.4.

4.1.1 Malaria parameters

The duration of the gonotrophic cycle (mosquito time spent in feeding mating-oviposition cycle) will be later defined in tables 5.1 and 5.2, according to $\tau_s = 4$ days. The time spent out of oviposition in gonotrophic cycle (mosquito time spent in feeding) is defined as $f = \frac{1}{\tau_s} = 0.25$ days^{-1}.

The human feeding rate – $\boldsymbol{a}$ – is a crucial measure of vector activity in Ross-Macdonald classical theory. It represents the average number of daily bites from a single mosquito. Most of the early successes in malaria are the result of effective vector control strategies in regions where explosive *Anopheles* breeding takes place during the tropical wet season (India and Africa). In our model this critical parameter is obtained from equation 4.1.

$$a = \frac{1}{\tau_s} P_Q \; n_b \; (1-u) \; \sigma \approx 0.238 \tag{4.1}$$

where the average number of mosquito individual daily bites (daily bites per mosquito) is obtained from $n_b = 2$, the animal feeding factor (% of mosquito human bites in all human and animal bites) results from $P_Q = 0.9$, and the barrier protection factor (IRS/ITN/LLIN) is defined as $u = 0.25$ – see tables 5.1 and 5.2, in chapter 5.

The mosquito-to-human transmission efficiency – $\boldsymbol{b}$ – is equivalent to the probability of M-to-H disease transmission from an infectious mosquito [1], and is obtained from equation 4.2, where the probability of mosquito-to-human transmission from one mosquito bite is obtained from $k_h = 0.2$, and $\overline{\nu} = 0.1$ represents the average baseline human population immunity against malaria.

$$b = k_h(1 - \overline{\nu}) = 0.18 \tag{4.2}$$

We have used this theoretical definition of $\boldsymbol{b}$, where all infected mosquito bites were counted in the model simulation, whether during or after latency, and not only from strictly infectious mosquitoes (positive for the presence of sporozoites in salivary glands) as in the theoretical prediction. Thus, the theoretical predicted value was higher than the value obtained from the simulation result.

In the simulation there is an effect derived from the mosquito mortality resulting from ITN exposure ($q_m^{(itn)} = 0.5$). In the model algorithm, that value was included in the overall mosquito mortality, lowering the number of mosquitoes that survived after latency. Thus, in the simulation, $\boldsymbol{b}$ is lower than the predicted theoretical value, as it includes mosquito bites from infected mosquitoes still in latency (and therefore, not yet infectious).

Finally, the Human-to-Mosquito transmission efficiency – $\boldsymbol{c}$ – is defined in equation 4.4, assuming a constant value of $k_m = 0.2$, and $w_h = 0.453$ (as an example), that corresponds to 68 days of positive gametocytemia in a total of 150 days of disease duration.

The presence of gametocytemia is obtained from equation 4.3 and will influence the Human-to-Mosquito transmission efficiency ($\boldsymbol{c}$) in equation 4.4 .

$$w_h = \frac{\tau_g}{\tau_d} = \frac{\tau_g}{150} \tag{4.3}$$

$$c = k_m w_h \approx 0.091 \tag{4.4}$$

[1] quoting from DL Smith, 2004 [343] we know that "The lifetime transmission potential of a mosquito is defined as the expected number of new infections that would be generated by a newly emerged adult. Let $\boldsymbol{b}$ denote the transmission efficiency from an infectious mosquito to an uninfected, susceptible human; in other words, $\boldsymbol{b}$ is the probability that an uninfected human becomes infected after being bitten by an infectious mosquito."

4.1.2 Secondary indices

Several important indices can be derived from the traditional Ross-Macdonald parameters. The sporozoite rate (Z) represents the fraction of infectious mosquitoes (average of surviving infected mosquito prevalence past latency). It is essential for the calculus of another critical index, the entomological inoculation rate (EIR). Z can be obtained from the average value of infected mosquitoes M_i multiplied by the fraction of mosquitoes surviving past latency (life expectancy above 10 days) according to equation 4.5.

$$Z = M_i e^{-q_m \tau_{lm}} \tag{4.5}$$

Another important index is the Parasite Rate X representing the fraction of human hosts that are infected (but not necessarily infectious). It is also important to stress out that the fraction of infected mosquitoes (not necessarily infectious) is defined by Y – see equation 3.8 and table 3.3, in chapter 3.

Z may also be obtained from the alternative equation 4.6:

$$Z = \frac{ace^{-q_m \tau_{lm}}}{q_m + acX} = \frac{0.0586814}{0.1 + 0.02158768 \times X} \tag{4.6}$$

Assuming a static analysis with $c = 1$ (D.L.Smith,2004) [343] we may still obtain a slightly overestimated version for Z, as in equation 4.7:

$$Z = \frac{ae^{-q_m \tau_{lm}}}{q_m + aX} = \frac{0.08759184}{0.1 + 0.02158768 \times X} \tag{4.7}$$

4.2 SIR deterministic model

Based upon the original Kermack-McKendrick equations it is possible to create several simplified compartment models. They include agent transitions between different compartments. In common practice, the SIR model is most usually used. It is based in 3 categories (or compartments): Susceptible (previously unexposed to the pathogen), Infected (currently colonized by the pathogen) and Recovered agents (that have successfully cleared the infection). By ignoring population demographics (no birth, death or migration) the simplified SIR model is perfectly acceptable and quite effective in transitions S-I, I-R and R-S. The differential SIR equations, considering that recovered patients become totally immune, are given in equations 4.8, 4.9 and 4.10.

$$\frac{\partial S}{\partial t} = -\beta SI \tag{4.8}$$

$$\frac{\partial I}{\partial t} = \beta SI - \gamma I \tag{4.9}$$

$$\frac{\partial R}{\partial t} = \gamma I \tag{4.10}$$

However, if immunity is gradually lost in time, without exposure to the infectious agent, we will then have a different set of equations – see equations 4.11, 4.12 and 4.13:

$$\frac{\partial S}{\partial t} = -\beta SI + \delta R \tag{4.11}$$

$$\frac{\partial I}{\partial t} = \beta SI - \gamma I \tag{4.12}$$

$$\frac{\partial R}{\partial t} = \gamma I - \delta R \tag{4.13}$$

In these equations, δ represents the rate of immunity loss in the recovered (R) category. In the presented model, two types of agents are involved: human individuals and mosquitoes. In such a case we will have two groups of equations: one applied to humans (equations 4.14, 4.15 and 4.16), and the other to mosquitoes (equations 4.17, 4.18 and 4.19) .

Humans:

$$\frac{\partial S_h}{\partial t} = -\beta_h S_h I_m + \delta_h R_h \tag{4.14}$$

$$\frac{\partial I_h}{\partial t} = \beta_h S_h I_m - \gamma_h I_h \tag{4.15}$$

$$\frac{\partial R_h}{\partial t} = \gamma_h I_h - \delta_h R_h \tag{4.16}$$

Mosquitoes:

$$\frac{\partial S_m}{\partial t} = -\beta_m S_m I_h + \delta_m R_m \tag{4.17}$$

$$\frac{\partial I_m}{\partial t} = \beta_m S_m I_h - \gamma_m I_m \tag{4.18}$$

$$\frac{\partial R_m}{\partial t} = \gamma_m I_m - \delta_m R_m \tag{4.19}$$

If the initial fraction of susceptible (S_0) is less than $\frac{\gamma}{\beta}$, then the infection will die out as a result of $\frac{dI}{dt} < 0$. This is well accepted as the "threshold phenomenon", described by Kermack and McKendrick [185].

For the impact of different initial conditions in our model, please refer to Appendix C.

4.2.1 Simplified Kermack-McKendrick SIS mathematical model

As a support to the present stochastic model, a corresponding Kermack-McKendrick SEIRS model was deduced. Exposed compartment represented a small constant fraction of the infected compartment. However, we used a simplified SIS version of the deterministic model, removing the exposed and recovered compartments. As such, the exposed compartment was included in the infectious group. It was assumed that malaria immunity from infection does not confer fully protection to human individuals from new infection episodes. All cured patients were directly moved from the infectious to the susceptible compartment, removing the recovered compartment. With these assumptions, a simplified SI mathematical model was used – see equations 4.14 to 4.19.

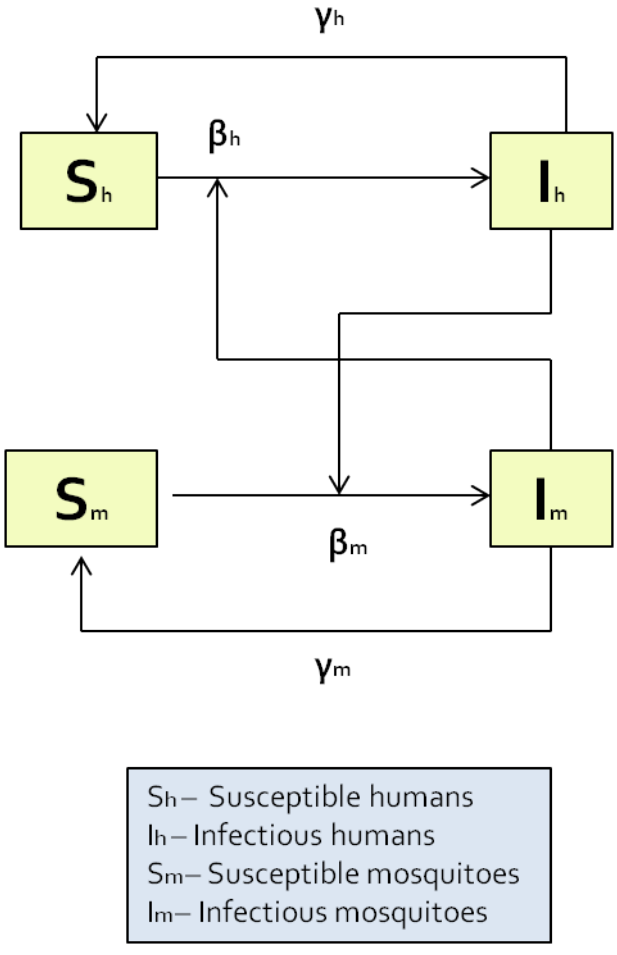

Figure 4.1: SIS deterministic model

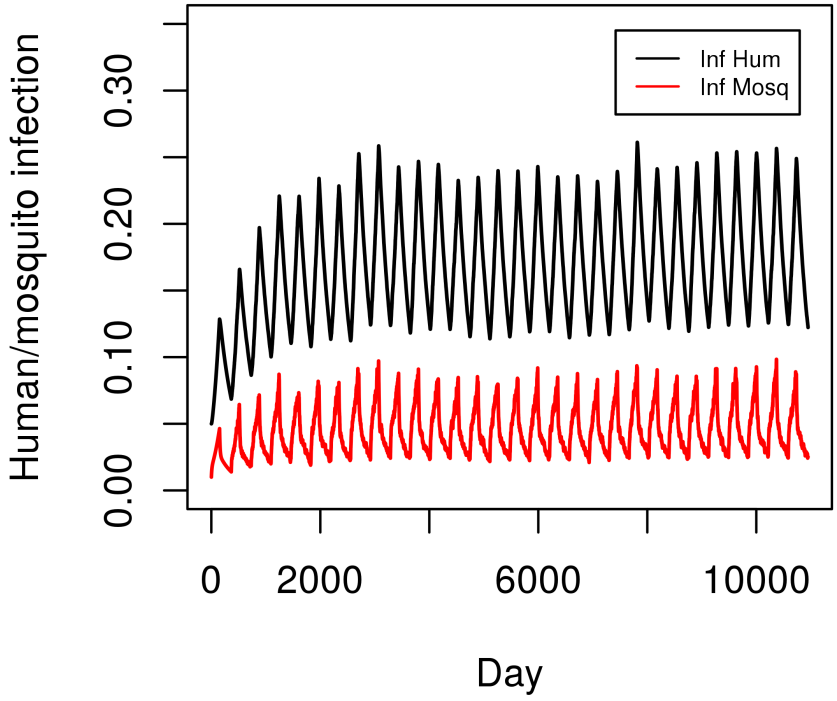

Figure 4.2: Malaria SIS deterministic model simulation resulting from equations 4.20 and 4.21 (with $\beta_h = 0.040$, $\beta_m = 0.040$, and $\gamma_h = 0.0067$, while γ_m depends on the mosquito mortality rate $q_m = 0.10$ days^{-1}, assumed constant in our model).

4.2.2 SIS model – differential equations

Humans:

$$\frac{\partial S_h}{\partial t} = -\beta_h S_h I_m + \gamma_h I_h \tag{4.20}$$

$$\frac{\partial I_h}{\partial t} = \beta_h S_h I_m - \gamma_h I_h \tag{4.21}$$

where oviposition length, ITN/IRS protection, skin protection against sporozoite mosquito-to-human transmission after mosquito bite, and drug prevention, are all included in β_h, and human immunity protection, drug therapy and human disease cure rate (q_h) are included in γ_h:

Mosquitoes:

$$\frac{\partial S_m}{\partial t} = -\beta_m S_m I_h + \gamma_m I_m \tag{4.22}$$

$$\frac{\partial I_m}{\partial t} = \beta_m S_m I_h - \gamma_m I_m \tag{4.23}$$

where oviposition length, ITN/IRS protection, skin protection against gametocyte human-to-mosquito transmission after mosquito bite, and drug prevention, are all included in β_h, and mosquito mortality rate (q_m) and drug therapy are included in γ_h – see equations 4.20 to 4.23, and figures 4.1 and 4.2.

4.2.3 Stability analysis of SIS differential equation model

Assuming differential equations in support of the SIS simplified model we obtain a set of equations – see equations 4.24 to 4.27:

$$s_h = \frac{S_h}{N_h} \tag{4.24}$$

$$s_m = \frac{S_m}{N_m} \tag{4.25}$$

$$i_h = \frac{I_h}{N_h} \tag{4.26}$$

$$i_m = \frac{I_m}{N_m} \tag{4.27}$$

We then have

$$\frac{S_h}{N_h} + \frac{I_h}{N_h} = 1 \tag{4.28}$$

and

$$s_m = 1 - i_m \tag{4.29}$$

$$s_h = 1 - i_h \tag{4.30}$$

Only two truly independent equations are needed for the purpose of stability analysis of critical equilibrium states – equations 4.31 and 4.32:

$$\frac{\partial i_h}{\partial t} = \beta_h i_m (1 - i_h) - \gamma_h i_h \tag{4.31}$$

$$\frac{\partial i_m}{\partial t} = \beta_m i_h (1 - i_m) - \gamma_m i_m \tag{4.32}$$

4.2.4 Critical points in a two-variable dynamical system

At the critical points it is assumed that:

$$\frac{\partial i_h}{\partial t} = 0 \tag{4.33}$$

$$\frac{\partial i_m}{\partial t} = 0 \tag{4.34}$$

From equations 4.35 and 4.36 :

$$f_h = \frac{\partial i_h}{\partial t} = \beta_h i_m (1 - i_h) - \gamma_h i_h \tag{4.35}$$

$$f_m = \frac{\partial i_m}{\partial t} = \beta_m i_h (1 - i_m) - \gamma_m i_m \tag{4.36}$$

we obtain equations 4.37 and 4.38 :

$$f_h^* = \beta_h i_m^* \left(1 - i_h^*\right) - \gamma_h i_h^* = 0 \tag{4.37}$$

$$f_m^* = \beta_m i_h^* \left(1 - i_m^*\right) - \gamma_m i_m^* = 0 \tag{4.38}$$

and equations 4.39 and 4.40 :

$$i_m^* = \frac{\gamma_h}{\beta_h} \left(\frac{i_h^*}{1 - i_h^*} \right) \tag{4.39}$$

$$i_h^* = \frac{\gamma_m}{\beta_m} \left(\frac{i_m^*}{1 - i_m^*} \right) \tag{4.40}$$

Differentiating f_h and f_m we obtain equations 4.41 to 4.44 :

$$\frac{\partial f_h}{\partial i_h} = -\beta_h i_m - \gamma_h \tag{4.41}$$

$$\frac{\partial f_h}{\partial i_m} = \beta_h \left(1 - i_h\right) \tag{4.42}$$

$$\frac{\partial f_m}{\partial i_h} = \beta_m \left(1 - i_m\right) \tag{4.43}$$

$$\frac{\partial f_m}{\partial i_m} = -\beta_m i_h - \gamma_m \tag{4.44}$$

Evaluating the Jacobian matrix at equilibrium points, we obtain the characteristic equation 4.45:

$$(\mathbf{J} - \lambda\mathbf{I}) = 0 \tag{4.45}$$

with the characteristic matrix 4.46:

$$\mathbf{J} = \begin{bmatrix} -\beta_h i_m - \gamma_h & \beta_h (1 - i_h) \\ \beta_m (1 - i_m) & -\beta_m i_h - \gamma_m \end{bmatrix} \tag{4.46}$$

Expanding the determinant we obtain equation 4.47:

$$\begin{bmatrix} -\beta_h i_m - \gamma_h - \lambda & \beta_h (1 - i_h) \\ \beta_m (1 - i_m) & -\beta_m i_h - \gamma_m - \lambda \end{bmatrix} = 0 \tag{4.47}$$

By using equations 4.48, 4.49 and 4.50:

$$\lambda^2 - Tr(\mathbf{J})\lambda + Det(\mathbf{J}) = 0 \tag{4.48}$$

$$\mathbf{B} = Tr(\mathbf{J}) = -\beta_h i_m - \gamma_h - \beta_m i_h - \gamma_m \tag{4.49}$$

Eigenvalues λ_1,λ_2	B	$B^2 - 4C$	**Type of point**	**Stability**
complex	> 0	< 0	spiral fixed point	unstable
complex	< 0	< 0	spiral fixed point	stable
complex	$= 0$	< 0	center	stable
real (opposite sign)	> 0	> 0	saddle	unstable
real (same sign, negative)	< 0	> 0	node	stable
real (same sign, positive)	> 0	> 0	node	unstable
real and identical (positive)	> 0	$= 0$	degenerate node	unstable
real and identical (negative)	< 0	$= 0$	degenerate node	stable

Table 4.1: Stability analysis of critical points

$$\mathbf{C} = Det(\mathbf{J}) = (\beta_h i_m + \gamma_h)(\beta_m i_h + \gamma_m) - \beta_h \beta_m (1 - i_h)(1 - i_m) \tag{4.50}$$

we obtain the following roots for the characteristic equation – see equations 4.51, 4.52 and 4.53:

$$\lambda^2 - \mathbf{B}\lambda + \mathbf{C} = 0 \tag{4.51}$$

$$\lambda_1 = \frac{\mathbf{B} + \sqrt{\mathbf{B}^2 - 4\mathbf{C}}}{2} \tag{4.52}$$

$$\lambda_2 = \frac{\mathbf{B} - \sqrt{\mathbf{B}^2 - 4\mathbf{C}}}{2} \tag{4.53}$$

From both roots, dynamical aspects of critical points may be determined – see table 4.1.

In our case, it is obvious from 4.49, that $\mathbf{B} < 0$. In this case, assuming that $B^2 - 4C \neq 0$, two options remain:

a) $B^2 - 4C > 0$ with a stable node.

b) $B^2 - 4C < 0$ with a stable spiral fixed point.

In both cases, the Human-Mosquito system reveals stability.

Part II

CONTRIBUTIONS

Chapter 5

An agent-based stochastic model of malaria transmission

5.1 Model background

Malaria is an infectious disease, caused by the *Plasmodium* parasite, which is still responsible for the death of nearly half a million individuals every year worldwide [286]. *P.falciparum (Pf)* is the most prevalent form of the malaria parasite in Africa, accounting for 99.7% of all estimated malaria cases in 2017 [286].

While some countries have had reasonable success in rolling back malaria through a well-planned preventive strategy, disease resurgence remains unpredictable. Different types of factors may contribute to such unpredictability. "Hidden" factors, such as the asymptomatic presence of gametocytes in human systemic circulation, which are the precursors of male and female gametes of the parasite, are essential in disease transmission. Migration of just a few asymptomatic human gametocyte carriers into African regions where the disease is controlled may act as a potential trigger in malaria outbreaks [217, 294]. The presence of gametocytes may be mitigated through the application of gametocidal drugs, such as primaquine or methylene blue.

Second, malaria transmission can be promoted due to the intrinsic heterogeneity in human demography and mosquito behavior [224]. For example, in a potential outbreak, human fatality rate may rise out of proportion due to the weaker immunity of local populations from reduced exposure to the parasite [364]. Or, in regions under anti-malaria massive drug administration, drug-resistant parasite strains can develop and consequently, through human migratory phenomena, they may be imported into areas of near eradication, locally strengthening malaria transmission [99, 217, 294].

Although the decisive role these factors can play on malaria transmission mech-

Tunable parameters	Symbol	Value
Probability of ivermectin treatment [14, 61, 196, 291, 357]	p_{iv}	0.00-0.10
Duration of positive gametocytemia [134, 181, 231]	τ_g	58-90 (days)
Fixed global parameters	**Symbol**	**Value**
Human individuals [70, 134, 237, 249]	H	2000
Female mosquitoes [70, 134, 237, 249]	M	4000
Duration of high transmission season [122, 123]	δ_s	150 (days)
Probability of a mosquito bite during the high season [122, 123]	p_{hs}	1.0
Probability of a mosquito bite during the low season [122, 123]	p_{ls}	0.50
Seasonality overall mosquito bite probability [122, 123]	s	0.7055
Fixed mosquito parameters	**Symbol**	**Value**
Duration of the gonotrophic reproductive cycle [110, 387]	τ_s	4 (days)
Fraction of mosquito feeding in human hosts (anthropophilic factor) [160, 190]	P_Q	0.90
Probability of daily mosquito mortality (general causes) [70, 110, 134, 181, 231, 387]	q_m	0.10
Average mosquito life expectancy [70, 110, 134, 181, 231, 387]	$\tau_m = \frac{1}{q_m}$	10 (days)
Average number of bites from one mosquito [134, 175, 181, 231, 237]	n_b	2 (per day)
Probability of mosquito infection after feeding on infectious human [20, 112, 181, 211, 229, 270, 271]	k_m	0.20
Maximum life time of one mosquito [231, 237]	τ_{max}	40 (days)
Minimum life time of one mosquito [231, 237]	τ_{min}	0 (days)
Time for parasite development inside the mosquito [70, 237]	τ_{lm}	10 (days)
Mosquito mortality after feeding on human host treated with ivermectin [14, 61, 196, 291]	q_{iv}	0.50
Initial infected mosquito rate [231, 237]	M_{i_0}	0.01

Table 5.1: Tunable parameters, and fixed global and mosquito parameters of the agent-based model for malaria spreading within two interacting communities of human individuals and mosquitos.

anisms is well established, the impact on malaria transmission resulting from the combined effect of different drug therapies in heterogeneous populations is still not fully understood.

The life cycle of *Pf* may be summarized as follows. The malaria vector, the mosquito, *Anopheles spp.*, usually lives, mates and feeds within a few miles distance from its birthplace [184]. To become infectious to humans, the mosquito needs to survive 10 or more days after feeding on a *Pf* gametocyte carrier. This time period is required to complete parasite sporogonic development inside the mosquito [110], after which, mosquito-to-human transmission becomes possible. Therefore, strict gametocidal drugs may not only block human-mosquito transmission, but can also have a strong impact on it. Other drug agents, such as ivermectin, have become a promising antimalarial interventions due to its anophelocide properties, preventing parasite's maturation inside the mosquito [61, 196, 283, 357]. It is known that mosquitoes, feeding on human hosts under ivermectin treatment, have a considerably lower life expectancy, with a large fraction of mosquito deaths occurring within 4 days after the blood meal [61, 196, 291].

Moreover, interventions including mass administration of ivermectin in prevention of several other African endemic parasites have resulted in a significant reduction of malaria incidence on those regions [14, 195, 250, 357].

To tackle the specific problem related with malaria transmission in a human community, several mathematical models have been proposed. Early models, such as those by Ross and Macdonald, were deterministic [231, 317], having nonetheless a significant relevance in malaria epidemiology [70, 71, 103, 197, 237, 273, 381] and being since then refined. More recent variants have been developed with the help of modern satellite imaging, precise weather and geographical information, computational agent-based modeling, and advanced statistics, such as hidden Markov processes, time-series analysis and big-data approaches [70, 100, 110, 115, 134, 180, 249, 324]. In particular, agent-based models strengthen the importance of malaria simulation for disease prevention [110, 137, 346]. Based on the classical susceptible-infected (SI) model by Kermack and McKendrick, stochastic modeling approaches were also proposed, with the aim of better implementing the uncertainties inherent to the disease dynamics [122].

Epidemiological field data of malaria transmission is commonly presented as human monthly or weekly disease incidence [24, 122], while mosquito infection rates are obtained from data collected through the use of mosquito trapping devices [39]. However, since both are important to understand the transmission dynamics, one should account for the combined effect of human and mosquito infection prevalence.

5.2 Model design

Malaria transmission is a complex infectious process involving two interacting compartments – human individuals and mosquitoes. Such a sophisticated coupled biological system is responsible for periodic oscillatory behavior of infection prevalence in stable dynamical systems in endemic equilibrium.

With the purpose of better defining the intrinsic dynamics involved in malaria transmission, we have created an agent-based computational stochastic model able to simulate the evolution in time of malaria incidence and human and mosquito infection prevalence.

Here, we introduce an agent-based model of *Pf* malaria endemic/epidemic behavior, incorporating both human-to-mosquito and mosquito-to-human transmission processes. The model assumes a typical isolated African village with limited access to drug therapy and is based on discrete Markov processes describing the succession of human-mosquito encounters, which are implemented through a Monte Carlo algorithm.

We parameterize some of the most important biological aspects of disease transmission, focusing mainly in the parameters describing the reduction of gametocytemia prevalence in the human host and the extension of ivermectin administration in the population. Several biological parameters were included in the model, while adjusted to a range of realistic values. Multiple time series simulations of disease prevalence were obtained and analyzed in terms of disease stability, proximity to phase transition and the possibility of disease elimination.

Special attention was devoted to the critical role of human gametocytemia in disease transmission and the possible intervention with gametocidal agents such as prima-quine and methylene blue. The assessment of therapeutic intervention with ivermectin – a less known but quite promising drug – was also included in the model dynamics. Tuning the parameter defining gametocytemia inside the human host, or the parameter controlling the fraction of the human population under ivermectin treatment, we uncover a phase transition between disease elimination and epidemic prevalence. In both cases, the transition is sensitive to minor changes in the parameters, and through mathematical analysis, we can predict critical values separating the two phases, disease elimination and endemic prevalence.

We start by describing the agent model and the main parameters driving *Pf* gametocytemia and human-mosquito infection dynamics. In chapter 7 (sections 7.1, 7.2 and 7.3) we present the model results while discussing its impact on possible clinical and medical strategies. In section 7.4 and chapter 12, we describe the model validation procedures by using data sets from several world regions.

We consider a system of $M = 4000$ mosquitoes and $H = 2000$ human individuals, where each population is divided into a number of healthy and infected indi-

viduals, represented by H_0 and M_0 and by H_i and M_i respectively: $H = H_0 + H_i$ and $M = M_0 + M_i$. Although, in reality, the density of mosquitoes is much higher, we model the number of mosquitoes as the effective fraction of the overall mosquito mass, imposing an average of two bites per day for each mosquito.

The flowchart describing the computer implementation of the agent model is sketched in figure 5.1 and is described as follows. The algorithm simulates a total time interval of 30 years and it starts by evaluating each individual agent (human host and mosquito), to ascertain if it became cured or not. In the case of human individuals, the recovered rate q_h is a fixed value, dependent on the average time τ_c it takes for one individual to be cured,

$$q_h = \frac{1}{\tau_c} \,. \tag{5.1}$$

In the case of mosquitoes, there is no explicit recovery rate. Every dead mosquito is replaced by a new healthy mosquito. As such, the mosquito recovery rate equals its global mortality rate q_m, to be determined by its baseline natural life expectancy, τ_m, the fraction p_{iv} of human hosts with whom the mosquito interacts that is under ivermectin treatment as well as the life expectancy $\tau_m^{(iv)}$ of a mosquito after exposure to ivermectin, and $q_m^{(itn)}$ which represents the mortality resulting from mosquito contact with ITN, LLIN and IRS barrier protection.

The parameter $q_m^{(itn)}$ will depend on the average time for mosquito death from barrier protection ($\tau_m^{(itn)}$), to be obtained from:

$$q_m^{(itn)} = \frac{1}{\tau_m^{(itn)}} \tag{5.2}$$

The average time for mosquito death from barrier protection ($\tau_m^{(itn)}$) relates to $q_m^{(itn)}$ in equation 5.2, and will be dependent on the effective human-mosquito contact rate before interaction with any form of barrier protection (r), the ITN/LLIN/IRS protection parameter (u), and the instant mosquito mortality directly resulting from barrier protection, represented later on as $q_m^{(itn)} = 0.5$ (after defining r in equation 5.5; it represents a 50 % probability of mosquito death upon contact with ITN/LLIN/IRS):

$$\tau_m^{(itn)} = \frac{1}{r \; u \; q_m^{(itn)}} \tag{5.3}$$

The final expression for the global mosquito mortality will then be obtained from:

$$q_m = (1 - p_{iv}) \left(\frac{1}{\tau_m} + \frac{1}{\tau_m^{(itn)}} \right) + p_{iv} \frac{1}{\tau_m^{(iv)}} \,. \tag{5.4}$$

The two rates, q_h and q_m, are not directly implemented in the agent model.

Fixed human parameters	Symbol	Value
Maximum time of human infection (includes time of parasite development) [50, 119, 231, 237]	τ_d	150 days
Minimum time of human infection (includes time of parasite development) [50, 119, 231, 237]	τ_0	25 days
Average human infectious period, cf. equation (5.1) [50, 119, 231, 237]	τ_c	87.5 days
Probability of human disease daily recovery [181, 231, 237]	$q_h = \frac{1}{\tau_c}$	0.011
Time for parasite development inside the human host [181, 237]	τ_{lh}	10 days
Human-to-mosquito gametocytemia transmission coefficient [134, 181, 231]	$w_h = \frac{\tau_g}{\tau_d}$	0.387-0.733
Probability of human infection after infectious mosquito bite [20, 112, 181, 211, 229, 270, 271]	k_h	0.20
Full human protection from acquired immunity [77, 106, 126, 231]	ν_{max}	0.30
Average initial human population acquired immunity [106, 126, 157, 158, 231]	ν_0	0.10
Time to immunity loss in case of absence of infection [77, 106, 126, 134, 158, 231, 270, 271]	τ_{ν_0}	2 years
Time to full immunity in case of persistent reinfection [77, 106, 126, 134, 158, 231, 270, 271]	τ_ν	5 years
Protection from LLIN/ITN/IRS barrier protection [181, 199, 271, 387]	u	0.25
Mosquito mortality due to LLIN/ITN/IRS protection [110, 181, 271, 387]	$q_m^{(itn)}$	0.50 days^{-1}
Fraction of children (age $<$ 5 years) in the population [106, 126, 134]	h_c	0.12
Gametocytemia probability in children $<$ 5 years of age [119, 134]	w_{h_c}	0.70
Human yearly mortality rate (global causes) [123, 237, 287]	μ_h	0.015
Human mortality rate from a single malaria episode [123, 237, 287]	μ_d	0.003
Time reset in elapsed infection time if human reinfection [231, 249, 345]	τ_ρ	0.50
Initial infected human rate [231, 237]	H_{i_0}	0.05

Table 5.2: Human parameters of the agent-based model for malaria spreading within two interacting communities of human individuals and mosquitos.

Instead, we impose a maximum time of human infection of $\tau_d = 150$ days and a minimum time of 25 days, uniformly distributed, yielding an average human infectious period of $\tau_c = 87.5$ days, a maximum mosquito lifetime of 40 days and a minimum lifetime of 0 days, uniformly distributed, yielding an average life expectancy of one mosquito $\tau_m = 10$ days, as well as a probability $q_{iv} = 0.5$ of one mosquito to die from feeding on a human host under ivermectin treatment. In case of an infectious mosquito bite in an infected human host, a human reinfection or super-infection occurs [1] and the disease time of that human individual is reset to half of the present disease time. Beyond 5 years of persistent human reinfections, the human host acquires maximum immunity and after 2 years with no infection events, the host loses immunity completely.

In case the mosquito succeeds in overcoming the barrier protection, the algorithm starts to ascertain if transmission will take place or not. This is done by computing the probability r for one mosquito and one human individual or another animal to contact through one bite, which is given by

$$r = \Big((1-s)p_{ls} + s\ p_{hs}\Big)\frac{P_Q}{\tau_s}\,, \tag{5.5}$$

where s is the fraction of time in the year with high disease transmission (percentage of time in rainy season), p_{ls} and p_{hs} represent the fractions of the year covered by the low and high seasons respectively, P_Q is the fraction of humans among all animals able to be bitten by one mosquito within the geographical region covered by the mosquito community, and τ_s is the duration of the gonotrophic reproductive cycle. In the agent model, we use values provided in previous studies, namely $p_{ls} = 0.5$, $p_{hs} = 1$, $P_Q = 0.9$ and $\tau_s = 4$ days. In our model a high value of human blood index was assumed, corresponding to a strong anthropophilic mosquito feeding, more typical of *An.gambiae* or *An.funestus*, and different from *An.arabiensis*. Moreover, inspired in Mozambique seasonality [122, 123], we consider 150 days for the duration of the high transmission season, i.e. $s = 150/365$. Notice that during transmission season, one considers a non-zero probability of transmission; in this way, disease transmission may occur during the whole year, although with higher intensity during the high-transmission season.

Upon updating the number of healthy human individuals and mosquitoes, the algorithm proceeds to generate one mosquito bite attempt. Here, one will use the probability $u = 0.25$ that long lasting insecticide-impregnated nets (LLIN), insecticide-impregnated nets (ITN) or indoor residual spraying (IRS) may protect human hosts from mosquito bites. This parameter u (previously introduced in equation 5.3), represents the degree of human population protection resulting from

[1] Persistent reinfection is defined as a new contact between an infected human host and an infected mosquito, during the period of active infection. In practice, since the average time of infection in one human is 87.5 days, one human host may reacquire a new malaria infection within three months after the initial infection episode, thus perpetuating disease transmission as well as immunity individual acquisition.

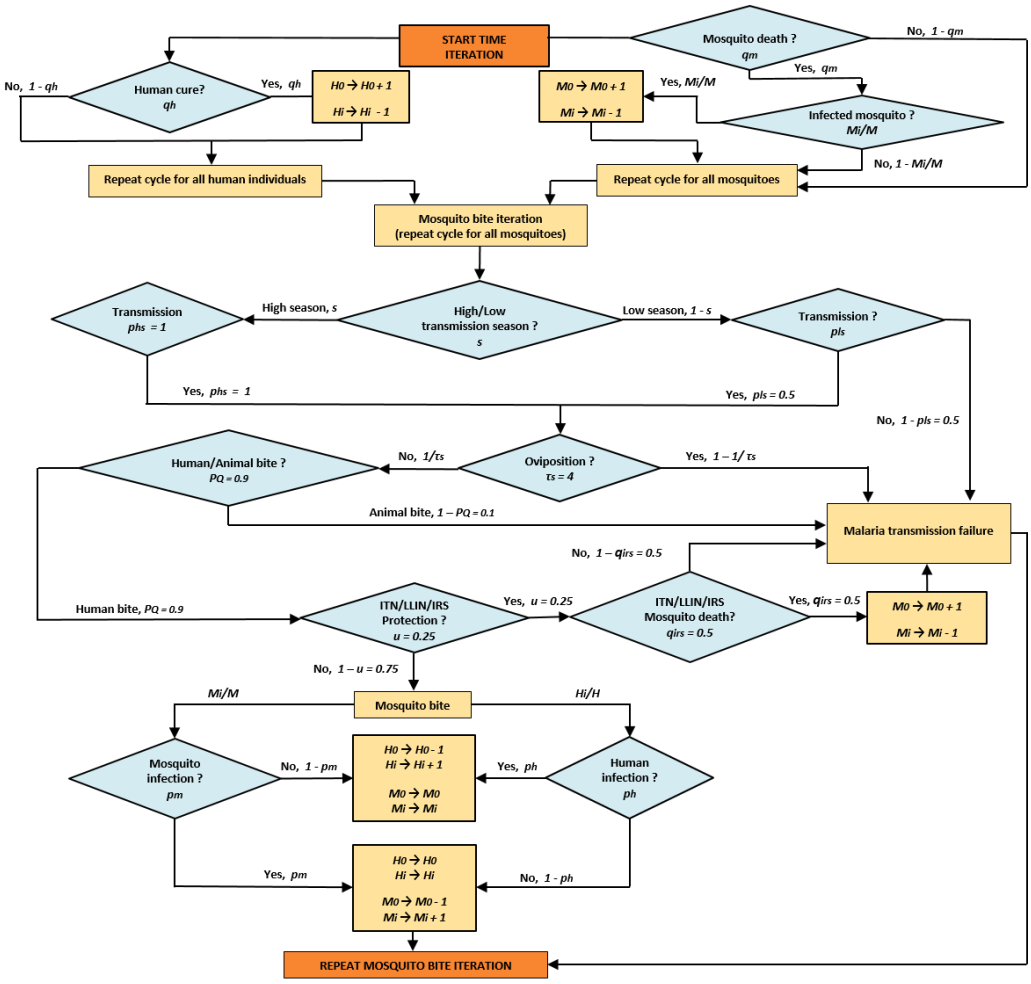

Figure 5.1: Flowchart of the agent-based model for human-mosquito interaction to reproduce scenarios of malaria spreading. Probabilities q_h and q_m are given in equations 5.1 and 5.4 respectively. The other probabilities are given in table 5.1. The probability for infecting a human or a mosquito depends on p_h and p_m, given in equations 5.7 and 5.8 respectively, and also on additional details concerning the dynamics of immunity acquisition of each human individual and the fraction of the human population composed by children (see text).

LLIN, ITN or IRS preventive measures, and simulates the probability of mosquito bite failure due to protective barrier. Likewise, the probability of mosquito bite success after surviving barrier protection assumes the form $(1 - u)$, and the final effective mosquito bite probability will result from the following expression (see figure 5.1):

$$R = r(1 - u) \tag{5.6}$$

In this case, we may use R as a the final simplified version of the global mosquito-human effective contact rate, after mosquito exposure to barrier protection preventive measures, as in equation 5.6.

Additionally, we include here the previously used barrier protection effect in killing the mosquito during the bite attempt – $q_m^{(itn)}$. In this model, the probability

of mosquito mortality induced by protective barriers was defined as $q_m^{(itn)} = 0.5$.

In the case one of the above factors succeeds, malaria transmission fails. In case all barriers fail, the algorithm finds one mosquito-human interaction through one bite. If the two interacting agents are infected or none of them is, both populations remain unchanged and the algorithm starts the next iteration. If only one individual (either human or mosquito) is infected, the algorithm ascertains if malaria transmission is successful.

The probability p_h for such single bite to effectively transmit the parasite from an infected mosquito to a healthy human depends on four factors, namely (i) the fraction M_i/M of infected mosquitoes, the probability k_h to get infected from one single mosquito bite [2] , the probability w_m that the mosquito is ready to transmit the parasite, and the probability ν of human individual immunity protection, yielding

$$p_h = \frac{M_i}{M} k_h w_m (1 - \nu) \tag{5.7}$$

and similarly, the probability for one single bite to effectively transmit the parasite from an infected human to a healthy mosquito is

$$p_m = \frac{H_i}{H} k_m w_h. \tag{5.8}$$

The probability w_m is obtained from the fraction of surviving mosquitoes past the period of parasite development, i.e.

$$w_m = e^{-q_m \tau_{lm}}\,, \tag{5.9}$$

where the parameter τ_{lm} is the period of parasite development in the mosquito. As for w_h it measures the fraction of time of the duration of positive gametocytemia from the maximal period of human infection,

$$w_h = \frac{\tau_g}{\tau_d}\,, \tag{5.10}$$

where τ_d is the maximal period of human infection and τ_g is the duration of positive gametocytemia.

In the agent model we fix $k_m = k_h = 0.2$, $\tau_{lm} = \tau_{lh} = 10$ days and $\tau_d = 150$ days – see tables 5.1 and 5.2.

Notice that the duration of positive gametocytemia is a tunable parameter used for varying w_h, which will be one of the important parameters in malaria transmission.

Since τ_d takes values between 58 and 90 days (see table 5.1), the probability

[2] The value of the probability to get infected from one single bite, either for humans as for mosquitoes, is given by the inverse of the number of infected mosquito bites necessary to infect one human or one mosquito and it estimated from controlled malaria infection, in laboratory settings [211, 229].

w_h varies between 0.387 and 0.733[3], a range that includes a phase transition from malaria eradication to malaria endemic behavior.

5.3 Human/mosquito infection equations

While assuming that H and M stand for the total of human individuals and mosquitoes, respectively, we will define the simplified fraction of infected humans h, as in $h = \frac{H_i}{H}$, where H_i represents the absolute count of infected humans.

Likewise, the fraction of infected mosquitoes m will be obtained from $m = \frac{M_i}{M}$ [4], where M_i stands for the absolute count of infected mosquitoes.

From that, it is clear that p_h and p_m will depend on both h and m.

By using simpler expressions for p_h and p_m we then may use:

$$\Phi_h = k_h w_m (1 - \nu) \tag{5.11}$$

and

$$\Phi_m = k_m w_h \tag{5.12}$$

resulting in:

$$p_h = m\Phi_h \tag{5.13}$$

and

$$p_m = h\Phi_m \tag{5.14}$$

From these equations, we have evidence of non-linearity in the coupled system $H - M$, as the human probability p_h depends both on human (k_h and ν) and mosquito (m and w_m) parameters.

Likewise, the mosquito probability p_m will depend both on mosquito (k_m) and human (h and w_h) parameters.

In this situation, non-linearity will only depend on variables h and m, as the the remaining parameters will be constant parameters, nested inside Φ_h and Φ_m.

From the simplified equations 5.13 and 5.14 we will then obtain the final probabilities of effective global human-mosquito disease transmission, P_h and P_m:

[3] Gametocyte detection threshold by light microscopy usually retrieves measurements between 5 and 10 gametocytes per μL. But with current molecular detection methods, that threshold may be as low as 0.1 per μL [181]. It is assumed that during the period of human disease, gametocytemia will occur according to a random stochastic process, with a predefined probability of human-to-mosquito transmission at every mosquito bite in the range of admissible values [181, 201].

[4] Not to be mistaken with mosquito density, originally described as m by Smith(2004) [343], but defined here as $\Delta_m = \frac{M}{H}$

$$P_h = R\ p_h \tag{5.15}$$

equivalent to:

$$P_h = R\ m\Phi_h \tag{5.16}$$

and

$$P_m = R\ p_m \tag{5.17}$$

equivalent to:

$$P_m = R\ h\Phi_m \tag{5.18}$$

From this, it is clear that functions P_m and P_h will also both depend on m and h, finally having:

$$P_h = P_h(h, m) \tag{5.19}$$

and

$$P_m = P_m(h, m) \tag{5.20}$$

This does not happen to q_h and q_m, which depend only on h and m, respectively, as we already know from equations 5.1 and 5.4:

5.4 Model rationale

It is assumed that a higher gametocyte density will result in higher human-to-mosquito transmission efficiency. Consequently, the concept of gametocytemia reduction is considered equivalent to the effects of treatment with gametocidal agents such as primaquine or methylene blue.

The agent model implements three additional aspects that are not usually taken into account in simulation of malaria transmission dynamics.

First, in the present model we simulate the use of ivermectin in a fraction of the human population (p_{iv}), assuming a global ivermectin-related mosquito fatality rate (q_{iv}) of 0.5. Ivermectin inhibits sporogony in the mosquito with evidence of a partial blocking effect on human-to-mosquito transmission. We used this mechanism for defining ivermectin treatment biodynamics in our computational model.

Second, to consider the effect of acquired immunity to malaria infection. Acquired immunity ν against malaria changes according to the history of infection

and the genetic traits of a particular human individual. The value of ν can increase in the case of repeated reinfections, or decrease, in case of no infection during a certain time. The time to acquire protective immunity after every infection episode is typically longer than that of the immunity loss. We consider that if the human host does not contact with the parasite during two years, he/she loses the acquired immunity against the parasite, while maximal immunity is gained after 5 years with persistent reinfection. Moreover, maximum protective immunity is different from complete protective immunity, as a human cannot be more than 30% immune, $\nu_{max} = 0.3$. Acquired immunity is parameterized through ν, while being incorporated in parameter p_h – see equation 5.7 – which is indicated in one of the boxes in the flowchart of figure 5.1.

Third, the extreme vulnerability to malaria infection of children under 5 years of age is a well-known critical factor in the disease morbidity and mortality. We therefore consider additional effects for the subgroup of children in the human population. A simplified age effect is considered: the fraction of children under 5 years of age represents 12% of the total human population, and for those children immunity is considered to be absent, with a higher gametocytemia prevalence during disease duration, namely during 70% of the time [50, 77, 106, 126, 134, 158].

Malaria unrelated human mortality is also considered in our model. However, its magnitude is assumed to be low, namely 0.015 cases per year, i.e. it has negligible effects in disease transmission. The system is always initialized with a fraction of infected mosquitoes of 1%, a fraction of infected humans of 5% and an initial acquired immunity of $\nu_0 = 0.1$ for every human individual[5].

Our model has its limitations. Some variables can be modelled with distributions which are derived from standard mathematical derivations, such as the time for human disease recovering, treated here as a stochastic variable exponentially distributed. Other random variables, however, not necessarily related with exponentially decaying processes were taken as uniformly random variables, e.g. variables related to mosquito biting behavior, human disease duration or gametocytemia occurrence, since no other forms of statistical distribution have been firmly established. Notice that the risk of using other distributions such as Gaussian, Poisson or Gamma distribution, can lead to scenarios and transition features different from those reported below, but such assumptions need further investigations and are out of the scope of the present dissertation.

Another simplification is the parameterization of ivermectin. It is known that ivermectin is an anti-mosquito drug with a fast-decaying rate: mosquitoes taking a blood meal containing this drug have an enhanced mortality rate that is directly related to the ivermectin concentration present in the blood.

This fact is incorporated in the model as a simplified procedure, defining mosquito mortality probability from ivermectin exposure as equal to 50% ($q_{iv} =$

[5]Except children under 5 years of age, who are assumed to have an acquired immunity of 0.0

0.5), similarly to other studies in this topic [196, 291].

5.5 Model assumptions

The chosen values of each model parameter are given in tables 5.1 and 5.2, and the algorithm keeps track of all attributes for each agent, human or mosquito, in a particular age, time since infection, and immunity status. Notice that only two parameters are modulated, namely the fraction p_{iv} of the human population subjected to ivermectin treatment and the effectiveness of gametocidal drugs, measured as the number τ_g of days of positive gametocytemia. All other parameters are kept at constant values and their values were chosen according to previous studies.

5.6 Model master equation

Stochastic processes that are continuous in time and space represent the mathematical background of diffusion processes. These processes result from probabilistic Markov transitions with a continuous sample path and infinitesimal and finite mean and variance. The present model uses a Markov transition process supporting the computational algorithm. It will be presented with further detail in Appendix A.

In our case, the presence of a diffusion process in malaria transmission will lead to the concept of transition probability density function which will become a solution of the forward and backward Kolgomorov differential equations from Markov chain theory, leading to the Fokker-Planck equation (FPE).

Combining human and mosquito terms, we obtain a two-dimensional (2D) Fokker-Planck equation.

We know that in general:

For

$$dX_t = \mu(X_t)dt + \Psi(X_t)dW_t \tag{5.21}$$

and by using vector notation we may obtain

$$\frac{\partial p(x,t)}{\partial t} = -\nabla \cdot [\mu(x)p(x,t)] + \frac{1}{2}\nabla \cdot (\nabla \cdot [\sum(x)p(x,t)]) \tag{5.22}$$

where $p(h,m,t) = [u(h,m,t), v(h,m,t)]$, $x = (h,m)$, $\mu(x) = \mu(h,m)$, $\mu_1 = h$, $\mu_2 = m$, and $\Psi(X_t) = \Psi(h,m)$ for the diffusion matrix coefficient.

Thus, we will have for the general 2D Fokker-Planck equation (FPE):

$$\frac{\partial p(x,t)}{\partial t} = -\sum_{i=1}^{2} \frac{\partial \mu_i p(x,t)}{\partial x_i} + \frac{1}{2}\sum_{i=1}^{2}\sum_{j=1}^{2} \frac{\partial^2}{\partial x_i \partial x_j}\{\sum_{ij}(x)p(x,t)\} \tag{5.23}$$

where $\sum_{ij}(x) = \Psi(x)\Psi(x)^T$

We may then use Itô formulation in a simpler form of the differential stochastic equation:

$$dX = A(h, m, t)\, dt + B(h, m, t)\, dW \tag{5.24}$$

And for the human-mosquito system:

$$\begin{aligned} \frac{\partial p(h,m,t)}{\partial t} &= -\frac{\partial A_h\, p(h,m,t)}{\partial h} - \frac{\partial A_m\, p(h,m,t)}{\partial m} \\ +\frac{1}{2}(\frac{\partial^2 B_{hh}\, p(h,m,t)}{\partial h^2} &+ 2\frac{\partial^2 B_{hm}\, p(h,m,t)}{\partial h \partial m} + \frac{\partial^2 B_{mm}\, p(h,m,t)}{\partial m^2}) \end{aligned} \tag{5.25}$$

Here, $A(h, m, t)$ stands for the 2D drift coefficient, and $B(h, m, t)$ stands for the 2×2 diffusion matrix coefficient.

In order to derive the 2D Fokker-Planck equation we must consider using a two-dimensional Taylor approximation. For the one- and two-dimensional Taylor approximations to the Fokker Planck equation, please consider checking them in Appendix B.

Chapter 6

Vector control

6.1 Mosquito density and malaria transmission

Since the early transmission models defined by Sir Ronald Ross in the first years of the XX century, it has been recognized that the epidemiology and control of malaria is inextricably linked to the ecology of *Anopheles* mosquito vectors [189]. In his early work, Ross clearly demonstrated the critical role of mosquito density in malaria transmission [317].

George Macdonald [231] reformulated the pioneering model of Ross [317] and identified mosquito vector longevity as the single most important variable in the force of transmission [167]. Since Macdonald important work (1957) it is well-established that small variations in mosquito density may result in substantial changes in human infection prevalence [231].

The effective implementation of several mosquito-control measures achieved reasonable success in South America during the 1910s. With the addition of effective mosquito larvicide agents (such as Paris Green spraying or widespread use of certain fish species like *Gambusia* with preferential feeding on *Anopheles* larvae) in ponds or other water depots, a significant suppression of the total mosquito burden was obtained, leading to a widespread reduction in malaria cases [351]. All these health policies were directed at reducing the total number of mosquitoes in heavy populated areas. The role of private foundations such as the Rockefeller foundation was particularly decisive in establishing better mosquito-control strategies to be implemented worldwide [351]. This anti-malaria strategy gained strength during the 1920s, with massive reduction of malaria cases in Italy and Sardinia, and later on during the 1930s in Bulgaria and India [351]. These strategies were responsible for effective malaria control in more temperate areas in America and Europe where malaria had been endemic for centuries.

Ross' equation for the basic reproductive number deduction, was supported on a well-established malaria SIR model, underscoring the importance played by mosquito density in disease resurgence events.

The ratio of mosquitoes to human individuals is defined here as the index Δ_m[1], to be included in all equations involving the basic reproductive number R_0 – see equations 3.16, 3.17, and 3.18. In the initial formulation of Ross-Macdonald theory, mosquito density assumed a decisive role in powering disease transmission, as shown in the definition of R_0 in Ross initial equation. The use of widespread insecticide-treated nets (ITN), long lasting insecticide-treated nets (LLIN) and insecticide indoor residual spraying (IRS) improved the global strategy of malaria elimination and reinforced the importance of effective vector control in disease prevention.

Disease elimination is more difficult in larger population aggregates. *Anopheles* flight is usually limited to a short distance range of less than 4 Km within larval breeding sites radius [184]. Thus, higher human population densities and shorter distances between housing in urban centers may facilitate an effective human contact with mosquitoes, resulting in higher disease transmission (pseudo-mass action).

Stochasticity also depends on human population size. This effect becomes more pronounced in simulations with smaller populations[224]. From research in smallpox eradication [17] we know that high disease transmission rates are higher in urban aggregations than in isolated villages. This form of human spatial heterogeneity may have a stronger impact in diseases where the parasite transmission cycle involves an intermediate vector, as it is the case in malaria transmission.

The research on chemicals led to the discovery of a new form of insecticide, dichlorodiphenyltrichloroethane (DDT), by a Swiss firm, Geigy, and its first effective use took place during the 1940s in North Africa (Algeria), and a few years later in the region of Rome, Italy, by aerial spraying of mosquito breeding sites. As a consequence of the selective use of this chemical substance, in water ponds, swamps and other high risk *Anopheles* breeding sites, as well as inside the interior of houses and barns in the region of Fiumicino, the number of mosquitoes fell drastically to zero, followed by the widespread reduction of malaria incidence in Rome. After World War II, new more selective insecticide chemicals were developed with success. The eradication of malaria in the island of Sardinia by the massive spraying with DDT was a clear demonstration that vector control would have to play a crucial role in any strategy concerning the reduction of disease transmission.

However, this early success suffered a temporary setback a few years later with the demonstration of the first cases of DDT resistance.

In the present research, mosquito density was assumed to be an important variable for analysis in the setting of dedicated simulations of our computational model.

Malaria is the result of a two-agents coupled disease transmission system, revealing heterogeneous cyclic seasonal behavior depending on the world region.

[1] representing mosquito density in the form of $\Delta_m = \frac{N_m}{N_h}$, based upon D.L.Smith,2004 [343]

During the XX century, vector control and larval source reduction assumed an important part in disease prevention. As a consequence of effective management of larval breeding sites (usually aquatic habitats) malaria transmission was significantly reduced in several world regions [189, 389].

Larval source management consists of habitat interventions aimed at the modification of permanent changes in water reservoirs and landscape as well as the manipulation of water-related activities such as adequate water drainage, biological control of the *Anopheles* mosquito, and the widespread use of larvicidal strategies.

An integrated vector control program including anopheline source suppression, environmental management with modified agricultural practice reducing potential larval breeding sites, and simple housing modifications resulting in effective human barrier protection could reduce transmission intensity from more than 300 to less than 1 infectious bite per person per year. Thus, decisive reductions of EIR could possibly result from proper environmental management in Africa [189].

Mosquito burden is directly related to rainfall intensity during the rainy season, as well as to the resulting increase in vegetation, facilitating the potential occurrence of new *Anopheles* larval breeding sites [74, 100, 207].

Environment and climate are among the most important factors in malaria transmission, particularly the factors of temperature, rain precipitation, humidity, vegetation, stationary water pools and human-vector interaction, as they affect the habitat and vector breeding sites. [394]

Although ivermectin may increase mosquito mortality, this effect is of a small magnitude and will not be able to significantly influence global mosquito density. However, the fact that ivermectin is more toxic to *Anopheles* in the first few days after mosquito feeding, amplifies its effectiveness as it kills mosquitoes in the early incubation stage, when the mosquito has not yet become infectious. It is also possible to define a significant linear correlation between mosquito density and ivermectin effectiveness [61, 196]. After being exposed to ivermectin, mosquitoes tend to die well before sporozoites can be detected in the salivary glands, and therefore becoming incapable of transmitting the disease to other human individuals. Such a fact explains the importance of ivermectin in malaria transmission. This action, in combination with the gametocidal effect induced by gametocidal agents such as primaquine could possibly improve disease prevention alongside other effective preventive measures. In the setting of a higher value of mosquito density, this protection will eventually become more significant.

6.2 Methods

With the purpose of determining the relevance of the size of mosquito burden in malaria transmission within a stable human population while assessing the merits of partial ivermectin use prevention, a small modification of the present model was

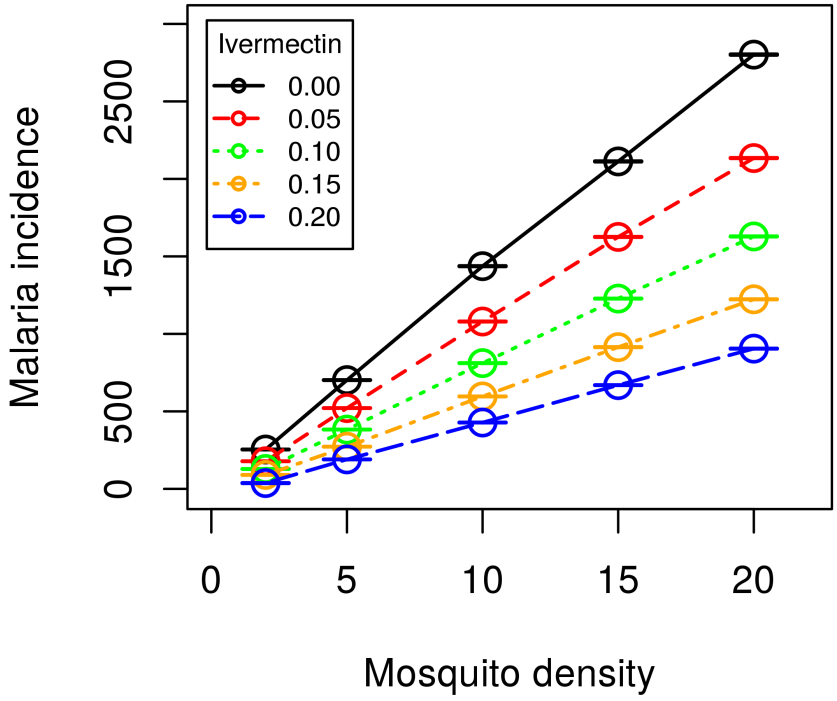

Figure 6.1: Average malaria incidence (number of diagnosed cases per 100 inhabitants, during a full year) at different levels of mosquito density (ranging from $\Delta_m = 2$ to $\Delta_m = 20$), and ivermectin prevention (from $p_{iv} = 0.00$ to $p_{iv} = 0.20$), in a full heterogeneity scenario. This scenario was defined in the form of $\frac{1}{\theta} = 4.0$, within a high human-to-mosquito transmission efficiency scenario ($w_h = 0.800$). Model simulations were repeated 10 times in all settings.

put in place, introducing specific initial parameters.

Multiple simulations were implemented by using different levels of mosquito density while evaluating the influence of ivermectin in malaria incidence. A constant value of $n_H = 200$ was defined for human inhabitants – a value roughly equivalent to the population of a small African village –, and different stages of mosquito density (Δ_m) were used in the range between two (equivalent to $n_M = 400$ mosquitoes) and twenty ($n_M = 4000$ mosquitoes). Ivermectin prevention was simulated assuming that a constant and randomly chosen fraction of the human population would be under that treatment.

6.3 Results and discussion

As expected from Ross-Macdonald theory, mosquito density was directly correlated with malaria incidence. However, the use of ivermectin in the human

population was quite effective in the reduction of malaria transmission at all levels of mosquito density, as can be seen in figure 6.1. Higher population coverage with ivermectin preventive treatment implied lower levels of malaria incidence in all mosquito density settings. These simulations were obtained in a full heterogeneity scenario with higher disease transmission and point out the use of ivermectin as a potential complement to other effective forms of malaria prevention.

In figure 6.1, as expected, we have found a linear dependence of malaria incidence on mosquito density, in the best Ross-Macdonald tradition. We have used a high heterogeneity ($\frac{1}{\theta} = 4.0$) and high human-to-mosquito transmission efficiency scenario ($w_h = 0.800$) in these model simulations in order to amplify baseline malaria incidence. Ivermectin prevention was shown to be quite effective in all different scenarios of mosquito density, in a proportional relation with the fraction of human population covered.

Chapter 7

Gametocytemia and ivermectin in disease dynamics

In the following sections, we will address separately the effect of gametocidal drugs and of ivermectin, choosing adequate values in the creation of three possible disease transmission scenarios:

- Scenario A: Stable endemic ($H_i > 0$ and $M_i > 0$).
- Scenario B: Disease eradication ($H_i = 0$ and $M_i = 0$).
- Scenario C: Critical phase transition between the endemic stage and disease eradication, where some of the simulations evolve to disease eradication, while others to endemic stability.

7.1 Assessing the effect of gametocytemia in phase transition

We have defined the effect of ivermectin as null when $p_{iv} = 0$, with illustrative examples for each scenario. In Scenario A we consider $\tau_g = 68$ days of gametocytemia, yielding a value of $w_h = 68/150 = 0.453$, while in Scenario B we consider $\tau_g = 60$ days of gametocytemia, i.e. $w_h = 0.400$. Finally, in Scenario C, we will have $\tau_g = 64$ days of gametocytemia, corresponding to $w_h = 0.427$. Results are shown in figure 7.1.

Figure 7.1 a) illustrates Scenario A, where both human and mosquito communities evolve in periodic cycles, reflecting the seasonal character of malaria incidence, with a significant variation between low and high transmission seasons. Here, none of the infected communities will evolve towards eradication. In figure 7.1 b) one observes the opposite: both communities will eventually be cured with no further cases of infection. In the plotted example disease eradication occurs at the tenth seasonal cycle (10 years to extinction).

In Scenario A, the result was $10\% \pm 5\%$ of infected humans and $1.3\% \pm 0.6\%$

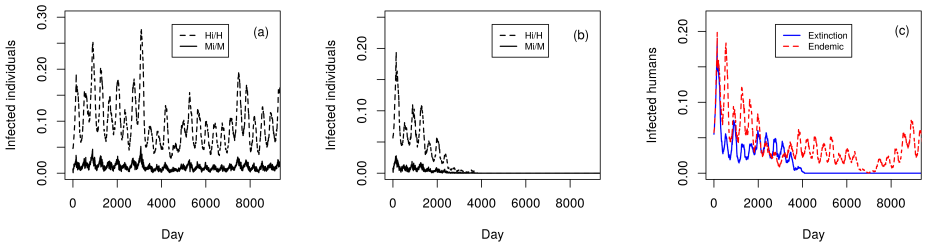

Figure 7.1: Illustration of the three scenarios tuned by gametocytemia parameter w_h: **(a)** Scenario A, disease epidemic prevalence ($w_h = 0.453$), **(b)** Scenario B, disease eradication ($w_h = 0.400$), and **(c)** Scenario C, transition between human infection ($\frac{H_i}{H}$) endemic prevalence and eradication ($w_h = 0.427$). In all cases $p_{iv} = 0$.

of infected mosquitoes, while in Scenario B, a smaller value was obtained with $1.4\% \pm 3\%$ of infected humans and $0.2\% \pm 0.4\%$ of infected mosquitoes.

In figure 7.1 c) we observe the intermediate situation, between endemic prevalence and eradication. Two different outcomes occur at identical gametocytemia levels: in red dashed lines we plot the evolution of human community in a simulation where the disease persists for more than 30 years and in blue solid lines, one observes the resulting community evolution towards a state of eradication, after around 11 years. This intermediate scenario occurs for $w_h \sim 0.42$. In the eradication case of Scenario C we obtained $1.4\% \pm 2.5\%$ of infected humans and $0.2\% \pm 0.3\%$ of infected mosquitoes, while in the endemic case, we witness a higher value of $4.2\% \pm 3.1\%$ of infected humans and $0.5\% \pm 0.4\%$ of infected mosquitoes.

Three important features must be addressed at this point. First, the time span needed for eradication at the transition value ($w_h \sim 0.427$) is considerably larger than for values below the transition. This is a common feature in critical phase transitions [350]. Second, the different outcomes from Scenarios A, B and C result from small changes in the total time duration of gametocytemia: the differences between scenarios A, B and C are not greater than 4 days, which represents gametocytemia differences of $\pm 2.7\%$. Consequently, small changes in gametocytemia status may result in significant changes on the level of epidemic outcome, a feature that shows the importance of gametocytemia in controlling malaria transmission. Third, disease persistence depends on very small values of mosquito infection prevalence (in Scenario C with epidemic outcome the average mosquito infection prevalence is $0.5\% \pm 0.4\%$, a value not much higher than the one in Scenario C with disease elimination, $0.2\% \pm 0.3\%$).

To better uncover the transition from endemic prevalence to eradication due to gametocytemia control, we generate 20 different realizations for a set of different w_h values within a range covering all three scenarios. Results are shown in figure 7.2 a). As one sees, while for Scenarios A and B, all realizations converged to the same state, prevalence or eradication respectively, for Scenario C one fraction of the

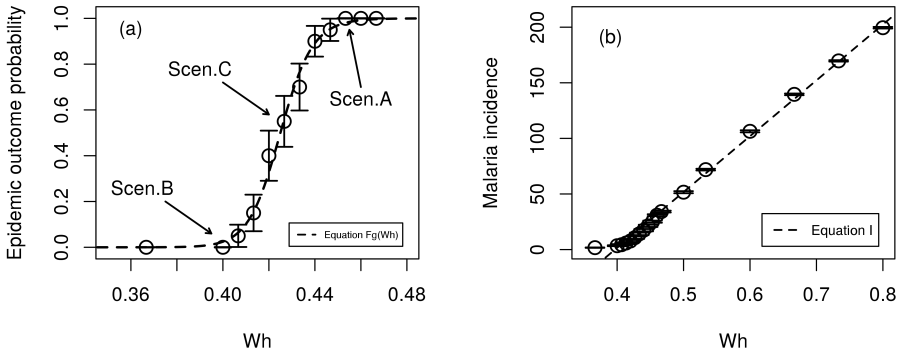

Figure 7.2: **(a)** Probability of epidemic outcome with changing gametocytemia duration at phase transition. The three scenarios illustrated in figure 7.1 are indicated with arrows. The function in equation 7.1 is plotted with dashed line. The fraction of infected humans is averaged over 20 realizations for each value of w_h. **(b)** Annual malaria incidence per 100 habitants and its correlation with the positive gametocytemia w_h. Correlations were computed by averaging 20 realizations for each value of w_h.

realizations ended in endemic prevalence while the rest converged to eradication. Therefore, we argue that there is a critical value of gametocytemia days that guarantees full recovery of the community.

A quantitative approach for estimating this transition gametocytemia value is to approximate the transition curve in figure 7.2 a) by a step function of the form

$$F_g(w_h) = \frac{1}{1 + \left(\frac{w_h^{(t)}}{w_h}\right)^{\alpha_g}}, \tag{7.1}$$

yielding an estimate for the transition gametocytemia value ($w_h^{(t)}$) in the range $0.420 \leq w_h^{(t)} \leq 0.427$, and for the exponent $\alpha_g = 60$. The functional form in equation (7.1), is a kind of Fermi-function, which, in this case, enables to parameterize the transition from eradication to prevalence with two single parameters, a critical value $w_h^{(t)}$ for which $F_g(w_h^{(t)}) = 1/2$, and a transition "length" α_g which controls how sensitive the transition is with respect to variations of gametocytemia around the critical value.

In real situations of malaria epidemics, there are several difficulties in properly determining the annual malaria incidence[1], which is an adequate measure for evaluating the gravity and extension of the epidemic. Through simulations, the annual malaria incidence can be easily calculated while it will also be possible to investigate how it relates with other variables. As shown in figure 7.2 b), we observe a clear linear relation between the average malaria incidence I and the gameto-

[1]Annual malaria incidence represents the instant expected average of malaria incidence per 100 inhabitants during one full year, if transmission conditions remain unchanged.

cytemia parameter w_h. In the plot, for each value of positive gametocytemia w_h we obtained the average of the annual malaria incidence over 20 different simulations. A linear regression of the simulation results yields

$$I = -199 + 502\ w_h\,, \tag{7.2}$$

with a coefficient of determination of $r^2 = 0.989$ and a p-value of $P < 0.001$. Notice that for $w_h < 199/502 \lesssim w_h^{(t)}$, close to the obtained transition value of gametocytemia, the annual incidence is negative, meaning that the system converges to a scenario of disease eradication. Only for values above the transition value one may find a positive malaria incidence.

7.2 The role of ivermectin in transmission prevention

To investigate the role of ivermectin we fix the value for the time of positive gametocytemia, since it appears to be independent from human-to-mosquito transmission efficiency. We choose a stable epidemic background with 90 days of gametocytemia, corresponding to a higher value of human-to-mosquito transmission efficiency – $w_h = 0.6$. To investigate the mosquito mortality due to ivermectin, we first focus on three different values of the fraction of human population under ivermectin treatment, namely $p_{iv} = 0, 0.05, 0.1$. In this case, we have used 10 simulations in every setting, with a reasonably small variance in malaria incidence results. Each of these three values illustrates one of three different regimes, respectively (i) absence of ivermectin treatment, (ii) weak ivermectin administration and (iii) moderate ivermectin administration.

Our results show that, while in the absence of ivermectin administration the mosquito mortality during the parasite development phase (mosquito latency) is 79.6%, that mortality increases to 84.4% for $p_{iv} = 0.05$, and to 88.1% in the case of $p_{iv} = 0.1$. Furthermore, mosquito mortality directly related to ivermectin was 15.2% in the case of $p_{iv} = 0.05$ (ivermectin prevention in 5% of the human population) and 26.3% for $p_{iv} = 0.1$ (ivermectin prevention in 10% of the human population). In the case of bite failure due to barrier protection, the mosquito mortality was considered relevant, and set at $q_{irs} = 0.5$[2].

We have also observed that, in the case of ivermectin random usage in 5% of the population ($p_{iv} = 0.05$), disease eradication may occur roughly 20 years later. But if ivermectin is administered to 10% of the human population ($p_{iv} = 0.1$), a disease eradication outcome may be possible much earlier (less than 4 years). Moreover, the administration of ivermectin induces a reduction in the frequency

[2]There is no precise knowledge concerning the probability for the mosquito to die due to ITN,IRS or LLIN barriers. We assumed a value of 0.5, which together with a coverage of ITN of 25%, results in a global mortality due to ITN barriers of $0.25 \times 0.5 = 0.125$. This value is probably below the real value, since in some African countries the LLIN/ITN/IRS coverage may be as high as 80%.

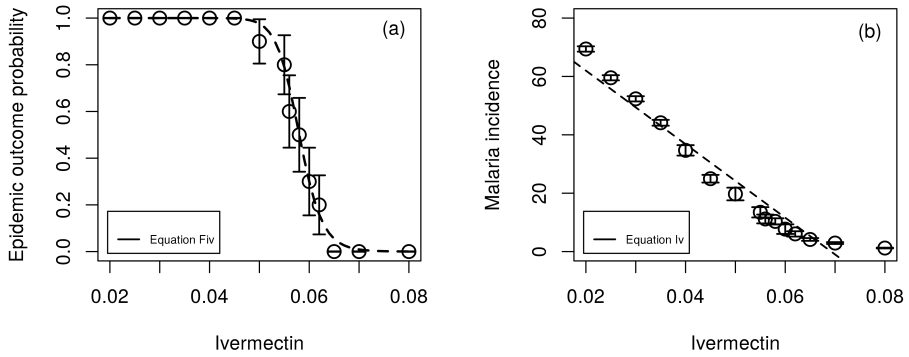

Figure 7.3: **(a)** Probability of epidemic outcome with probability of ivermectin treatment at phase transition, and approximate fit function. The function in equation (7.3) is plotted with dashed line. Here we run 10 trials for each value of p_{iv} in the range $0.02 \leq p_{iv} \leq 0.08$. **(b)** Annual malaria incidence per 100 habitants and correlation with ivermectin treatment probability (p_{iv}). The function in equation (7.4) is plotted with dashed line. Positive gametocytemia is fixed at $w_h = 0.6$.

of healthy mosquito bites in an infected human (not shown).

Varying the fraction p_{iv} also uncovers a continuous phase transition from prevalence to eradication. See figure 7.3 a). Differently from the transition by gametocytemia variation, here the phase transition is only visible for high gametocytemia levels, typically $w_h = 0.6$ or larger. A possible explanation for this is the strong inhibitory effect of ivermectin on human-to-mosquito disease transmission.

In figure 7.3 a), a phase transition from epidemic prevalence to disease eradication can be observed. Here, the critical value of the human fraction with ivermectin is approximately $p_{iv} = 0.058$. Higher p_{iv} values induce faster disease eradication scenarios. Similarly to equation 7.1, the step function can be modelled through the function

$$F_{iv}(p_{iv}) = 1 - \frac{1}{1 + \left(\frac{p_{iv}^{(t)}}{p_{iv}}\right)^{\alpha_{iv}}} . \tag{7.3}$$

The fitting parameters here are $p_{iv}^{(t)} = 0.058$ and $\alpha_{iv} = 25$.

Comparison of figures 7.2 a) and 7.3 a), indicates that a more intensive use of ivermectin in the human population is qualitatively equivalent to a shorter gametocytemia time needed to maintain disease prevalence. The outcome of massive administration of ivermectin in a fraction of the human population reveals strong correlation with an effective reduction on the duration of positive gametocytemia. Consequently, both the probability of ivermectin treatment p_{iv} and annual malaria incidence are anticorrelated, as shown in figures 7.3 b). Here, we run 10 simulations for each value of p_{iv} ranging from 0.020 to the value 0.058, which corresponds to the obtained critical value at the phase transition in figure 7.3 a). The linear

regression in figure 7.3 b) yields

$$I_v = 87 - 1260\ p_{iv} \tag{7.4}$$

with a Pearson correlation of $r^2 = 0.930$ and a p-value of $P < 0.001$. Similarly to what we have discussed above for equation 7.2, here, we observe a positive malaria incidence only for values of ivermectin prevention in the range of $p_{iv} \lesssim 87/1260 \lesssim p_{iv}^{(t)}$.

7.3 Combined use of gametocidal agents and ivermectin: a copula approach for predicting optimal administration intensities

As shown in the previous section 7.2, in a stable epidemic status, with 90 days of positive gametocytemia ($w_h = 0.60$), after the use of ivermectin in 5% of the human population ($p_{iv} = 0.05$), there is a reduction in the fraction of infected human hosts – compare figure 7.4 a) with figure 7.4 b). However, this reduction is not robust enough to achieve complete disease eradication. Similarly, after a reduction in the days of positive gametocytemia, namely from 90 to 70 days (from $w_h = 0.6$ to $w_h = 0.467$), with no ivermectin treatment, there is a weakening in disease transmission, although also not robust enough to achieve disease eradication (see figure 7.4 c). But, by combining both effects, namely with a gametocytemia reduction from 90 to 70 days and ivermectin preventive treatment in 5% of the population, disease eradication is rapidly attained – see figure 7.4 d).

Apparently, the combination of these separate strategies may lead to a stronger action in suppressing malaria infection in the human population. Our quantitative analysis however provides a framework for deriving an estimation of how strong these strategies should be, when used in combination, in order to achieve full disease elimination. Assuming both factors to be independent from each other, a first order approximation to estimate the number of infected humans would be $\hat{H} = F_g(w_h)F_{iv}(p_{iv})H$, and disease elimination would be the region in parameter space (w_h, p_{iv}) satisfying

$$F_g(w_h)F_{iv}(p_{iv}) < \frac{1}{H}\,. \tag{7.5}$$

The fact that the time period of the parasite development in the mosquito is generally longer than 10 days (see table 5.1), may explain the reason for the effectiveness of ivermectin in preventive campaigns directed to other endemic parasites in Africa. However, this effect may not be only related to an overall reduction in the number of mosquitoes, but also to a selective interference in the process of parasite development towards sporozoite inside the mosquito, and a preferential killing of infected mosquitoes. Therefore, both factors are correlated, and the

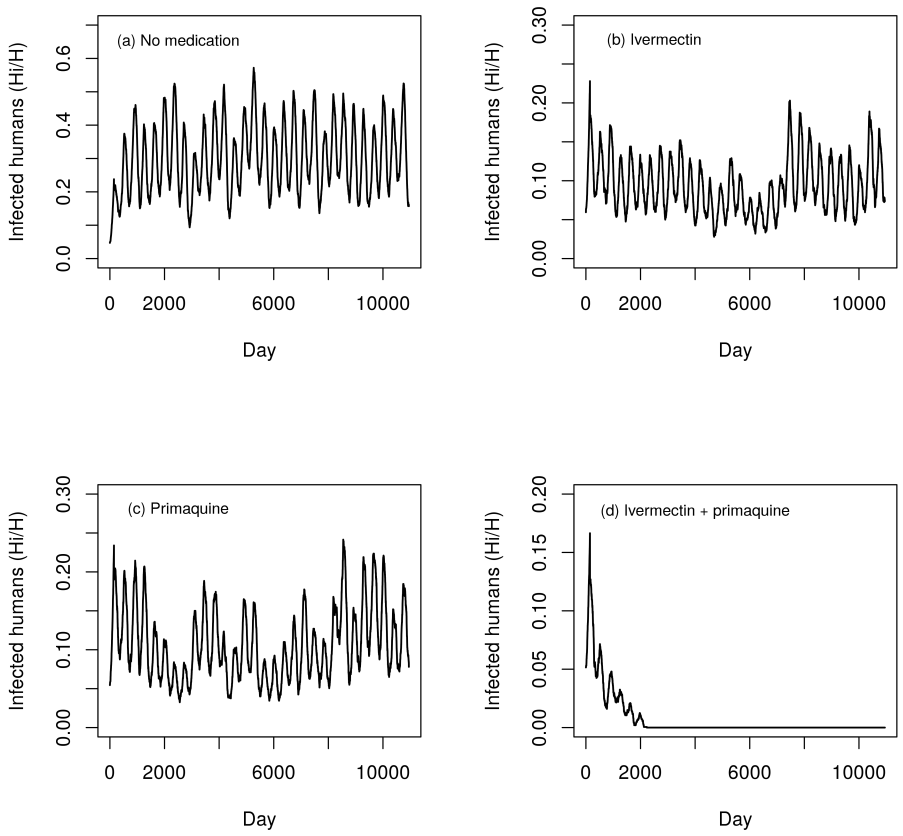

Figure 7.4: **(a)** The evolution of the number of infected humans in an epidemic status with $w_h = 0.6$ with $p_{iv} = 0$. **(b)** Application of ivermectin treatment with $p_{iv} = 0.05$ to the situation shown in (a), keeping positive gametocytemia at $w_h = 0.6$. **(c)** Application of gametocytemia reduction with primaquine from $w_h = 0.6$ to $w_h = 0.467$, without ivermectin ($p_{iv} = 0$). **(d)** Combined gametocytemia reduction with primaquine and ivermectin treatment in epidemic status, with $w_h = 0.467$ with $p_{iv} = 0.05$.

prediction presented above is biased towards a worst-case scenario.

7.4 Model validation and consistency tests: comparison with malaria transmission results in Chimoio

In this section, we intend to validate the agent model simulations against empirical data, namely time series at weekly intervals collected at Chimoio region in Mozambique [122]. In this African region, malaria is endemic revealing a trend, which increases during the four to five months of the wet season (high transmission season) and decreases during the rest of the year (low transmission season). The empirical time series includes a total of 490 561 malaria cases in a population of $H = 324816$ human individuals, recorded from January 1st, 2006, to December 31st, 2014. During these 9 years, weekly malaria incidence I_w was analyzed in

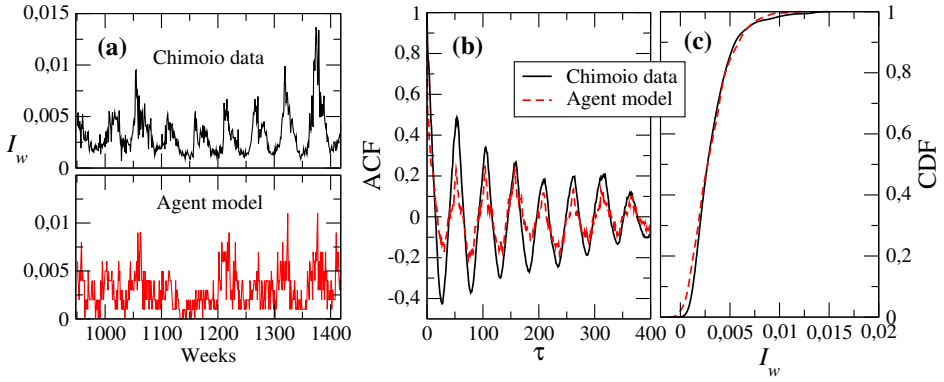

Figure 7.5: **(a)** Time series of weekly malaria incidence I_w, comparing empirical data from Ref. [122] (top) against data from one realization of the agent model (bottom), where 64 days of gametocytemia was used ($w_h = 0.427$). **(b)** Auto-correlation function of the weekly malaria incidence from the empirical data (solid line), compared with the auto-correlation from the agent model simulation. **(c)** Cumulative density functions (CDF) of the malaria incidence for both empirical and simulation sets of data. In all cases $p_{iv} = 0$.

both the empirical set of data and in simulated data generated by the agent model. Figure 7.5 a) shows both time series during 9 years (468 weeks).

From the total time of 30 years covered by the simulation, we discarded the first 14 weeks to weaken the influence of the initial conditions and to synchronize seasonality with Mozambique empirical data. Considering total simulation time, we have used three partial 468 weeks' time series (from weeks 15 to 482, 483 to 950 and 951 to 1418) which were very similar in global behavior (data not shown). For presentation purposes we have used the last one of these 3 time-series (from week 951 to 1418), revealing good correlation between our model and Mozambique empirical data, as in the horizontal axis label of figure 7.5 a). The reason for excluding so many years of data was related to the necessity of using a time gap identical to the one of Mozambique empirical series (468 weeks). Since we scaled both populations to a maximum number of individuals, we neglect here demographic effects, which stand as a good approximation, as long as the human population density does not exceed the radius of activity of individual mosquitoes[3].

The simulation uses 64 days of positive gametocytemia ($w_h = 0.427$), which relates to a value of human-to-mosquito disease transmission efficiency close to that found at phase transition – see figure 7.2 a). The present validation procedure only relates to the transmission model, not including therapeutic interventions with ivermectin. The model validation for ivermectin treatment will be discussed later in section 12.5. A more detailed model validation procedure will be presented in chapter 12.

[3]In realistic conditions, the mosquito population size is usually an unknown parameter, with spatial heterogeneous distribution according to topography, vegetation and water conditions for larval breeding. Consequently, it can only be guessed as an approximation, resulting from data obtained with the help of mosquito traps and larval water count in water reservoirs, or indirectly from counting mosquito bites.

In figure 7.5 b) we plot the auto-correlation functions of the empirical data from Chimoio, Mozambique, and of the model simulation results. The autocorrelation is defined as

$$\gamma(\tau) = \frac{\langle (I_w(t+\tau) - \bar{I}_w)(I_w(t) - \bar{I}_w) \rangle}{\sigma^2_{I_w}}, \tag{7.6}$$

where $\bar{I}_w$ and $\sigma^2_{I_w}$ are respectively the mean and variance of the incidence series and $\langle \cdot \rangle$ represents the average over time t. Apart from a deviation of the local extremes, the periodicity of the simulated scenario matches rather well with the real seasonal oscillation period (~ 1 year). To quantify the similarity between real data and agent model simulation results, we have computed the usual performance metrics, namely the mean absolute error (MAE)

$$\text{MAE} = \frac{1}{n} \sum_{t=1}^{n} \left| \hat{I}_w(t) - I_w(t) \right| \tag{7.7}$$

with $\hat{I}_w(t)$ and $I_w(t)$ representing the simulated and real incidence values in $n = 468$ (weeks), the mean absolute percentage error (MAPE)

$$\text{MAPE} = \frac{1}{n} \sum_{t=1}^{n} \left| \frac{\hat{I}_w(t) - I_w(t)}{I_w(t)} \right| \tag{7.8}$$

and the root mean square error

$$RMSE = \left[\frac{1}{n} \sum_{t=1}^{n} (\hat{I}_w(t) - I_w(t))^2 \right]^{1/2}. \tag{7.9}$$

The computation yields MAE= 0.00152, MAPE= 0.558 and RMSE= 9.54×10^{-5}. The simulation is within fluctuations of 50% of real incidence values.

We also compare the distribution of simulated and real incidence values, as plotted in figure 7.5 c): the cumulative distributions match rather well, with a small Kolmogorov-Smirnov score (0.22) having a p-value smaller than 0.001.

Importantly, in all simulations, mosquito and human infections are strongly related, showing a similar oscillatory pattern. Moreover, only a small fraction of the mosquito population survived beyond the parasite development inside the mosquito (10 days), which supports the presence of strong correlation between endemic prevalence status in humans and mosquitoes in all endemic scenarios [249].

Our model assumes rules based on classical and neoclassical assumptions, including several parameters from the classical Ross-MacDonald model [231, 317, 343].

The two main quantities in this classical model are the annual entomological inoculation rate EIR, which is defined as the number of bites per year on a human

Description	Theory	Model
Basic reproductive number (R_0)	**1.619**	**0.973**
Annual entom. inoculation rate (EIR)	**0.961**	**0.965**
Fraction of infected mosquitoes (Δ_m)	2	2
Human feeding rate (a)	0.238	0.239
Sporozoite rate (Z)	—	0.006
Force of infection (λ)	0.47	0.284
Mosquito-to-Human transmission (b)	0.18	0.108
Human-to-Mosquito transmission (c)	0.091	0.090
Human recovery rate (q_h)	0.011	0.011
Mosquito daily mortality (q_m)	0.1	0.1

Table 7.1: Classical Ross parameters from theory and model simulation for endemic scenario A close to phase transition, i.e. with 68 days of gametocytemia ($w_h = 0.453$). The two main quantities, reproductive number R_0 and the annual entomological inoculation rate EIR are within the classical theoretical values.

host from an infectious mosquito, and the reproductive number R_0, which represents the number of infected humans generated from one single infectious mosquito in a population of susceptible and non-immune individuals.

For evaluation of our model, we have compared the values obtained in model simulations with the expected theoretical ones, which are given in references [317, 343]. Results are given in table 7.1. For estimating the annual entomological inoculation rate, we have used the definition

$$EIR = 365\,\Delta_m\,a\,Z, \tag{7.10}$$

where Δ_m represents the mosquito density (number of mosquitoes per human individual, $\Delta_m = \frac{N_m}{N_h}$), $\boldsymbol{a}$ is the human feeding rate given by (see table 5.1 and section 5.2), $a = (P_Q n_b(1-u)\sigma)/\tau_s$, and Z is the sporozoite rate (fraction of infectious mosquitoes). In estimating the reproductive number, we have used the Ross definition [317]

$$R_0 = \frac{\Delta_m\ a^2 bc}{q_h q_m}\,, \tag{7.11}$$

where $\boldsymbol{b}$ is the mosquito-to-human transmission efficiency, $b = k_h(1-\bar{\nu})$, $\boldsymbol{c}$ is the human-to-mosquito transmission efficiency, $c = k_m w_h$, and q_h and q_m are given by equations 5.1 and 5.4, respectively. As indicated in table 7.1, the expected theoretical values of both these quantities are well reproduced by the model simulations. When compared with Ross theory, the lower value of R_0 found in the model simulations, is related to the fact that the $\boldsymbol{b}$ value in the simulation only takes into account bites from infectious mosquitoes.

7.5 Towards improved medical strategies

Here, we have introduced an agent model for assessing the effect of gametocytemia and drug administration in epidemiological scenarios of malaria. Our model was calibrated by considering various aspects of the disease dynamics and supported by field data. We uncover the existence of a phase transition between an absorption state with disease elimination, and an endemic/epidemic regime.

Because several parameters from our model were based on the Mozambique epidemic environment, validation of the model implementation took place by the comparison of model simulation results with field collected data series for malaria incidence in the typical seasonal endemic malaria region of Chimoio, Mozambique. Importantly, this field data time-series covered a long time period of malaria incidence, namely 9 years [122]. Although the parameter values in table 5.1 are case-dependent, they are within the range of typical values described in the literature.

In complex models, phase transition stands as a critical concept in stochastic simulation. Its precise definition is useful to identify the occurrence of a state transition between disease elimination and endemic stability, which can be used for better preventive planning. At critical equilibrium points, malaria transmission dynamics was defined taking into account the predicted rational use of anti-malarial strategies in the near future.

Special attention was given to the role of gametocytemia in human-to-mosquito transmission. All our model simulations assumed the duration of positive gametocytemia to be in the range of 0.4 to 0.8 of total infection time. With a small variation in gametocytemia prevalence it was possible to define all tested transition phases. These small changes in gametocytemia were considered as a model for effective gametocidal treatment, such as the administration of primaquine or methylene blue [117, 148, 176, 181, 201, 221, 355]. Transition phases were clearly defined, promoting a better understanding of the disease dynamics, as well as of the points of sudden stochastic transition from epidemic prevalence to disease elimination.

In the present model, we also analyzed preventive intervention with ivermectin, a well-known agent with capability of interfering with human-to-mosquito transmission. An intervention with ivermectin may be highly selective in targeting recently infected mosquitoes, by killing them before the complete development of the parasite could take place. This aspect bears no relation to gametocytemia prevalence [61, 196, 291, 357]. Apparently, the role of mosquito mortality from ivermectin in disease transmission does not significantly interfere with the effect of gametocidal drug intervention.

However, notice that, in this model, the action of primaquine is based on

its general properties as a gametocidal agent. For simplicity, we have assumed gametocytemia duration reduction in *P.falciparum* as the main drug effect, neglecting its action on other forms of *Plasmodium*. Methylene blue can be used as an alternative potential gametocidal agent, but our model intends to catch general spreading regimes and therefore, we have not focused on any other major drug characteristics.

Moreover, while the results may be encouraging, showing that ivermectin coverage as low as 5-10% can have a significant impact, the next step in research should be in the direction of considering drug pharmacokinetic properties, which could afterwards provide insight on how this prolonged coverage could take place with the current drug formulations.

The detailed biochemical mechanisms that trigger gametocytogenesis in *Plasmodium* are not well known.

However, this process may be influenced by host immunity and anti-malaria therapy [181, 201]. For human-to-mosquito transmission to be effective, male and female stage V gametocytes must be present in the blood during mosquito feeding. Once inside the mosquito midgut, gametocytes will mature to gametes promoting fertilization and maturation to zygote stage, ookinete, oocyst, and finally to the sporozoite stage, the infectious form of the parasite present in mosquito salivary glands. Common gametocidal drug agents (primaquine, artemisinin and methylene blue [41, 117, 148, 176, 221, 300, 355]) usually fail to act in the early stages of gametocyte maturation. But their inhibitory action on gametocytes in stage V may be very effective in reducing the time of gametocytemia duration [201].

Vector control, by itself, is not enough to eradicate disease transmission. Long standing cyclic positive gametocytemia in a few human individuals may perpetuate transmission for a long time, and more attention should be directed towards human disease reservoirs as possible hot-spots for chronic mosquito infection. Preventing mosquito infection from these hot-spot human reservoirs by reducing the time of positive gametocytemia with the help of a selective mosquito-killing-after-bite prevention strategy with ivermectin, may turn out to be more effective in the fight against malaria.

It is known that drug resistance may not only be the result of mass drug administration, but also a consequence of new mutations. The combined intervention of gametocidal agents and ivermectin can also be useful in reducing pressure in areas where drug resistance is becoming a major problem as a result of new mutations in the background of mass drug administration [93, 105]. Our results seem to indicate that such a theoretical possibility may deserve serious consideration in future malaria prevention campaigns.

Dynamical aspects of human therapy with drug agents such as artemisinin or quinine (with specific intervention in disease status and gametocytemia probability), population heterogeneity and human migration were not included in the

present analysis, but will be dealt separately in chapters 8 and 9. Model simulations assumed the existence of a typical and isolated African village with limited drug availability.

Our computational model allowed us to test the combined use of different preventive interventions with antimalarial agents like ivermectin (killing mosquitoes during parasite's development) or primaquine (gametocytemia reduction) that could significantly influence disease outcome, and therefore contribute to a better knowledge of disease transmission dynamics in different endemic scenarios. With the present model, it was possible to recreate simulations for regions with different disease status and with specific seasonality conditions, and to anticipate future events as a result of selective interventions in certain human subgroups, in all simulations.

From the main findings of this agent-based model, a set of valuable insights are possible. First, in endemic locations, small differences in gametocytemia prevalence in human populations, obtained from preventive intervention in a small fraction of the population with gametocidal drugs [117, 148, 176, 221, 300, 355], may result in very different outcomes, despite the relative stability of classical human-to-mosquito infectiousness parameter $\boldsymbol{c}$.

Second, the demonstrated mosquito-killing properties of ivermectin in the first days after a mosquito feed, may potentiate the effect of gametocidal agents with drastic interference in human-to-mosquito transmission efficiency. This preventive action may also benefit from its combined use with LLIN/ITN/IRS.

Third, our model indicates that with a combined ivermectin and primaquine scissor-like intervention, malaria elimination may be possible in small African villages after a short period of time.

Chapter 8

Heterogeneity in malaria transmission

8.1 Heterogeneity background

The presence of heterogeneity in malaria may influence disease transmission in multiple ways [5]. It may concern to different human and vector densities, to several forms of diversity in human age distribution, cultural, social, and genetic population backgrounds, as well as to a variable host-acquired immunity from previous infections. It may also relate to differences in climate conditions, land topography, local altitude, housing structure, human migration and the unequal use of preventive and treatment measures [235, 261]. Indeed, heterogeneous mosquito biting has been reported as a possible factor for enhancing malaria transmission: human hosts who are bitten most will later on infect a larger number of mosquitoes [344], and will be more likely to behave simultaneously as super-receivers as well as super-spreaders [83, 367]. Moreover, not all human beings are equally attractive to mosquitoes. Multiple factors seem to influence mosquito feeding routine. During day-time, the mosquito vision apparatus seems to be the most effective mosquito guidance system. However, at night-time, olfactory cues may play a more important role in mosquito host-seeking behavior. The affinity of the disease vector *Anopheles* is related to the presence of specific odors in the human host, namely different chemical stimulus called kairormones such as the CO_2 percentual fraction in human exhaled air, or the presence of some aliphatic carboxylic acids in the human skin. Human respiratory CO_2 exhaling may be the single most important factor conditioning mosquito feeding preferences [261]. Also, different *Anopheles* subspecies may display different levels of anthropophilic mosquito feeding habits [9, 98, 233, 276]. Furthermore, infectious hosts may display higher mosquito bite attractiveness as a result of the presence of high levels of gametocytemia [84, 97, 206].

However, till the 90's, most of the models of malaria dynamics assumed ho-

mogeneous transmission, while a precise and objective quantitative approach to realistic scenarios was still lacking. In 1997, Woolhouse defined a specific model for the presence of heterogeneity in malaria transmission, naming it the rule 20/80 [386]. This rule assumes that 80% of all mosquito bites will occur in 20% of the human population, being inspired in Wilfredo Pareto's original work on the distribution of world wealth [295, 296]. This smaller super-spreader subgroup [83] concentrates the effect of repeated biting leading to a proportional increase in the risk of disease transmission to human hosts. Also, it stands as a privileged reservoir with higher probability of mosquito reinfection because of higher gametocytemia levels. In identical endemic conditions, this factor alone may increase several-fold the probability of disease transmission [386]. We will refer to this Pareto-Woolhouse (PW) rule as the PW-rule. For a review comparing the major malaria transmission models, see reference [346].

Spatial variation in malaria incidence and exposure to infected mosquitoes in Tanzania has been related to the presence of clusters of higher malaria incidence among infants [43]. These were defined as hot-spots of malaria transmission, with higher mosquito bite exposure. In this case, while a small group of children (around 10%) experienced several malaria episodes, there was no clinical evidence of malaria symptoms in two thirds of all the children. A stronger human exposure to *Anopheles* mosquito may also result from spatial factors such as a closer distance to vector breeding sites, prolonged outdoor human activities, and human genetics responsible for odor production more attractive to mosquitoes [45]. In some African villages, the existence of hot-spots supports continuing transmission during the dry season, while acting as a source of infection for the rest of the village during the wet season [45]. Within a few districts of Bangladesh with stable hot-spots, malaria incidence distribution was remarkably similar to the heterogeneity 20/80 rule described by Woolhouse [274, 386].

In the present chapter we provide quantitative evidence that malaria spreading effectiveness is strongly sensitive to heterogeneous affinity. Section 8.2 describes the agent-based malaria model used in simulating different scenarios of malaria spreading, introducing a parameter for measuring heterogeneous affinity. In sections 8.3, 8.4 and 8.5, we investigate the possible transitions from elimination to disease persistence, focusing on the role of three parameters: heterogeneous affinity, level of drug administration, i.e. the fraction of human population at risk undertaking ivermectin treatment, and human-to-mosquito (H-to-M) transmission efficiency. In particular, in section 8.5.3 we address the issue of mosquito survival. Later on, in chapter 12, section 12.5, we will use a model validation procedure evaluating the impact of ivermectin human treatment in mosquito survival, when compared to similar results obtained from previous research [61, 342]. In section 8.6, we discuss further which measurable quantities can in real situations better predict malaria incidence. We look at how heterogeneity interacts with gametocytemia in boosting H-to-M disease transmission in section 8.7. Section 8.8

concludes the chapter.

8.2 Modeling heterogeneity in malaria transmission

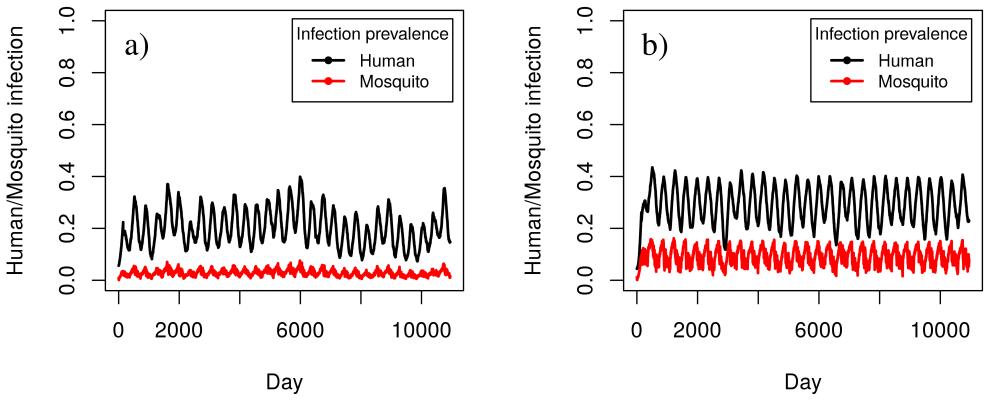

Figure 8.1: Human and mosquito infection prevalence **(a)** in a scenario of homogeneous affinity, namely 20% of the human individuals receive 20% of mosquitos bites, and **(b)** in a heterogeneous scenario when 20% of the human individuals receive 80% of mosquitos bites. In both cases intermediate human-to-mosquito transmission efficiency is considered, $w_h = 0.500$.

Comparing two typical scenarios, one in which the number of bites are distributed uniformly among the human population - see figure 8.1 a) -, and another where PW-rule 20/80 is applied – see figure 8.1 b) -, the model predicts that heterogeneity clearly promotes malaria persistence in both mosquito and human populations.

There are many factors influencing heterogeneous affinity in mosquito and human populations. Some of the most important are the existence of hot-spots, genetic propensity, migratory human behavior and specific geophysical conditions. Instead of considering these different factors separately, we will look at their collective effect in a small fraction of human individuals receiving most of mosquito bites. In other words, we will parameterize a sort of Pareto rule in its more modern formulation, according to Woolhouse [386].

Our model extends the agent-based malaria model introduced in chapter 5 and in reference [326], now incorporating heterogeneous affinity. We consider a system of $N_m = 4000$ mosquitoes and $N_h = 2000$ human individuals, both including healthy and infected individuals, henceforth represented as M_0 and H_0 and as M_i and H_i respectively ($N_m = M_0 + M_i$ and $N_h = H_0 + H_i$). Although the density of mosquitoes in the field may be higher than the one here considered, we model the number of mosquitoes as a smaller effective fraction of the overall mosquito mass that randomly feeds on a human individual, on average, twice a day, with

uniform distribution, and ranging from no bites to four daily bites. The algorithm keeps track of all attributes for each agent, human or mosquito, in a particular age, time since infection, and immunity status. All simulations take place during a time period of 30 years. More details and a flowchart describing the computer implementation of the agent-based model is given in chapter 5 and reference [326].

Heterogeneous affinity is here defined by the PW-rule parameter

$$\theta = \frac{P_h}{P_b}, \tag{8.1}$$

giving the quotient between the percentage P_h of the group with the most bitten humans and the percentage P_b of the bites that the group will receive. The algorithm defines a human subgroup consisting of 20% of the human population. This subgroup will be bitten with a probability between 20% (full homogeneity $\theta = 1$) and 80% (full Pareto heterogeneity 20/80, corresponding to $\frac{1}{\theta} = 4$). Next, we describe the relation between the basic reproduction number of the Ross-Macdonald model [230, 317], and the heterogeneity affinity rule introduced above. The basic reproductive number R_0 represents the number of secondarily infected humans that result from a single infectious human, and it has been defined as

$$R_0 = \frac{\Delta_m \; a^2 bc}{q_h q_m}(1+\alpha) = \bar{R}_0(1+\alpha), \tag{8.2}$$

where Δ_m represents the mosquito density [1], a is the human feeding rate, b and c represent respectively the mosquito-to-human (M-to-H) and human-to-mosquito (H-to-M) transmission efficiencies, and q_h and q_m are, respectively, the human daily recovery rate and the mosquito daily mortality rate. Parameter $\alpha \geq 0$ has been used in previous studies accounting for the effects of heterogeneous affinity [5, 11, 38, 45, 83, 108, 261, 386] and corresponds to the so-called *index of biting disparity*, which has been included by assuming that the previous basic reproductive number corresponds to the *homogeneous* basic reproductive number $\bar{R}_0$.

From empirical studies [43, 45, 83, 386], parameter α is known to assume values in the range $0 < \alpha < \alpha_{max} \lesssim 4$. Next, we introduce an explicit definition for α, to map it from parameter θ:

$$\alpha = \alpha_{max}\left(1 - \exp\left(-\frac{(\log\theta)^2}{2\sigma^2}\right)\right), \tag{8.3}$$

where $\sigma = |\log(20/80)|$ to settle PW-rule 20/80 as the heterogeneous affinity deviated from homogeneous state by one standard deviation, and $\alpha_{\max} = 4$. A sketch of α as defined in equation 8.3 as a function of θ, while equation 8.1, is shown in the inset of Figure 8.2.

In the present chapter, there is the intention to define a specific metrics for heterogeneity quantification in the form of its possible impact on local disease trans-

[1] Here, we use $\Delta_m = \frac{M}{H}$ as the mosquito density, instead of m from D.L.Smith,2004 [343]

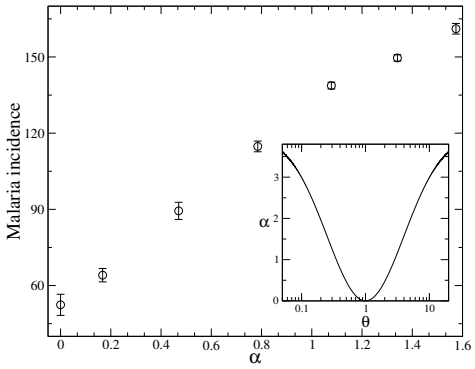

Figure 8.2: Malaria incidence as a function of heterogeneous affinity α as defined in equation 8.3. The inset shows the change in heterogeneous affinity with θ, as defined in equation 8.1.

mission, equivalent to the effect of a small migrating gametocyte-carrier population in the increase of disease resurgence risk. The utility of preventive treatment with ivermectin in the context of high heterogeneity in disease transmission while in the presence of different levels of background gametocytemia in the human population is also analyzed in terms of effective disease prevention. This intervention may be used as an adjuvant therapy to other anti-human-to-mosquito transmission measures resulting in gametocytemia reduction, by the use of effective drugs such as artemisinin, primaquine or methylene blue [41, 55, 212, 333]. Therefore, following the study presented in chapter 7, one may also consider two important aspects of malaria spreading in the presence of heterogeneity which enable us to use our previous results in the discussion of a possible new insight into improving the control of malaria transmission. The two aspects are:

(i) gametocytemia reduction by the use of specific treatment with primaquine, methylene blue or artemisinin derivatives.

(ii) ivermectin prevention.

8.3 Human-to-mosquito transmission and drug administration in a heterogeneity setting

At least two mosquito bites are required to complete the human-mosquito-human malaria transmission cycle. However, it is the presence of gametocytes in the blood at the human-to-mosquito transmission stage that stands as the most critical step in the persistence of malaria transmission.

Because human hosts can present a wide range of gametocytemia levels at different occasions, and during a finite time period, the effectiveness of human-to-mosquito transmission assumes a stochastic nature, conditioning some form of heterogeneity in the process. In the present model, human-to-mosquito transmission efficiency w_h was defined as the fraction between the number τ_g of days with

positive gametocytemia and the expected total duration τ_d of the disease, as [326]

$$w_h = \frac{\tau_g}{\tau_d} \,. \tag{8.4}$$

Here, we consider the typical value $\tau_d = 150$ days. The period with potential gametocyte production is usually longer than the disease symptomatic phase, which is of shorter duration. The assumed value of 150 days represents a reasonable approximation to the upper range of the expected average disease duration. Gametocytemia duration was defined as an essential model parameter, tunable through a dynamically equivalent action by the potential use of a gametocidal drug agent. In the present model, heterogeneity was analyzed at different levels of disease H-to-M transmission (from $w_h = 0.400$ to $w_h = 0.800$).

In the case of heterogeneous transmission, the combination of several anti-malarial strategies is crucial to achieve epidemic control [5]. The possibility of quarantine may be ineffective in malaria asymptomatic patients. Even gametocyte-carriers may briefly show only asexual forms of the most dangerous parasite *P.falciparum* (*Pf*) in their peripheral blood. With new laboratory assays for early disease diagnosis, diagnostic accuracy on migrant population may improve. But to decide which migrants should be treated with effective anti-malaria treatment at admittance is debatable.

Ivermectin has proven effective against *P.falciparum* infection, by selective killing of *Anopheles* mosquitoes shortly after a successful bite, before the parasite is able to complete its sporogony development [61, 62, 196, 250, 291], and apparently without any form of direct toxicity to the parasite [28]. This ivermectin selective killing action on biting mosquitoes may be extremely effective in disease prevention, by reducing the need for treatment with artemisinin derivatives, and thus lowering the risk of artemisinin drug-resistance expansion.

Ivermectin prevention was introduced in the present model as an adjustable parameter δ_{iv}, according to a previously published definition [326]. The δ_{iv} parameter results from the product of ivermectin administration probability p_{iv} (in the range between 0.0, with no ivermectin prevention, and 0.50, with ivermectin prevention in 50% of the human population) and the ivermectin-induced mosquito mortality constant parameter (q_{iv}=0.50):

$$\delta_{iv} = p_{iv} \times q_{iv} \,. \tag{8.5}$$

This mathematical implementation of the ivermectin effect is based on the knowledge that approximately half of all mosquitoes will die during the first four days after feeding on a human-host under ivermectin treatment [61]. As described below, we will validate such implementations in our model, looking into mosquito survival distribution curves, and comparing them with Chaccour original results – see section 12.5 [61]. We also evaluate if there is any correlation between mosquito

mortality as a result of ivermectin human treatment when compared to mosquito mortality occurring during the parasite incubation period inside the mosquito, according to what would be expected from theoretical predictions.

8.4 Predictive rates for assessing the strength of malaria transmission and the annual entomological inoculation

Field malaria transmission is difficult to monitor, requiring various methods to measure different aspects of disease transmission [352]. Here, we consider three metrics to monitor the intensity of malaria transmission: a) malaria incidence (MI), b) parasite rate (X) for human individuals, and c) sporozoite rate (Z) for mosquitoes.

Malaria incidence is defined as the confirmed malaria cases per person per unit of time, and more particularly, as the annual number of malaria-confirmed cases per 100 inhabitants at risk. The parasite rate X is given by the fraction of infected humans, and is also known as the prevalence of infection in humans [343, 344]. This rate is obtainable from the slide positivity rate (SPR), which is defined as the number of microscopy-confirmed malaria tests per 100 suspected cases examined [172]. SPR is useful in establishing temporal trends in malaria, and simple to implement at peripheral health facilities. It only considers laboratory confirmed cases of malaria, and may also be derived from rapid diagnostic testing (RDT-PR) [47]. SPR has been associated with malaria incidence and identified as a strong predictor of malaria transmission in Yunnan province, China [37]. The sporozoite rate Z represents the fraction of infected mosquitoes [308, 343].

Although these two indices, Z and X, are commonly used separately in malaria research [343], we have combined their behavior with respect to heterogeneity, introducing a "global infection rate" $G = ZX$ parameter, which is given by the product of both rates:

$$G \sim ZX\,, \tag{8.6}$$

where G represents an improved rate in the form of a squared percentage.

Related with these predictive rates is the annual entomological inoculation rate (EIR) defined as

$$\mathrm{EIR} = 365\ \Delta_m\ a\ Z \tag{8.7}$$

where, as stated above, Δ_m represents the mosquito density, and $\boldsymbol{a}$ is the human feeding rate [343].

8.5 From disease persistence to elimination in a scenario of increasing heterogeneity

8.5.1 Heterogeneity and ivermectin

The present model was implemented for sets of ten simulations in three heterogeneity scenarios, defined by the following values of heterogeneity affinity: low ($\theta = 1, 0.66$), intermediate ($\theta = 0.5, 0.4$) and strong ($\theta = 0.33, 0.29, 0.25$). See equation 8.1. These values are equivalent to the set of PW-rules 20/20, 20/30, 20/40, 20/50, 20/60, 20/70 and 20/80, respectively. Our results show a consistent linear correlation between 30-years average malaria incidence and increasing levels of heterogeneity, suggesting that heterogeneity strongly promotes malaria transmission (Figure 8.2).

Next, we analyze how heterogeneity in disease transmission is influenced by ivermectin treatment. In the absence of ivermectin administration, malaria incidence is three times higher in high heterogeneity simulations related to the PW-rule 20/80 ($\theta = 0.25$), for which around 150 cases *phy* are observed, when compared to simulations in full homogeneity ($\theta = 1.0$) where one observes ~ 50 cases *phy*. The curve in figure 8.3 a) for $p_{iv} = 0$ clearly shows this pattern. Moreover, this pattern is significantly reduced if ivermectin is used by even a small fraction of 5% of the general population, and a major decline in malaria incidence – very close to disease elimination – can be achieved by using ivermectin treatment in 20% of the general population, in the high heterogeneity scenario (PW-rule 20/80, $\theta = 0.25$).

An important feature is revealed in figure 8.3 b): isolines of constant malaria incidence fit approximately a linear relation $\alpha + sp_{iv}$ with $s \simeq -18$. If malaria incidence is plotted as a function of this linear relation, we uncover a transition from disease persistence to elimination at $\alpha - 18p_{iv} \sim -1$. Our results suggests that an increase in malaria transmission due to heterogeneity can be overcome when the population fraction under ivermectin treatment is such that $p_{iv} \gtrsim (\alpha + 1)/18$.

8.5.2 The role of transmission efficiency combined with ivermectin treatment in heterogeneous scenario

In the present model, human-to-mosquito transmission efficiency w_h is related to the time of gametocytemia duration and reveals strong correlation with malaria incidence in highly-heterogeneity scenarios. However, this correlation is consistently suppressed with higher rates of ivermectin prevention, as shown in Figure 8.4 a).

In this case, as shown in figure 8.4 b), isolines of constant malaria incidence fit approximately a linear relation $w_h + sp_{iv}$ with $s \simeq -4.2$, and malaria incidence is approximately proportional to this linear combination.

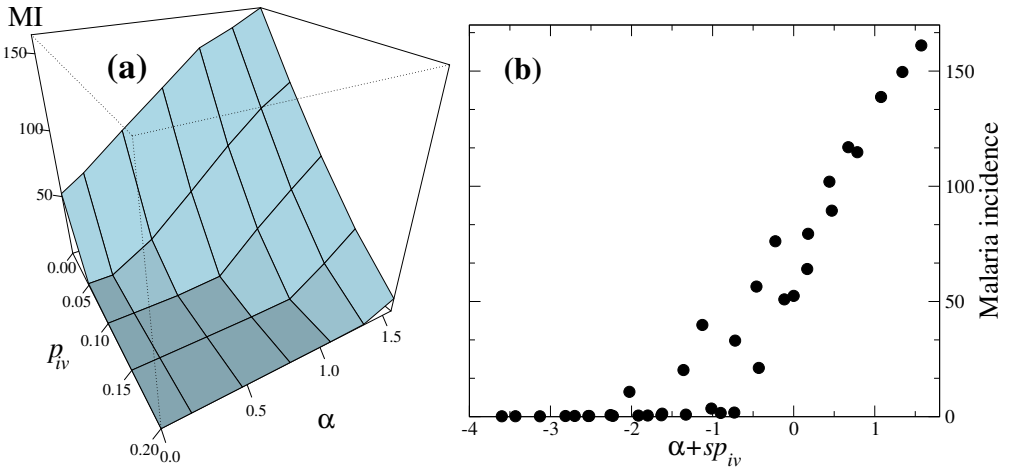

Figure 8.3: **(a)** Malaria incidence as a function of the heterogeneous affinity α and the ivermectin probability p_{iv}, showing that isolines of malaria spreading are approximately a linear combination of both variables.
(b) Malaria incidence as a function of the linear combination $\alpha+sP_{iv}$ with $s = -18$, showing a transition from disease persistence to elimination. In all cases, the human-to-mosquito transmission efficiency is held constant at $w_h = 0.5$.

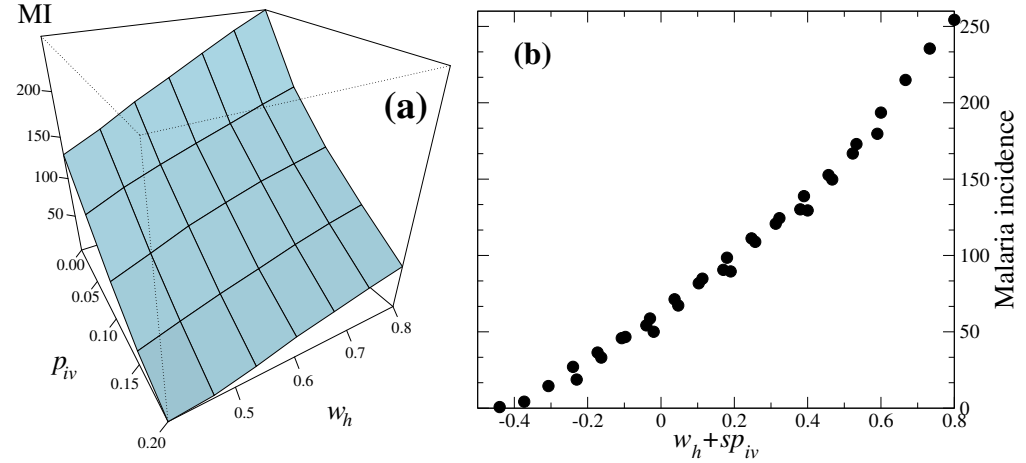

Figure 8.4: **(a)** Malaria incidence as a function of the human-to-mosquito transmission efficiency w_h and the ivermectin probability p_{iv}, showing that isolines of malaria spreading are approximately linear combination of both variables. Therefore, we plot in **(b)** the malaria incidence as a function of the linear combination $w_h + sP_{iv}$ with $s = -4.2$, clearly showing a gradual transition from elimination to endemic prevalence. In all cases the PW-rule 20/80 was used, corresponding to $\theta = 0.25$.

8.5.3 Mosquito survival patterns

In the present model, ivermectin is responsible for a consistent reduction in mosquito life expectancy resulting in lower chances for *Plasmodium* parasites to mature to the stage of sporozoite inside the mosquito, after feeding on a gametocyte-carrier human host. With a higher fraction of human hosts on ivermectin treatment, mosquito mortality is higher during the initial period of mosquito lifetime before the necessary ten days for parasite maturation inside the mosquito gut – see figure

8.5.

Average mosquito mortality, during the 10 days parasite incubation time period as a direct result of ivermectin treatment, is influenced by the fraction of human hosts on ivermectin treatment. Mosquito mortality was consistently stable and independent of different heterogeneity levels in all simulations with identical model parameters. In figure 8.5 a) we show the mosquito survival distribution curve for 30-years' time for different values of ivermectin probability and fit it with an exponential function

$$N = A \exp(\gamma t) \tag{8.8}$$

with γ and A, which vary linearly with p_{iv}, as shown in figures 8.5 b) and 8.5 c).

The intersection point in figure 8.5 a) around 10 days coincides approximately with the parasite incubation time period inside the mosquito, as ivermectin-induced mosquito mortality is typically higher during the first ten days of treatment, and becomes residual thereafter.

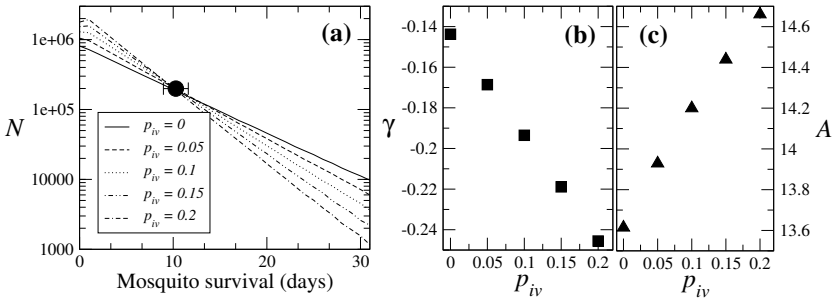

Figure 8.5: **(a)** Mosquito survival distribution curve for 30-years' time series (5 samples), uncovering an intersecting point around 10 days. The exponential fit $N = A \exp(\gamma t)$ has parameters, γ and A, which vary linearly with P_{iv} as shown in **(b)** and **(c)**. In all cases, high heterogeneity ($\theta = 0.25$) and low human-to-mosquito transmission efficiency ($w_h = 0.5$) is fixed.

8.6 Towards parameters for assessing malaria incidence

8.6.1 Utility of *Plasmodium* infection metrics

An important issue addressed in our model concerns the presentation of malaria burden results. For that purpose, we have used a point-analysis of annual malaria incidence per 100 inhabitants as a reliable metrics of malaria transmission intensity. However, we have also tested an alternate rate resulting from the combination of two other well-known and reliable infection rates: sporozoite rate (Z) and parasite rate (X).

We defined the G-rate as the result from the product of both sporozoite and

parasite rates – see equation 8.6. With the background of different heterogeneity scenarios, we have found a consistent correlation of the G-rate with malaria annual incidence, when compared to the established role of the parasite rate in defining the intensity of malaria transmission. Comparing the different plots in figure 8.6, one sees that in the presence of transmission heterogeneity, malaria incidence correlates better with the G-rate, rather than with any of the other rates, Z or X, separately.

8.6.2 Performance of classical Ross-Macdonald parameters in heterogeneity scenarios

We have determined the combined influence of ivermectin treatment on two important Ross-Macdonald model classical metrics, at different levels of heterogeneity affinity: the annual entomological inoculation rate (EIR), defined in equation 8.7, and the basic reproductive number (R_0), at different levels of heterogeneity – see figures 8.7 a) and 8.7 b).

As expected, mosquito mortality progressively increases with higher percentual use of ivermectin in the general population. When ivermectin treatment rate reaches the value of 0.20, i.e. nearly 93% of all mosquito deaths occur during the 10-days after the initial blood meal, when the parasite is still developing into the next transmissible form, explaining the effectiveness of this drug in blocking disease transmission.

Nonetheless, our simulations indicate that EIR is a better indicator than R_0 in the prediction of malaria transmission, as shown in figures 8.7 c) and 8.7 d). A possible explanation for this observation is that EIR values are consistently higher with increasing levels of heterogeneity.

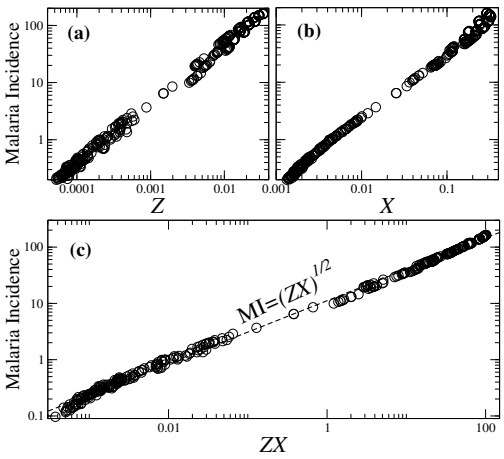

Figure 8.6: Scatter-plot between annual malaria incidence per 100 inhabitants and **(a)** the Z-rate, **(b)** the X-rate and **(c)** the ZX-rate. In each case we merge different levels of heterogeneity and at three different levels of ivermectin treatment, namely p_{iv}=0.00, 0.10 and 0.20. Independently of the heterogeneous affinity and ivermectin probability, there is a very accurate relationship given by $MI \sim \sqrt{ZX}$.

Additional simulations were performed for other classical Ross-Macdonald model parameters, such as the human feeding rate $\boldsymbol{a}$, mosquito-to-human trans-

mission parameter $\boldsymbol{b}$ and human-to-mosquito transmission parameter $\boldsymbol{c}$, with different results according to the heterogeneity level. While $\boldsymbol{a}$ is not significantly affected by heterogeneity, we find a consistent reduction in $\boldsymbol{b}$ with increasing levels of heterogeneity; on the contrary, $\boldsymbol{c}$ is positively and linearly correlated with higher heterogeneity levels.

The level of heterogeneity at which $\boldsymbol{c}$ became higher in magnitude than $\boldsymbol{b}$ was above the level corresponding to the PW-rule 20/60, where we had previously found an inversion of human infection prevalence. From this relation between $\boldsymbol{b}$ and $\boldsymbol{c}$, one may assume the possible existence of some form of proportionality of the fraction $\frac{c}{b}$ with the *biting disparity index* α.

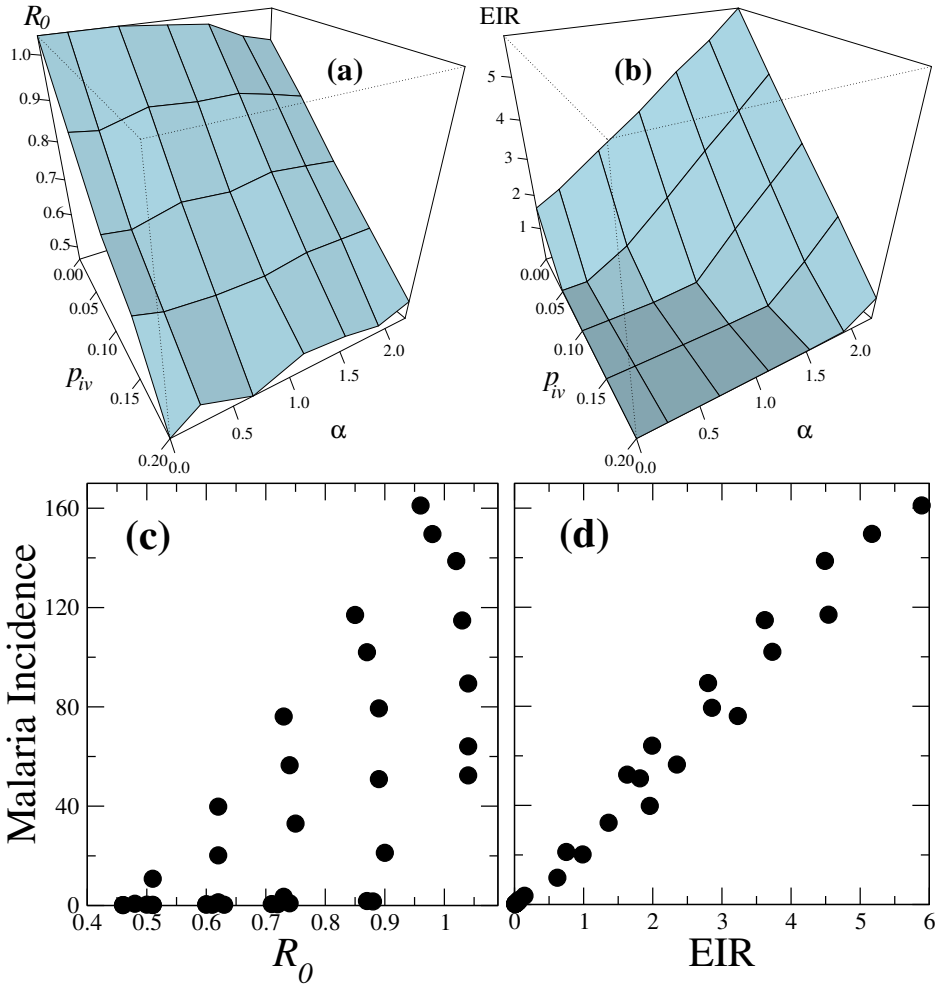

Figure 8.7: **(a)** The basic reproduction number, equation (8.2), and **(b)** the annual entomological inoculation rate, equation (8.7), both as function of the ivermectin probability p_{iv} and heterogeneous affinity α. In **(c)** and **(d)** we show the scatterplots of the basic reproduction number and annual entomological inoculation rate, respectively, with the corresponding values of malaria incidence. Clearly, there is a significantly stronger correlation of malaria incidence with EIR than with R_0.

8.7 Gametocytemia and heterogeneity in disease transmission

In our model, the intensity of human-to-mosquito transmission efficiency is represented by the variable w_h, which is roughly equivalent to the fraction of time with the presence of positive gametocytemia in human infected individuals. This variable is strongly correlated to the H-to-M transmission efficiency parameter $\boldsymbol{c}$ in R_0 original equation [317, 343], while being essential to the dynamics of human infectiousness to mosquitoes. This aspect of malaria transmission becomes particularly relevant in the presence of transmission hot-spots in the setting of human and mosquito population heterogeneity [274, 367, 386].

In the present model, we have investigated how the presence of heterogeneity could affect the 2D probability density function of human and mosquito infection prevalence (see figures 8.8 and 8.9).

We have also looked into the possibility of interaction between human-to-mosquito infectiousness and the presence of transmission heterogeneity hot-spots, and how this interaction was modified by the intensity of ivermectin intervention (see figures 8.10 and 8.11).

From figures 8.8 and 8.9 it is possible to show that the 2D human-mosquito infection prevalence probability density function is strongly affected by the presence of increasing heterogeneity. In the present simulation with full homogeneity ($\frac{1}{\theta} = 1.0$) there is evidence of the presence of a form of power-law in the human-mosquito infection prevalence 2D distribution function. With the presence of increasing heterogeneity ($\frac{1}{\theta} \in [2.0 - 4.0]$) it becomes evident that the dynamical human-mosquito infection trajectories evolve towards more stable 2D attractors – see figures 8.8 and 8.9, from a) to d).

8.8 Discussion and conclusion

We addressed heterogeneity as an important aspect in disease transmission, with severe impact in disease prevention strategy. To that end, we have used a previously described agent-based malaria model to simulate malaria transmission in scenarios of varying heterogeneous affinity, aiming to identify parameters that potentiate transition from disease persistence to elimination. Emphasis was drawn upon the role of preventive interventions, such as mass administration of ivermectin treatment (possibly in combination with gametocidal therapy), as well as on the adaptability of field malaria transmission indicators to accurately predict malaria incidence.

Human-to-mosquito transmission, which is directly related to the time length

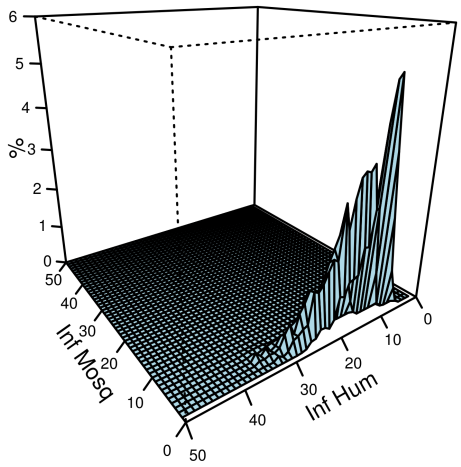

a)

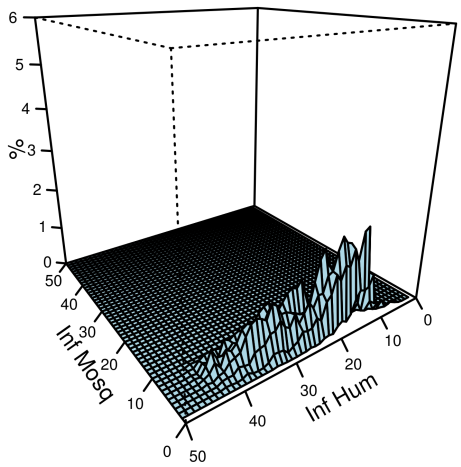

b)

Figure 8.8: 3-D probability density function (PDF) of human and mosquito *Pf* infection prevalence at constant H-to-M transmission efficiency ($w_h = 0.500$), in the setting of lower levels of heterogeneity:
(a) Homogeneneity ($\frac{1}{\theta} = 1.0$) **(b)** Mild heterogeneity ($\frac{1}{\theta} = 2.0$)

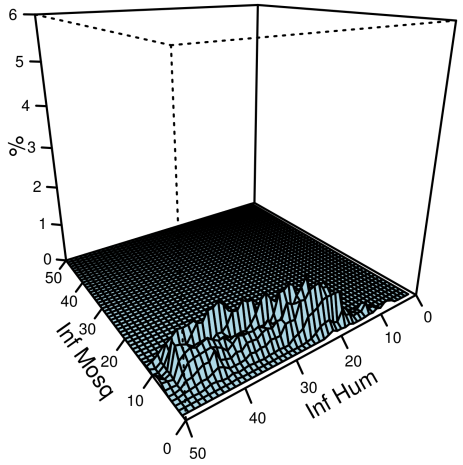

c)

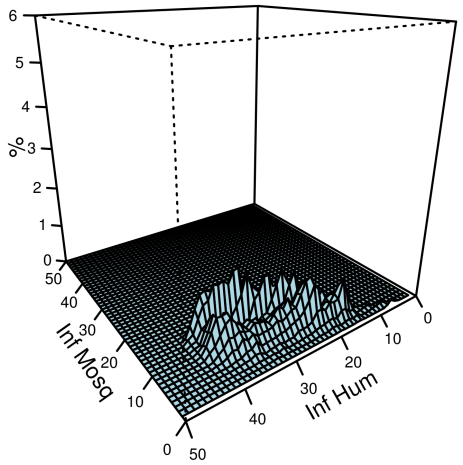

d)

Figure 8.9: (Cont. figure 8.8) 3-D probability density function (PDF) of human and mosquito *Pf* infection prevalence at constant H-to-M transmission efficiency ($w_h = 0.500$), in the setting of higher levels of heterogeneity:
(c) Intermediate heterogeneity ($\frac{1}{\theta} = 3.0$) **(d)** Full heterogeneity ($\frac{1}{\theta} = 4.0$).

of positive gametocytemia (w_h) is fundamental in disease transmission. Mass administration of ivermectin can potentially inhibit transmission due to its lethal effect on mosquito populations, immediately after feeding, and therefore, not allowing for complete gametocyte maturation to take place inside the mosquito, long before completing the 10 days incubation period. Such effect is potentiated in the settings of high mosquito density and high human-to-mosquito transmission [61, 196, 326].

We found that in the presence of strong heterogeneity, the product between the sporozoite and the parasite infection rates becomes a reliable indicator in predicting malaria transmission, performing better than the parasite rate and sporozoite rate, separately, in identical heterogeneity settings, particularly when taking into consideration the possibility of mass administration of ivermectin. Also, we have found that among classical Ross-Macdonald model metrics, EIR is much more sensitive than R_0 in predicting malaria incidence in high heterogeneity scenarios.

In the present model simulation, with different levels of heterogeneity ($\frac{1}{\theta}$) and human-to-mosquito transmission efficiency (w_h), we have found an additive influence of the two variables in increasing malaria incidence – see figure 8.10 a). However, this effect could be effectively reversed with the help of ivermectin prevention in increasing fractions of the human population – see figures 8.10 a) and b), and 8.11 c) and d).

The assumptions of our model intend to assess the impact of heterogeneity in malaria transmission. In an agent-model, the assessment takes place at a more qualitative level. In other words, while keeping its simplicity to facilitate the exploration of different scenarios, our results provide evidence for an impressive efficiency of ivermectin administration, at least at a qualitative level. We describe the quantitative output of our simulations, parameterized according to the knowledge about both populations and drug features, and well supported by reliable qualitative assumptions. However, we point out that the adopted validation procedure did not include quantitative conclusions, only possible with clinical trials, which are of course beyond the scope of a computational agent-based simulation.

Moreover, our model is based upon a stochastic agent-based model, previously published [326]. The model is implemented based in a detailed multi-parameter calibration, including information from empirical knowledge about mosquitoes, human-mosquito interaction and pharmacological features of ivermectin. Here, the additional assumption is derived from a well-established concept in economy and ecology, which is strongly connected to the presence of transmission hot-spots and disease super-spreading events, as we now report in the manuscript: 20% of the causes are responsible for 80% of the consequences. Our model of heterogeneity was implemented as a mathematical tool replicating that concept, in accordance with the first use of the 20/80 rule in infectious disease research by Woolhouse, in 1997 [386].

To better explore the robustness of our results against variations of heteroge-

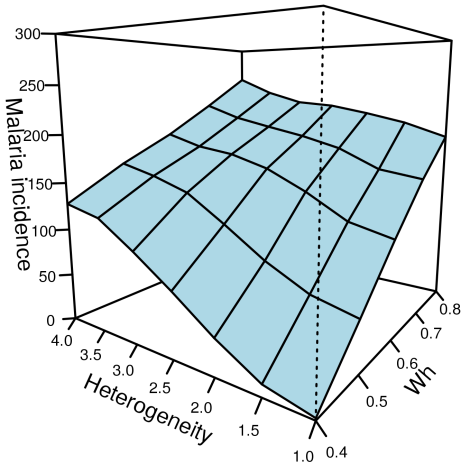

a)

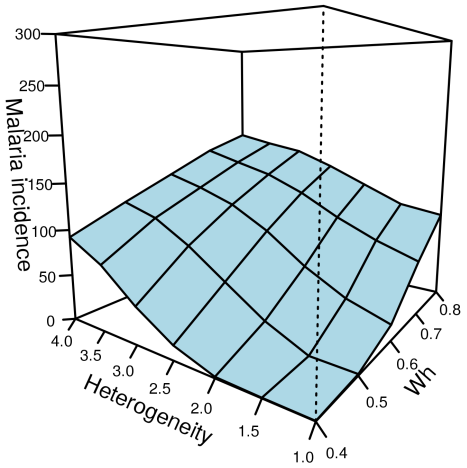

b)

Figure 8.10: Malaria incidence (number of diagnosed cases per 100 inhabitants, during a full year) as a result of the interaction between human-to-mosquito transmission efficiency (w_h) and heterogeneity, ranging from homogeneity ($\frac{1}{\theta} = 1.0$) to full heterogeneity ($\frac{1}{\theta} = 4.0$), with different levels of ivermectin prevention: **(a)** $p_{iv} = 0.00$ **(b)** $p_{iv} = 0.05$

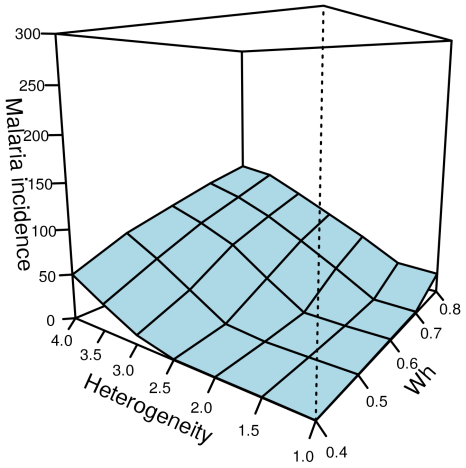

c)

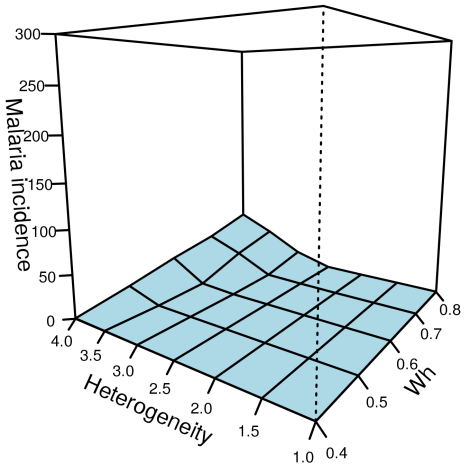

d)

Figure 8.11: (Cont. figure 8.10) Malaria incidence (number of diagnosed cases per 100 inhabitants, during a full year) as a result of the interaction between human-to-mosquito transmission efficiency (w_h) and heterogeneity, ranging from homogeneity ($\frac{2}{\theta} = 1.0$) to full heterogeneity ($\frac{1}{\theta} = 4.0$), with different levels of ivermectin prevention: **(c)** $p_{iv} = 0.10$ **(d)** $p_{iv} = 0.20$

neous affinity, we introduce a parameter that measures that affinity. Our results show a linear relationship between the level of heterogeneous affinity and the minimal level of ivermectin administration. Again, the specific linear coefficients are not taken as a trustworthy result, but the linear relationship between the minimum level of drug administration and the level of heterogeneity can be presented as one conclusion in this study. One particular aspect uncovered in our simulations is the evidence that the annual entomological inoculation rate seems to be a better predictor than other widely used quantifiers, such as the basic reproduction number, R_0.

We have previously shown the critical influence of heterogeneity in amplifying malaria transmission three-fold in our model simulations with full heterogeneity ($\frac{1}{\theta} = 4.0$). We have also proved that ivermectin was effective in suppressing disease transmission. In the present section we have looked at how heterogeneity ($\frac{1}{\theta}$) interacts with human-to-mosquito transmission efficiency (w_h), in different settings of θ and w_h.

In figures 8.8 and 8.9 we may witness different 2D probability density functions relating percentual infection prevalence between mosquitoes and human individuals in different heterogeneity settings. Mosquito infection prevalence was consistently higher in the presence of high heterogeneity scenarios ($\frac{1}{\theta} = 4.0$). leading as a result to higher human infection prevalence.

By looking at figures 8.10 and 8.11 it is also clear that ivermectin was efective in the presence of both high heterogeneity and high H-to-M transmission efficiency. In figure 8.11 d) malaria transmission was successfully suppressed with the implementation of partial ivermectin prevention in the human population.

Overall, our model emphasizes the importance of considering heterogeneity, when predicting malaria transmission, showing that the effect of mass drug administration of ivermectin, is not only dependent of ivermectin intensity and human-to-mosquito transmission efficiency, but that it is also clearly influenced by the presence of heterogeneity in disease transmission.

Heterogeneity is clearly illustrated by the presence of transmission hot-spots, which have been shown to be geographically distinct, and able to present substantial diversity in temporal transmission dynamics [34]. The role of these hot-spots in malaria transmission may assume special importance in small villages in close proximity to high *Anopheles* mosquito density and larval active breeding sites. Children, as well as recent immigrants coming from malaria high-risk regions should also be considered as transmission hot-spots heterogeneity sources.

In our view, a combined treatment strategy with gametocidal drugs (such as artemisinin, primaquine, or methylene blue) and mass administration of ivermectin, specifically targeting transmission hot-spots, may stand as a promising alternative in dealing with the risk of malaria resurgence in high heterogeneity settings, deserving further consideration in future field trials.

Chapter 9

Migration and malaria transmission

9.1 Introduction

Malaria eradication persists as troublesome in some world regions where it is endemic [288, 289]. Although several countries have claimed significant reductions in malaria incidence and mortality, sporadic outbreaks may occur. In some parts of Africa and Asia, the possibility of malaria resurgence is still a danger to the indigenous population. In later disease resurgence, global population immunity is usually reduced after years of low parasite exposure. In such a case, a strong malaria comeback with higher mortality may be anticipated [217].

Changing weather conditions may also precipitate malaria resurgence in countries with poor malaria surveillance, widespread human migration, and lack of anti-malaria institutional measures aiming to the general population as well as to medical professionals [253].

Caminade et al. (2014), used an adequate climate and hydrological model predicting an overall global net increase in climate suitability for malaria transmission as well as a net increase in the population at risk. These climate and human changes are set to occur at a faster pace during the 2050s decade [56].

In different world regions, human migratory movement has been formally implicated in the risk of malaria endemic resurgence [99, 121, 218, 294, 306]. Human migration may be responsible for widespread infectious disease outbreaks, making it impossible to predict local disease resurgence events. All over the world, population flow is continuous. For cultural, economic, social, or touristic reasons, or in mass emigration movements, human individuals travel to or from locations with significant potential risk of malaria transmission. Different factors may be implicated in such migratory movements. War, demographical expansion, low economic development and poorer living conditions in Africa have been at the source

of most of the human migration movements. Touristic travel stands as a potential threat to countries that have achieved successful disease eradication.

Human migration originating from places with higher malaria prevalence may result in perpetual endemic renewal in regions where the disease had previously been eliminated. In countries with good conditions to *Anopheles* breeding and no firm policy of prompt RDT/ACT administration to potential gametocyte-carriers, the risk of disease resurgence may become significant.

It is well-known that after human infection, submicroscopic gametocytes may persist in blood circulation for a very long time, usually up to two months, sometimes even more than that. The migration of these silent gametocyte carriers may be responsible for new epidemic episodes in regions where malaria was assumed to have been eradicated. A long time after disease elimination, human population will have lost a significant part of its previous protecting immunity, thus becoming more vulnerable to a fatal disease outcome. The possibility of renewed malaria seeding within a healthy population, originating from a few asymptomatic malaria gametocyte-carrier patients, represents a consistent risk for malaria resurgence in places with stable *Anopheles* persistence. These malaria migration hot-spots have been dismissed in preventive campaigns, and scientific consensus about the correct policy to enforce malaria prevention in migrant asymptomatic patients is still unclear [5, 43, 45]. Thus, some malaria outbreaks may in fact be the consequence of population movements from endemic areas to non- or low-endemic areas [227]. Migratory movement persists as a perpetual menace to malaria-free regions presenting with adequate geophysical conditions favoring *Anopheles* survival [11, 58, 227, 235, 241]. These favorable *Anopheles* breeding conditions consist of a stable tropical temperature (from 16° to 32°C), during a long rainy season with above average humidity and good local breeding sites for the *Anopheles* larvae, usually with a *Normalized Difference Vegetation Index* (NDVI) above 0.350 [173, 184, 306, 337].

While the importance of migration in malaria resurgence has been ignored until recently, persistent malaria within a healthy population, originating from a few asymptomatic malaria gametocyte-carrier patients, may fuel up malaria resurgence in regions with good conditions to *Anopheles* breeding.

In the past, population movement has contributed to several episodes of malaria resurgence. The arrival of infective human individuals to a non-infected population may easily trigger the spread of an infectious disease in that population. This fact may explain the failure of several malaria eradication campaigns in the 1950s and 1960s. Also, human population movement patterns have promoted the dispersal of drug resistant parasite strains [305].

Martens et al. (2000) had already stressed the fact that, not considering adequately the role of population movement in malaria transmission, could have been responsible for the failure of several malaria eradication campaigns. The movement of infected individuals from areas where malaria was still endemic to

other areas where malaria had been considered eradicated was considered to be an important trigger of local disease resurgence [241].

Mukandavire (2010) used a deterministic mathematical model to evaluate the implications of infective immigrants´ arrival to a malaria high risk region [262]. Also, Yukich considered human movement, even in a small scale, an important risk factor for the resurgence of malaria. Evidence of human movement interaction with vector habitat and features of the environment were found to be determinant in the epidemiology of malaria [393].

While *Pf* infection in humans may last up to 12 months, some patients may develop malaria symptoms more than 2 months after returning from traveling abroad from malaria-endemic countries [107]. Although rare, *Pf* transfusion-related transmission has been sporadically reported. In 2001, Mungai et al. described the occurrence of 32 cases of malaria after blood transfusion in the USA from 1963 to 1999 [107, 263].

9.2 Impact of human migration

9.2.1 Europe

At the present rate of climatic change, Southern Europe may entail a reasonable risk of malaria resurgence in the foreseeable future. Warmer temperatures allowing for better mosquito survival conditions along with the constant inflow of immigrants from countries where malaria is still endemic may facilitate the occurrence of endogenous malaria outbreaks, in southern Europe. The wide presence of *An.atroparvus* in countries like Spain and Portugal assumes a potential risk for malaria resurgence [319].

Anopheles species are potential vectors of malaria in Finland, and presumably have existed there since prehistoric times [168]. During the XIX century, the movement of large numbers of human individuals to several working sites in Finland such as the Saimaa canal (1845–54), the lowering of some lakes (during the XIX century), or the building of the railway (1862–71) have brought temporary populations to uninfected areas. Some of those workers could have been *Plasmodium* carriers, a consistent explanation for malaria resurgence in Finland during the XIX century [168].

Most of all severe malaria cases in Europe were related to tourists returning home after acquiring the infection in African countries [205] or to migration movements from non-European origin. Several *Anopheles* species are known to be specific of Europe – where mosquito survival conditions are harsher than in Africa – with particular relevance to *An.atroparvus*, *An.labranchiae* and *An.sacharovi*.

In recent years, first-time arrival immigrants in Paris, France, especially pregnant women on mefloquine prophylaxis, were apparently more likely to develop prolonged *P.falciparum* infection (up to 3 years) with higher parasitemia rates,

while remaining asymptomatic [107].

Despite a consistent migratory flow of refugees from Africa to southern Europe, malaria resurgence risk in Europe remains low. Possibly as a consequence of the low anthropophilic potential in the local *Anophelline* population. Also, *P.falciparum* persistence in immigrants may be of shorter duration when compared to the long time spent while traveling from the country of origin [58]. Imported cases from Africa to the United Kingdom rose from 803 in 1987 to 1,165 in 1993 [241]. From 2006 to 2014, 190 patients with severe falciparum malaria were reported in 12 European countries.

Temperatures above 30°C suppress both parasite and mosquito survival [253]. However, *Plasmodium* sporogony duration is clearly dependent on local temperatures, with full suppression at low temperature values, well below 16°C [168].

In the face of persistent gametocytemia in human individuals, stable conditions to disease transmission stand as an important factor in disease transmission. Malaria elimination is possible at a low annual malaria incidence level – less than 2 cases/1000 inhabitants, per year [259]. In such a situation, a small migration flux may not be able to trigger disease resurgence. However, a persistent immigration flux could promote a mildly stabilizing effect on disease dynamics while being responsible for a small increase in the number of infected individuals [224]. People that travel away to areas with strong malaria endemicity, may return later as gametocyte-carriers, promoting new malaria cases at home [11].

At low transmission levels the cycle of human-mosquito reinfection could occur with reduced intensity, so that disease elimination would become possible. Yet, the risk of disease resurgence may persist for a very long time during the low transmission dry season in the presence of a few asymptomatic gametocyte human-carriers in the general population. In regions with a long-wet season potentiating vector breeding and malaria transmission, disease elimination could still become possible during the low transmission dry season. In those conditions, the possibility of disease resurgence may clearly depend on disease importation as a consequence of human migration.

9.2.2 Central and Far East Asia

Feng et al. reported that in China during 2012, a total of 2428 malaria cases were imported (89.0% of all diagnosed cases). *P.falciparum* (58.6%) and *P.vivax* (37.5%) were responsible for the vast majority of these cases. It became clear that imported malaria persisted as a severe threat to the malaria elimination program in China [120].

During 2012, in the Chinese province of Yunnan, cross-border migration persisted as the main source of *P.falciparum* importation [388]. Clinical *P.falciparum* malaria was related to human travel across the border, especially from China to Myanmar. Individuals living in the proximity of the border between China and

Myanmar were at a higher risk of infection, with the presence of high-incidence clusters along the border extension [388]. Internally migrating populations could also play a role in spreading malaria across district boundaries.[274]. Malaria propagation has been attributed to short and medium distance population movement. Migration movement across the border between Bangladesh and Myanmar has also been implicated in malaria resurgence inside Bangladesh [274].

During a five-year epidemiological survey in Faridabad, India, the occurrence of malaria was clearly related to labor migration, with an infection rate close to 39%, because of the new arrival of malaria-infected migrant workers, fueling local disease transmission. In these places, the distance from the potential breeding sources of anophelines to the villages and nearby migrant settlements was well within the average anopheline flight range of 500 meters [329].

In the former Soviet Union, massive importation of malaria from Afghanistan became a harsh reality during the 1980s. After the disappearance of the Soviet Union there was an unprecedented return to Russia of infected individuals from former soviet republics such as Tajikistan and Azerbaijan. Intensive labor migration triggered several malaria outbreaks in Russia at the time, probably aggravated by climate change, facilitating *Anopheles* breeding [253].

9.2.3 Central and South America

More recently, in Venezuela, malaria resurgence has become a major health issue. Also, several malaria cases have been reported in neighboring regions from Brazil and Colombia. By 1931, Venezuela had the highest malaria incidence rate in Latin America. Several years later (1961) after the implementation of several effective malaria preventive measures, Venezuela was considered by the WHO as the first country in the world to eliminate malaria [113]. However, due to progressive recent economic degradation and social unrest in the country, malaria became once again the focus of malaria spreading to other South American countries (Colombia, Peru and Brazil) as a consequence of intensive human migration outflow. Also in Nicaragua, malaria risk has increased since 2017, probably because of infective individuals migration from Venezuela. These events underline the potential of malaria resurgence risk as a result of combined human migration and climate change [113].

9.2.4 Africa

In Africa, several examples remind us of the importance of human migration in disease flares and endemic persistence (Réunion island, Cape Verde, S. Tomé e Príncipe, and borders between Zanzibar and Tanzania, and South Africa, Mozambique and Zimbabwe) [140, 217, 241, 294]. In Mozambique, malaria resurgence has been related to the arrival of migrant workers, possibly parasite carriers, to the sugar estates back in the 1960s and early 1970s [241]. During the 1980s, malaria

prevalence decreased from 35% to 0.6% after effective implementation of chloroquine prophylaxis combined with an IRS-based eradication program in the island of Príncipe. However, due to financial difficulties, this preventive campaign was suspended, leading later (1984) to a severe malaria outbreak with significant mortality in small children. With the development of multiple DDT-resistant *Anopheles* strains, the situation rapidly deteriorated [217]. Also, *Pf* was detected in 29% of immigrant asymptomatic children from Liberia upon arrival in the United States (Minnesota) [107]. In June 2009, malaria resurgence occurred in the island of Príncipe. This malaria rebound was apparently related to imported cases from the main island of São Tomé [217]. And a recent malaria outbreak in Cape Verde islands has been related to human travel from nearby continental Africa [99]. Meanwhile, in northwest Ethiopia, Malede et al. reported that imported malaria were 19.5 % of all malaria cases [235]. Finally, in the island of Réunion, malaria resurgence occurred after disease transmission had been suppressed. Imported malaria cases were detected mainly in Réunion residents returning from holidays or from visiting family and friends in the surrounding regions (Comoros, Madagascar and Mayotte) [294].

9.3 Methods to implement the impact of migration

9.3.1 Human migration

A dedicated algorithm was included in the main model for simulation of a persistent migration flow of human individuals, introducing the possibility that human healthy individuals could be replaced by infected humans according to a hypothetical prevalence of *Pf* infection, with random disease duration and malaria immunity.

This way, two probabilities were defined: A daily human migration probability π_{mig} parameterized at a constant value of small $\pi_{mig} = 0.0005$ (corresponding to the daily arrival chance of a single immigrant in 2000 human individuals), and a variable disease probability of malaria infection in individual human immigrants (π_{dis}, ranging from 0.00 to 0.50).

The global disease immigration rate was defined as δ_{mig}, resulting from the product of both previous probabilities, according to equation 9.1:

$$\delta_{mig} = \pi_{mig} \times \pi_{dis} \tag{9.1}$$

δ_{mig} was defined in a range between 0.00 (no immigration) and $0.00025 = 0.5 \times 0.0005$ (equivalent to the daily arrival chance of a single infectious immigrant in a total of 4000 human individuals). This flow was kept at a constant rate for the whole duration of the simulation.

Two different heterogeneity settings were used in the model simulations –

figure 9.1:
a) Homogeneity ($\frac{1}{\theta} = 1.0$).
b) Full heterogeneity ($\frac{1}{\theta} = 4.0$).

A low immigration scenario was considered, departing from the standard initial conditions used in the model ($H_{i0} = 0.05$ and $M_{i0} = 0.01$). This scenario evaluated immigration impact in a small village with an initially low disease burden. Phase transition from stable epidemic to disease eradication was defined through repeated model simulations. The follow-up time period was defined as 30 years. The mosquito model characteristics suffered no modifications from the previous model.

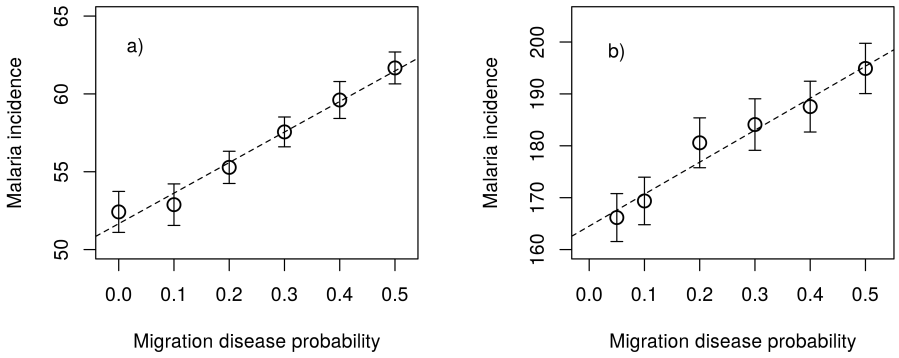

Figure 9.1: The impact of disease migration in malaria incidence (disease prevalence in a single immigrant – π_{dis} – in the range between 0.00 and 0.50, corresponding to a global migration disease rate δ_{mig} between 0.00 and 0.00025) obtained as the number of malaria diagnosed cases per 100 inhabitants, during a full year, with mild human-to-mosquito transmission efficiency ($w_h = 0.500$), no ivermectin prevention ($p_{iv} = 0.00$), and different heterogeneity settings:
(a) Homogeneity ($\frac{1}{\theta} = 1.0$)
(b) Full heterogeneity ($\frac{1}{\theta} = 4.0$)

From figure 9.1, one may witness that even a small immigration rate of malaria patients can have a significant impact in potentiating malaria transmission. With full heterogeneity this impact is higher than in the homogeneity setting – figures 9.1 a) and b).

9.3.2 Ivermectin prevention

The preventive action of ivermectin was determined in different transmission scenarios. Assuming a constant 50% probability of mosquito death after a bite in an ivermectin-treated human host ($q_{iv} = 0.50$), the probability of treatment with ivermectin (p_{iv}) varied in the range between 0.00 (no ivermectin treatment) and 0.20 (20% of the human population under ivermectin treatment).

In the present model, the use of ivermectin is included, as a treatment probability randomly assigned to every human individual $p_{iv} = 0.00$ to 0.010, with

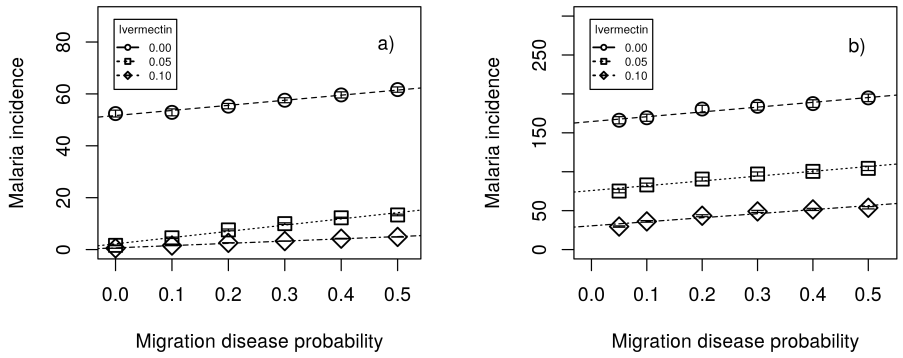

Figure 9.2: The impact of disease migration in malaria incidence (disease prevalence in a single immigrant π_{dis} in the range between 0.00 and 0.50, corresponding to a global migration disease rate δ_{mig} between 0.00 and 0.00025) as the number of malaria diagnosed cases per 100 inhabitants, during a full year, with mild human-to-mosquito transmission efficiency ($w_h = 0.500$), in different heterogeneity settings and different levels of ivermectin prevention (from $p_{iv} = 0.00$ to $p_{iv} = 0.10$):
(a) Homogeneity ($\frac{1}{\theta} = 1.0$).
(b) Full heterogeneity ($\frac{1}{\theta} = 4.0$).

constant mosquito mortality $q_{iv} = 0.50$ defined during a short period of time (usually less than 4 days) after the bite, in a randomly selected human individual among the whole human population. This way, 50% of all mosquitoes biting ivermectin-treated human individuals will be removed from the simulation and replaced by healthy ones.

The impact of partial ivermectin prevention in the immigration model in human population was assessed in terms of yearly malaria incidence per 100 inhabitants – figures 9.2 and 9.3.

9.4 Results and discussion

In malaria transmission, several factors come into play. Following a single malaria episode, the long and unpredictable persistence of gametocytes in human blood will play a decisive role in perpetuating chronic mosquito reinfection. Submicroscopic gametocytes may persist in blood circulation for a very long time, possibly lasting more than two months. The migration of these silent gametocyte carriers may be responsible for new epidemic episodes in regions where malaria had been considered extinct. A long time after disease extinction, human population will have lost a significant part of its protecting immunity, thus becoming more vulnerable, and leading to a higher malaria fatality rate, especially among children. This gametocyte reservoir will become critical in disease resurgence, making it harder to attain long lasting disease elimination. In our simulations, we have

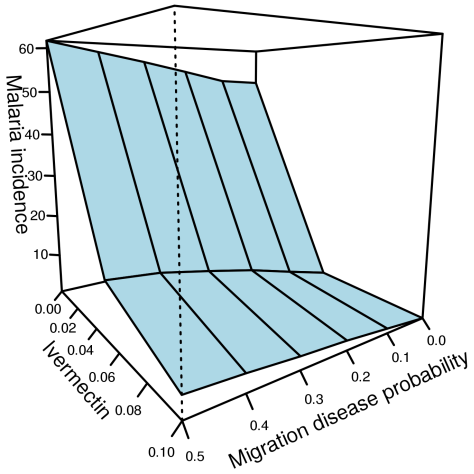

a)

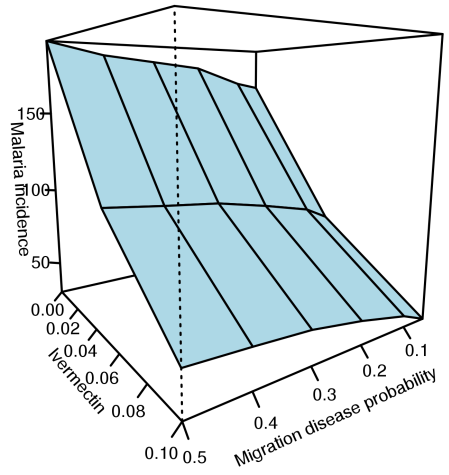

b)

Figure 9.3: Malaria incidence, human migration of malaria patients (disease prevalence in a single immigrant π_{dis} in the range between 0.00 and 0.50, corresponding to a global migration disease rate δ_{mig} between 0.00 and 0.00025), and ivermectin prevention, in the setting of mild human-to-mosquito transmission efficiency ($w_h = 0.500$):
(a) Homogeneity ($\frac{1}{\theta} = 1.0$).
(b) Full heterogeneity ($\frac{1}{\theta} = 4.0$).

shown that a small but constant inflow of asymptomatic gametocyte-carriers into a disease-free community may perpetuate malaria transmission in that setting – see figure 9.1. That effect revealed significant synergism with the presence of population heterogeneity. This migration effect could be significantly inhibited with the help of massive ivermectin treatment in the population – see figures 9.2 and 9.3.

Thus, the presence of these silent gametocyte carriers in a region with a significant burden of the vector *Anopheles* mosquito stands as a potential threat and may reignite a reinfection human-to-mosquito cycle, leading to sustained disease transmission.

From figure 9.3, it is possible to compare the migration impact on malaria incidence between different heterogeneity settings with different levels of ivermectin prevention. Malaria incidence was much higher in the presence of full heterogeneity, as expected from what we had learned in chapter 8.

With the implementation of partial ivermectin prevention, it was possible to strongly inhibit malaria transmission in the setting of a constant immigration rate of infectious patients or asymptomatic gametocyte carriers – see figures 9.2 and 9.3. Malaria transmission suppression induced by ivermectin was effective and consistent in both heterogeneity settings and at different levels of human migration.

As global warming may ultimately change present conditions for malaria transmission in the foreseeable future, malaria eradication will persist as a global health problem in some regions of the world where it is endemic. Although several countries have claimed significant reductions in malaria incidence and mortality, the epidemic is still not contained, with sporadic outbreaks worldwide [253, 393]. In some parts of Africa and Asia, the possibility of malaria resurgence persists as a potential danger for the indigenous population. After a long period of time with low malaria incidence, global population immunity is significantly reduced, as a consequence of years of low parasite exposure. In the event of disease resurgence, a strong malaria comeback with higher mortality rates can be anticipated. [217]

Chapter 10

Seasonal malaria transmission

10.1 Historical background

Worldwide, malaria assumes a periodic seasonal behavior as vector density is strongly dependent on climatic conditions, especially local temperature range, water precipitation and humidity.

Macdonald [231] reformulated the original model of Ross [317] and defined mosquito vector longevity as the single most important variable with influence in the force of transmission [167]. Anthropogenic climate change may directly affect the behavior and geographical distribution of the *Anopheles* mosquito as well as the biological cycle of the *Plasmodium* parasite, while influencing environmental factors such as the presence of vegetation and the availability of adequate mosquito breeding sites, with potential impact in disease incidence [242].

The prevalence of infection is strongly related to vector density – see chapter 6. Areas of high malaria transmission are less sensitive to changes in mosquito density than low transmission areas, and areas of low transmission appear to be highly sensitive to sudden reductions in mosquito density [17]. Mosquito population abundance is also well correlated with the duration of the rainy season. In most of Africa malaria endemic regions, disease resurgence is usually expected in the weeks following a long period of time with high precipitation leading to increased vegetation density, persistent water accumulation, and the creation of multiple potential *Anopheles* breeding sites. Therefore, seasonal variation in malaria incidence as a result of climatic change was included here as an independent critical component in our computational model.

Climate is a decisive factor in malaria transmission. In certain world regions where malaria is hyperendemic, specific geophysical conditions such as an ideal temperature range (between 19 and 32^{o} C), the occurrence of significant rain precipitation or of special terrain features adequate for mosquito larval breeding, are responsible for a seasonal pattern conditioning improved vector survival conditions. Higher *Anopheles* life expectancy and stronger mosquito emergence typically oc-

curs during a period of time lasting between 2 and 7 months every year. This climate pattern is usually periodic, occurring once or twice every year, with a stable time duration. During the rainy season, mosquito emergence will overcome mosquito mortality, leading to increased malaria transmission with a seasonal pattern.

Malaria weather modeling has evolved in recent years. Seasonal climate forecasting is currently based upon up to six months of time window. However, chaotic behavior is still responsible for significant probabilistic uncertainty in rain precipitation affecting climate models. Some of those models produced a far more accurate prediction of the potentially devastating impact of El Nino event in Africa, during the years of 1997/1998 [167]. Therefore, the seasonal variation in mosquito numbers is critical to mosquito and parasite weather dependent dynamics [167]. Hyperendemic malaria occurs in regions where disease transmission is higher during the rainy season. The time length of this season will necessarily affect the intensity of global disease spreading throughout the year. The temperature range, as well as seasonal rainfall along with some land topographic features such as higher vegetation density, will facilitate mosquito breeding, leading to higher mosquito density and higher disease transmission. The duration of the wet season is probably one of the most important factors conditioning malaria incidence.

10.2 Methods

In the present model, seasonality was simulated assuming a 3- to 6-month duration wet season with higher malaria transmission, followed by nine to six months with a lower transmission potential, equivalent to half of the rainy season transmission efficiency. This model of seasonal dynamics was consistent with different seasonal patterns in different African regions [122]. Malaria incidence was measured depending on a variable percentage duration of high transmission season $\Delta_s = \frac{\delta_s}{365}$, where Δ_s was in the range between 0.25 (corresponding to $\delta_s = 90$ days) and 0.49 (corresponding to $\delta_s = 180$ days). All model simulations were repeated 10 times, in a full homogeneity scenario ($\frac{1}{\theta} = 1.0$), with a high constant value of human-to-mosquito transmission efficiency scenario ($w_h = 0.800$), and different levels of ivermectin prevention (p_{iv} from 0.0 to 0.15).

10.3 Results and discussion

In the present model simulations malaria incidence was consistently higher in the setting of a longer rainy season. There was a clear linear correlation between malaria incidence and the duration of the rainy season in a wide range of its percentual duration (from 0.25 to 0.49). Also, a significant reduction in malaria incidence was the result of ivermectin prevention in a fraction of the human population (between $p_{iv} = 0.0$ and $p_{iv} = 0.15$).

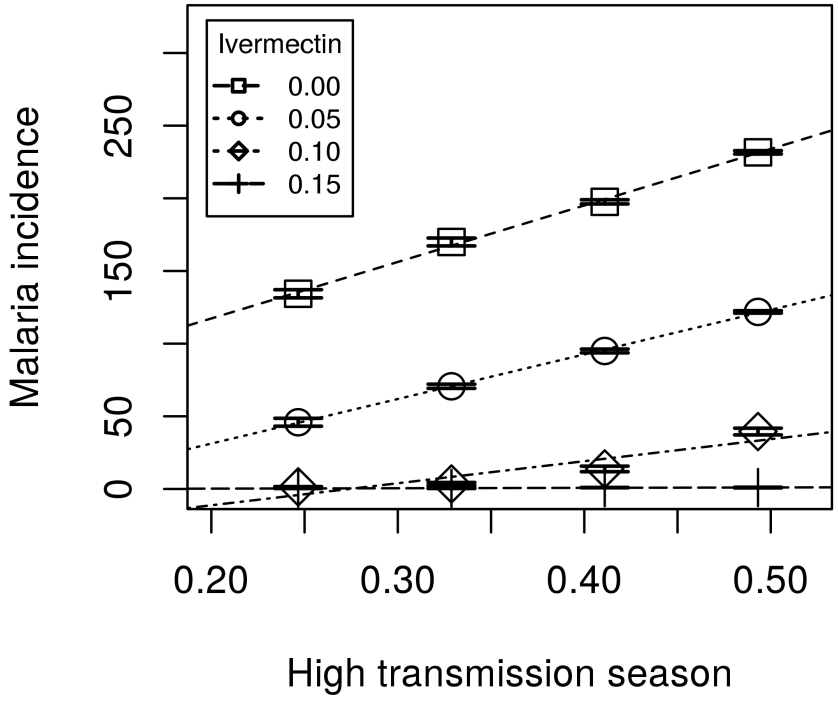

Figure 10.1: Malaria incidence and percentual duration of high transmission season (Δ_s) where Δ_s lies in the range between 0.25 and 0.49, in a full homogeneity scenario ($\frac{1}{\theta} = 1.0$), with a constant high value of human-to-mosquito transmission efficiency scenario ($w_h = 0.800$), and different levels of ivermectin prevention (p_{iv} from 0.0 to 0.15).

From our model simulations, the use of ivermectin was especially effective when p_{iv} was above 0.15 – see figure 10.1. By comparing time series simulations at high transmission seasons ($w_h = 0.800$) with different time lengths (90 vs. 180 days of significant rainfall during a whole year), we have witnessed different levels of malaria incidence depending on the rainy season duration. And by looking at disease transmission suppression induced by ivermectin prevention it was clear that the partial use of ivermectin in the human population could assume an effective role in achieving disease elimination, when complemented with vector density reduction in the presence of a heavy and prolonged rainy season – see figure 10.2.

Longer rainy seasons facilitate mosquito breeding sites by promoting widespread vegetation growth (NDVI > 0.350) leading to multiples sites with better conditions for adequate larval development followed by higher mosquito density a few weeks later. The consequence of seasonality in improved mosquito breeding was clear in our simulations with a longer wet season – see figures 10.1 and 10.2. However, with a low fraction of the population under ivermectin treatment it was

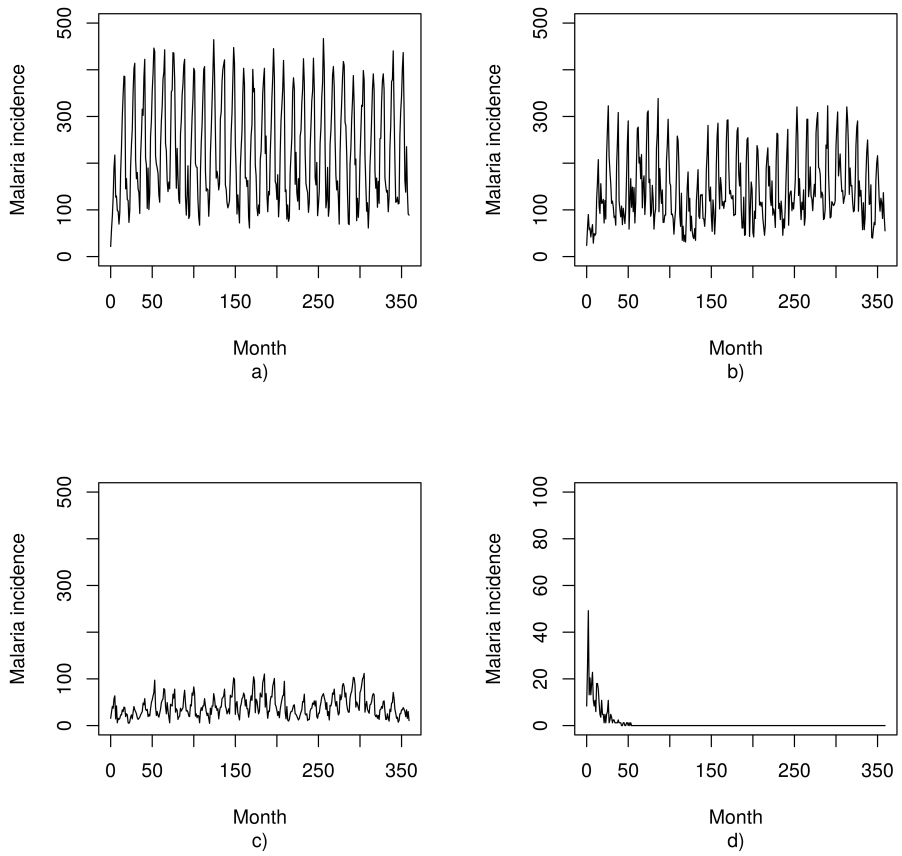

Figure 10.2: **(a)** High seasonality with 180 days of high malaria transmission season, and no ivermectin treatment, **(b)** Low seasonality with 90 days of high malaria transmission season, and no ivermectin treatment, **(c)** High seasonality with 180 days of high malaria transmission season, and ivermectin treatment in 10 % of the population, and **(d)** Low seasonality with 90 days of high malaria transmission season, and ivermectin treatment in 10 % of the population. All scenarios relating to a human population with full homogeneity ($\theta = 1.0$) and high H-to-M disease transmission ($w_h = 0.800$).

possible to suppress disease transmission in the setting of longer rainy seasons – see figures 10.1, and 10.2 c) and d). Our data suggests that ivermectin alone could adequately reduce malaria incidence in tropical regions devastated by prolonged rain precipitation.

Chapter 11

Hurst exponent and malaria transmission

11.1 Introduction

In this chapter we propose a different approach to estimate effective *Plasmodium* transmissibility levels, which reflect submicroscopic gametocytemia in individuals within a specific community, based on collected time series of local malaria incidence.

Time series models have been used as important tools and metrics, not only in epidemiology, but also in economics, geophysics, biology and ecology [46]. One of them, the so-called Hurst exponent, was introduced by Hurst in 1951 [169] in the context of hydrology planning, namely during the study of flooding levels in the river Nile. The Hurst exponent is a measure of memory in a time series of values. Applying it to the series of Nile flooding levels, based upon Egyptian ancient hydrology data collected during earlier 847 years, Hurst was able to estimate the rate at which the autocorrelation of that series decreased as the time interval between measurements increased. In this way, Hurst used the collected data to model the flooding levels of the Nile, and with that assess optimum dam sizes to contain extreme rain events. Soon the applicability of the Hurst exponent extended to many other fields, particularly in the study of financial theory [57] and complex phenomena with evidence of fractal features [238–240]. However, while different time series models have been implemented in epidemic infections in general [13, 23, 122, 144, 204, 266, 302, 324], and in malaria incidence forecasting in particular [64, 334] – mostly auto-regressive and linear models – the application of the Hurst exponent in malaria spreading is still lacking.

Of particular importance in malaria transmission is the level of gametocytes in the blood circulation. Gametocytes are the parasite forms which mediate transmission from humans to mosquitoes and, therefore, are also obvious targets in implementing preventive actions such as vaccine immunization or anti-malarial drugs.

Submicroscopic gametocytemia detection is difficult and often not as precise as statistical data collection from e.g. malaria incidence varying heterogeneously from one community to another [326, 327].

To relate gametocytemia levels with malaria incidence time series we introduce a methodology based upon the use of the Hurst exponent. To the best of our knowledge, this is the first analysis of empirical data of malaria incidence series using Hurst exponent to derive an estimate of a hidden variable, namely the level of transmissibility or easiness of spreading within the community from which the series of malaria incidence is collected.

We show that the Hurst exponent can grasp long-range dependencies close to the phase transition between disease elimination and stable prevalence scenarios of malaria. In a more general scope, complexity in time series may also be related to the level of information entropy, which is commonly used to address emergence phenomena and self-organization. Here, we analyze the effects of memory in time series of malaria incidence. Two types of memory have been defined in random stochastic processes, long and short memory, where the transition between these regimes may be represented as a phase transition in the context of a stochastic random process. We focus on Hurst exponent estimation and Shannon entropy at different levels of disease transmission intensity, applied to malaria time series derived from simulations with a previously introduced agent-based model [326] with different (parameterized) levels of gametocytemia, as well as to different empirical malaria time series.

Our objective is to properly identify malaria transmission patterns, as well as to link long-range dependence processes in malaria incidence time series to the occurrence of phase transition near disease elimination. We also test the importance of Hurst exponent estimation and Shannon entropy as sound predictors of the presence of long-range dependence and long memory processes in malaria transmission. In particular, we show that from simple models connecting gametocytemia levels and measures easily extractable from empirical series of malaria incidence, such as incidence levels, Hurst exponent, and entropy, we are able to predict an indicator of "effective" gametocytemia for regions where malaria incidence is regularly monitored. Our study uses eight different empirical series, shown in figure 11.1.

We start in section 11.2 by describing the different empirical data sets analyzed in this study and the agent-model used to produce simulated scenarios of different transmissibility levels, parameterized by the gametocytemia level. Moreover, we briefly describe the basic tools, namely the Hurst exponent and Shannon entropy, explaining how they are computed from series of malaria incidence. In sections 11.3 and 11.4 we describe qualitatively the behavior of Hurst exponent and entropy, and the form of autocorrelation function decay, in eight different malaria empirical time series examples, respectively. In section 11.5 we derive models to fit the values of the three observables, namely the malaria incidence, the Hurst exponent and the entropy for different simulated scenarios, as a function

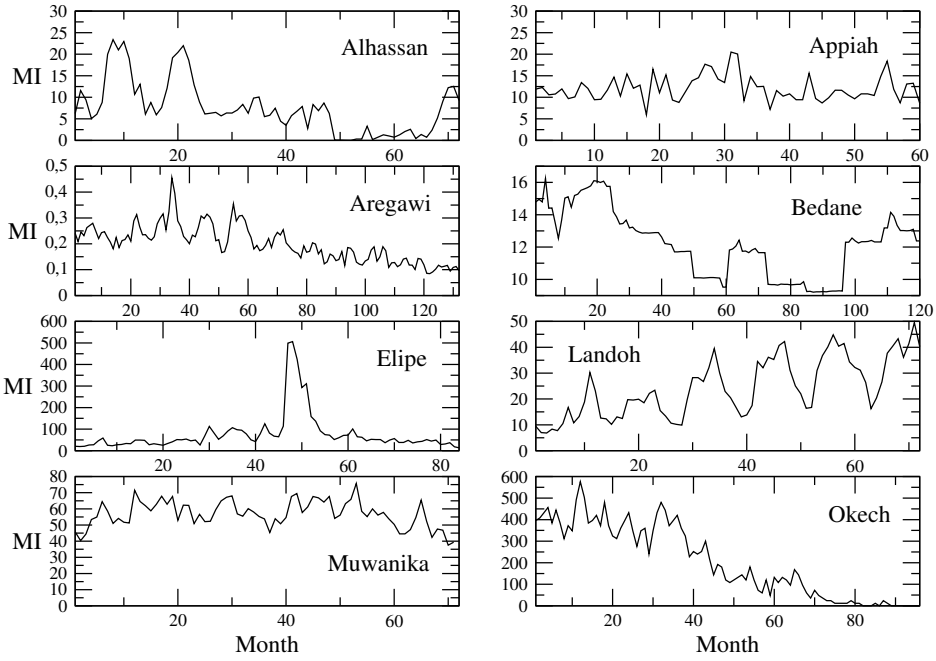

Figure 11.1: Eight different series of malaria incidence from different studies in the literature: Alhassan et al (Kasena Nankana municipality in Ghana, 2017) [12], Appiah et al (Ejisu-Juaben municipality in Ghana, 2015) [23], Aregawi et al (Ethiopia, 2014) [24], Bedane et al (Kucha district in Ethiopia, 2016) [33], Gomez-Elipe et al (Karuzi in Burundi, 2007) [147], Landoh et al (Est Mono district in Togo, 2012) [209], Muwanika et al (Uganda, 2017) [267], Okech et al (Kenya, 2008) [278].

of the gametocytemia level. Using these fitted expressions we then measure the average malaria incidence, Hurst exponent and entropy of the empirical data sets. Introducing these values in the fitted expressions we retrieve an estimate of the associated "effective" gametocytemia level, i.e. the effective transmissibility level in each empirical case. In section 11.6 we adopt a qualitative approach to Hurst exponent and entropy with a case-by-case description. The robustness of 36-month averages of the Hurst exponent and entropy is analyzed in section 11.7. Finally, in section 11.8 we discuss limitations of our approach, as well as possible extensions.

11.2 Data, modeling methods and analysis tools

11.2.1 Empirical series of malaria incidence

The empirical part of our investigation comprehends eight series of malaria incidence as presented in figure 11.1. These series are available from previous studies namely Alhassan et al (Kasena Nankana municipality in Ghana, 2017) [12], Appiah et al (Ejisu-Juaben municipality in Ghana, 2017) [23], Aregawi et al (Ethiopia, 2014) [24], Bedane et al (Kucha district in Ethiopia, 2016) [33], Gomez-Elipe et al (Karuzi in Burundi, 2007) [147], Landoh et al (Est Mono district in Togo, 2012) [209], Muwanika et al (Uganda, 2017) [267], Okech et al (Kenya, 2008) [278]. The

data sets were chosen as representative of regions with malaria incidence diversity in Africa. They have a time duration ranging from 60 [23] to 132 months [24], while showing different trends and periodicity – see figure 11.1 and table 11.1. Malaria incidence was measured at each month as the expected number of new malaria cases per 100 inhabitants in a full year, if malaria incidence were to be kept constant. In this way, to obtain the precise incidence at each month, the yearly presented graphical value must be divided by 12 months.

As can be seen from figure 11.1, the eight cases differ in their level of malaria transmission and epidemic behavior. All empirical series show some form of irregular periodicity as a consequence of climate seasonality. Declining malaria incidence is clear in series from Aregawi and Okech, as well as in Alhassan and Bedane, although with a final disease outbreak in these last two cases. High levels of malaria transmission occur in Gomez-Elipe (identified solely as Elipe time series in some of the figures for clarity) during a brief period of time. Malaria incidence remains quite stable in Muwanika, Appiah and Landoh empirical series, with a consistent upward trend in the last case.

11.2.2 Agent model for malaria spreading

To combine results from empirical data with simulations from the agent model introduced and developed in previous works [326, 327], we conduct a series of simulations at different levels of disease transmission efficiency. Human-to-mosquito (H-to-M) transmission was defined in terms of the fraction of human disease days with the presence of gametocytemia in blood circulation, henceforth represented as w_h.

Six different scenarios were considered, corresponding to a wide range of different levels of positive gametocytemia duration and disease transmission efficiency, namely 110 days of positive gametocytemia during 150 days of expected disease duration (i.e. $w_h = 110/150 = 0.733$), 90 days ($w_h = 0.600$), 75 days ($w_h = 0.500$), 70 days ($w_h = 0.467$), 68 days ($w_h = 0.453$), and 63 days ($w_h = 0.420$). For the simulations, we consider a system of $N_m = 4000$ mosquitoes and $N_h = 2000$ human individuals, both including healthy and infected individuals. We have modeled the number of mosquitoes as a small but effective fraction of the overall mosquito mass that randomly feeds on a human individual, twice daily on average. The simulation time lasts 30 years while evaluating each human individual in terms of disease duration and human-to-mosquito transmission.

The algorithm keeps track of several attributes for each agent, whether human or mosquito, at a particular age, such as the time spent since the first day of infection, and the individual immunity status. Beyond 5 years of persistent human reinfections, the human host will develop partial protective immunity at the maximum possible level, while losing it after 2 years without infection. The computational cycle includes a realistic mosquito daily mortality routine. Dead mosquitoes are to be replaced by uninfected mosquitoes. Human disease duration

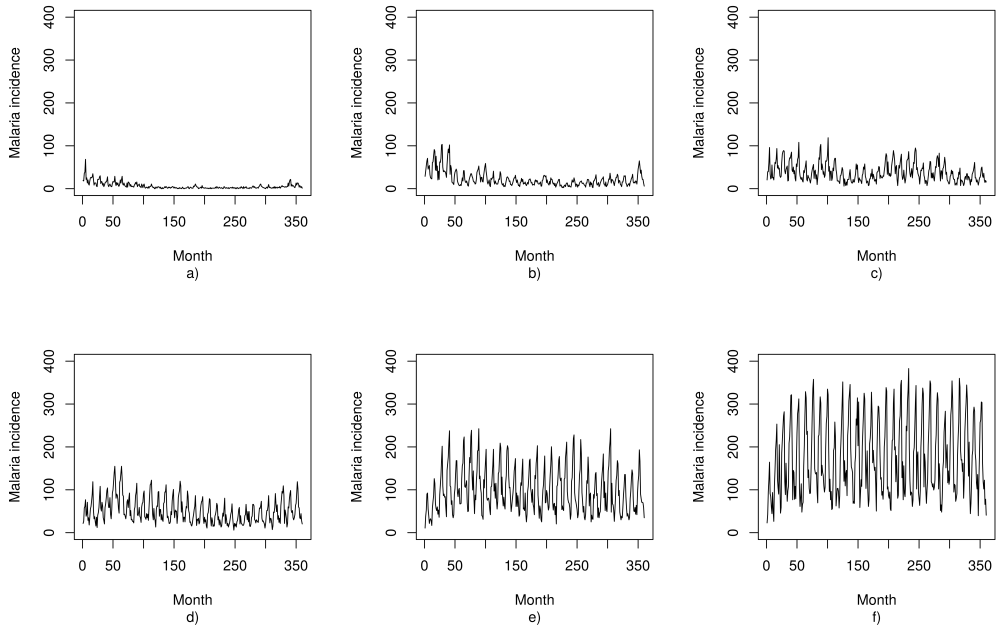

Figure 11.2: Six different simulations of malaria incidence using different scenarios of gametocytemia, namely **a)** 63 days ($w_h = 0.420$), **b)** 68 days ($w_h = 0.453$), **c)** 70 days ($w_h = 0.467$), **d)** 75 days ($w_h = 0.500$), **e)** 90 days ($w_h = 0.600$), and **f)** 110 days of positive gametocytemia during 150 days of expected disease duration (i.e. $w_h = 110/150 = 0.733$).

reflects realistic human recovery from malaria.

Human-to-mosquito transmission efficiency (w_h) is also stochastically defined and directly dependent on the number of days with positive gametocytemia. Upon updating the number of healthy human individuals and mosquitoes, the algorithm generates one episode of mosquito feeding in a human individual, with the possibility of protection from long lasting insecticide-impregnated nets (ITN), insecticide-impregnated nets (ITN) or indoor residual spraying (IRS). Our model is inspired in Mozambique seasonality [122, 123], considering 150 days for the duration of the high transmission season – see figure 11.2.

Relevant details as well as the flowchart describing the computer implementation of the agent-based model are given in chapter 5, and in reference [326].

Using the present model we analyzed the behavior of the human-mosquito coupled system, resulting from a complex interaction between the two compartments. Human-to-mosquito transmission efficiency (w_h) was used to define the probability of a sustained presence of gametocytemia in human blood circulation, as well as the survival probability of infected mosquitoes beyond latency. These aspects are considered critical in disease transmission. Our model simulations use gametocytemia as an independent variable affecting human-to-mosquito transmission. Different levels of gametocytemia define different stages of disease transmission efficiency. Theoretical gametocytemia reduction is considered equivalent to an ef-

fective treatment with gametocidal agents such as primaquine or methylene blue in a fraction of the human population.

11.2.3 Hurst exponent and entropy to assess memory effects in stochastic series

We use two different metrics to assess memory in series of malaria incidence, empirical and simulated, investigating whether long-range dependencies could occur close to phase transition near disease elimination when compared to more stable epidemic scenarios. The Hurst exponent is defined as

$$\frac{R}{D} = kT^H \tag{11.1}$$

where the first member represents the rescaled range as a dimensionless ratio between R (represents the maximal range of all observations) and D (represents the standard deviation of all observations). An explicit mathematical definition is given below in equations 11.4 and 11.5. T stands for the time index (number of observations in the time series), k is some constant to be determined and H represents the Hurst exponent.

With Hurst exponent estimation it became possible to distinguish among three different regimes characterizing the time series: (i) the *anti-persistent* regime, characterized by $0.0 < H < 0.5$, when if the series increases (resp. decreases) in one period it is very likely that it will decrease (resp. increase) in the next period, (ii) the *persistent* regime, characterized by $0.5 < H < 1$, when if the series decreases (resp. increases) in one period it is very likely that it will decrease (resp. increase) in the next period, and (iii) the *memory-less* regime characterized by $H = 0.5$, when the process is uncorrelated in time.

A Hurst exponent estimation close to 0.5 (random walk process) is found in empirical time series with heavier disease transmission. In malaria time series from our model simulations, transitions from prevalence to disease elimination are characterized by values of the Hurst exponent larger than 0.5 and close to 1, a footprint of a persistence time series.

As for entropy, it is related with the complexity of the time series [322, 330]. The complexity of stochastic processes may be calculated with the use of entropy-based measures. For that purpose, several functions may be employed. The significance of complexity, emergence phenomena and self-organization may provide us with useful information concerning continuous as well as discrete systems, in the form of time series results.

Information entropy is supported by the equation:

$$S = -\sum_{i=1}^{N_b} P(x_i) \log P(x_i)\,, \tag{11.2}$$

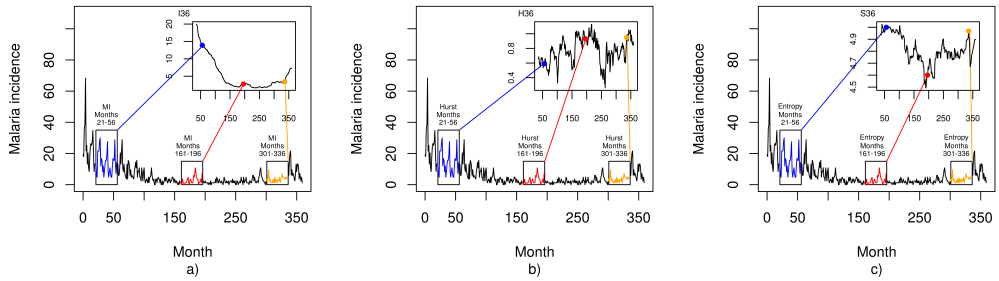

Figure 11.3: **(a)** Illustration of how 36-month moving average malaria incidence, symbolized as I_{36} is obtained from an original series of monthly malaria incidence values either empirical or simulated. Similar procedures are used to compute **(b)** H_{36} and **(c)** S_{36}. See text for details. In this case, we used a simulation with an agent-based with low human-to-mosquito transmission efficiency, namely $w_h = 0.420$.

where the Boltzman $P(x)$ is the probability density function of the observable x, which in its discretized form is estimated by an histogram, finite set of values $P(x_i)$ for the set of bin-points x_i. The log function is base 2. Information theory defines entropy in terms of information uncertainty in the evolution of time series results. Other entropy related terms such as mutual information may be used as alternative methods for time series analysis in malaria.

11.2.4 Estimating Hurst exponent and entropy in series of malaria incidence

Both Hurst exponent and Shannon entropy are influenced by the length of the time-series sample. Therefore, we introduce a standardization procedure, which is independent of the length of the time series.

The procedure is illustrated in figure 11.3 and is as follows. We define a 36-month moving average malaria incidence, symbolized as $I_{36}(m)$, at month m, as the average malaria incidence in the previous 36 months:

$$I_{36}(m) = \frac{1}{36} \sum_{n=m-35}^{m} I(n)\,, \tag{11.3}$$

where $I(n)$ is the monthly malaria incidence measured or simulated, composing the series of values.

In the Alhassan malaria time series (Kasena Nankana municipality in Ghana, 2017) [12] one can see a declining trend in malaria incidence in the form of a decreasing moving average of 36 months (I_{36}), from $\sim$ 11 to $\sim$ 4 cases per 100 inhabitants, per year [*phy*], despite the small final outbreak in the last 6 months. Consistent with this declining trend in I_{36} we may also witness a decreasing trend in S_{36} as well as a rising trend in H_{36} after month 55. In this case, the behavior of both Hurst exponent and entropy in the preceding 36 months is well correlated

with the malaria incidence trend.

The Gomez-Elipe time series (Karuzi in Burundi, 2007) [147] is quite different from the remaining empirical examples. It shows a consistent stable pattern of malaria incidence below 110 cases *phy*, until month 45, peaking at $\sim$ 500 cases *phy*, around month 48, with a fast downward trend to $\sim$ 60 cases *phy* at month 56, and a slower decline thereafter to a final value of $\sim$ 20 cases *phy* – see figure 11.1. The 36-months malaria incidence (I_{36}) reveals a consistent upward trend peaking at month 64, with a downward pattern thereafter. In this case, we find a persistent oscillatory behavior in the value of H_{36} during the entire time series, usually ranging above 0.9. But, in parallel with the outbreak in malaria incidence we see a sudden fall in H_{36} to values close to 0.6 (closer to random noise) at around month 48. Entropy in the form of a 36-months moving average (S_{36}) reveals a similar behavior in relation to I_{36} from month 48 onwards.

The Landoh malaria time series (Est Mono district in Togo, 2012) [209] reveals a consistent upward trend in malaria incidence in the form of a mild increase in the 36 months moving average (I_{36}) during the whole time series, ranging from the initial $\sim$ 18 cases *phy*, to a peak at $\sim$ 30 cases *phy* in month 72.

Consistent with the steady upward trend in I_{36} during the entire time series, we find a declining trend in the 36-months moving average of Hurst exponent (H_{36}) from a peak of $\sim$ 0.85 at month 47, to an all-low value of $\sim$ 0.55. Along with this downward trend in H_{36}, there is a consistent wave-like increase in entropy in the form of a 36-months moving average (S_{36}), during the entire time series. In the Landoh time series, the behavior of H_{36} and S_{36} is reasonably well correlated with the behavior of I_{36} in time.

In a similar form, but with an opposite trend to the Landoh time series, the Okech time series (Kenya, 2008) [278] also reveals a steady decreasing trend. In the Okech time series, malaria incidence consistently decreases from an initial peak of $\sim$ 400 cases *phy*, to a final value close to 50 cases *phy*. Consistent with the steady downward trend in I_{36} during the entire time series, we find an upward trend in the 36-months moving average of Hurst exponent (H_{36}) from an all-low of $\sim$ 0.6 at month 42, to a peak of $\sim$ 1.2 at month 82. Along with this upward trend in H_{36}, there is also a consistent decrease in entropy in the form of a 36-months moving average (S_{36}), during the whole time series. In the Okech time series, the behavior of H_{36} and S_{36} is also quite correlated with the behavior of I_{36} in time.

Because, Hurst exponent (H) and Shannon entropy (S) are influenced by the length of the time-series sample, we also consider a 36-month moving window estimate. In the case of the Hurst exponent, we assume the following identity:

$$\Delta_{I_{36}} = \left(\sum_{k=1}^{t} (I(k) - I_{36}(T)) \right) \tag{11.4}$$

and compute the quantities R and D as

Series	I_{36} **36 Months**	H_{36} **36 Months**	S_{36} **36 Months**	**Duration** *Months*
Aregawi,2014 [24]	0.208 ± 0.05	0.7766 ± 0.14	5.138 ± 0.01	132
Alhassan,2017 [12]	7.091 ± 2.81	1.014 ± 0.14	4.792 ± 0.18	72
Bedane,2016 [33]	11.63 ± 1.36	1.077 ± 0.09	5.161 ± 0.01	120
Appiah,2015 [23]	12.44 ± 0.13	0.9229 ± 0.06	5.121 ± 0.01	60
Landoh,2012 [209]	24.54 ± 4.31	0.7326 ± 0.08	5.065 ± 0.02	72
Muwanika,2017 [267]	58.76 ± 1.11	0.8254 ± 0.12	5.160 ± 0.01	71
Elipe,2007 [147]	101.0 ± 28.2	0.9367 ± 0.10	4.710 ± 0.17	84
Okech,2008 [278]	203.4 ± 120	1.018 ± 0.16	4.881 ± 0.28	96

Table 11.1: Table with the empirical values of average malaria incidence I (malaria cases per 100 inhabitants, per year), Hurst exponent H and Shannon entropy S, concerning a 36-month time frame. Error indicate standard deviations from the series by using moving windows of 36 months.

$$R(T) = \max_{t=1,\ldots,T}(\Delta_{I_{36}}) - \min_{t=1,\ldots,T}(\Delta_{I_{36}}) \tag{11.5a}$$

$$D(T) = \left(\frac{1}{36}\sum_{k=T-35}^{n}(I(k) - I_{36}(T))^2\right)^{1/2} \tag{11.5b}$$

Having the series of 36 values $R(T)/D(T)$ for each window, we then apply equation (11.1) to find fitting values for k and for the Hurst exponent H.

As for Shannon entropy, an estimate of the probability density is first computed given by the set of values $P(I_i)$ for an assumed set of bin values I_i, with $i = 1, \ldots, N_b$, of malaria incidence (I) and then equation (11.2) applied, running the sum only over the 36 incidence values observed within each time-window.

In this way, we have computed the average of malaria incidence I, H and S for 36-month windows, independently of the size of the empirical series. In order to quantify I, H and S for each empirical case, we then obtain the average of the corresponding time series and compute its standard deviations. Table 11.1 shows the empirical values of the three observables. Notice that, in these cases, higher moments seem to be not very relevant, which can be seen comparing the average in table 11.1 with the median and quartiles in table 11.2.

11.3 Qualitative analysis and robustness assessment of Hurst exponent and entropy in empirical time series behavior

While the eight empirical cases show a broad range of values for malaria incidence and Hurst exponent, the entropy seems much more resistant to changes.

Series	I_{36} Q_{50}	I_{36} Q_{25}	I_{36} Q_{75}	H_{36} Q_{50}	H_{36} Q_{25}	H_{36} Q_{75}	S_{36} Q_{50}	S_{36} Q_{25}	S_{36} Q_{75}
Aregawi,2014	0.22	0.16	0.26	0.80	0.66	0.90	5.14	5.13	5.14
Alhassan,2017	7.43	4.36	9.68	0.94	0.90	1.15	4.77	4.68	4.96
Bedane,2016	11.2	10.4	12.4	1.10	1.00	1.15	5.16	5.16	5.16
Appiah,2015	12.5	12.4	12.5	0.93	0.87	0.96	5.12	5.12	5.12
Landoh,2012	24.0	21.0	28.4	0.76	0.70	0.80	5.06	5.05	5.08
Muwanika,2017	59.0	58.2	59.7	0.81	0.77	0.90	5.16	5.16	5.16
Elipe,2007	115	83.5	122	0.95	0.89	1.00	4.67	4.59	4.72
Okech,2008	211	89.1	310	1.06	0.98	1.13	4.96	4.85	5.08

Table 11.2: Table with the empirical values of median, quartile 25 and 75 from the series of malaria incidence, entropy, and Hurst exponent, using moving windows of 36 months.

The cases of Alhassan, Elipe and Okech form a group separated from the other time series which form a second group. We will address these cases in more detail when building the model for effective human-to-mosquito transmissibility (gametocytemia).

We have also looked at the way those indices behaved in a typical low-transmission empirical time series such as obtained from Okech,2008 [278]. In this empirical time series, when Hurst exponent was evaluated in 36-months partial intervals ($H36$), it revealed a clear inverse correlation with malaria annual incidence. Furthermore, Shannon entropy consistently decreased with progressive lower values of malaria incidence. This correlation pattern was like the one found in model simulations when comparing high and low transmission scenarios.

By consistently searching for evidence of the presence of long-range dependence in malaria time series we looked into the time evolution of information (Shannon) entropy in scenarios with stronger disease transmission, and compared results with those from other time series of lower disease transmission. Our model simulations, at low levels of disease burden near a eradication-prevalence transition from consistently found malaria time series with lower information entropy. In section 11.6 we describe in more detail the eight particular cases.

Table 11.3 shows the correlation between the three properties, I, H and S, for the eight empirical data sets. One finds evidence of linear correlation between malaria incidence and Hurst exponent or Shannon entropy in seven of the eight presented empirical malaria time series. The case of Bedane is the exception.

The estimation of the Hurst exponent by R/S-analysis may be biased due to the short length of 36 months [19, 32, 149]. To ascertain how robust the results with 36-month windows are, we repeated our estimates for 24- and 48-month averages. The correlation is also reasonably evident in the 48-months' time frame. Entropy is clearly more linearly correlated to malaria incidence than Hurst exponent. In summary, the data shown in table 11.3 suggests the presence of significant linear correlation between malaria incidence, and Hurst exponent or Shannon entropy.

	24 months		36 months		48 months	
Pearson r^2	(I,H)	(I,S)	(I,H)	(I,S)	(I,H)	(I,S)
Aregawi,2014	0.048	0.216	0.323	0.223	**0.727**	0.012
Alhassan,2017	0.528	**0.657**	**0.638**	**0.879**	0.530	**0.746**
Bedane,2016	0.006	0.107	0.094	0.027	0.000	0.181
Appiah,2015	0.336	**0.620**	0.222	0.353	0.299	0.534
Landoh,2012	0.310	0.339	0.436	**0.633**	**0.722**	**0.743**
Muwanika,2017	0.043	0.547	0.175	**0.748**	0.449	**0.903**
Elipe,2007	0.074	**0.886**	0.012	**0.655**	0.590	**0.683**
Okech,2008	0.068	**0.603**	0.414	0.069	0.013	**0.949**

Table 11.3: Table with Pearson correlation coefficient r^2, between pairs among the three metrics, namely malaria incidence I, Hurst exponent H and Shannon entropy S. The three metrics were computed for three different time-windows, namely 24, 36 and 48 months. See also section 11.7. Results with $r^2 > 0.600$ are highlighted in bold.

In section 11.7 we present a more detailed comparison between 36-month averages with 24- and 48-month averages.

11.4 Autocorrelation function and stochastic memory in malaria empirical series

The autocorrelation function (ρ_k) behavior has been used with reasonable success in different research fields, from financial to hydrology, and climate data time series. It measures the linear relationship between two sequential values of a time series with a specific time lag k. The autocorrelation function (ρ_k) expresses the magnitude of that correlation between k lagged values:

$$\rho_k = \frac{\sum_{t=1}^{N-k}(x_t - \overline{x})(x_{t+k} - \overline{x})}{\sum_{t=1}^{N}(x_t - \overline{x})^2} \tag{11.6}$$

Figure 11.4 shows the autocorrelation function for each empirical case.

The algebraic decay of the empirical autocorrelation function ρ_k is strongly connected to the memory of stochastic processes such as long memory in the form of *Long Range Dependence* (LRD). The existence of LRD assumes the presence of stationarity in the time series. A memory parameter d is defined in relation to the slope of the autocorrelation function (ρ) decay. When $d > 0$ the term *persistent* defines the time series, with progressively larger values in time. In the opposite case we have $d < 0$ with the presence of *anti-persistence*, where positive values will tend to alternate with negative values and vice versa. Here, we borrow the concept as defined in reference [128]: *For $d < 0$ we have anti-persistence; i.e. positive values tend to be followed by negative values and vice versa.* In the special case of $d = 0$, the process will correspond to the presence of white noise, without evidence of autocorrelation, and corresponding to a pure Markovian process [128].

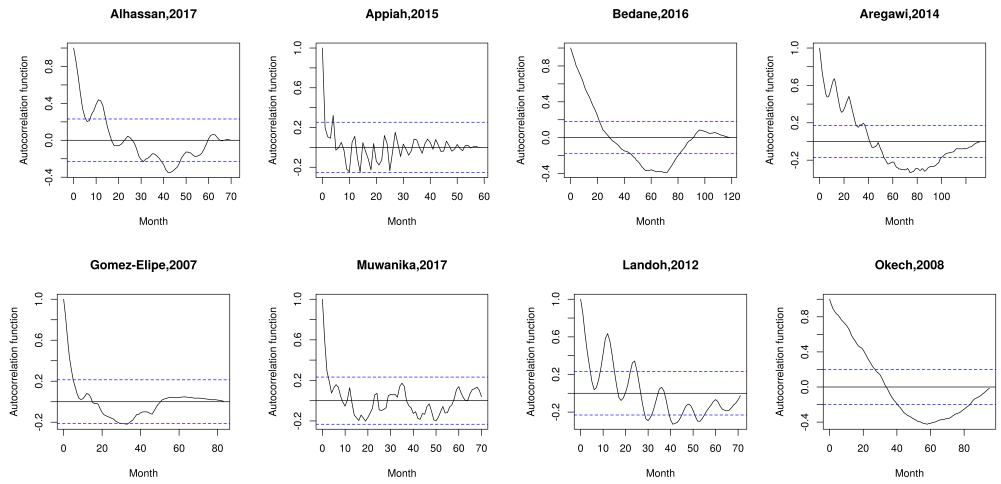

Figure 11.4: Malaria empirical series: Autocorrelation function from **(a)** Alhassan et al (Kasena Nankana municipality in Ghana, 2017) [12]. **(b)** Appiah et al (Ejisu-Juaben municipality in Ghana, 2015) [23], **(c)** Bedane et al (Kucha district in Ethiopia, 2016) [33], **(d)** Aregawi et al (Ethiopia, 2014) [24], **(e)** Gomez-Elipe et al (Karuzi in Burundi, 2007) [147], **(f)** Muwanika et al (Uganda, 2017) [267], **(g)** Landoh et al (Est Mono district in Togo, 2012) [209], **(h)** Okech et al (Kenya, 2008) [278].

The decay in time of the autocorrelation function ρ_k in a stochastic process correlates with the presence of memory persistence of past events in the present state of the system. In the case of fast ρ_k exponential decay the system memory will be short. With slower ρ_k decays (corresponding to a power law process) memory will be longer in relation to the presence of LRD.

For the present eight empirical time series the autocorrelation function ρ_k did reveal similar decay patterns. The ρ_k decay seems to deviate from exponential decay in most of the cases, what would have been expected in the case of a pure white noise Markovian process, thus suggesting the presence of memory persistence in all empirical series shown. The slow ρ_k decay is usually related to the presence of time series non-stationarity. In more than half of the presented examples, a persistent and undulatory expression of ρ_k values because of seasonality and periodicity in disease transmission overlaps with the background decaying trend.

11.5 A more quantitative malaria model for predicting effective gametocytemia

Figure 11.5 shows the result obtained for the I, H and S in the six different scenarios of gametocytemia levels. From figure 11.5 a) we observe that the six simulations cover all different incidence regimes, ranging from low incidence ($I \sim 0$) to high incidence ($I \sim 1$). For the same simulations, the Hurst exponent shown in figure 11.5 b), shows a clear decrease in the memory pattern with the increase of the gametocytemia level w_h.

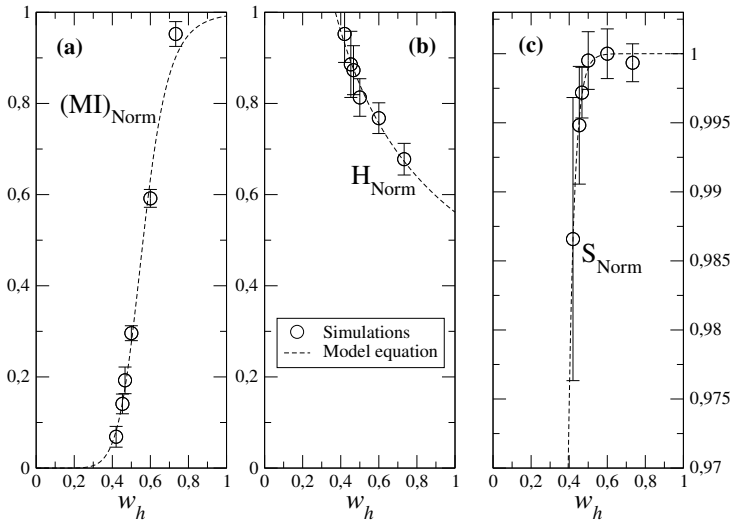

Figure 11.5: **(a)** Evaluation of the normalized continuous step function of malaria incidence in time series from model simulations at different settings of human-to-mosquito transmission efficiency ($0.420 < w_h < 0.733$). Hurst exponent is consistently close to 1.0 at phase transition (when $w_h \sim 0.420$) and decreasing to values ~ 0.5 (close to a random walk stochastic state) with higher values of $w_h \sim 0.700$ in higher disease transmission epidemic stage. For the same series **(b)** evaluation of Hurst exponent and **(c)** evaluation of Shannon entropy. In each case we simulated the agent model 10 times.

As for the dependence of the entropy S, shown in figure 11.5 c), we also observe a transition to large entropy values as w_h increases, but the transition seems much more abrupt. At phase transition near disease extinction, we have consistently found lower values of information entropy, clearly defining a stochastic process with long memory. At higher disease transmission rates (higher w_h) entropy became higher and more stable, evolving towards a short memory stochastic process. This dichotomy defines the nature of transmission stability and may be useful in defining how distant a malaria time series is from a situation of disease extinction.

11.5.1 Models for the three observables as function of parameter gametocytemia

Having described the values of the incidence, Hurst exponent and entropy obtained in six simulations with an agent model for malaria spreading, we now derive models for each one of these observables as a function of the central parameter in our approach, the gametocytemia level w_h.

Notice that, being a parameter which cannot be measured directly from empirical series of malaria incidence, a model from simulations relating the observables with this parameter, will enable us to predict the "effective" gametocytemia level (i.e., the transmissibility) in empirical cases.

To model the malaria incidence I we consider a continuous step function vary-

ing from $I = 0$ for w_h to $I = 1$ for $w_h = 1$:

$$I = \frac{1}{1 + \left(\frac{A}{w_h}\right)^{\alpha}} . \tag{11.7}$$

The dashed line in figure 11.5 a) shows a function given by equation 11.7 for $A = 0.562$ and $\alpha = 8.3$. Here, parameter A gives the gametocytemia level which brings the malaria incidence to the level of 50%, while the value of parameter α indicates how abrupt the transition from eradication to prevalence occurs when increasing the gametocytemia level.

Through inspection of figure 11.5 b), we choose to model the Hurst exponent H by a power law

$$H = B w_h^{\beta} , \tag{11.8}$$

for which the best fit yields $B = 0.56$ and $\beta = 0.58$. Here, parameters have no direct interpretation.

Finally, to address the abrupt transition observed for the entropy when the gametocytemia level varies, we choose a step function tunned by an exponential of w_h:

$$S = \frac{1}{1 + Ce^{-\gamma w_h}} , \tag{11.9}$$

with the best fit yielding $C = 10136$ and $\gamma = 32$. The parameter C tunes how low the entropy is for the extreme case of $w_h = 0$, while, similarly to parameter α, the γ controls how abrupt the transition from that minimum level to $S = 1$ occurs.

11.5.2 Prediction of effective gametocytemia in empirical cases

In relation to the prediction of "effective" gametocytemia in the empirical cases we first invert the functions defined in equations 11.7, 11.8 and 11.9 with respect to the gametocytemia level. We call to the values obtained estimates of gametocytemia, which in general do not coincide:

$$w_h^{(I)} = A\left(\frac{1}{I} - 1\right)^{-1/\alpha} , \tag{11.10a}$$

$$w_h^{(H)} = \left(\frac{H}{B}\right)^{-1/\beta} , \tag{11.10b}$$

$$w_h^{(S)} = -\frac{1}{\gamma}\log\left(\frac{1}{C}\left(\frac{1}{S} - 1\right)\right) . \tag{11.10c}$$

In the case that all three models to predict w_h retrieve the same value we can assume almost zero error (maximum consistency of the models). In general, there will be deviations between the three predictions for gametocytemia level. Therefore, we take as estimate $\hat{w}_h$ for the gametocytemia level the average of the three independent predictions, and the corresponding error $\sigma_{\hat{w}_h}$ the largest deviation of

the independent predictions from that estimate:

$$\hat{w}_h = \frac{1}{3}\left(w_h^{(I)} + w_h^{(H)} + w_h^{(S)}\right), \tag{11.11a}$$

$$\sigma_{\hat{w}_h} = \max\left(|\hat{w}_h - w_h^{(I)}|, |\hat{w}_h - w_h^{(H)}|, |\hat{w}_h - w_h^{(S)}|\right). \tag{11.11b}$$

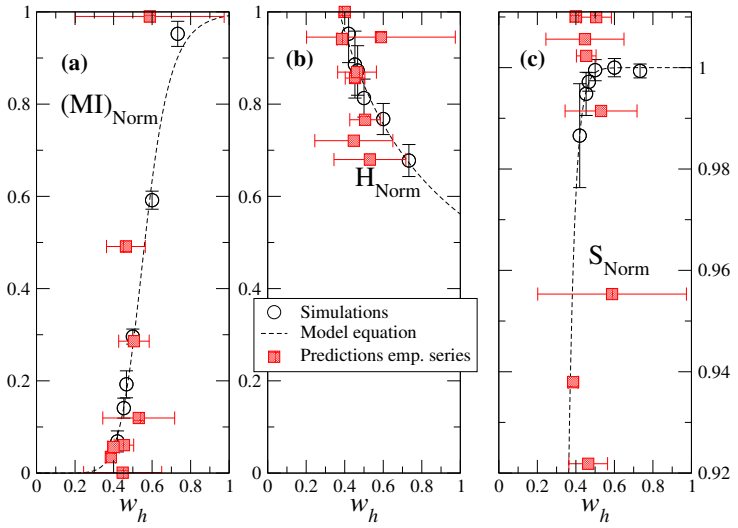

Figure 11.6: Repeating figure 11.5 with the effective gametocytemia for each empirical series (see text).

Figure 11.6 repeats the models drew for the simulations of the agent-based model, together with the estimate for the eight empirical series. While malaria incidence and the Hurst exponent retrieve reasonably acceptable predictions, the entropy seems to be very sensitive. The reason for this may be related with the fact that values of entropy are all very similar, making difficult to derive a numerical model which distinguishes between the different values. Moreover, the errors are typically large, showing a broad range of different predictions depending on which models are used – see equations 11.10.

In figure 11.6 we plot the curves in figure 11.5 together with estimates for the eight empirical cases. To predict the gametocytemia in empirical data sets, we assume that the range of values of I, H and S observed for the collection of empirical series, covers the range of admissible values between a minimum and a maximum. The same occurs for the collection of simulations we have done, but since there is no guarantee of proper calibration, minimum and maximum values may be different. Still, if assuming that simulations should cover the same range of possibilities in the empirical cases, we normalize the range of observed values in the empirical cases to the range observed for the simulations. This is a necessary step to predict effective gametocytemia, as explained below.

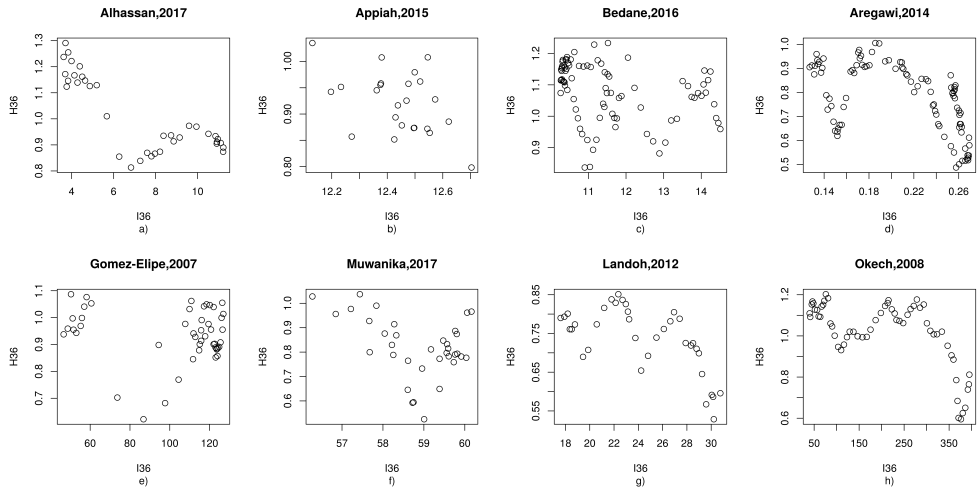

Figure 11.7: Illustration of how 36-month moving average malaria incidence in the x-axis, symbolized as I_{36} relates to 36-months Hurst exponent H_{36} in th y-axis in malaria empirical time series: **(a)** Alhassan et al (Kasena Nankana municipality in Ghana, 2017) [12]. **(b)** Appiah et al (Ejisu-Juaben municipality in Ghana, 2015) [23], **(c)** Bedane et al (Kucha district in Ethiopia, 2016) [33], **(d)** Aregawi et al (Ethiopia, 2014) [24], **(e)** Gomez-Elipe et al (Karuzi in Burundi, 2007) [147], **(f)** Muwanika et al (Uganda, 2017) [267], **(g)**Landoh et al (Est Mono district in Togo, 2012) [209], **(h)** Okech et al (Kenya, 2008) [278].

11.6 Qualitative analysis of Hurst exponent and entropy: case-by-case description

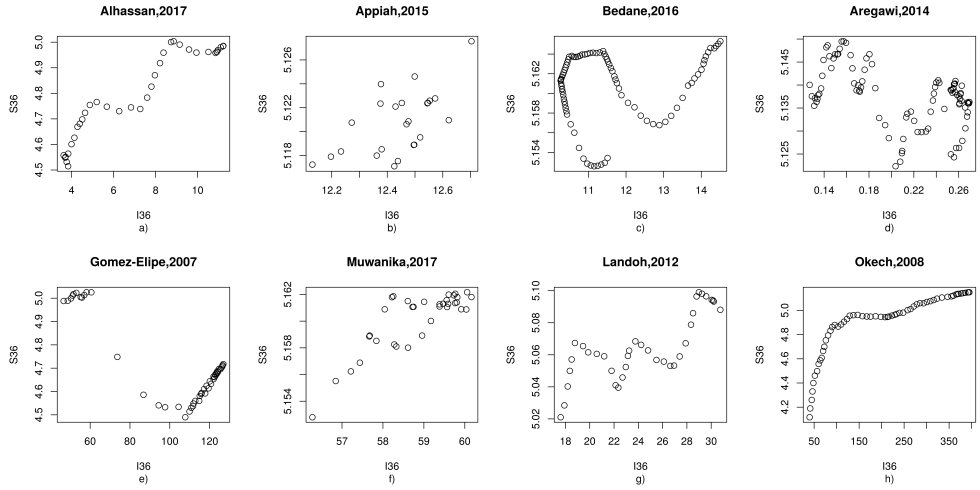

Figure 11.8: Illustration of how 36-month moving average malaria incidence in the x-axis, symbolized as I_{36} relates to 36-months entropy S_{36} in th y-axis in malaria empirical time series: **(a)** Alhassan et al (Kasena Nankana municipality in Ghana, 2017) [12]. **(b)** Appiah et al (Ejisu-Juaben municipality in Ghana, 2015) [23], **(c)** Bedane et al (Kucha district in Ethiopia, 2016) [33], **(d)** Aregawi et al (Ethiopia, 2014) [24], **(e)** Gomez-Elipe et al (Karuzi in Burundi, 2007) [147], **(f)** Muwanika et al (Uganda, 2017) [267], **(g)** Landoh et al (Est Mono district in Togo, 2012) [209], **(h)** Okech et al (Kenya, 2008) [278].

Alhassan (2017)

In the Alhassan malaria time series (Kasena Nankana municipality in Ghana, 2017) [12] one can see a declining trend in malaria incidence in the form of a decreasing moving average of 36 months (I_{36}), from $\sim$ 11 to $\sim$ 4 cases per 100 inhabitants, per year [*phy*], despite the small final outbreak in the last 6 months. Consistent with the declining trend in I_{36} we may also witness a decreasing trend in S_{36} as well as a rising trend in H_{36} after month 55. In this case, the behavior of both Hurst exponent and entropy in the preceding 36 months is well correlated with the malaria incidence trend – see figures 11.7, 11.8 and 11.9.

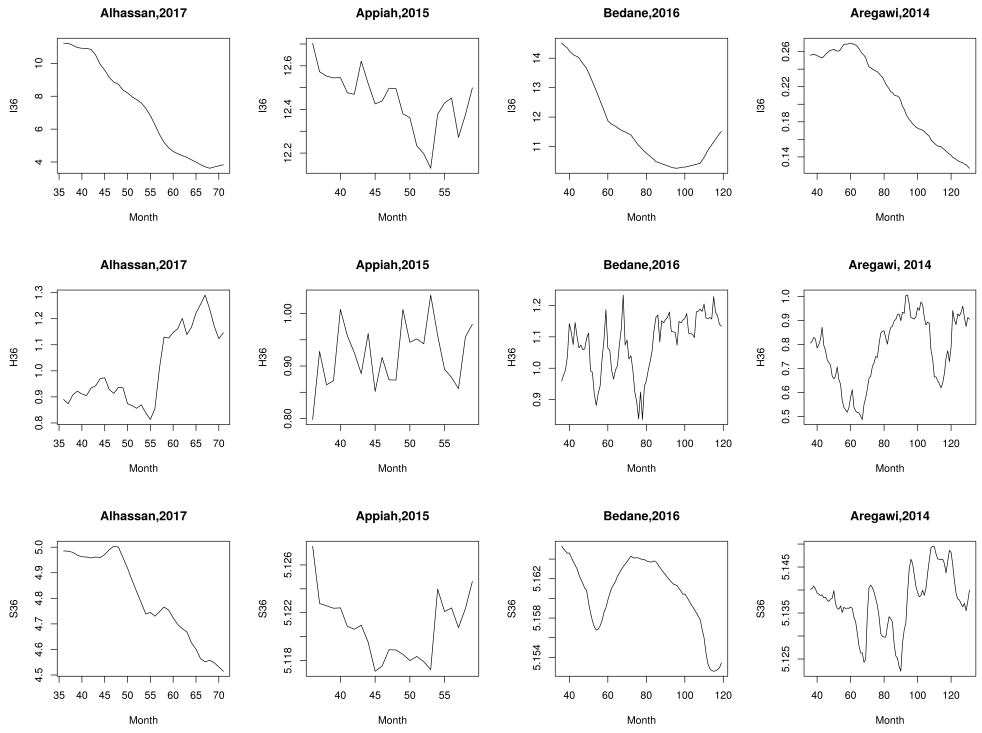

Figure 11.9: Comparative depiction of I_{36} (top), H_{36} (middle) and S_{36} (bottom) for (from left to right) Alhassan et al (Kasena Nankana municipality in Ghana, 2017) [12], Appiah et al (Ejisu-Juaben municipality in Ghana, 2015) [23], Bedane et al (Kucha district in Ethiopia, 2016) [33], and Aregawi et al (Ethiopia, 2014) [24].

Appiah (2015)

By looking at the Appiah malaria time series (Ejisu-Juaben municipality in Ghana, 2015) [23] it is detectable an irregular oscillation of malaria incidence superimposed on a stable trend in malaria incidence $\sim$ 12.4 cases *phy*, with a range between a peak incidence of $\sim$ 20 cases *phy* at 32 months, and an all-low of $\sim$ 5 cases *phy* at 18 months – see figure 11.1. Consistent with the initial declining trend in I_{36} until month 53 we may also witness a declining trend in S_{36} as well as a rising trend in H_{36}. In the present case, the behavior of both Hurst exponent and entropy in the initial 53 months is well correlated with the malaria incidence trend – see figures

11.7, 11.8 and 11.9.

Bedane (2016)

In relation to the Bedane malaria time series (Kucha district in Ethiopia, 2016) [33] we can witness an initial declining trend in malaria incidence in the form of a decreasing moving average of 36 months (I_{36}) lasting until month 98, from $\sim$ 15 cases *phy*, to $\sim$ 10 cases *phy*, followed by a small final upsurge in I_{36} to $\sim$ 11.5 cases *phy*. Consistent with the initial declining trend in I_{36} until month 98 we may also witness a delayed declining trend in S_{36} from months $\sim$ 70 to $\sim$ 115 as well as a rising trend in H_{36} from months $\sim$ 60 to $\sim$ 80, despite the presence of a superimposed irregular oscillatory noise pattern. In this case, the behavior of both Hurst exponent and entropy in the initial $\sim$ 98 months partially shows some degree of correlation with the global malaria incidence trend – see figures 11.7, 11.8 and 11.9.

Aregawi (2014)

In the Aregawi malaria time series (Ethiopia, 2014) [24] we can witness an initial small upper trend in malaria incidence in the form of an increasing moving average of 36 months (I_{36}) in the initial $\sim$ 62 months, with $\sim$ 0.26 cases per 100 inhabitants, per year, declining thereafter to less than $\sim$ 0.12 cases per 100 inhabitants, per year.

Consistent with the initial small upper trend in I_{36} we also witness a declining trend in H_{36} after month 62. In this case, entropy revealed an atypical behavior, peaking a littler later at month $\sim$ 72. Along with a declining trend in I_{36} after month 62, one can witness a consistent rise in H_{36} lasting to the end of the time series despite a transitory fall at month $\sim$ 105, with a rapid recovery at month $\sim$ 114. In Aregawi time series the behavior of S_{36} was more unpredictable, with a more delayed response. This fact may be somehow related to the low malaria incidence in the time series.

However, in the present case, the behavior of the Hurst exponent in the form of a 36-months moving average (H_{36}), in the initial 65 months, still reveals some degree of correlation with the global malaria incidence trend – see figure 11.9. At such low levels of malaria incidence ($\sim$ 0.2 *phy*) this behavior could be interpreted as a possible outlier result – see figures 11.7, 11.8 and 11.9.

Gomez-Elipe (2007)

The Gomez-Elipe time series (Karuzi in Burundi, 2007) [147] is quite different from the remaining empirical examples. It shows a consistent stable pattern of malaria incidence below 110 cases *phy*, until month 45, peaking to $\sim$ 500 cases *phy*, around month 48, with a rapid fall to $\sim$ 60 cases *phy* at month 56, and with a slower decline thereafter to a final value of $\sim$ 20 cases *phy* – see figure 11.1. The

36-months malaria incidence (I_{36}) reveals a consistent upward trend peaking at month 64, with a downward pattern thereafter.

In this case, we find a persistent oscillatory behavior in the value of H_{36} during the entire time series, usually ranging above 0.9. But, coinciding with the outbreak in malaria incidence at month 48 it is possible to see a sudden fall in H_{36} to values close to 0.6 (closer to random noise). Entropy in the form of a 36-months moving average (S_{36}) reveals a parallel correlated behavior to I_{36} from month 48 onwards. Despite the presence of a superimposed oscillatory noise pattern, the behavior of the Hurst exponent and entropy also shows some degree of correlation, with the malaria incidence trend, globally – see figures 11.7, 11.8 and 11.10.

Muwanika (2017)

In the Muwanika malaria time series (Uganda, 2017) [267] we may witness an initial small upper trend in malaria incidence in the form of a mild increase in the 36 months moving average (I_{36}) during the initial $\sim$ 47 months, with a peak at $\sim$ 60 cases *phy*, declining thereafter to $\sim$ 56 cases *phy*.

Consistent with the initial small upper trend in I_{36} until month 47 we may also witness a declining trend in H_{36} from an initial value $\sim$ 0.9 to $\sim$ 0.5 close to month 45. From month 47 onwards, H_{36} consistently increases to values close to 1.0 (long memory process) in parallel with the steady decline in I_{36}. In the present case, entropy, in the form of a 36-month moving average (S_{36}), reveals a consistent decreasing trend, shadowing the decline in I_{36} beginning at $\sim$ month 47. In the Muwanika time series, the behavior of H_{36} and S_{36} is globally correlated with the behavior of I_{36} in time – see figures 11.7, 11.8 and 11.10.

Landoh (2012)

The Landoh malaria time series (Est Mono district in Togo, 2012) [209] reveals a consistent upper trend in malaria incidence in the form of a mild increase in the 36 months moving average (I_{36}) during the whole time series, ranging from the initial $\sim$ 18 cases *phy*, to a peak at $\sim$ 30 cases *phy* in month 72.

Consistent with the steady upper trend in I_{36} during the entire time series, we find a declining trend in the 36-months moving average of Hurst exponent (H_{36}) from a peak of $\sim$ 0.85 at month 47, to an all-low value of $\sim$ 0.55. Along with this downward trend in H_{36}, there is a consistent increase in entropy in the form of a 36-months moving average (S_{36}), during the entire time series, despite its undulatory behavior. In the Landoh time series, the behavior of H_{36} and S_{36} is reasonably well correlated with the behavior of I_{36} in time – see figures 11.7, 11.8 and 11.10.

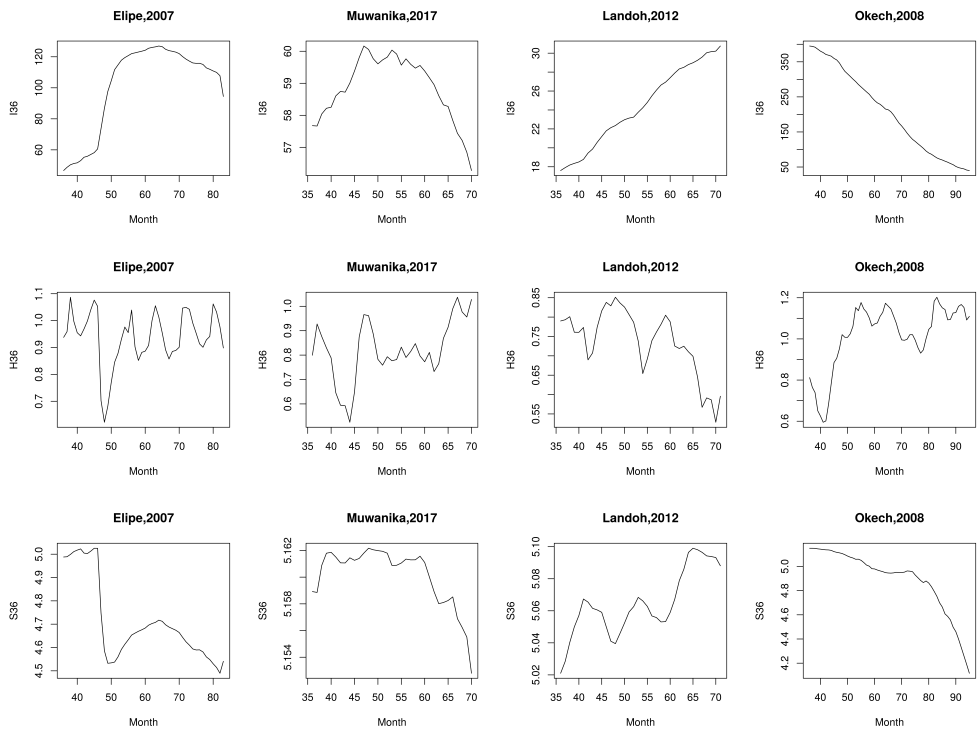

Figure 11.10: (Cont. figure 11.9): Gomez-Elipe et al (Karuzi in Burundi, 2007) [147], Muwanika et al (Uganda, 2017) [267], Landoh et al (Est Mono district in Togo, 2012) [209], Okech et al (Kenya, 2008) [278].

Okech (2008)

In a similar form, but with an opposite trend to the Landoh time series, the Okech time series (Kenya, 2008) [278] also reveals a steady decreasing trend. In the Okech time series, malaria incidence consistently decreases from an initial peak of ~ 400 cases *phy*, to a final value close to 50 cases *phy*.

Consistent with the steady downward trend in I_{36} during the entire time series, we find an upper trend in the 36-months moving average of Hurst exponent (H_{36}) from an all-low of ~ 0.6 at month 42, to a peak of ~ 1.2 at month 82. Along with this upper trend in H_{36}, there is a consistent decrease in entropy in the form of a 36-months moving average (S_{36}), during the whole time series. In the Okech time series, the behavior of H_{36} and S_{36} is also quite correlated with the behavior of I_{36} in time – see figures 11.7, 11.8 and 11.10.

11.7 Inspecting the robustness of 36-month averages

The results in the previous section were derived using average values in windows of 36 months, i.e. three years. While the number of points is small, it covers three annual cycles. As it is known – and as shown in chapter 10 and Appendix D – malaria spreading shows periodic behavior following annual seasonality.

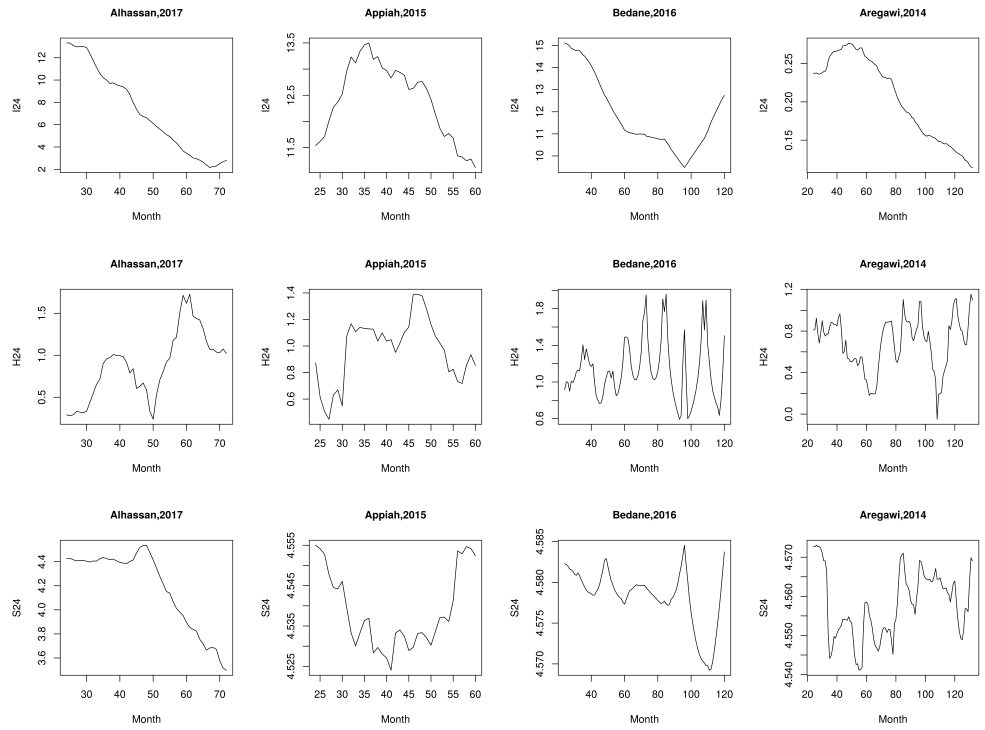

Figure 11.11: Comparative depiction of I_{24} (top), H_{24} (middle), S_{24} (bottom) for (from left to right): Alhassan et al (Kasena Nankana municipality in Ghana, 2017) [12], Appiah et al (Ejisu-Juaben municipality in Ghana, 2015) [23], Bedane et al (Kucha district in Ethiopia, 2016) [33], and Aregawi et al (Ethiopia, 2014) [24].

To evaluate the robustness of the estimated values for malaria incidence, Hurst exponent and entropy, shown in the previous section, we present next the results for estimates obtained from two and four annual cycles, i.e. 24 and 48 months respectively. Results are shown in figures 11.11 to 11.14.

11.8 Discussion and conclusions

The utility of time series models is still a long way from becoming standard practice in malaria prevention. Differences in climate and geographic factors between world regions act as confounding factors in the strictly mathematical time series approach, lowering malaria forecast precision. In recent years the Box-Jenkins theory has become a consistent development in malaria forecasting [2, 46, 122, 220]. However, little attention has been devoted to Hurst theory, information entropy, short and long memory stochastic processes and long-range dependence. It is remarkable that Hurst theory was initially implemented in the field of hydrology, as malaria surges are clearly correlated with rainfall, temperature and climate seasonality [169].

Malaria epidemic time series consistently present different memory patterns depending on disease transmission intensity. By comparing time series from our model simulations to real data malaria time series from different parts of the

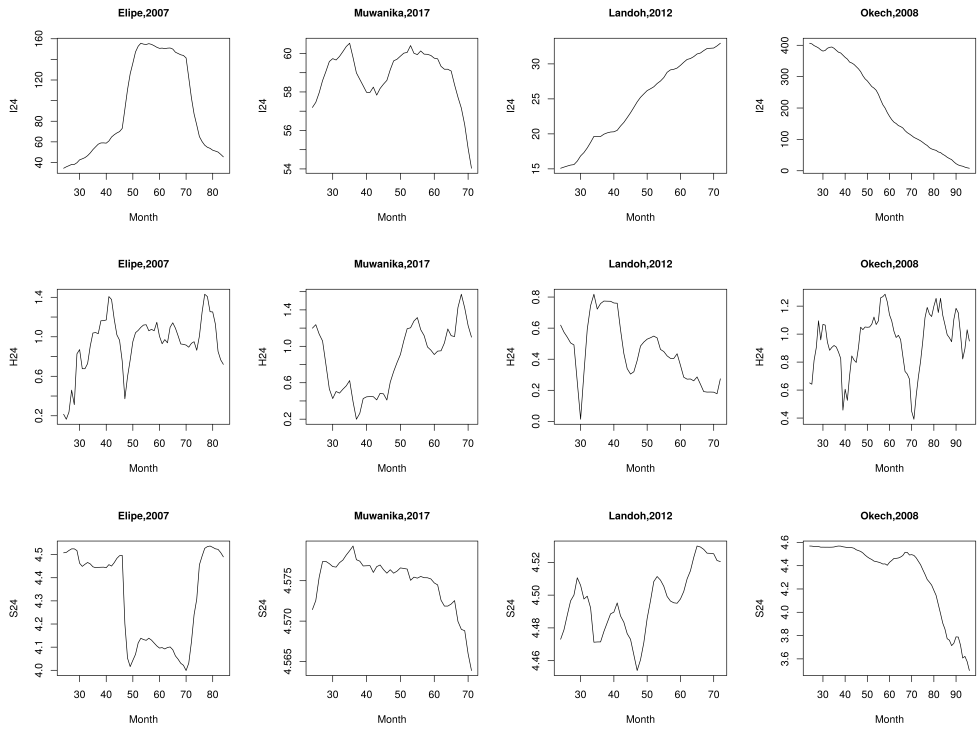

Figure 11.12: (Cont. figure 11.11): Gomez-Elipe et al (Karuzi in Burundi, 2007) [147], Muwanika et al (Uganda, 2017) [267], Landoh et al (Est Mono district in Togo, 2012) [209], and Okech et al (Kenya, 2008) [278].

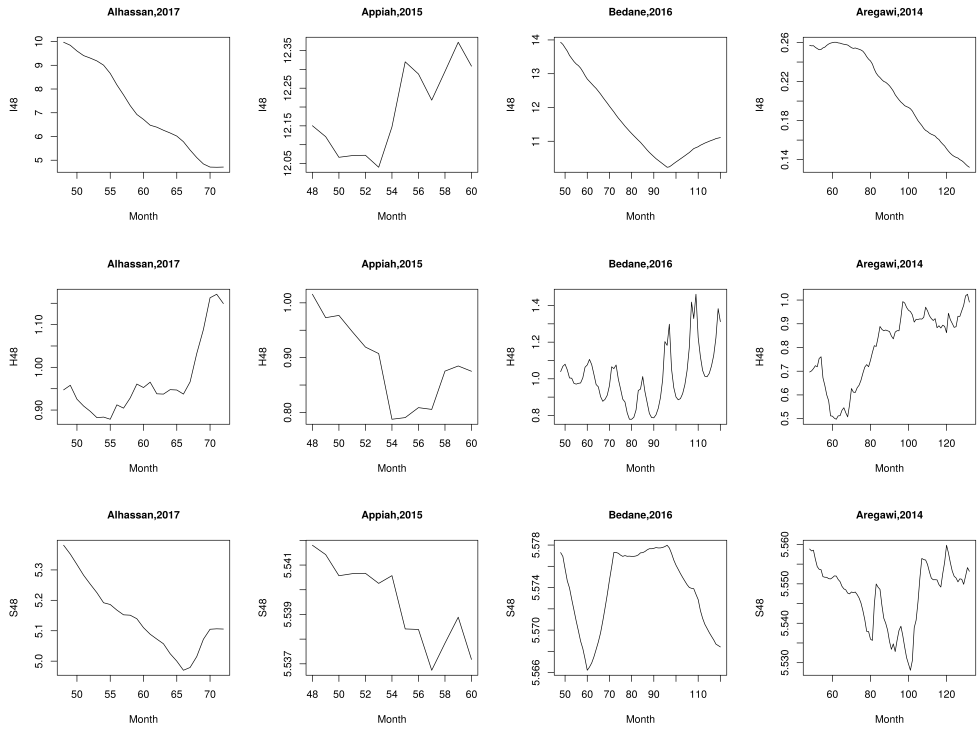

Figure 11.13: Comparative depiction of I_{48} (top), H_{48} (middle), S_{48} (bottom) for (from left to right): Alhassan et al (Kasena Nankana municipality in Ghana, 2017) [12], Appiah et al (Ejisu-Juaben municipality in Ghana, 2015) [23], Bedane et al (Kucha district in Ethiopia, 2016) [33], and Aregawi et al (Ethiopia, 2014) [24].

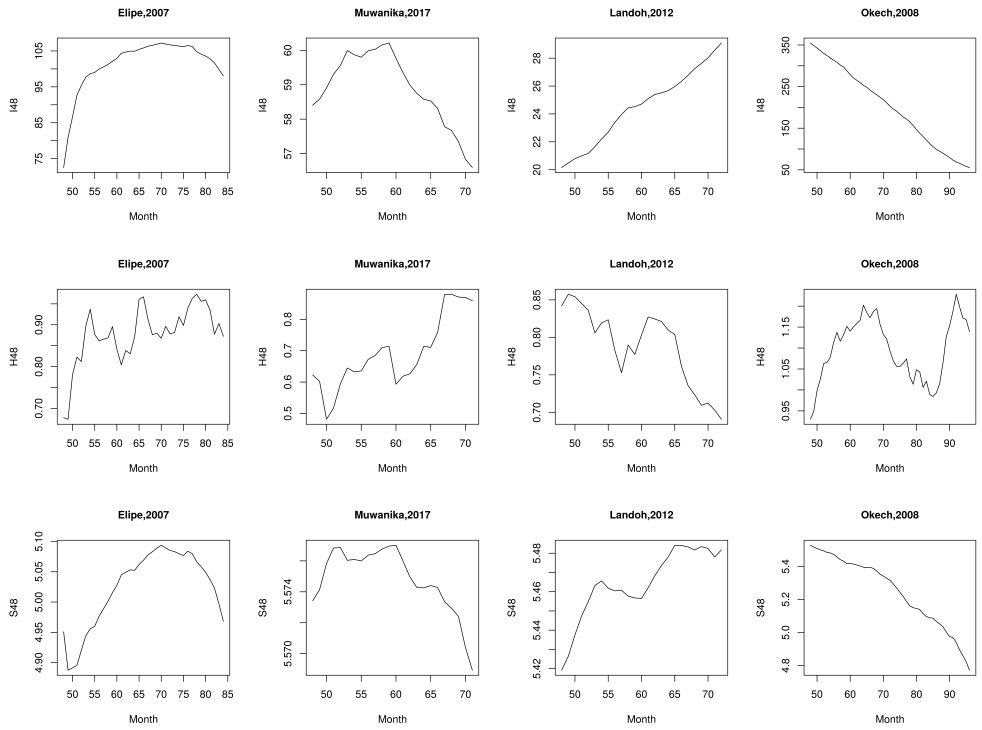

Figure 11.14: (Cont. figure 11.13): Gomez-Elipe et al (Karuzi in Burundi, 2007) [147], Muwanika et al (Uganda, 2017) [267], Landoh et al (Est Mono district in Togo, 2012) [209], and Okech et al (Kenya, 2008) [278].

world, it was possible to obtain a better definition of epidemic stability according to disease transmission efficiency, from field data time series results. In stationary time series, long memory processes have been related to the presence of long-range dependence (LRD) between present and past results [150].

At low H-to-M disease transmission intensity, time series patterns were consistent with the presence of LRD. However, at high disease transmission intensity, this pattern reverted to a low-memory process. By looking at the present model time series with changing w_h, one could witness significant differences in stochastic memory patterns. Also, in the presented empirical time series, Hurst exponent and entropy correlated reasonably well with different epidemic growth rates. A similar pattern was evident when looking at malaria incidence correlation with Hurst exponent and Shannon entropy. As these parameters may be affected by the time series length, their use in a normalized setting should be considered as a reliable option.

By using the standardized forms of Hurst exponent (H_{36}) and entropy measurement (S_{36}) it was possible to define the type of memory of stochastic malaria incidence time series with greater precision. This fact may be of significant relevance as both parameters may become additional and useful tools in malaria forecasting.

In this chapter we used a 36-month standard time length for a specific analysis. We considered it a compromise between a shorter time length (24 months) with

less information available to Hurst exponent estimation, and a longer time length (48 months) with less data available for analysis in shorter empirical time series, such as the series of Appiah et al [23] (60 months). The standard method to estimate Hurst exponent, based in the quotient R/S [85, 127, 128, 131, 150, 192], could be substituted by other alternative methods, namely the generalized Hurst exponent (GHE).

GHE is a modern approach to Hurst analysis with some specific advantages, applied in the analysis of complex and inhomogeneous time series in electrocardiography (ECG) signals, and it has been shown to be a promising tool for the study of atrial fibrillation (AF) organization from the surface ECG [178]. It is usually recommended in the presence of short time series where it has been shown to be slightly more efficient. It has been used mainly in the assessment of stability of financial firms applied to the stock market. However, GHE does not assign equal importance to different events in the timeline. It usually tends to overestimate more recent events reducing the significance of older past events. For this reason, we chose the standard estimation method.

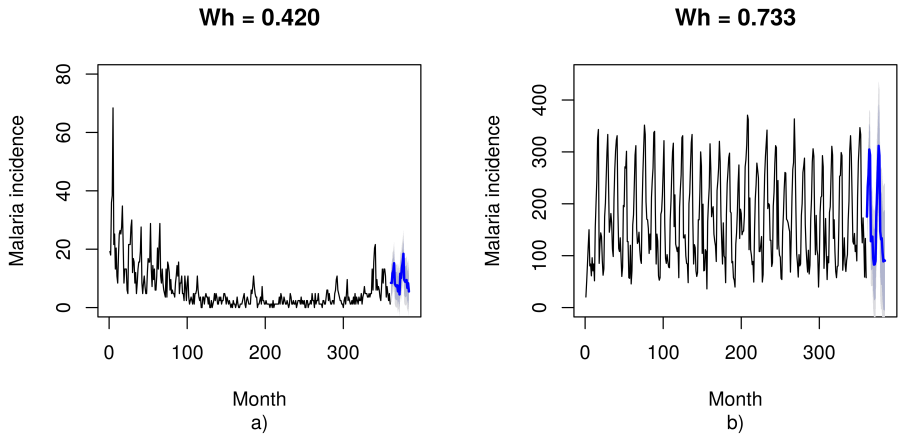

Figure 11.15: Model simulation (black) and SARIMA model forecasting (blue) of model simulation at phase transition: (a) Low human-to-mosquito transmission efficiency ($w_h = 0.420$); (b) High human-to-mosquito transmission efficiency ($w_h = 0.733$).

Being a standard approach in time series analysis, we also performed SARIMA models for the simulation and empirical cases. Figures 11.15 and 11.16 show two illustrative cases of each. In the case of the seasonal component, the regressive component of the SARIMA term vanishes in Okech model and we have $(P, D, Q) = (0, 1, 1)$. On the contrary, the seasonal SARIMA model of Landoh is purely a regressive model with one time differencing, and we have $(P, D, Q) = (1, 1, 0)$. SARIMA forecast of both empirical series is presented in figure 11.16, while its equations and coefficients are available in tables D.5 and D.6 in Appendix D. These results will be presented with further detail in the appendix concerning Box-Jenkins theory, ARIMA and SARIMA models – see Appendix D.

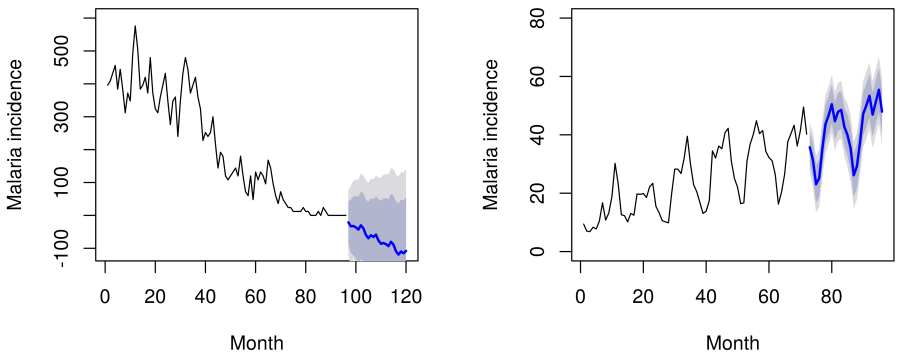

Figure 11.16: **(a)** Empirical time series (black) and SARIMA model forecasting (blue) from Okech,2008 [278] empirical time series along with declining malaria incidence. SARIMA forecast predicts rapid disease elimination evolving towards negative values. **(b)** Empirical time series (black) and SARIMA model forecasting (blue) from Landoh,2012 [209] empirical time series along with a steady increase in malaria incidence. SARIMA forecast predicts a trend of progressive disease spreading.

Overall, our results seem to indicate that in malaria incidence time series, long-range dependence may occur close to phase transition between epidemic stability and disease elimination. The presence of these long-memory stochastic processes in malaria incidence time series could become an additional and useful tool in the early detection of epidemic resurgence, as well as a potential improvement in malaria prevention strategy.

Chapter 12

Model validation

12.1 Introduction

Validation of theoretical or computational models stands as one of the most demanding tasks in model building. The global soundness of the model algorithm should be considered a critical goal in the validation process, as models may fail because of deep concept faults that are not apparent from the start. Defining adequately the model parameters stand as a crucial step in building realistic models. The choice of adequate parameters should be tested in different model scenarios, while modulating its values in accordance with the expected outcome from model simulations. And when the model output consists in simulated time series malaria data, validation procedures may require comparison with the outcome of similar empirical real-world time series. For quality strategy planning, an accurate analysis of model procedures will be essential. Computational models pretend to create a valid representation of the real world. Assuming the *Occam´s razor* perspective, a simpler model will usually be more effective than a high complexity model, for that purpose. However, real world behavior may occur as a non-linear, stochastic, multi-dimensional and sometimes chaotic process.

Several inconsistencies in designing a model may result from poor insight into the model dynamics. Model parameters are to be estimated beforehand, frequently in the absence of consistent empirical data. The interaction between different model parameters must be defined in advance during the conception phase, and later on verified, calibrated and corrected, in order to define a satisfactory and realistic model design.

12.2 Model validation methodology

In the present dissertation, model validation required multiple validating procedures. The model algorithm was implemented with a C++ code that was thoroughly debugged, paying close attention to details, while being checked for incon-

sistencies in the expected output. As the model procedure included dedicated subroutines based on specific model assumptions, a detailed framework was adopted for verification of intermediate results during the simulation procedure. This way, model inconsistencies were detected and corrected. A graphical methodology was adopted for comparison of simulated and empirical time series. Six different empirical malaria time series were used as standards, in relation to six model simulations with similar disease transmission coefficients. Model simulations were defined in a 30-years' time frame; a smaller fraction of the whole simulation was considered for compared analysis. The graphical method also included an evaluation of autocorrelation function, as well as of the cumulative probability distribution function of malaria incidence in the form of box plot data presentation. Deterministic quantitative measures were also used in the form of conventional statistical tests such as the Kolmogorov-Smirnov test, and other alternative but no less powerful methods such as the Anderson-Darling and the Kuiper test. Other deterministic quantitative measures were also used for error estimation procedure, such as the mean absolute error (MAE), the mean absolute percentage error (MAPE), the root mean squared error (RMSE), and Theil´s inequality coefficient (U) – see equation 12.1.

$$U = \frac{\sqrt{\frac{1}{n}\sum_{i=1}^{n}\left(y_i - \hat{y}_i\right)^2}}{\sqrt{\frac{1}{n}\sum_{i=1}^{n} y_i^2} + \sqrt{\frac{1}{n}\sum_{i=1}^{n} \hat{y}_i{}^2}} \tag{12.1}$$

An extensive model validation procedure was defined with the aim of comparing time series from model simulations with real world malaria incidence empirical time series.

The following comparative metrics were used:

a) Comparative graphical presentation of malaria incidence between model simulation and real-world empirical time series with seasonal periodicity synchronization;
b) Cumulative probability distribution function (CDF) comparison between model simulation and empirical time series;
c) Study of auto-correlation and cross-correlation functions of model simulation and empirical time series;
d) Error estimation between model and empirical time series with MAE, MAPE and RMSE;
e) Statistical measures with Kolmogorov-Smirnov, Anderson-Darling, and Kuiper testing;
f) Theil´s inequality coefficient (U) comparing malaria incidence in model simulation and empirical time series;

Model consistency was evaluated with several parameters from classical Ross-Macdonald theory (EIR, R_0, a, b and c). Several questions were asked: Were the results consistent with model expectations?
Were the results stable and consistent in all simulations with the same parameter

specifications?
Model calibration – how was it done?

Model simulations were analyzed with small changes in the model initial parameters correlating changes in gametocytemia and ivermectin treatment with malaria incidence. Validation of the influence of ivermectin in model stability was defined by looking at mosquito survival probability distribution and its relation to the time of parasite latency inside the mosquito, as well as to the direct mortality from ivermectin. Simulation of mosquito survival distribution was compared to empirical mosquito survival results from previous research [61].

Outcome was also evaluated with different initial conditions for consistency of results – see Appendix C.

12.3 Model verification and calibration

It is the aim of model verification to check the consistency of a computer simulation model, as well as of all its related mathematical and logical internal processes. In the present model, verification was implemented by using multiple settings of model parameters in different biological scenarios, while checking the likelihood of the expected simulation outcome. Unexpected data output as well as illogical results were cross-checked for incongruencies in the model algorithm. This procedure was applied to different disease transmission scenarios, at different levels of model parameters, dedicating special attention to the consistency of simulation outcomes, and assuring that those results were adequate to model predictions. Intermediate results were also checked and compared to expected values from the original conceptual model.

12.4 Empirical time series validation

A significant group of 5 empirical malaria time series was used in model validation – see table 12.1. Each empirical time series was matched to a single model simulation presenting a similar average value of malaria incidence, thus assuming that human-to-mosquito transmission efficiency (w_h) was equivalent in both series. From the 30-years-long time sequence of all model simulations, an identical duration time sequence was selected for testing purposes, and compared to the matching empirical series, while synchronizing for seasonal periodicity. This way it was possible to test both time series in terms of matching graphical differences, inequality scores, and cumulative probability distribution curves. The empirical malaria time series from Ferrão,2017, previously presented in section 7.4, was the only one of the five with original results presented in the form of weekly malaria incidence, and was also included here for comparison purposes. The four remaining empirical time series had original results presented in the form of monthly malaria

time incidence. Malaria incidence results were recalculated in order to present final results in the form of annual malaria incidence per 100 inhabitants (*phy*) – see table 12.1.

Empirical series	**Duration**	**Empirical malaria incidence**
	Months	*phy* (±SE)
Landoh,2012	72	21.7 (±1.2)
Ganguly,2016	72	40.3 (±2.7)
Alhassan,2017	72	7.6 (±0.7)
Chirombo,2020	156	7.3 (±0.4)
Ferrão,2017	108	3.9 (±0.1)

Table 12.1: Empirical time series and average malaria incidence.

Empirical series	**Equivalent model**	**Model malaria incidence**
	w_h	*phy* (±SE)
Landoh,2012	0.433	19.2 (±1.2)
Ganguly,2016	0.480	41.9 (±2.5)
Alhassan,2017	0.413	7.9 (±0.6)
Chirombo,2020	0.420	7.5 (±0.4)
Ferrão,2017	0.427	3.7 (±0.1)

Table 12.2: Average malaria incidence in empirical time series and model simulations with similar human-to-mosquito transmission efficiencies: $0.413 < w_h < 0.480$.

Empirical series	**Equivalent model**	**MAE**	**MAPE**	**RMSE**
	w_h	*	%	*
Landoh,2012	0.433	7.567	0.384	10.042
Ganguly,2016	0.480	15.2	0.503	20.2
Alhassan,2017	0.413	4.240	6.586	5.523
Chirombo,2020	0.420	3.974	1.253	5.260
Ferrão,2017	0.427	1.852	0.547	2.483

Table 12.3: Quantitative error estimation (mean absolute error, mean absolute percentage error, and root mean square error) concerning the difference between empirical time series and model simulations with similar human-to-mosquito transmission efficiencies: $0.413 < w_h < 0.480$.

* Metrics – Annual malaria incidence per 100 inhabitants

12.4.1 Landoh,2012

In 2012, Landoh presented *P.falciparum* malaria results from the Est Mono district, Togo, during a time interval between 2005 and 2010 [209]. The covered region spreads over an area of 2,474 square kilometers with a population that was estimated at 89,060 inhabitants during the year 2010. The climate is generally tropical and presents two rainy seasons, the first lasting from April to July, and the second one lasting from September to November, with an average monthly

Empirical series	**Equivalent model**	**Kolmogorov-Smirnov**	**Theil**
	w_h		U
Landoh,2012	0.433	0.194	0.220
Ganguly,2016	0.480	0.111	0.217
Alhassan,2017	0.413	0.222	0.289
Chirombo,2020	0.420	0.141	0.301
Ferrão,2017	0.427	0.220	0.278

Table 12.4: Quantitative statistical measures (Kolmogorov-Smirnov test, and Theil's inequality coefficient – U) in relation to the difference between probability distribution curves of empirical time series and model simulations with similar human-to-mosquito transmission efficiencies: $0.413 < w_h < 0.480$.

Empirical series	**Equivalent model**	**Anderson-Darling**	**Kuiper**
	w_h		
Landoh,2012	0.433	0.030	0.236
Ganguly,2016	0.480	0.018	0.181
Alhassan,2017	0.413	0.037	0.361
Chirombo,2020	0.420	0.008	0.276
Ferrão,2017	0.427	0.017	0.329

Table 12.5: Quantitative statistical measures (Anderson-Darling and Kuiper tests) in relation to the difference between probability distribution curves of empirical time series and model simulations with similar human-to-mosquito transmission efficiencies: $0.413 < w_h < 0.480$.

precipitation of 79 mm (±3.1 mm) and an average annual precipitation of 949 mm (±37.4 mm). Malaria transmission is seasonal, with peaks related to the rainfall periods. The average malaria incidence (MI) – 21.7 annual malaria cases per 100 inhabitants – was obtained from the 6-years long empirical time series [209].

In figure 12.1 we can find evidence of a strong similarity between the empirical time series from Landoh (2012) and a model simulation with human-to-mosquito transmission efficiency ($w_h = 0.433$). This similarity is further supported by the presence of periodic seasonal synchronization in both time series, by using a bootstrap model simulation partial time series lasting 72 months – from month 247 to 318 – from a total of 360 months of available simulation.

Also, by looking at the cumulative probability distribution function (CDF) of both time series, it is noticeable that both functions reveal very close cumulative probability distributions – see figure 12.2 a).

This notion is also supported by close probability distribution violin plots of both time series. In figure 12.3 one may also notice the presence of close similarity in autocorrelation functions in both time series.

Quantitative error estimation

When using quantitative error estimation to compare the empirical time series from Landoh (2012) and a synchronized partial time series from a similar model

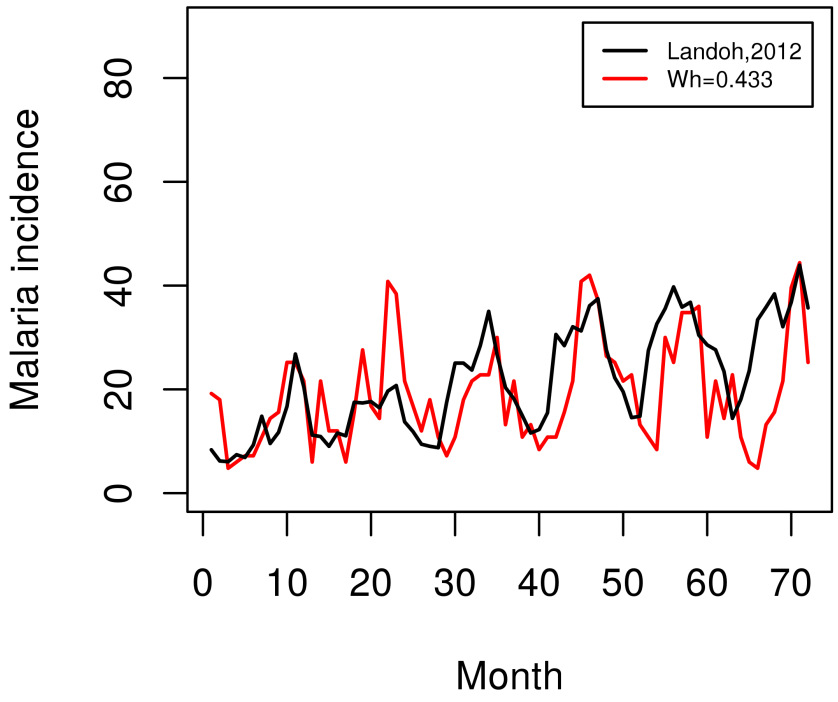

Figure 12.1: Monthly malaria incidence empirical time series from Landoh,2012 (black) [209] and model simulation with human-to-mosquito transmission efficiency $w_h = 0.433$ (red).

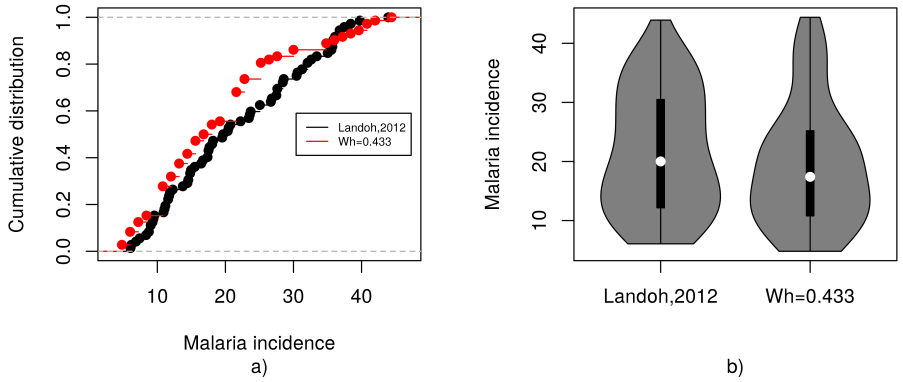

Figure 12.2: **(a)** Cumulative probability distribution curves from malaria empirical time series in Landoh,2012 (black) [209], and from model simulation with human-to-mosquito transmission efficiency $w_h = 0.433$ (red). **(b)** Monthly malaria incidence violin plot from empirical time series in Landoh,2012, and model simulation malaria incidence in empirical series from with human-to-mosquito transmission efficiency $w_h = 0.433$.

simulation with $w_h = 0.433$, one finds small differences between both time series of the mean absolute error (MAE), the mean absolute percentage error (MAPE) and the root mean squared error (RMSE) – see table 12.3.

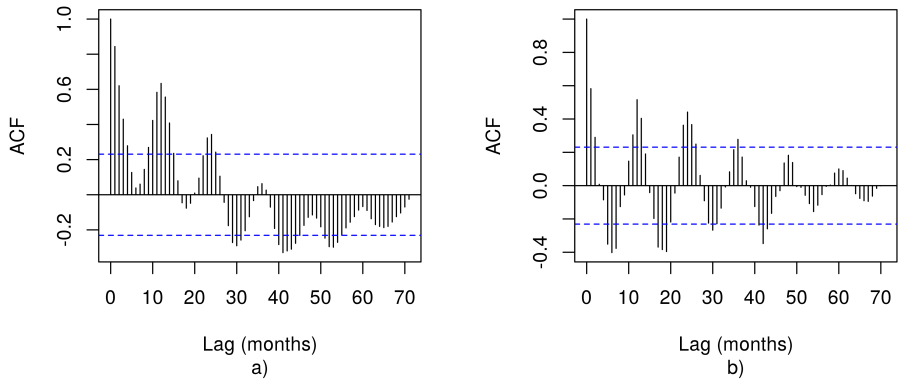

Figure 12.3: **(a)** Autocorrelation function from malaria empirical time series in Landoh,2012 [209]. **(b)** Autocorrelation function from model simulation with human-to-mosquito transmission efficiency $w_h = 0.433$.

Quantitative statistical measures

It is also possible to compare time series by using quantitative statistical measures of statistical proximity between the probability distribution function of two time series. In our model validation we found evidence of similarity between both time series in terms of the statistical measures variants that were used: a) Kolmogorov-Smirnov testing; b) Anderson-Darling testing; c) Kuiper testing.

Finally, we found a small estimated difference between the empirical time series from Landoh,2012 and the time series from a model with similar H-to-M transmission efficiency – $w_h = 0.433$ – in terms of Theil's inequality coefficient, with a acceptably small value of $U = 0.220$ – see tables 12.4 and 12.5.

12.4.2 Ganguly,2016

In 2016, Ganguly presented a malaria *P.vivax* and *P.falciparum* forecasting SARIMA model calibrated with data from Kolkata, India, during a 6 years' time interval between 2008 and 2013 [130]. The covered region spreads over an urban region in the county of Kolkata.

Malaria incidence empirical results were presented in the metrics of malaria monthly incidence per 100 inhabitants (phm), averaging 40.3 annual cases per 100 inhabitants – see table 12.2. Average malaria incidence (MI) in the model simulation was estimated at 41.9 annual cases per 100 inhabitants (phy), by using a bootstrap model simulation partial time series lasting 72 months – from month 213 to 284 – from a total of 360 months of available simulation – see table 12.2.

This was a very close result to Ganguly,2016 empirical time series – see tables 12.1 and 12.2.

This similarity is further supported by the presence of periodic seasonal synchronization in both time series, by using a bootstrap model simulation partial time series lasting 72 months – from month 247 to 318 – from a total of 360 months of available simulation.

In figure 12.4 we can find evidence of a strong similarity between the empirical time series from Ganguly (2016) and a model simulation with human-to-mosquito transmission efficiency ($w_h = 0.480$). This similarity is further supported by the presence of periodic synchronization of seasonality in both time series.

By looking at the cumulative probability distribution function (CDF) of both time series, it is noticeable that both functions reveal close cumulative probability distributions – see figure 12.5 a). This similarity is also documented in the comparative probability distribution violin plot of both time series as well as in figure 12.6 where it is possible to find a similar autocorrelation function in both time series.

Quantitative error estimation

By using quantitative error estimation to compare the empirical time series from Ganguly (2016) and a synchronized partial time series from a model simulation with $w_h = 0.480$, one finds small differences between both time series of the mean absolute error (MAE), the mean absolute percentage error (MAPE) and the root mean squared error (RMSE) – see table 12.3.

Quantitative statistical measures

It was also possible to compare both time series by using quantitative statistical measures that compare statistical proximity between two probability distribution functions. In the model validation procedure, we found small values concerning 3 statistical measures commonly used variants of this methodology: a) Kolmogorov-Smirnov testing; b) Anderson-Darling testing; c) Kuiper testing. The small differences found are consistent with a strong degree of similarity between the empirical time series from Ganguly (2016) and the time series obtained from the model simulation with $w_h = 0.480$.

Finally, we also evaluated the estimated difference between empirical (Ganguly,2016) and model simulation ($w_h = 0.480$) time series, in terms of Theil's inequality coefficient, finding a small value of $U = 0.217$ – see tables 12.4 and 12.5.

12.4.3 Alhassan,2017

In 2017, Alhassan presented a malaria ARIMA forecasting model based upon time series analysis of malaria results from Kasena Nankana municipality in Ghana, during a 6 years' time interval, between 2010 and 2015 [12]. The covered region has

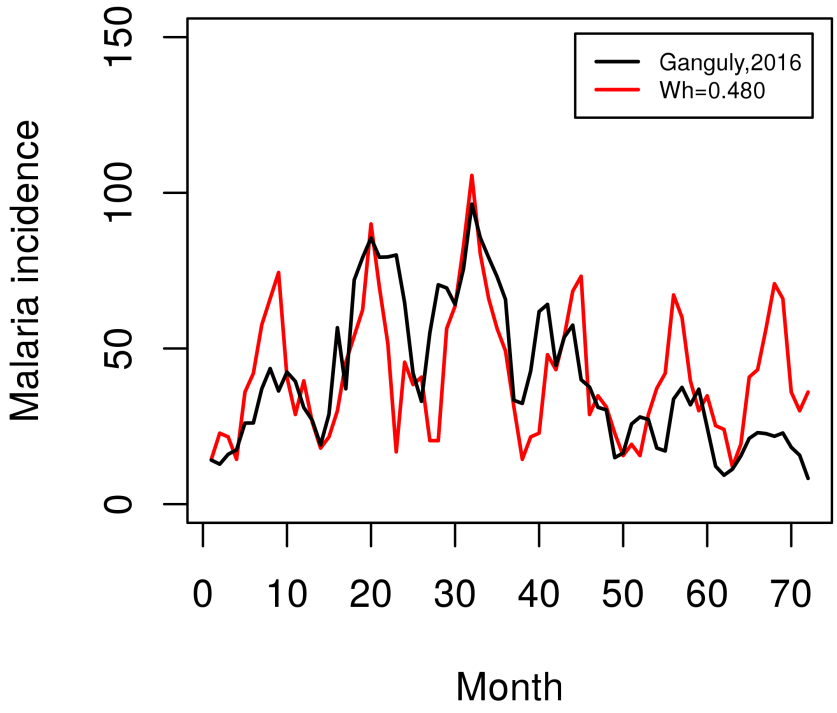

Figure 12.4: Monthly malaria incidence empirical time series from Ganguly,2016 (black) [130] and model simulation with human-to-mosquito transmission efficiency $w_h = 0.480$ (red).

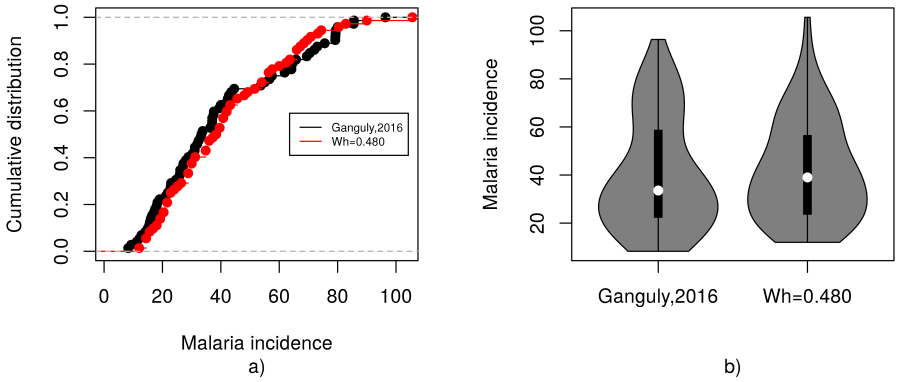

Figure 12.5: **(a)** Cumulative probability distribution curves from malaria empirical time series in Ganguly,2016 (black) [130], and from model simulation with human-to-mosquito transmission efficiency $w_h = 0.480$ (red). **(b)** Monthly malaria incidence violin plot from empirical time series in Ganguly,2016, and model simulation malaria incidence in empirical series from with human-to-mosquito transmission efficiency $w_h = 0.480$.

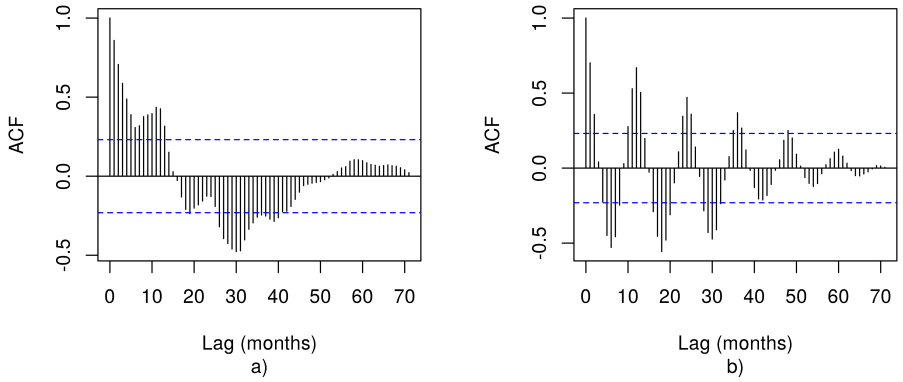

Figure 12.6: **(a)** Autocorrelation function from malaria empirical time series in Ganguly,2016 [130]. **(b)** Autocorrelation function from model simulation with human-to-mosquito transmission efficiency $w_h = 0.480$.

an estimated population of 109,944 inhabitants, according to the 2010 Municipality Population and Housing Census [264]. Malaria incidence empirical results in the original time series were presented in the form of malaria monthly incidence of cases (phm). Malaria incidence (MI) was estimated by dividing the empirical result by the region population total ($109,944$), while multiplying this result by $1,200$, thus obtaining the final result in the form of annual malaria cases per 100 inhabitants (phy), as in equation 12.2. Empirical average malaria incidence was 7.6 annual cases per 100 inhabitants during the 6-years' time period, ranging from the lowest value of 464 monthly cases, equivalent to $\frac{464 \times 1200}{109,944} = 5.1$ annual cases per 100 inhabitants, to the highest value of 2141 monthly cases, corresponding to $\frac{2141 \times 1200}{109,944} = 23.3$ annual cases per 100 inhabitants – see table 12.1 and equation 12.2.

$$phy = \frac{phm \times 1,200}{109,944} \tag{12.2}$$

In figure 12.7 we can confirm the presence of a significant similarity between the empirical time series from Alhassan (2017) and a model simulation with human-to-mosquito transmission efficiency ($w_h = 0.413$). This similarity is reinforced by the presence of periodic seasonal synchronization in both time series, by using a bootstrap model simulation partial time series lasting 72 months – from month 260 to 331 – from a total of 360 months of available simulation.

Also, by looking at the cumulative probability distribution function (CDF) of both time series, on can see that both functions present similar cumulative probability distributions – see figure 12.8 a).

This notion is further supported by the probability distribution violin plot of both time series. In figure 12.9 one may also notice the presence of some similarity

of the autocorrelation function in both time series.

Quantitative error estimation

When using quantitative error estimation to compare the empirical time series from Alhassan (2017) and a synchronized partial time series from a model simulation with $w_h = 0.413$, one finds small differences in the mean absolute error (MAE), the mean absolute percentage error (MAPE) and the root mean squared error (RMSE) between both time series – see table 12.3.

Quantitative statistical measures

It is also possible to compare time series by using quantitative statistical measures that compare statistical proximity between the probability distribution function of two time series. In our model validation we have used 3 well accepted statistical measures variants of this methodology: a) Kolmogorov-Smirnov testing; b) Anderson-Darling testing; c) Kuiper testing.

Finally, we also found a striking similarity between the empirical time series from Alhassan (2017) and the model simulation time series with human-to-mosquito transmission efficiency corresponding to $w_h = 0.413$ in terms of an acceptable small value of Theil's inequality coefficient ($U = 0.289$) – see tables 12.4 and 12.5.

12.4.4 Chirombo,2020

In 2020, Chirombo presented a spatial-temporal model reporting results from a time series of childhood malaria incidence in Malawi. Rainfall is heterogeneous across Malawi, ranging from an average annual precipitation of 700 mm in low altitude areas to 2500 mm in high altitude areas. The country includes 5 different climatic regions involving 28 districts. Results were presented at the district level, in the form of monthly malaria confirmed and suspected cases during a time period lasting 162 months (from 2004 to 2017) [68]. Several climate and non-climate variables were included in the model. Malaria data from the Dedza region was compared to a model simulation with similar average malaria monthly incidence, and a human-to-mosquito transmission efficiency of $w_h = 0.433$. Empirical average malaria incidence was estimated at 7.3 annual cases per 100 inhabitants during the 162-month time period – see table 12.1. To synchronize seasonal periodicity, a model simulation with a human-to-mosquito transmission efficiency of $w_h = 0.420$, an average malaria incidence of 7.5 annual cases per 100 inhabitants, and a time duration lasting from month 173 to month 328 was compared to the empirical time series from Chirombo,2020 – see figure 12.10.

In figure 12.10 we can confirm the presence of a significant similarity between the empirical time series from Chirombo (2020) and a model simulation with human-to-mosquito transmission efficiency of $w_h = 0.420$. This similarity is

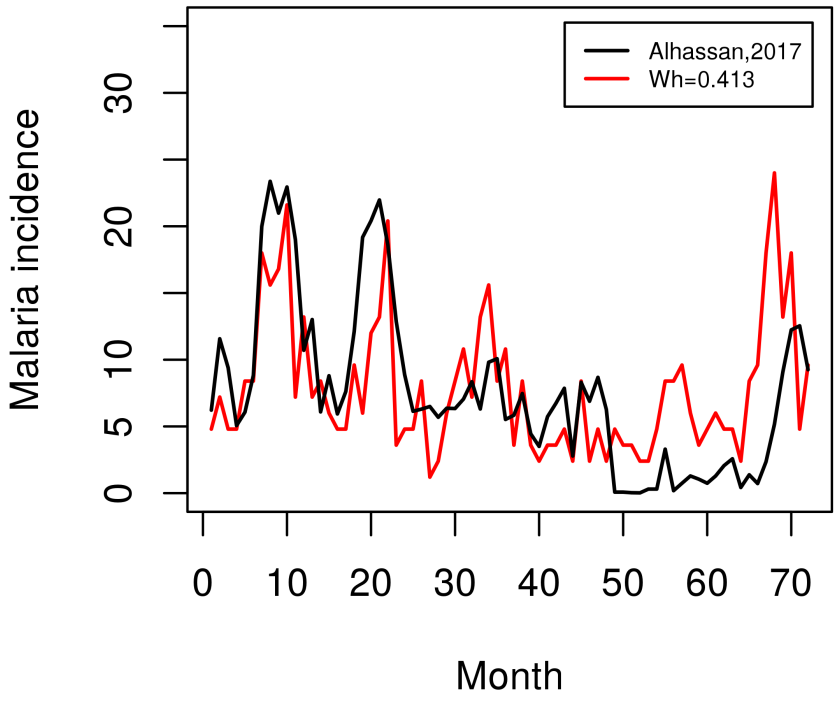

Figure 12.7: Monthly malaria incidence empirical time series from Alhassan,2017 (black) [12] and model simulation with human-to-mosquito transmission efficiency $w_h = 0.413$ (red).

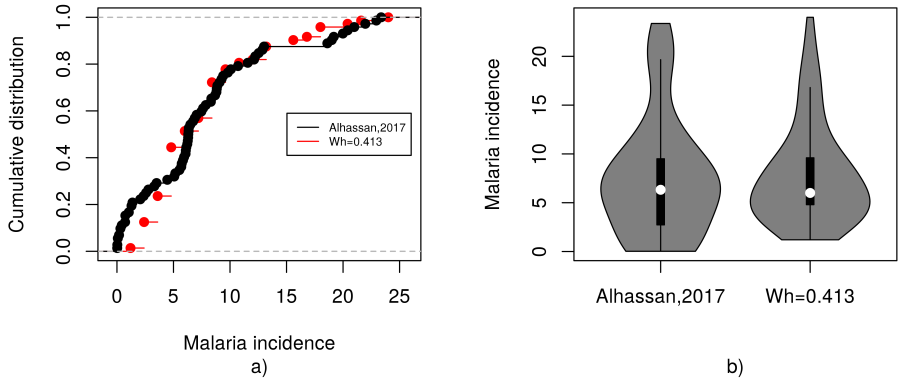

Figure 12.8: **(a)** Cumulative probability distribution curves from malaria empirical time series in Alhassan,2017 (black) [12], and from model simulation with human-to-mosquito transmission efficiency $w_h = 0.413$ (red). **(b)** Monthly malaria incidence violin plot from empirical time series in Alhassan,2017, and model simulation malaria incidence in empirical series from with human-to-mosquito transmission efficiency $w_h = 0.413$.

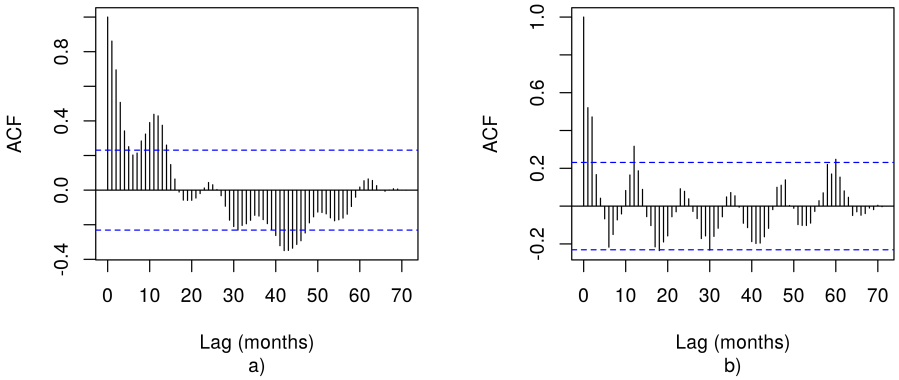

Figure 12.9: **(a)** Autocorrelation function from malaria empirical time series in Alhassan,2017 [12]. **(b)** Autocorrelation function from model simulation with human-to-mosquito transmission efficiency $w_h = 0.413$.

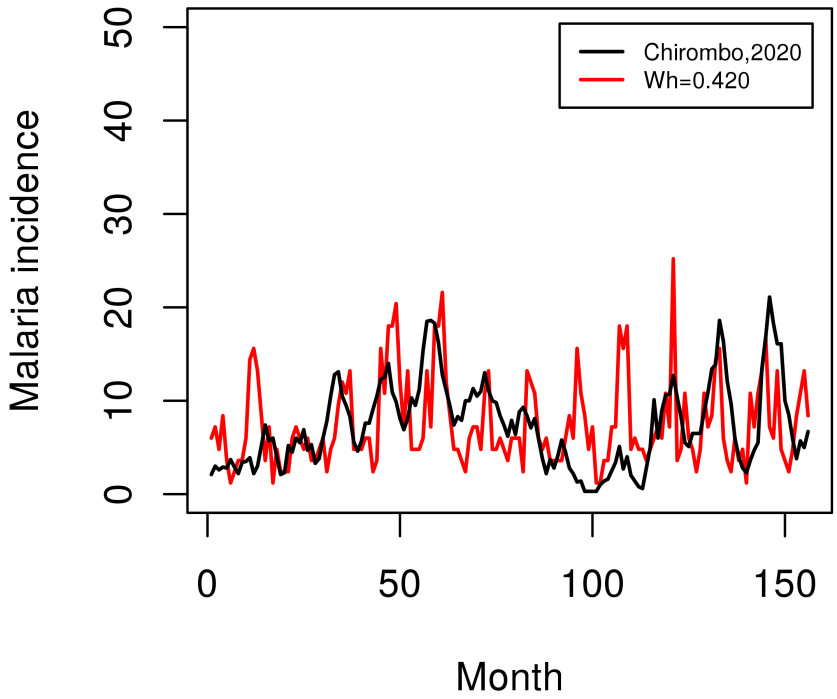

Figure 12.10: Monthly malaria incidence empirical time series from Dedza region in Chirombo,2020 (black) [68] and model simulation with human-to-mosquito transmission efficiency $w_h = 0.420$ (red).

reinforced by the presence of periodic seasonal synchronization in both time series, by using a bootstrap model simulation partial time series lasting 72 months – from month 173 to 328 – from a total of 360 months of available simulation.

Also, by looking at the cumulative probability distribution function (CDF) of both time series, on can see that both functions present similar cumulative probability distributions – see figure 12.11 a).

This notion is further supported by the probability distribution violin plot of both time series. In figure 12.12 one may also notice the presence of some similarity of the autocorrelation function in both time series.

Quantitative error estimation

When using quantitative error estimation to compare the empirical time series from Chirombo (2020) and a synchronized partial time series from a model simulation with $w_h = 0.420$, one finds small differences in the mean absolute error (MAE), the mean absolute percentage error (MAPE) and the root mean squared error (RMSE) between both time series – see table 12.3.

Quantitative statistical measures

It is also possible to compare time series by using quantitative statistical measures that compare statistical proximity between the probability distribution function of two time series. In our model validation we have found small values of three widely used statistical measures: a) Kolmogorov-Smirnov testing; b) Anderson-Darling testing; c) Kuiper testing. This fact supports the notion of strong similarity between the empirical time series from Chirombo (2020) and a model simulation with $w_h = 0.420$.

Finally, we found a striking similarity between the empirical time series from Chirombo (2020) and the model simulation time series with human-to-mosquito transmission efficiency corresponding to $w_h = 0.420$ in terms of an acceptable small value of Theil's inequality coefficient ($U = 0.301$) – see tables 12.4 and 12.5.

12.4.5 Ferrão,2017

The specific details of Ferrão (2017 empirical time series were previously described in section 7.4. As it happens, Ferrão (2017) is also the only empirical time series originally presented in the form of weekly malaria incidence. Its results were included in this chapter in the form of a more simplified version.

Quantitative error estimation

When using quantitative error estimation to compare the empirical time series from Ferrão (2017) and a synchronized partial time series from a model simulation with $w_h = 0.427$, it is possible to find small differences in the mean absolute error

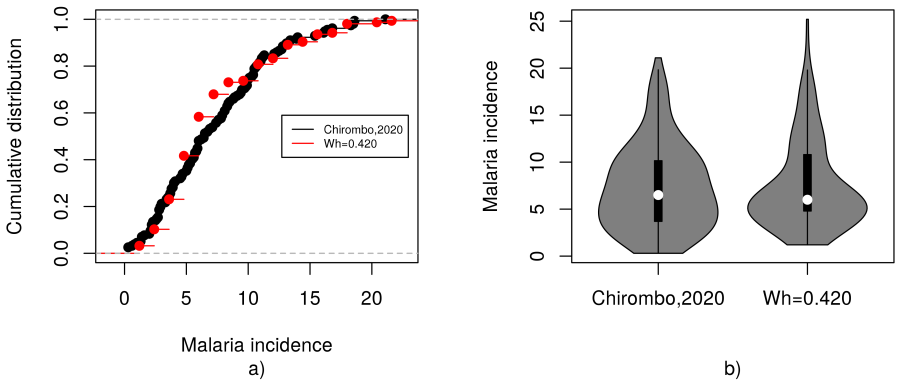

Figure 12.11: **(a)** Cumulative probability distribution curves from malaria empirical time series (Dedza region) in Chirombo,2020 (black) [68], and from model simulation with human-to-mosquito transmission efficiency $w_h = 0.420$ (red). **(b)** Monthly malaria incidence violin plot from empirical time series (Dedza region) in Chirombo,2020, and model simulation malaria incidence in empirical series from with human-to-mosquito transmission efficiency $w_h = 0.420$.

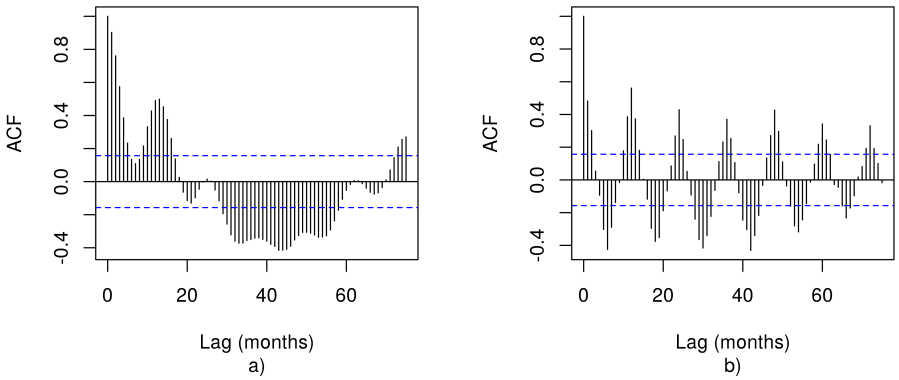

Figure 12.12: **(a)** Autocorrelation function from malaria empirical time series (Dedza region) in Chirombo,2020 [68]. **(b)** Autocorrelation function from model simulation with human-to-mosquito transmission efficiency $w_h = 0.420$.

(MAE), the mean absolute percentage error (MAPE) and the root mean squared error (RMSE) between both time series – see table 12.3.

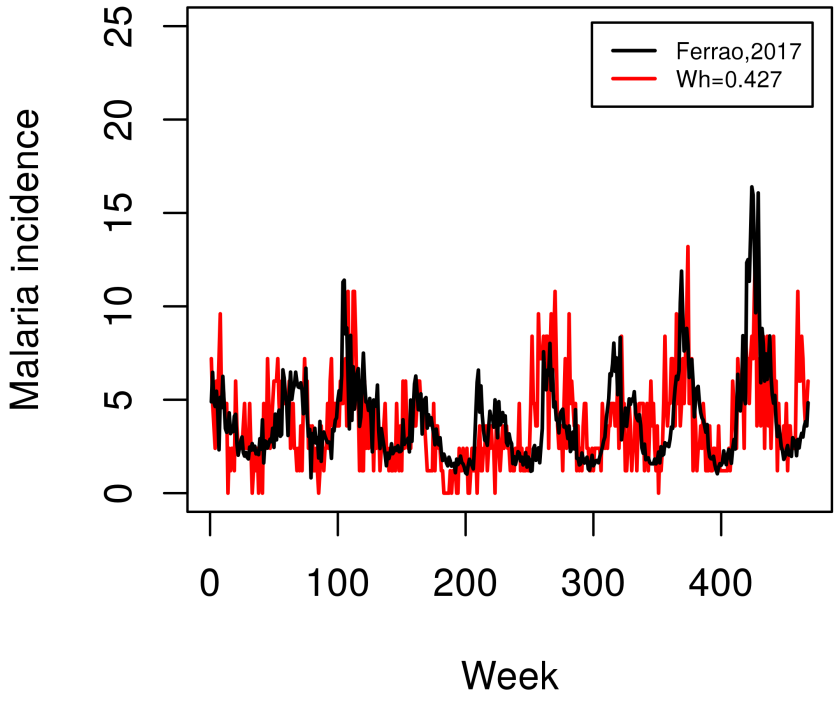

Figure 12.13: Weekly malaria incidence empirical time series from Ferrão,2017 (black) [122] and model simulation with human-to-mosquito transmission efficiency $w_h = 0.427$ (red).

Quantitative statistical measures

It was also possible to compare time series by using quantitative statistical measures that compare statistical proximity between the probability distribution function of two time series. In our model validation we have found small values of three widely used statistical measures: a) Kolmogorov-Smirnov testing; b) Anderson-Darling testing; c) Kuiper testing. This fact supports the notion of strong similarity between the empirical time series from Ferrão (2017) and a model simulation with $w_h = 0.427$.

Finally, we find a striking similarity between the empirical time series from Ferrão (2017) and the model simulation time series with human-to-mosquito transmission efficiency corresponding to $w_h = 0.427$ in terms of an acceptable small value of Theil's inequality coefficient ($U = 0.278$) – see tables 12.4 and 12.5.

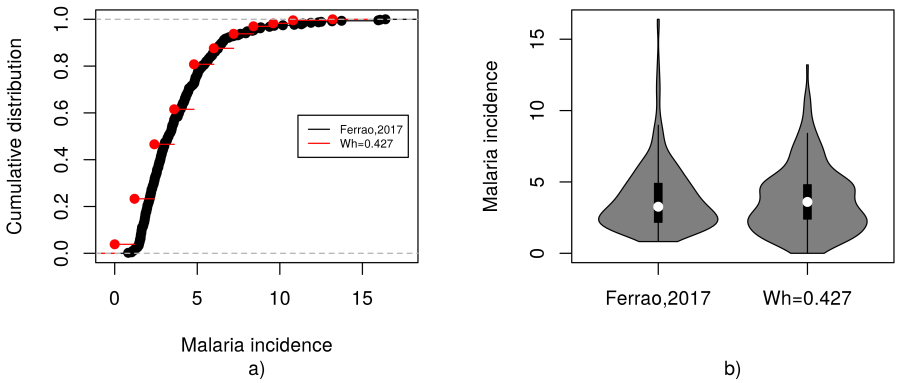

Figure 12.14: **(a)** Cumulative probability distribution curves from malaria empirical time series in Ferrão,2017 (black) [122], and from model simulation with human-to-mosquito transmission efficiency $w_h = 0.427$ (red). **(b)** Weekly malaria incidence violin plot from empirical time series in Ferrão,2017 and model simulation malaria incidence in empirical series from with human-to-mosquito transmission efficiency $w_h = 0.427$.

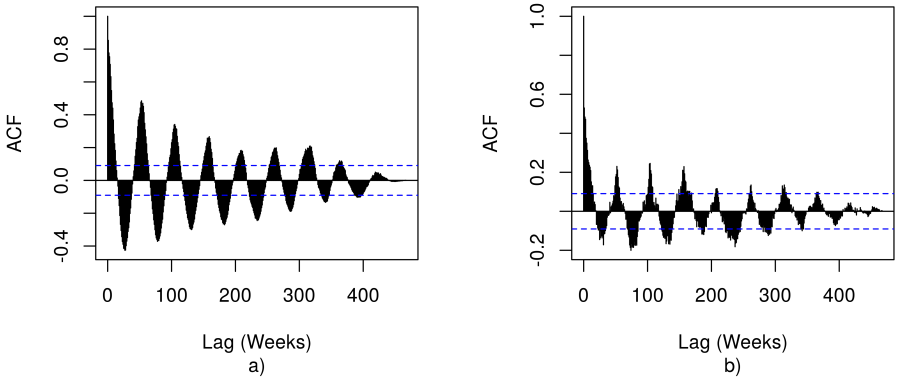

Figure 12.15: **(a)** Autocorrelation function from malaria empirical time series in Ferrão,2017 [122]. **(b)** Autocorrelation function from model simulation with human-to-mosquito transmission efficiency $w_h = 0.427$.

12.5 Ivermectin model validation

A theoretical approach to model validation is usually difficult to implement when evaluating a computational algorithm equivalent to the use of ivermectin in a human population. Still, in this section we describe a model validation procedure by graphically comparing results from our model, incorporating the ivermectin as a quantitative parameter in terms of mosquito survival, with data from previous research [61].

As shown in figure 12.16, the differences found in mosquito survival between the ivermectin human treatment group and the human control group are small. However, notice that mosquito survival at 12 days is slightly higher in the model simulation – close to 20% – when compared to the residual survival in the empirical data [61]. This difference can be explained by the implementation of a more conservative computational algorithm in our model, in terms of mosquito survival. Globally, our model survival curves were quite similar in shape to those of Chaccour's original paper, suggesting that this ivermectin model may reproduce acceptable model simulations, with mosquito survival results within the expected range.

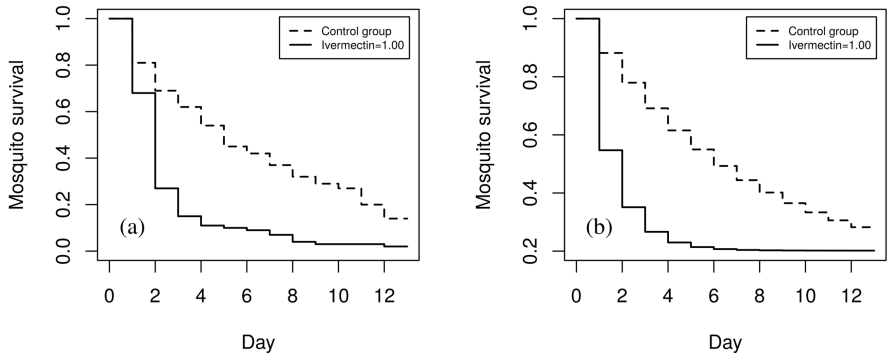

Figure 12.16: Validation of ivermectin model: **(a)** Mosquito survival curve in empirical series as result of ivermectin treatment in 100% of all human individuals when compared to the untreated human control group [61], and **(b)** mosquito survival curve because of model simulation of ivermectin treatment in 100% of all human individuals when compared to a model simulation with no treatment in the control group.

12.6 Ross-Macdonald theoretical validation

A critical aspect of model verification consists in checking the similarity of its predictions against the results from well-established previous models. Ross-Macdonald theory is mathematically sound and well supported on a few concepts related to malaria transmission such as the human feeding rate – $\boldsymbol{a}$ –, the mosquito-to-human and human-to-mosquito transmission efficiencies – $\boldsymbol{b}$ and $\boldsymbol{c}$, respectively -, the entomological inoculation rate – EIR -, and the basic reproduction number – R_0. Outcomes from a reliable malaria model should be in line with expected results from these parameters.

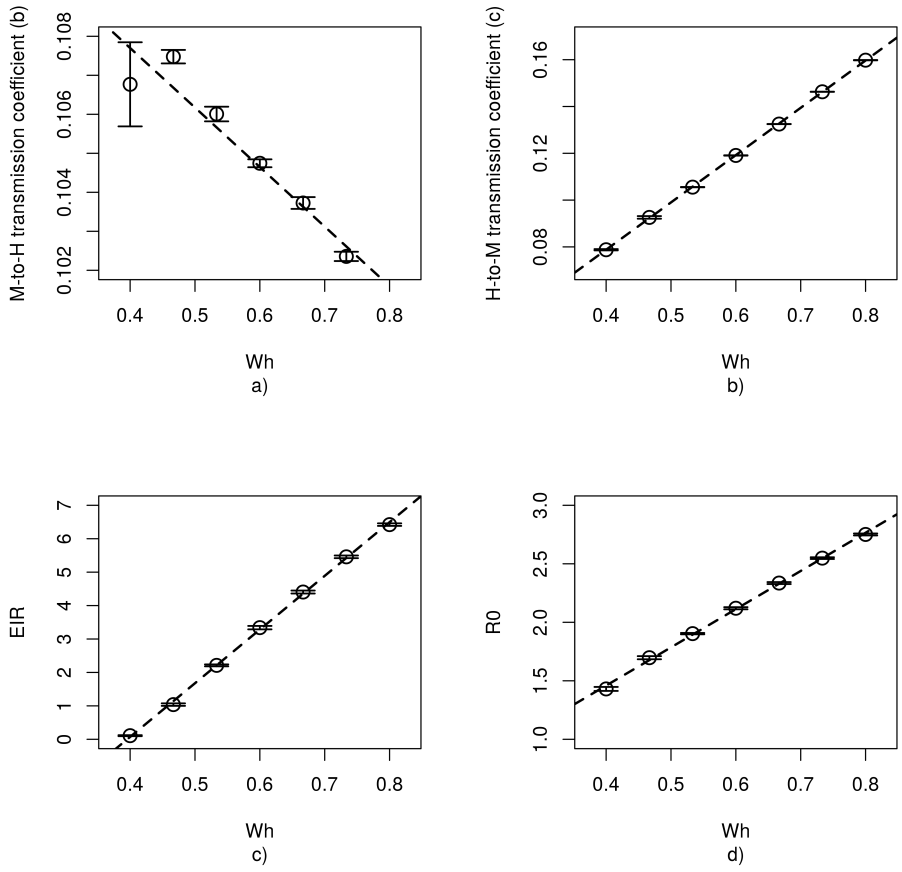

Figure 12.17: Correlation of Ross-Macdonald parameters b, c, EIR and R_0 with human-to-mosquito gametocytemia transmission efficiency (w_h), in 10 model simulations at all levels:
(a) b (Ross-Macdonald M-to-H transmission efficiency),
(b) c (Ross-Macdonald H-to-M transmission efficiency),
(c) EIR (Entomological inoculation rate), and
(d) R_0 (Basic reproductive number).

In the present model simulations, three different scenarios were tested in order to check model validity:

a) Variable human-to-mosquito transmission efficiency ($\boldsymbol{c}$) from Ross-Macdonald theory and w_h in the present model simulation;

b) Variable use of ivermectin prevention corresponding to the percentage of human individuals under ivermectin treatment – p_{iv};

c) Identical system settings in different initial conditions of human and mosquito infection prevalence.

These five Ross-Macdonald parameters were derived in all model simulations and verified in terms of model dynamics and output in different model settings – see tables 12.6 to 12.10.

12.6.1 Ross-Macdonald parameters and H-to-M gametocytemia transmission efficiency

In model simulations with different values of human-to-mosquito gametocytemia transmission efficiency ($0.400 < w_h < 0.800$) there is clear evidence of correlation of the model parameter w_h with Ross-Macdonald $\boldsymbol{c}$ parameter – see tables 12.6 and 12.7, and figure 12.17. The use of gametocidal agents such as primaquine or methylene blue was considered dynamically equivalent to a reduction in w_h values in model simulations. In all different levels of w_h, Ross-Macdonald parameters were in line with theoretical expectations.

w_h (**G**)	$\overline{a}$ (± SE)	$\overline{b}$ (± SE)	$\overline{c}$ (± SE)	$\overline{EIR}$ (± SE)	$\overline{R_0}$ (± SE)
0.400	0.2381	0.1068	0.0788	0.1086	1.4305
(60)	(± 0.0005)	(± 0.0011)	(± 0.0003)	(± 0.0150)	(± 0.0170)
0.467	0.2384	0.1075	0.0926	1.0378	1.6974
(70)	(± 0.0003)	(± 0.0002)	(± 0.0006)	(± 0.0370)	(± 0.0130)
0.533	0.2381	0.1060	0.1055	2.2114	1.9032
(80)	(± 0.0004)	(± 0.0002)	(± 0.0001)	(± 0.0290)	(± 0.0060)
0.600	0.2380	0.1047	0.1191	3.3403	2.1201
(90)	(± 0.0005)	(± 0.0001)	(± 0.0001)	(± 0.0510)	(± 0.0090)
0.667	0.2380	0.1037	0.1325	4.4056	2.3353
(100)	(± 0.0003)	(± 0.0002)	(± 0.0000)	(± 0.0044)	(± 0.0080)
0.733	0.2382	0.1024	0.1463	5.4586	2.5484
(110)	(± 0.0004)	(± 0.0001)	(± 0.0000)	(± 0.0400)	(± 0.0070)
0.800	0.2378	0.1014	0.1598	6.4218	2.7508
(120)	(± 0.0003)	(± 0.0001)	(± 0.0000)	(± 0.0380)	(± 0.0080)

Table 12.6: Correlation of Ross-Macdonald parameters with different levels of gametocytemia duration in days of positivity (**G**) and respective human-to-mosquito transmission efficiency (w_h), in groups of 10 model simulations at all levels.

From table 12.6 and figure 12.17 it is possible to assume that a drug intervention with gametocidal agents would have a major impact in Ross-Macdonald

c parameter, EIR and R_0, along with a much smaller impact in Ross-Macdonald ***b*** parameter, and with virtually no influence in ***a*** parameter. The respective w_h ANOVA correlation table 12.8 points out to the same conclusion.

p_{iv}	$\overline{a}$ (± SE)	$\overline{b}$ (± SE)	$\overline{c}$ (± SE)	$\overline{EIR}$ (± SE)	$\overline{R_0}$ (± SE)
0.00	0.2380 (± 0.0005)	0.1047 (± 0.0001)	0.1191 (± 0.0001)	3.340 (± 0.0513)	2.120 (± 0.0092)
0.02	0.2384 (± 0.0004)	0.0997 (± 0.0001)	0.1186 (± 0.0000)	2.280 (± 0.0297)	2.017 (± 0.0056)
0.04	0.2384 (± 0.0004)	0.0943 (± 0.0003)	0.1184 (± 0.0001)	1.200 (± 0.0602)	1.903 (± 0.0100)
0.06	0.2385 (± 0.0004)	0.0883 (± 0.0001)	0.1182 (± 0.0002)	0.280 (± 0.0586)	1.780 (± 0.0180)
0.08	0.2385 (± 0.0004)	0.0794 (± 0.0002)	0.1176 (± 0.0003)	0.046 (± 0.0045)	1.592 (± 0.0319)

Table 12.7: Correlation of Ross-Macdonald parameters with different levels of ivermectin prevention (p_{iv}) in groups of 10 model simulations at all levels.

p_{iv}	$\overline{a}$	$\overline{b}$	$\overline{c}$	$\overline{EIR}$	$\overline{R_0}$
F	4.998	206.4	117.1	76.6	189.2
P	0.111	7.31×10^{-4}	1.69×10^{-3}	3.14×10^{-3}	8.32×10^{-4}

Table 12.8: ANOVA table with **F** and **P** values of correlation of Ross-Macdonald parameters with different levels of ivermectin prevention (p_{iv}), in groups of 10 model simulations at all levels.

12.6.2 Ross-Macdonald parameters and ivermectin prevention

Ivermectin prevention affected the outcome of Ross-Macdonald parameters in model simulations at different levels of p_{iv}. From tables 12.7 and 12.8 and figure 12.18 it is possible to conclude that ivermectin had a major impact in Ross-Macdonald ***b*** parameter, EIR and R_0, along with a much smaller impact in Ross-Macdonald ***c*** parameter, and with virtually no influence in ***a*** parameter. The respective p_{iv} ANOVA correlation table – table 12.8 points out the same conclusion.

It is possible to conclude that gametocidal drug intervention will play a complementary role with ivermectin prevention in reducing disease transmission, as was shown in previous chapters concerning the role of gametocytemia suppression reducing ***c*** and ivermectin prevention reducing ***b*** in phase transition.

12.6.3 Ross-Macdonald parameters and initial conditions

With different initial conditions there was no significant change in Ross-Macdonald parameters in all model simulations – see also Appendix C. The stability of the human-mosquito dynamical system was in line with the expected stability in all Ross-Macdonald parameters – see tables 12.9 and 12.10.

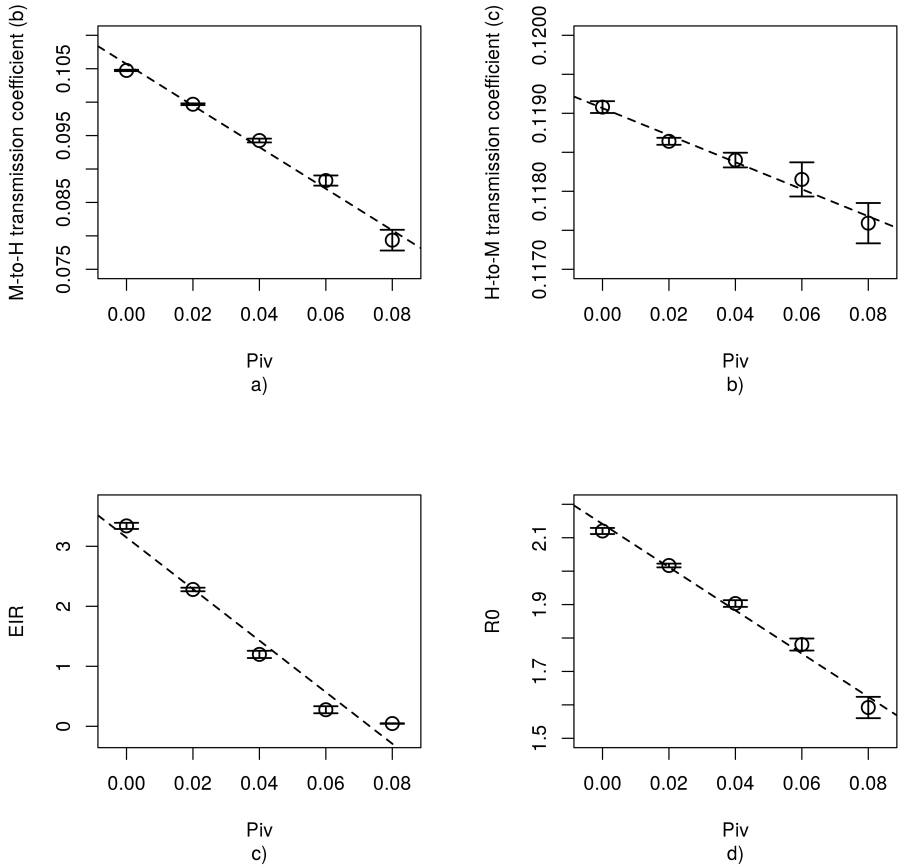

Figure 12.18: Correlation of Ross-Macdonald parameters b, c, EIR and R_0 with ivermectin prevention (p_{iv}), in 10 model simulations at all levels:
(a) b (Ross-Macdonald M-to-H transmission efficiency),
(b) c (Ross-Macdonald H-to-M transmission efficiency),
(c) EIR (Entomological inoculation rate), and
(d) R_0 (Basic reproductive number).

Hi_0	Mi_0	$\overline{a}$ (± SE)	$\overline{b}$ (± SE)	$\overline{c}$ (± SE)	$\overline{EIR}$ (± SE)	$\overline{R_0}$ (± SE)
0.05	0.01	0.2377	0.0943	0.1026	5.884	1.639
		(± 0.0005)	(± 0.0002)	(± 0.0000)	(± 0.0351)	(± 0.0088)
1.00	0.00	0.2374	0.0935	0.1025	5.918	1.621
		(± 0.0003)	(± 0.0002)	(± 0.0001)	(± 0.0250)	(± 0.0047)
0.00	1.00	0.2386	0.0944	0.1025	6.002	1.654
		(± 0.0004)	(± 0.0002)	(± 0.0001)	(± 0.0327)	(± 0.0062)
1.00	1.00	0.2382	0.0938	0.1025	6.006	1.638
		(± 0.0006)	(± 0.0002)	(± 0.0001)	(± 0.0404)	(± 0.0089)
0.50	0.50	0.2378	0.0939	0.1025	5.941	1.633
		(± 0.0002)	(± 0.0002)	(± 0.0001)	(± 0.0191)	(± 0.0049)

Table 12.9: Stability of Ross-Macdonald parameters with independence in 5 different initial conditions of human and mosquito infection prevalence in groups of 10 model simulations.

Initial conditons (Hi_0/Mi_0)	$\overline{a}$	$\overline{b}$	$\overline{c}$	$\overline{EIR}$	$\overline{R_0}$
F	0.361	0.129	3.418	1.713	0.006
P	0.590	0.744	0.162	0.282	0.945

Table 12.10: ANOVA table of correlation of Ross-Macdonald parameters and respective **F** and **P** values, with different initial conditions of human (Hi_0) and mosquito (Mi_0) infection prevalence, in groups of 10 model simulations at all levels.

Part III

DISCUSSION

Chapter 13

Discussion

13.1 Phase transition and gametocytemia

It was our original objective to explore all the possibilities of stochastic modeling in malaria research. Our model was presented in detail in chapter 5. The relevance of human-to-mosquito malaria transmission is anchored in the potential duration of gametocytemia in human hosts and captured in the parameter defined in our model as w_h expressing the percentage of time spent with positive gametocytemia during full disease duration. Special attention was devoted to the detection of a phase transition between epidemic stability and disease elimination. The potential use of the drug ivermectin as a selective *Anopheles* suppressor of mosquitoes during the mosquito latency stage (parasite maturation inside the mosquito before reaching the sporozoite stage) was further investigated. We assumed a copula approach (gametocidal agent primaquine + ivermectin) as a potentially effective intervention in reducing malaria transmission – see figure 13.1.

We have also investigated the role of heterogeneity in disease dynamics. Heterogeneity was defined in terms of a Pareto distribution model. Other factors affecting heterogeneity in disease transmission were also considered such as the importance of vector control, seasonality and human migration. We have tested the combined use of the sporozoite rate (Z) and the parasite rate (X) as an index correlating well with the intensity of disease transmission in the presence of heterogeneity. Finally, we looked into the presence of long memory in the stochastic process of malaria transmission by measuring Hurst exponent and Shannon entropy in model simulation and empirical time series.

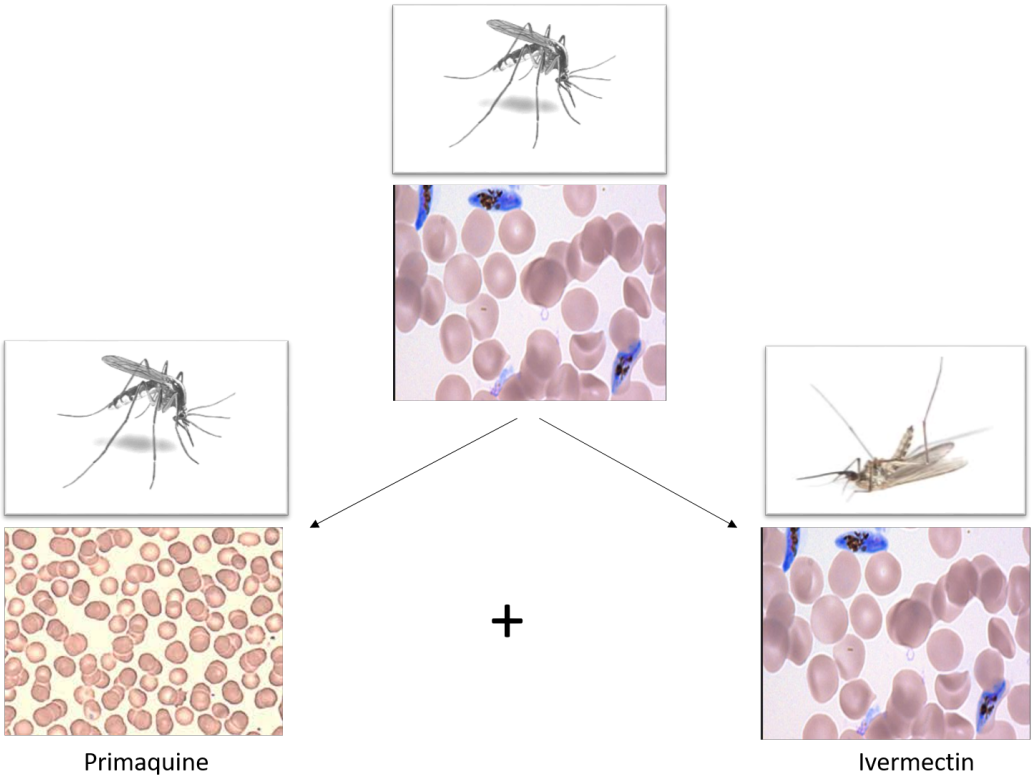

Figure 13.1: Copula approach with the gametocidal agent primaquine and the selective mosquito killer ivermectin in a more effective strategy suppressing malaria transmission.
(Images from Adobe Stock, https://openeducationalberta.ca, https://www.myjoyonline.com and https://www.wwarn.org [154])

Several points of this dissertation are open to discussion. The presence of gametocytes in the human blood during mosquito feeding is a critical factor in disease persistence. While the stochastic nature of this event may affect disease transmission with unpredictable consequences in a single time instant, ultimately it will not change the outcome resulting from a single mosquito bite in an infected human host. The presence of a phase transition in relation to the time spent with the presence of positive gametocytemia in the human blood is therefore a critical issue in defining more effective strategies in disease prevention. According to our model, the use of gametocidal agents (such as primaquine or methylene blue) could achieve a significant reduction in human-to-mosquito disease transmission, to a point where disease elimination could become feasible.

In terms of the theoretical implications of this strategy in the Ross-Macdonald model, our data also supports the concept that a combined use of this gametocidal approach, lowering the value of human-to-mosquito transmission efficiency $\boldsymbol{c}$, along with drug prevention with ivermectin in human hosts (lowering the value of mosquito-to-human transmission efficiency $\boldsymbol{b}$) could become a more effective way of reducing disease transmission.

Combining this strategy with adequate vector control (lowering the value of

mosquito density Δ_m [1]), while increasing the value of daily mosquito mortality q_m, adopting the widespread use of LLIN/ITN/IRS barrier measures (lowering the value of the human feeding rate $\boldsymbol{a}$), and implementing an effective anti-heterogeneity approach more hot-spot-oriented while increasing the value of θ and lowering the value of $\alpha(\theta)$ – see equations 8.2 and 8.3 – it may be feasible a consistent reduction of the basic reproduction number R_0, well below the disease elimination threshold.

13.2 Heterogeneity in malaria transmission

We have addressed heterogeneity as a critical aspect in disease transmission, and a potentially useful target in disease prevention strategy. Our agent-based malaria model simulating malaria transmission scenarios was used as a benchmark in testing for the presence of heterogeneous affinity. Several parameters were identified with influence in the interaction of infectious mosquitoes and healthy human individuals more vulnerable to mosquito biting, and assuming the role of active and attracting hot-spots in disease spreading. Our main focus was in predicting malaria incidence in the presence of a systematic administration of ivermectin treatment alone or in combination with gametocidal therapy such as primaquine or methylene blue.

Human-to-mosquito transmission, which is directly related to the time length of positive gametocytemia (w_h), is fundamental in disease transmission. In this setting, the mass administration of ivermectin has the potential for inhibiting disease transmission by killing mosquitoes with a lethal effect on mosquito populations immediately after feeding, while suppressing gametocyte maturation inside the mosquito before completing the 10 days incubation period. Such effect was magnified by the presence of a high mosquito density [61, 196, 326].

An important aspect of malaria prevention strategies is based upon the implementation of early disease diagnosis with RDT with the use of reliable metrics for the accurate measurement of disease incidence. From the results obtained in our model simulations it was possible to assume that the isolated single use of one of the usual disease prevalence metrics (sporozoite rate Z or parasite rate X) could reveal less accuracy in the presence of heterogeneity in disease transmission, favoring their combined use in malaria metrics.

We have shown that in the presence of increased heterogeneity, by multiplying the sporozoite rate Z by the parasite infection rate X it was possible to create a reliable indicator $G = ZX$ for prediction of malaria incidence, performing better than any of the two rates, separately, in identical heterogeneity settings, particularly in the setting of mass administration of ivermectin.

[1] Here, we use the definition $\Delta_m = \frac{M}{H}$ for mosquito density, instead of the parameter m adopted by D.L.Smith,2004 [343]

Considering classical Ross-Macdonald model metrics, we have also shown that EIR was quite more sensitive than R_0 in predicting malaria incidence in the presence of high heterogeneity scenarios.

Our model shows that it is essential to consider heterogeneity as an important factor, when predicting malaria transmission, while emphasizing that the effect of mass drug administration of ivermectin, is not only dependent on ivermectin intensity and human-to-mosquito transmission efficiency, but also clearly influenced by the presence of heterogeneity in human and mosquito populations.

The existence of transmission hot-spots plays a decisive role in disease transmission dynamics [34]. These hot-spots in malaria transmission may become decisive in small villages in close proximity to high *Anopheles* mosquito density and larval active breeding sites. Children and recent immigrants coming from malaria high-risk regions should also be considered as transmission hot-spots.

We have also shown that the dynamical behavior of the 2D probability density function of the dynamical human-mosquito infection system in phase space may somehow be affected by the presence of heterogeneity in disease transmission. This concept could be used in the implementation of more effective hot-spot-oriented strategies.

From our perspective the combined treatment strategy with gametocidal drugs (such as artemisinin, primaquine, or methylene blue) and mass administration of ivermectin, specifically targeting transmission hot-spots, may become an effective alternative in preventing disease resurgence in high heterogeneity settings.

The importance of establishing a malaria prevention strategy hot-spot-oriented was highlighted in previous chapters. Furthermore, our data shows that reducing the duration of gametocytemia in human hosts along with lowering the impact of heterogeneity in disease transmission in combination with the use of ivermectin in transmission hot-spots could result in significant benefits in reducing malaria transmission.

13.3 Vector control, migration and seasonality

Our data supports the traditional view by Ross and Macdonald that vector control remains one of the most important weapons in malaria prevention. In the present model, mosquito density was strongly correlated with the level of malaria incidence. Our data supports the notion that ivermectin is also effective in reducing disease transmission in higher mosquito density regions. This aspect should not be neglected in future malaria preventive strategies.

Also, the possibility of disease resurgence from the importation of silent malaria carriers as a result of human migration has become a reason of concern for Public Health officials. The occurrence of malaria outbreaks in world regions where malaria incidence had been marginally low for decades may be apparently related with several cases of human migration from malaria affected regions. Our model also revealed that migration could be a significant risk factor of disease resurgence, and that specific measures allowing for early malaria diagnosis in migrant populations could result in better control of disease transmission, especially in regions with low infection prevalence.

In the world regions where malaria transmission is seasonal and periodic, there is a relation between the length of the rainy season and mosquito breeding. A longer wet season implies a stronger disease transmission. In the present model, it was possible to test the impact of different time lengths of seasonal rain precipitation in epidemic resilience. As expected, longer periods of high transmission during the wet season led to higher malaria incidence. However, by using ivermectin, it was possible to inhibit disease transmission, partially neutralizing that seasonality effect. Our data supports the notion that ivermectin could be useful in malaria prevention during the rainy season, in world regions with high malaria incidence.

13.4 Time series analysis of malaria epidemics

Malaria epidemic time series consistently revealed a specific memory pattern depending on the intensity of disease transmission. This behavior was considered useful in predicting the evolution of the epidemic. Malaria time series could also be analyzed with an effective application of different ARIMA models. ARIMA models in respect to the Box-Jenkins theory, are quite useful in malaria model simulations as well as in empirical time series – see Appendix D. At low disease transmission intensity, the time series behavior was shown to be consistent with a long-memory process, defined as long-range dependence. At high disease transmission intensity, this pattern apparently evolved towards a low-memory process. Significant results were obtained with other alternative metrics of long-range dependence such as the Hurst exponent and the Shannon information entropy. Hurst exponent was quite useful in predicting malaria epidemic behavior and phase transition proximity.

Shannon entropy was also quite helpful in predicting higher disease transmission.

13.5 Model validation

In the present dissertation, an extensive model validation strategy was adopted, that involved graphical as well as analytical validation and verification procedures. The graphical comparison of malaria empirical time series with model simulations in terms of average malaria incidence was defined as the standard benchmark procedure. A wide set of malaria empirical time series were used for the purpose of validating our model. The similarity of cumulative probability distribution functions and of autocorrelation functions added further information in support of our model validation. Along with the graphical procedures described above, several analytical procedures were also implemented with the aim of consolidating the graphical information. Commonly used statistical measures and error estimation procedures were used as reliable analytical tools in support of model validation. For validation of the ivermectin model a special procedure was implemented comparing mosquito survival distribution curves with empirical results from field data. A specific procedure comparing the present model simulation of ivermectin intervention and empirical data was particularly helpful. As a supplementary procedure, the results from model simulations were tested in terms of compliance with the Ross-Macdonald theory. Standard Ross-Macdonald parameters were obtained from model simulations and verified in relation to the expected malaria dynamics.

13.6 An integrated strategy towards malaria elimination

Malaria prevention strategy should involve two types of intervention: Vector control and human protection (see figures 13.2 and 13.3).

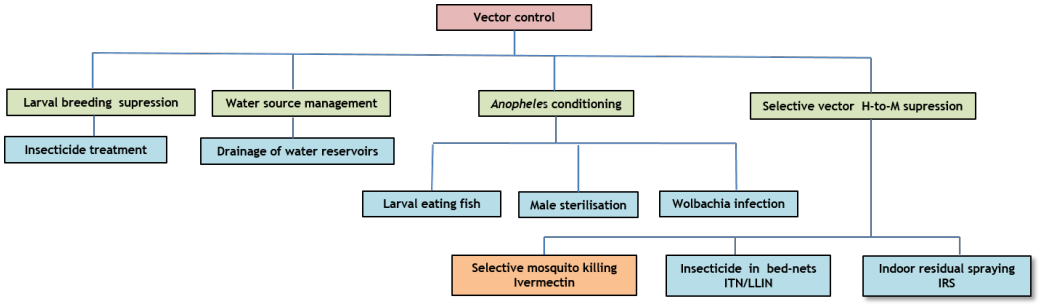

Figure 13.2: Global malaria strategy related to vector control. Highlighted in yellow is the strategic arm related to the use of ivermectin as a selective vector control agent.

Since Ross and Macdonald original work, vector control has assumed the most relevant aspect of malaria prevention. The discovery of the insecticide DDT and the usefulness of vector source suppression of water masses as potential larval breeding sites led to drastic reductions of malaria incidence worldwide. Despite later drawbacks such as growing insecticide resistance as well as major difficulties in handling the climate impact in geographical water management, vector control still assumes today a prominent role in malaria control. Also, source management by the introduction of larval-eating fish species could potentially contribute to a more adequate vector control strategy – see figure 13.2. An additional strategy has been recently found that promotes *Anopheles* conditioning with the use of mosquito male sterilization and increased vector mortality as a consequence of *Wolbachia* vector infection [146, 385, 392].

But malaria strategy is also strongly based upon human protection. Whether in the form of barrier protection with ITN/LLIN and IRS, or in the form of increasing human immunity against malaria. In regions with a stable number of new infections or reinfections, human individuals will acquire a reasonable form of protective immunity, that although it might not stop them from getting infected, still it will strongly reduce disease mortality and morbidity – see figure 13.3. The early use of rapid diagnostic tests in the presence of malaria clinical suspicion (RDT) is a sound approach to reducing disease mortality and morbidity, allowing for a more specific and effective use of artemisinin-combined therapy (ACT). However, asymptomatic gametocyte carriers will be able to retransmit the disease to healthy mosquitoes, thus increasing the burden of infectious vector, while increasing the chance of new infections in healthy human individuals.

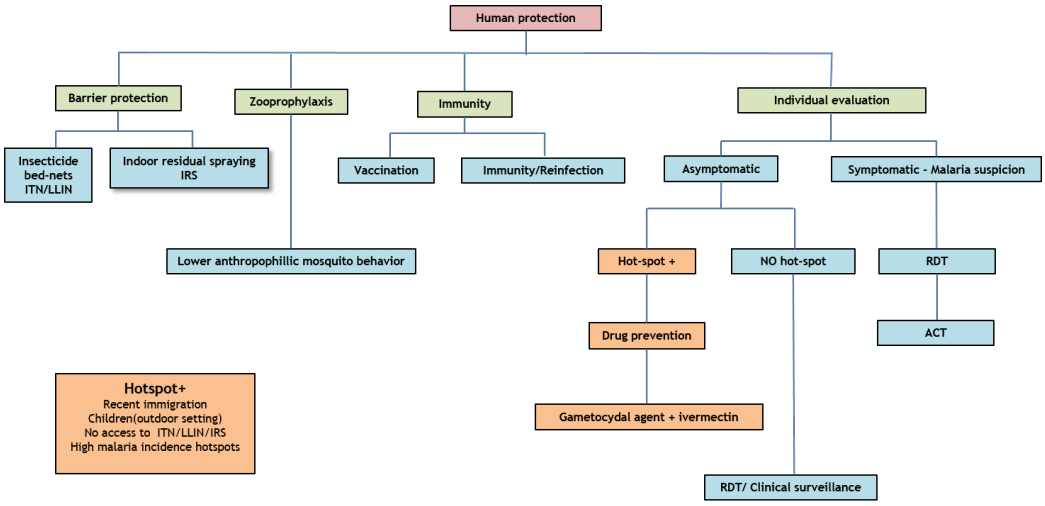

Figure 13.3: Global malaria strategy related to human protection. Highlighted in yellow is the strategic arm related to the combined use of gametocidal agents and ivermectin in a transmission hot-spot. In a heterogeneity setting, the definition of transmission hot-spot is given in the lower left box.

The importance of heterogeneity in malaria transmission gives support to the idea of a specific strategy dealing with transmission hot-spots and disease super-spreading. For that purpose, more specific effective measures could be used in targeting asymptomatic recent immigrants from high-risk areas, young children with frequent outdoor activities, and human individuals with no ITN/LLIN or IRS protection and living in the proximity of significant larval breeding sites or in regions with high malaria incidence – see figure 13.3.

The usefulness of ivermectin + gametocidal agents in prevention could improve the strength of malaria control strategy by selective reduction of potentially new infected mosquitoes before they ever become infectious. This highly selective action of ivermectin will not significantly modify mosquito density, but it will selectively reduce human infection risk. This intervention, if complemented with the use of an effective gametocyte reduction strategy (such as primaquine or methylene blue) could be very effective in improving malaria prevention strategy while potentially reducing the risk of parasite drug resistance to more effective medication such as artemisinin or quinine – see table 13.2 and figure 13.3.

13.7 Conclusions

The results described in the current dissertation confirm the validity of the present stochastic model of malaria transmission – see table 13.1. Gametocytemia levels are crucial to disease human-to-mosquito transmission efficiency and present a phase transition between epidemic stability and disease elimination. Our results highlight the possible benefit of using gametocidal agents in malaria prevention. They may also be very effective in reducing disease transmission in the presence of strong heterogeneity.

The use of ivermectin in facilitating disease elimination at gametocytemia phase transition may have a significant potential benefit in disease prevention by increasing early mosquito mortality during the disease incubation period, thus reducing human-to-mosquito transmission efficiency. Its effect may be combined with the use of gametocidal agents in a copula approach, with improved results in disease transmission suppression – see figure 13.1.

The presence of heterogeneity in disease transmission may be responsible for a $\sim 300\%$ increase in disease transmission as a result of hot-spot disease transmission and super-spreading events.

The use of an improved disease burden metrics like the $G = ZX$ score may be used as a more precise instrument of infection prevalence evaluation in the setting of heterogeneity and disease transmission hot-spots. Our results may be used in identifying these disease hot-spots in the presence of significant heterogeneity in disease transmission.

Ivermectin was also effective in reducing disease transmission in the presence of transmission heterogeneity. The combined effect of gametocidal agents and ivermectin may further reduce disease transmission in that specific setting.

Other aspects of heterogeneity were taken into consideration, such as the impact of vector control, silent-carriers migration, and seasonality in disease resurgence. It was shown here that ivermectin was also quite effective in reducing disease transmission in all these settings.

The human-mosquito stochastic dynamical system revealed non-chaotic and non-linear behavior, with stable stochastic closed trajectories circling around well-defined stability points – centers. The dynamical system revealed periodic behavior, insensitive to different status of human and mosquito infection initial conditions.

Time series Box-Jenkins methodology was useful in building better malaria forecasting models. We have shown that Hurst exponent and Shannon entropy evaluated in empirical time series of fixed time length (36 months) may also be useful in forecasting disease transmission. The use of Hurst exponent and Shannon

entropy in malaria incidence time series was extremely helpful in malaria forecasting.

PhD conclusions
Gametocytemia defines *Plasmodium* Human-to-Mosquito transmission (w_h)
Gametocytemia transition phase: epidemic stability vs. disease elimination
Primaquine + ivermectin effective in reducing disease transmission
Heterogeneity increases disease transmission $\sim$ 3x
Ivermectin reduces disease transmission in hot-spots (heterogeneity)
Utility of $G = ZX$ score in disease metrics in the presence of heterogeneity
Vector density, seasonality and human migration promote disease transmission
Ivermectin reduces disease transmission in the presence of:
increased vector density
seasonality
human migration
Heterogeneity interacts with gametocytemia, amplifying disease transmission
Human-Mosquito stochastic system with non-chaotic and non-linear behavior
Stable stochastic closed trajectories around stability points (centres)
Utility of Box-Jenkins time series theory in malaria forecasting models
Utility of Hurst exponent in malaria forecasting models
Utility of Shannon entropy in malaria forecasting models

Table 13.1: PhD conclusions

Summing up:

Computational stochastic models adopting Monte Carlo algorithms are well accepted as a reliable tool in malaria research. Our stochastic model provided adequate simulation data of malaria transmission in different epidemiological situations. Results from model simulations in different epidemiological settings were consistent with was expected from Ross-Macdonald models. Gametocytemia levels in infected human hosts stand as decisive aspect of malaria transmission to be adequately addressed in malaria research.

We have shown the existence of a phase transition in gametocytemia levels between an epidemic stable infection status and potential malaria elimination. This phase transition could be influenced with the help of a preventive strategy of ivermectin administration to a fraction of the human population at risk. This effect suggests that the combined use of a gametocidal agent (such as primaquine or methylene blue) and ivermectin could offer a reliable malaria preventive strategy, thus reducing the need for the use of artemisinin compound therapy as well as the risk of drug resistance induction.

Our data supports the notion that a global malaria preventive strategy should include the following combined steps – see table 13.2, and figures 13.2 and 13.3:

1. Vector control – reduction of mosquito density and active suppression of mosquito anthropophilic behavior.

2. Barrier protective measures – ITN/LLIN/IRS and vaccination.

3. Use of combined gametocidal agents (primaquine or methylene blue) and

Integrated drug strategy in malaria prevention
Gametocidal agent (primaquine) + ivermectin
Human barrier protection (LLIN/ITN/IRS)
Vector control
Targeting malaria hot-spots (strong heterogeneity)
RDT – early malaria diagnosis
Population with high malaria incidence
Children (lower immunity)
During rainfall season
Presence of high mosquito density
Proximity of larval active breeding sites
Human migration from high malaria risk regions
Malaria prediction metrics
$G = ZX$ index (setting of high heterogeneity)
SARIMA model
Hurst exponent
Shannon entropy

Table 13.2: Proposing a global approach to malaria

ivermectin after RDT diagnosis and specific treatment with artemisinin, or in preventive drug campaigns.

4. Suppression of transmission heterogeneity with the use of selective measures oriented to silent carriers, super-spreaders, and transmission hot-spots.

5. Use of Box-Jenkins methodology combined with Hurst exponent and Shannon entropy monthly evaluation of 36-months long strips of malaria incidence time series in malaria incidence forecasting.

The mixed use of all these interventions may support a more effective malaria preventive strategy, improving drug resistance to artemisinin-combined therapy.

Chapter 14

Bibliography

[1] A. Abdel-Wahab, A.A Abdel-Muhsin, E. Ali, S. Suleiman, S. Ahmed, D. Walliker, and H.A. Babiker. Dynamics of Gametocytes among *Plasmodium falciparum* Clones in Natural Infections in an Area of Highly Seasonal Transmission. *The Journal of infectious diseases*, 185(12): 1838–1842, 2002.

[2] T. A. Abeku, S. J. De Vlas, G. Borsboom, A. Teklehaimanot, A. Kebede, D. Olana, G. J. Van Oortmarssen, and J. D. F. Habbema. Forecasting malaria incidence from historical morbidity patterns in epidemic-prone areas of Ethiopia: A simple seasonal adjustment method performs best. *Trop. Med. Int. Heal.*, 7(10):851–857, 2002.

[3] R. Abellana, C. Ascaso, J. Aponte, F. Saute, D. Nhalungo, A. Nhacolo, and P. Alonso. Spatio-seasonal modeling of the incidence rate of malaria in Mozambique. *Malar. J.*, 7:228, 2008.

[4] G. J. Abiodun, O. S. Makinde, A. M. Adeola, K. Y. Njabo, P. J. Witbooi, R. Djidjou-Demasse, and J. O. Botai. A dynamical and zero-inflated negative binomial regression modelling of malaria incidence in Limpopo province, South Africa. *Int. J. Environ. Res. Public Health*, 16(11), 2019.

[5] M.A. Acevedo, O. Prosper, K. Lopiano, N. Ruktanonchai, T.T. Caughlin, M. Martcheva, C.W. Osenberg, and D.L. Smith. Spatial heterogeneity, host movement and mosquito-borne disease transmission. *PLoS One*, 10(6): e0127552, 2015.

[6] S. Adamala. Time Series Analysis: A Hydrological Prospective. *American Journal of Scientific Research and Essays*, 1(1):31–40, 2016.

[7] J.B. Aguilar and J.B. Gutierrez. An epidemiological model of malaria accounting for asymptomatic carriers. *Bulletin of Mathematical Biology*, 82:42, 2020.

[8] N. Ahmed, J.E. Macías-Díaz, A. Raza, D. Balanu, M. Rafiq, Z. Iqbal, and M.O. Ahmad. Design, Analysis and Comparison of a Nonstandard Computational Method for the Solution of a General Stochastic Fractional

Epidemic Model. *Axioms*, 11:10, 2022.

[9] M.C. Akogbéto, A.S. Salako, F. Dagnon, R. Aïkpon, M. Kouletio, A. Sovi, and M. Sezonlin. Blood feeding behaviour comparison and contribution of *Anopheles coluzzii* and *Anopheles gambiae*, two sibling species living in sympatry, to malaria transmission in Alibori and Donga region, northern Benin, West Africa. *Malar. J.*, 17(1):307, 2018.

[10] M.Z. Alam, S.M.N. Arifin, H.M. Al-Amin, M.S. Alam, and M.S. Rahman. A spatial agent-based model of *Anopheles vagus* for malaria epidemiology: Examining the impact of vector control interventions. *Malar. J.*, 16(1): 1–20, 2017.

[11] K. Alemu, A. Worku, Y. Berhane, and A. Kumie. Spatiotemporal clusters of malaria cases at village level, northwest Ethiopia. *Malar. J.*, 13(1):1–8, 2014.

[12] E.A. Alhassan, A.M. Isaac, and A. Emmanuel. Time Series Analysis of Malaria Cases in Kasena Nankana Municipality. *International J. Stat. Appl.*, 7(2):43–56, 2017.

[13] R. Allard. Use of time-series analysis in infectious disease surveillance. *Bull. World Health Organ.*, 76(4):327–333, 1998.

[14] H. Alout, B.J. Krajacich, J.I. Meyers, and et al. Evaluation of ivermectin mass drug administration for malaria transmission control across different West African environments. *Malar. J.*, 13(1):1–10, 2014.

[15] M. Amadi, A. Shcherbacheva, and H. Haario. Agent-based modelling of complex factors impacting malaria prevalence. *Malar. J.*, 20:185, 2021.

[16] N. Amek, N. Bayoh, M. Hamel, and et al. Spatial and temporal dynamics of malaria transmission in rural Western Kenya. *Parasit. Vectors*, 5(1):86, 2012.

[17] R.M. Anderson and R.M. May. *Infectious diseases of humans: Dynamics and control.* Oxford Science publications, 1991.

[18] E. Andrei and E. Bugudui. Econometric Modeling of GDP Time Series. *Theoretical and Applied Economics, XVIII*, 10(563):91–98, 2011.

[19] A.A. Anis and E.H. Lloyd. The expected value of the adjusted rescaled Hurst range of independent normal summands. *Boometrika*, 63(1):111–116, 1976.

[20] K. Annan and C.D. Mukinay. Stability and Time-Scale Analysis of Malaria Transmission in Human-Mosquito Population. *Int. J. Syst. Sci. Appl. Math. 2017*, 2(1):1–9, 2017.

[21] R. Anokye, E. Acheampong, I. Owusu, and E.I. Obeng. Time series analysis of malaria in Kumasi: Using ARIMA models to forecast future incidence. *Cogent Social Sciences*, 4:1461544, 2018.

[22] M.Y. Anwar, J.A. Lewnard, S. Parikh, and et al. Time series analysis of

malaria in Afghanistan: using ARIMA models to predict future trends in incidence. *Malar. J.*, 15(1):566, 2016.

[23] S.T. Appiah, H. Otoo, and I.B. Nabubie. Times Series Analysis Of Malaria Cases In Ejisu- Juaben Municipality. *Int. J. Sci. Technol. Res.*, 4(6): 220–226, 2015.

[24] M. Aregawi, M. Lynch, W. Bekele, and et al. Time series analysis of trends in malaria cases and deaths at hospitals and the effect of antimalarial interventions, 2001-2011, Ethiopia. *PLoS One*, 9(11):e106359, 2014.

[25] S.M.N. Arifin, Y. Zhou, G.J. Davis, J.E. Gentile, G.R. Madey, and F.H. Collins. An agent-based model of the population dynamics of *Anopheles gambiae*. *Malar. J.*, 13(1):424, 2014.

[26] E. Atcheson, K. Bauza, and A. Reyes-Sandoval. A probabilistic model of pre-erythrocytic malaria vaccine combination in mice. *PLoS One*, 14(1): 1–26, 2019.

[27] E. Avila-Vales and B. Buonomo. Analysis of a mosquito-borne disease transmission model with vector stages and nonlinear forces of infection. *Ric. di Mat.*, 64(2):377–390, 2015.

[28] R. Azevedo, A.M. Mendes, and M. Prudêncio. Inhibition of *Plasmodium* sporogonic stages by ivermectin and other avermectins. *Parasites Vectors*, 12:549, 2019.

[29] T. Bakary, S. Boureima, and T. Sado. A mathematical model of malaria transmission in a periodic environment. *J. Biol. Dyn.*, 12(1):400–432, 2018.

[30] F.N. Baliraine, Y.A. Afrane, D.A. Amenya, M. Bonizzoni, A.M. Vardo-Zalik, D.M. Menge, A.K. Githeko, and G. Yan. A cohort study of *Plasmodium falciparum* infection dynamics in Western Kenya Highlands. *BMC Infectious Diseases*, 10:283, 2010.

[31] A. Baltac. Economic and Financial Analysis Based on Time Series Method. *International Journal of Academic Research in Accounting, Finance and Management Sciences*, 5(3):77–82, 2015.

[32] J. Barunik and L. Kristoufek. On Hurst exponent estimation under heavy-tailed distributions. *Physica A: Statistical Mechanics and its Applications*, 389(18):3844–3855, 2010.

[33] A.S. Bedane, T.K. Tanto, and T.F. Asena. Malaria Distribution in Kucha District of Gamo Gofa Zone, Ethiopia: A Time Series Approach. *Am. J. Theor. Appl. Stat.*, 5(2):70–79, 2016.

[34] P. Bejon, T.N. Williams, A. Liljander, and et al. Stable and unstable malaria hotspots in longitudinal cohort studies in Kenya. *PLoS Med.*, 7(7), 2010.

[35] D.B. Belay, Y.G. Kifle, A.T. Goshu, J.M. Gran, D. Yewhalaw, L. Duchateau, and A. Frigessi. Joint Bayesian modeling of time to malaria

and mosquito abundance in Ethiopia. *BMC Infect. Dis.*, 17:1–12, 2017.

[36] S.E. Bellan. The importance of age dependent mortality and the extrinsic incubation period in models of mosquito-borne disease transmission and control. *PLoS One*, 5(4), 2010.

[37] Y. Bi, W. Hu, H. Liu, Y. Xiao, Y. Guo, S. Chen, L. Zhao, and S. Tong. Can slide positivity rates predict malaria transmission? *Malar. J.*, 11:1–8, 2012.

[38] J. Biggs, J. Raman, J. Cook, and et al. Serology reveals heterogeneity of *Plasmodium falciparum* transmission in northeastern South Africa: implications for malaria elimination. *Malar. J.*, 16:48, 2017.

[39] A. Bomblies, J. Duchemin, and E.A.B. Eltahir. A mechanistic approach for accurate simulation of village scale malaria transmission. *Malar. J.*, 8:223, 2009.

[40] S. Bosson-Amedenu. Nonseasonal ARIMA Modeling and Forecasting of Malaria Cases in Children under Five in Edum Banso Sub-district of Ghana. *Asian Res. J. Math.*, 4(3):1–11, 2017.

[41] H. Bosson-Vanga, J. Franetich, V. Soulard, and et al. Differential activity of methylene blue against erythrocytic and hepatic stages of *Plasmodium*. *Malar. J.*, 17(1):143, 2018.

[42] T. Bousema and C. Drakeley. Epidemiology and Infectivity of *Plasmodium falciparum* and *Plasmodium vivax* Gametocytes in Relation to Malaria Control and Elimination. *Clinical Microbiology Reviews*, 24(2):377–410, 2011.

[43] T. Bousema, C. Drakeley, S. Gesase, and et al. Identification of hot spots of malaria transmission for targeted malaria control. *J. Infect. Dis.*, 201 (11):1764–1774, 2010.

[44] T. Bousema, L. Okell, S. Shekalaghe, and et al. Revisiting the circulation time of *Plasmodium falciparum* gametocytes: molecular detection methods to estimate the duration of gametocyte carriage and the effect of gametocytocidal drugs. *Malar. J.*, 9:136, 2010.

[45] T. Bousema, J.T. Griffin, R.W. Sauerwein, , and et al. Hitting hotspots: Spatial targeting of malaria for control and elimination. *PLoS Med.*, 9(1): 1–7, 2012.

[46] G.E.P. Box and Jenkins G.M. Time series analysis: Forecasting and control. *Holden day: San Francisco*, 1970.

[47] R.M. Boyce, R. Reyes, M. Matte, M. Ntaro, E. Mulogo, F.C. Lin, and M.J. Siedner. Practical implications of the non-linear relationship between the test positivity rate and malaria incidence. *PLoS One*, 11(3):1–9, 2016.

[48] O.J. Brady, H.C. Slater, P. Pemberton-Ross, and et al. Role of mass drug administration in elimination of *Plasmodium falciparum* malaria: a consensus modelling study. *Lancet Glob Health*, 5:e680–87, 2017.

[49] M.T. Bretscher, N. Maire, N. Chitnis, I. Felger, S. Owusu-Agyei, and T. Smith. The distribution of *Plasmodium falciparum* infection durations. *Epidemics*, 3(2):109–118, 2011.

[50] M.T. Bretscher, N. Maire, I. Felger, S. Owusu-Agyei, and T. Smith. Asymptomatic *Plasmodium falciparum* infections may not be shortened by acquired immunity. *Malar. J.*, 14:294, 2015.

[51] M.T. Bretscher, J.T. Griffin, A.C. Ghani, and L.C. Okell. Modelling the benefits of long - acting or transmission - blocking drugs for reducing *Plasmodium falciparum* transmission by case management or by mass treatment. *Malar. J.*, 16:341, 2017.

[52] O.J.T. Briët, P. Vounatsou, D.M. Gunawardena, G.N.L. Galappaththy, and P.H. Amerasinghe. Models for short term malaria prediction in Sri Lanka. *Malar. J.*, 7:76, 2008.

[53] T. Britton, T. House, A.L. Lloyd, D. Mollison, S. Riley, and P. Trapman. Five challenges for stochastic epidemic models involving global transmission. *Epidemics*, 10:54–57, 2015.

[54] M.G. Buhnerkempe, M.G. Roberts, A.P. Dobson, H. Heesterbeek, P.J. Hudson, and J.O. Lloyd-Smith. Eight challenges in modelling disease ecology in multi-host, multi-agent systems. *Epidemics*, 10:26–30, 2015.

[55] G. Camarda, P. Jirawatcharadech, R.S. Priestley, and et al. Antimalarial activity of primaquine operates via a two-step biochemical relay. *Nature Communications*, 10:3226, 2019.

[56] C. Caminade, S. Kovatsc, J. Rocklov, and et al. Impact of climate change on global malaria distribution. *PNAS*, 111(9):3286–3291, 2014.

[57] A. Carbone, G. Castelli, and H.E. Stanley. Time-dependent Hurst exponent in financial time series. *Physica A*, 344:267—271, 2004.

[58] F. Castelli and G. Sulis. Migration and infectious diseases. *Clin. Microbiol. Infect.*, 23(5):283–289, 2017.

[59] S.N. Catlin, P. Guttorp, and J.L. Abkowitz. The kinetics of clonal dominance in myeloproliferative disorders. *Blood*, 106(8):2688–2692, 2005.

[60] CDC. Malaria life cycle. 2022. URL `https://www.cdc.gov/malaria/about/biology/index.html`.

[61] C. Chaccour, J. Lines, and C.J.M. Whitty. Effect of Ivermectin on Anopheles gambiae Mosquitoes Fed on Humans: The Potential of Oral Insecticides in Malaria Control. *J. Infect. Dis.*, 202(1):113–116, 2010.

[62] C.J. Chaccour. Advancing the repurposing of ivermectin for malaria. *www.thelancet.com*, 393, 2019. URL `http://dx.doi.org/10.1016/S0140-6736(18)32613-8`.

[63] C.J. Chaccour, K.C. Kobylinski, Q. Bassat, T. Bousema, C. Drakeley, P. Alonso, and B.D. Foy. Ivermectin to reduce malaria transmission: a

research agenda for a promising new tool for elimination. *Malar. J.*, 12:153, 2013.

[64] C. Chatfield. *The Analysis of Time Series.* Chapman & Hall/CRC, 2006.

[65] C. Chatterjee and R.R. Sarkar. Multi-step polynomial regression method to model and forecast malaria incidence. *PLoS One*, 4(3):e4626, 2009.

[66] S. Chaturvedi and S. Dwivedi. Estimating the malaria transmission over the Indian subcontinent in a warming environment using a dynamical malaria model. *J Water Health*, 18(3):358–374, 2020.

[67] B.E. Chekol and H. Hagras. A Big-Bang Big-Crunch Type-2 Fuzzy Logic-based System for Malaria Epidemic Prediction in Ethiopia. *Journal of Engineering and Computer Sciences*, 21(2):64–74, 2020.

[68] J. Chirombo, P. Ceccato, R. Lowe, D.J. Terlouw, M.C. Thomson, A. Gumbo, P.J. Diggle, and J.M. Read. Childhood malaria case incidence in Malawi between 2004 and 2017: spatio-temporal modelling of climate and non-climate factors. *Malar. J.*, 19:5, 2020.

[69] N. Chitnis, J.M. Cushing, and J.M. Hyman. Bifurcation analysis of a mathematical model for malaria transmission. *SIAM J. Appl. Math.*, 67(1): 24–45, 2006.

[70] N. Chitnis, D. Hardy, and T. Smith. A Periodically-Forced Mathematical Model for the Seasonal Dynamics of Malaria in Mosquitoes. *Bull. Math. Biol.*, 74(5):1098–1124, 2012.

[71] N. Chitnis, A. Schapira, C. Schindler, M.A. Penny, and T.A. Smith. Mathematical analysis to prioritise strategies for malaria elimination. *J. Theor. Biol.*, 455:118–130, 2018.

[72] S.E. Choi, M.L. Brandeau, and E. Bendavid. Cost-effectiveness of malaria preventive treatment for HIV-infected pregnant women in sub-Saharan Africa. *Malar. J.*, 16(1):1–10, 2017.

[73] T.S. Churcher, E.J. Dawes, R.E. Sinden, G.K. Christophides, J.C. Koella, and M. Basáñez. Population biology of malaria within the mosquito: density-dependent processes and potential implications for transmission-blocking interventions. *Malar. J.*, 9:311, 2010.

[74] T.S. Churcher, R.E. Sinden, N.J. Edwards, and et al. Probability of transmission of malaria from mosquito to human is regulated by mosquito parasite density in naïve and vaccinated hosts. *PLoS Pathog.*, 13(1): e1006108, 2017.

[75] E. Cleary, M.W. Hetzel, P.M. Siba, C.L. Lau, and A.C.A. Clements. Spatial prediction of malaria prevalence in Papua New Guinea: a comparison of Bayesian decision network and multivariate regression modelling approaches for improved accuracy in prevalence prediction. *Malar. J.*, 20:269, 2021.

[76] J.E. Coalson, L.M. Cohee, A.G. Buchwald, and et al. Simulation models predict that school-age children are responsible for most human-to-mosquito *P. falciparum* transmission in southern Malawi. *Malar. J.*, 17:147, 2018.

[77] L.E. Coffeng, C.C. Hermsen, R.W. Sauerwein, and S.J. de Vlas. The Power of Malaria Vaccine Trials Using Controlled Human Malaria Infection. *PLOS Comp Biol*, 13(1):e1005255, 2017. ISSN 1553-7358.

[78] J.M. Cohen, D.L. Smith, C. Cotter, A. Ward, G. Yamey, O.J. Sabot, and B. Moonen. Malaria resurgence: A systematic review and assessment of its causes. *Malar. J.*, 11:122, 2012.

[79] J.M. Cohen, S. Dlamin, J.M. Novotny, D. Kandula, S. Kunene, and Tatem. A.J. Rapid case-based mapping of seasonal malaria transmission risk for strategic elimination planning in Swaziland. *Malar. J.*, 12:61, 2013.

[80] K.A. Collins, A. Ouedraogo, W.M. Guelbeogo, and et al. Investigating the impact of enhanced community case management and monthly screening and treatment on the transmissibility of malaria infections in Burkina Faso: study protocol for a cluster-randomised trial. *BMJ Open*, 9:e030598, 2019.

[81] F.J. Colón-González, M.O. Sewe, A.M. Tompkins, H. Sjödin, A. Casallas, J. Rocklöv, C Caminade, and R. Lowe. Projecting the risk of mosquito-borne diseases in a warmer and more populated world: a multi-model, multi-scenario intercomparison modelling study. *Lancet Planet Health*, 5:e404, 2021.

[82] J. Cook, B. Aydin-Schmidt, I.J. González, and et al. Loop-mediated isothermal amplification (LAMP) for point-of-care detection of asymptomatic low-density malaria parasite carriers in Zanzibar. *Malar. J.*, 14:43, 2015.

[83] L. Cooper, S.Y. Kang, D. Bisanzio, and et al. Pareto rules for malaria super-spreaders and super-spreading. *Nature Communications*, 10:3939, 2019.

[84] S. Cornet, A. Nicot, A. Rivero, and S. Gandon. Both infected and uninfected mosquitoes are attracted toward malaria infected birds. *Malar. J.*, 12(1):1–8, 2013.

[85] C.S. Corrêa, D.A. Schuch, A.P. Queiroz, G. Fisch, F.N. Corrêa, and M.M. Coutinho. The Long-Range Memory and the Fractal Dimension: a Case Study for Alcântara. *J. Aerosp. Technol. Manag.*, 9(4):461–468, 2017.

[86] F.E.G. Cox. History of the discovery of the malaria parasites and their vectors. *Parasites & vectors*, 3(1):5, 2010.

[87] M. Craig, D. Le Sueur, and B. Snow. A climate-based distribution model of malaria transmission in sub-Saharan Africa. *Parasitol. Today*, 15(3): 105–111, 1999.

[88] V. Crowell, O.J.T. Briët, D. Hardy, N. Chitnis, N. Maire, A. Di Pasquale, and T.A. Smith. Modelling the cost-effectiveness of mass screening and treatment for reducing *Plasmodium falciparum* malaria burden. *Malar. J.*, 12:4, 2013.

[89] X. Cui, D. Xue, and T. Li. Fractional-order delayed Ross–Macdonald model for malaria transmission. *Nonlinear Dyn*, 107:3155–3173, 2022.

[90] C.B. Cunha and B.A. Cunha. Brief history of the clinical diagnosis of malaria: from Hippocrates to Osler. *J Vector Borne Dis*, 45(September): 194–199, 2008.

[91] J. Cunningham, S. Jones, Gatton M.L., and et al. A review of the WHO malaria rapid diagnostic test product testing programme (2008–2018): performance, procurement and policy. *Malar. J.*, 18:387, 2019.

[92] D.J. Daley and J. Gani. *Epidemic Modelling: An introduction.* Cambridge University Press, 1999.

[93] S. Dama, H. Niangaly, A. Ouattara, and et al. Reduced ex vivo susceptibility of *Plasmodium falciparum* after oral artemether-lumefantrine treatment in Mali. *Malar. J.*, 16(1):59, 2017.

[94] E.D. Dan, O. Jude, and O. Idochi. Modelling and Forecasting Malaria Mortality Rate using SARIMA Models (A Case Study of Aboh Mbaise General Hospital, Imo State Nigeria). *Science Journal of Applied Mathematics and Statistics*, 2(1):31–41, 2014.

[95] C.E. Dangerfield, J.V. Ross, and M.J. Keeling. Integrating stochasticity and network structure into an epidemic model. *J. R. Soc. Interface*, 6: 761–774, 2009.

[96] E.L. Darkoh, J.A. Larbi, and E.A. Lawer. A Weather-Based Prediction Model of Malaria Prevalence in Amenfi West District, Ghana. *Malar. Res. Treat.*, page 7820454, 2017.

[97] C.M. De Moraes, N.M. Stanczyk, H.S. Betz, H. Pulido, D.G. Sim, A.F. Read, and M.C. Mescher. Malaria-induced changes in host odors enhance mosquito attraction. *Proc. Natl. Acad. Sci.*, 111(30):11079–11084, 2014.

[98] T. Dekker, W. Takken, G.J. Knols, E. Bouman, S. van de Laak, A. de Bever, and P.W.T. Huisman. Selection of biting sites on a human host by *Anopheles gambiae s.s.*, *An. arabiensis* and *An. quadriannulatus*. *Entomologia Experimentalis et Applicata*, 87:295–300, 1998.

[99] A.J. DePina, E.H.A. Niang, A.J.B. Andrade, and et al. Achievement of malaria pre-elimination in Cape Verde according to the data collected from 2010 to 2016. *Malar. J.*, 17:236, 2018.

[100] J.O. Depinay, C.M. Mbogo, G. Killeen, and et al. A simulation model of African *Anopheles* ecology and population dynamics for the analysis of malaria transmission. *Malar. J.*, 3(1):29, 2004.

[101] W. Deressa, A. Ali, and Y. Berhane. Review of the interplay between population dynamics and malaria transmission in Ethiopia. *Ethiop.J.Health Dev.*, 20(3):137–144, 2006.

[102] N.P. Devi and R.K. Jauhari. Climatic variables and malaria incidence in Dehradun, Uttaranchal, India. *J. Vector Borne Dis.*, 43(1):21–28, 2006.

[103] K. Dietz, L. Molineaux, and A. Thomas. A malaria model tested in the African Savannah. *Bull. World Health Organ.*, 50(3-4):347–357, 1974.

[104] D. Dingli, A. Traulsen, and J.M. Pacheco. Stochastic Dynamics of Hematopoietic Tumor Stem Cells. *Cell Cycle*, 6(4):e1–e6, 2007.

[105] A.M. Dondorp, S. Yeung, L. White, C. Nguon, N.P.J. Day, D. Socheat, and L. Seidlein. Artemisinin resistance: current status and scenarios for containment. *Nature reviews. Microbiology*, 8(4):272–280, 2010.

[106] D.L. Doolan, C. Dobano, and J.K. Baird. Acquired Immunity to Malaria. *Clin. Microbiol. Rev.*, 22(1):13–36, 2009.

[107] E. D'Ortenzio, N. Godineau, A. Fontanet, S. Houze, O. Bouchaud, S. Matheron, and J.L. Le Bras. Prolonged *Plasmodium falciparum* infection in immigrants, Paris. *Emerg. Infect. Dis.*, 14(2):323–326, 2008.

[108] C. Dye and G. Hasibeder. Population dynamics of mosquito-borne disease: Effects of flies which bite some people more frequently than others. *Trans. R. Soc. Trop. Med. Hyg.*, 80(1):69–77, 1986.

[109] O. Ebhuoma, M. Gebreslasie, and L. Magubane. Modeling malaria control intervention effect in KwaZulu-Natal, South Africa using intervention time series analysis. *Journal of Infection and Public Health*, 10(3):334–338, 2017.

[110] P.A. Eckhoff. A malaria transmission-directed model of mosquito life cycle and ecology. *Malar. J.*, 10:e303, 2011.

[111] N. Endo and E.A.B. Eltahir. Prevention of malaria transmission around reservoirs: an observational and modelling study on the effect of wind direction and village location. *Lancet Planet. Heal.*, 2(9):e406–e413, 2018.

[112] V. Ermert, A.H. Fink, A.E. Jones, and A.P. Morse. Development of a new version of the Liverpool Malaria Model. II. Refining the parameter settings and mathematical formulation of basic processes based on a literature review. *Malar. J.*, 10(1):35, 2011.

[113] J. Espinoza. Malaria Resurgence in the Americas: An Underestimated Threat. *Pathogens*, 8(1):11, 2019.

[114] L. Esteva, A.B. Gumelb, and C.V. León. Qualitative study of transmission dynamics of drug-resistant malaria. *Mathematical and Computer Modelling*, 50:611–630, 2009.

[115] D.A. Ewing, C.A. Cobbold, B.V. Purse, M.A. Nunn, and S.M. White. Modelling the effect of temperature on the seasonal population dynamics of temperate mosquitoes. *J. Theor. Biol.*, 400:65–79, 2016.

[116] C.M. Eze, O.C. Asogwa, C.U. Onwuamaeze, N.M. Eze, and C.I. Okonkwo. On the Fourier Residual Modification of Arima Models in Modeling Malaria Incidence Rates among Pregnant Women. *American Journal of Theoretical and Applied Statistics*, 9(1):1–7, 2020.

[117] A.C. Eziefula, R. Gosling, J. Hwang, and et al. Rationale for short course primaquine in Africa to interrupt malaria transmission. *Malar. J.*, 11(1): 360, 2012.

[118] R.M. Fairhurst and T.E. Wellems. *Plasmodium species (Malaria).* Number 6th Ed. Elsevier. Churchill Livingstone, 2005.

[119] I. Felger, M. Maire, M.T. Bretscher, and et al. The dynamics of natural *Plasmodium falciparum* infections. *PLoS One*, 7(9):e45542, 2012.

[120] J. Feng, H. Yan, X.Y. Feng, L. Zhang, M. Li, Z.G. Xia, and N. Xiao. Imported malaria in China, 2012. *Emerg. Infect. Dis.*, 20(10):1778–1780, 2014.

[121] J. Feng, L. Zhang, F. Huang, J.H. Yin, H. Tu, and Z.G. Xia. Ready for malaria elimination: zero indigenous case reported in the People's Republic of China. *Malar. J.*, 17:315, 2018.

[122] J.L. Ferrão, J.M. Mendes, and M. Painho. Modelling the influence of climate on malaria occurrence in Chimoio Municipality, Mozambique. *Parasites and Vectors*, 10(1):1–12, 2017.

[123] J.L. Ferrão, J.M. Mendes, M. Painho, and S. Zacarias. Malaria mortality characterization and the relationship between malaria mortality and climate in Chimoio, Mozambique. *Malar. J.*, 16:212, 2017.

[124] C.P. Ferreira, S.P. Lyra, F. Azevedo, D. Greenhalgh, and E. Massad. Modelling the impact of the long-term use of insecticide-treated bed nets on *Anopheles* mosquito biting time. *Malar. J.*, 16(1):1–11, 2017.

[125] J.L. Ferrão, D. Earland, A. Novela, R. Mendes, and K.M. Searle. Malaria Temporal Variation and Modelling Using Time-Series in Sussundenga District, Mozambique. *Int. J. Environ. Res. Public Health*, 18:5692, 2021.

[126] A.N. Filipe, E.M. Riley, C.J. Drakeley, C.J. Sutherland, and A.C. Ghani. Determination of the Processes Driving the Acquisition of Immunity to Malaria Using a Mathematical Transmission Model. *PLoS Comput Biol*, 3 (12):e255, 2007.

[127] M.N. Flynn and W.R.L.S. Pereira. Ecological diagnosis from biotic data by Hurst exponent and the R/S analysis adaptation to short time series. *Biomatemática*, 23:1–14, 2013.

[128] C.L.E. Franzke, S.M. Osprey, P. Davini, and N.W. Watkins. A Dynamical Systems Explanation of the Hurst Effect and Atmospheric Low-Frequency Variability. *Scientific Reports*, 5:9068, 2015.

[129] V.J. Gabriel and L.F. Martins. On the forecasting ability of ARFIMA

models when infrequent breaks occur. *Econom. J.*, 7(2):455–475, 2004.

[130] K.S. Ganguly, S. Modak, A.K. Chattopadhyay, K.S. Ganguly, T.K. Mukherjee, A. Dutta, and D. Biswas. Forecasting Based On a SARIMA Model of Urban Malaria for Kolkata. *Am. J. Epidemiol. Infect. Dis.*, 4(2): 22–33, 2016.

[131] M.N.L. Garcia and J.P.R. Requena. Different methodologies and uses of the Hurst exponent in econophysics. *Estudios de Economia Aplicada*, 37 (2):96–108, 2019.

[132] F. Gasse. Hydrological changes in the African tropics since the Last Glacial Maximum. *Quaternary Science Reviews*, 19:189–211, 2000.

[133] M.L. Gatton, J. Dunn, A. Chaudhry, S. Ciketic, J. Cunningham, and Q. Cheng. Implications of parasites lacking *Plasmodium falciparum* histidine-rich protein 2 on malaria morbidity and control when rapid diagnostic tests are used for diagnosis. *J. Infect. Dis.*, 215(7):1156–1166, 2017.

[134] J. Gaudart, O. Touré, N. Dessay, A.I. Dicko, S. Ranque, L. Forest, J. Demongeot, and O.K. Doum. Modelling malaria incidence with environmental dependency in a locality of Sudanese savannah area, Mali. *Malar. J.*, 8:61, 2009.

[135] A.A. Gebremeskel and H.E. Krogstad. Mathematical Modelling of Endemic Malaria Transmission. *American Journal of Applied Mathematics*, 3(2): 36–46, 2015.

[136] J.E. Gentile, S.S.C. Rund, and G.R. Madey. Modelling sterile insect technique to control the population of *Anopheles gambiae*. *Malar. J.*, 14(1): 92, 2015.

[137] J. Gerardin, A.L. Ouédraogo, K.A. Mccarthy, P.A. Eckhoff, and E.A. Wenger. Characterization of the infectious reservoir of malaria with an agent-based model calibrated to age-stratified parasite densities and infectiousness. *Malar. J.*, 14:231, 2015.

[138] J. Gerardin, C.A. Bever, D. Bridenbecker, and et al. Effectiveness of reactive case detection for malaria elimination in three archetypical transmission settings: a modelling study. *Malar. J.*, 16(1):248, 2017.

[139] J. Gerardin, A. Bertozzi-Villa, P.A. Eckhoff, and E.A. Wenger. Impact of mass drug administration campaigns depends on interaction with seasonal human movement. *Int. Health*, 10(4):252–257, 2018.

[140] A.A.M. Gerritsen, P. Kruger, M.F.S. Van Der Loeff, and M.P. Grobusch. Malaria incidence in Limpopo Province, South Africa, 1998-2007. *Malar. J.*, 7:1–8, 2008.

[141] B. Getnet and S. Ayalew. Developing Stochastic Model For Forecasting Malaria Cases In Addis Zemen, South Gondar, Ethiopia: A Time Series

Analysis. *Nat. Sci.*, 15(4):64–77, 2017.

[142] A.C. Ghani, C.J. Sutherland, E.M. Riley, C.J. Drakeley, J.T. Griffin, R.D. Gosling, and J.A.N. Filipe. Loss of Population Levels of Immunity to Malaria as a Result of Exposure-Reducing Interventions: Consequences for Interpretation of Disease Trends. *PLoS ONE*, 4(2):e4383, 2009.

[143] F. Girond, L. Randrianasolo, L. Randriamampionona, and et al. Analysing trends and forecasting malaria epidemics in Madagascar using a sentinel surveillance network: a web-based application. *Malar J.*, 16(1):72, 2017.

[144] A. Golestani and R. Gras. Can we predict the unpredictable? *Sci. Rep.*, 4: 1–6, 2014.

[145] E. Gomes, C. Capinha, J. Rocha, and C. Sousa. Mapping risk of malaria transmission in mainland Portugal using a mathematical modelling approach. *PLoS One*, 11(11):1–17, 2016.

[146] F.M. Gomes, B.L. Hixsona, M.D.W. Tynera, and et al. Effect of naturally occurring *Wolbachia* in *Anopheles gambiae s.l.* mosquitoes from Mali on *Plasmodium falciparum* malaria transmission. *Proc. Nat. Acad. Sci. of the United States of America*, 114(47):12566–12571, 2017.

[147] A. Gomez-Elipe, A. Otero, M. van Herp, and A. Aguirre-Jaime. Forecasting malaria incidence based on monthly case reports and environmental factors in Karuzi, Burundi, 1997-2003. *Malar. J.*, 6:129, 2007.

[148] B.P. Gonçalves, A.B. Tiono, A. Ouédraogo, and et al. Single low dose primaquine to reduce gametocyte carriage and *Plasmodium falciparum* transmission after artemether-lumefantrine in children with asymptomatic infection: a randomised, double-blind, placebo-controlled trial. *BMC Med.*, 14(1):40, 2016.

[149] M.A.S. Granero, J.E.T. Segovia, and J.G. Pérez. Some comments on Hurst exponent and the long memory processes on capital markets. *Physica A: Statistical Mechanics and its Applications*, 387:5543–5551, 2008.

[150] T. Graves, R. Gramacy, N. Watkins, and C. Franzke. A brief history of long memory: Hurst, Mandelbrot and the road to ARFIMA, 1951-1980. *Entropy*, 19:437, 2017.

[151] J.T. Griffin. Is a reproduction number of one a threshold for *Plasmodium falciparum* malaria elimination? *Malar. J.*, 15(1):389, 2016.

[152] J.T. Griffin, T. D. Hollingsworth, L.C. Okell, and et al. Reducing *Plasmodium falciparum* malaria transmission in Africa: A model-based evaluation of intervention strategies. *PLoS Med.*, 7(8):e1000324, 2010.

[153] J.T. Griffin, N.M. Ferguson, and A.C. Ghani. Linking the incidence and age patterns of clinical malaria to parasite prevalence using a mathematical model. *Malar. J.*, 11(Suppl 1):P115, 2012.

[154] WWARN Gametocyte Study Group. Gametocyte carriage in

uncomplicated *Plasmodium falciparum* malaria following treatment with artemisinin combination therapy: a systematic review and meta-analysis of individual patient data. *BMC Medicine*, 14:79, 2016.

[155] W. Gu and R.J. Novak. Predicting the impact of insecticide-treated bed nets on malaria transmission: The devil is in the detail. *Malar. J.*, 8(1): 1–10, 2009.

[156] W. Gu, G.F. Killeen, C.M. Mbogo, J.L. Regens, J.I. Githure, and C. John. An individual-based model of *Plasmodium falciparum* malaria transmission on the coast of Kenya. *Trans. R. Soc. Trop. Med. Hyg.*, 97:43–50, 2003.

[157] D. Gurarie and F.E. McKenzie. A stochastic model of immune-modulated malaria infection and disease in children. *Math. Biosci.*, 210:576–597, 2007.

[158] D. Gurarie, S. Karl, P.A. Zimmerman, C.H. King, T.G. St.Pierre, and T.M.E. Davis. Mathematical Modeling of Malaria Infection with Innate and Adaptive Immunity in Individuals and Agent-Based Communities. *PLoS One*, 7(3):e34040, 2012.

[159] M.J. Harris, S.I. Hay, and J.M. Drake. Early warning signals of malaria resurgence in Kericho, Kenya. *Biology letters*, 16(3):1–6, 2020.

[160] H. Hasyim, M. Dhimal, J. Bauer, D. Montag, D.A. Groneberg, U. Kuch, and R. Müller. Does livestock protect from malaria or facilitate malaria prevalence? A cross-sectional study in endemic rural areas of Indonesia. *Malar. J.*, 17(1):302, 2018.

[161] S.I. Hay, D.J. Rogers, G.D. Shanks, M.F. Myers, and R.W. Snow. Malaria early warning in Kenya. *Trends Parasitol.*, 17(2):95–99, 2001.

[162] S.I. Hay, J. Cox, D.J. Rogers, S.E. Randolph, D.I. Stern, G.D. Shanks, M.F. Myers, and R.W. Snow. Climate Change and the Resurgence of Malaria in the East African Highlands. *Nature*, 415(6874):905–909, 2002.

[163] U. Helfenstein. The use of transfer function models, intervention analysis and related time series methods in epidemiology. *International Journal of Epidemiology*, 20(3):808–815, 1991.

[164] H.W. Hethcote. The Mathematics of Infectious Diseases. *Soc. Ind. Appl. Math. Rev.*, 42(4):599–653, 2000.

[165] T.D. Hollingsworth, J.R.C. Pulliam, S. Funk, J.E. Truscott, V. Isham, and A.L. Lloyd. Seven challenges for modelling indirect transmission: Vector-borne diseases, macroparasites and neglected tropical diseases. *Epidemics*, 10:16–20, 2014.

[166] L. Hong. Decomposition and Forecast for Financial Time Series with High-frequency Based on Empirical Mode Decomposition. *Energy Procedia*, 5:1333–1340, 2011.

[167] M.B. Hoshen and A.P. Morse. A weather-driven model of malaria transmission. *Malar. J.*, 3(1):32, 2004.

[168] L. Huldén, L. Huldén, and K. Heliövaara. Endemic malaria: An 'indoor' disease in northern Europe. Historical data analysed. *Malar. J.*, 4:1–13, 2005.

[169] H.E. Hurst. The Long-Term Storage Capacity of Reservoir. *Transactions of the American Society of Civil Engineers*, 116(1):770–799, 1951.

[170] H.H. Hussien, F.H. Eissa, and K.E. Awadalla. Statistical Methods for Predicting Malaria Incidences Using Data from Sudan. *Malaria Research and Treatment*, 4205957:1–9, 2017.

[171] M.A. Janssen and W.J.M. Martens. Modeling Malaria as a Complex Adaptive System. *Artif. Life*, 3(3):213–236, 1997.

[172] T.P. Jensen, H. Bukirwa, D. Njama-Meya, D. Francis, M.R. Kamya, P.J. Rosenthal, and G. Dorsey. Use of the slide positivity rate to estimate changes in malaria incidence in a cohort of Ugandan children. *Malar. J.*, 8 (1):1–8, 2009.

[173] T.H. Jetten and W. Takken. Anophelism without malaria in Europe. A review of the ecology and distribution of the genus *Anopheles* in Europe. *Wageningen Agric. Univ. Papers*. 5:69, 1994.

[174] X. Jin, S. Jin, and D. Gao. Mathematical Analysis of the Ross–Macdonald Model with Quarantine. *Bulletin of Mathematical Biology*, 82(47):1–26, 2020.

[175] A. Jindal. Agent-Based Modeling and Simulation of Mosquito-Borne Disease Transmission. *Proc. 16th Int. Conf. Auton. Agents Multiagent Syst. - AAMAS (2017)*, 2017.

[176] C.C. John. Primaquine plus artemisinin combination therapy for reduction of malaria transmission: promise and risk. *BMC Med.*, 14:65, 2016.

[177] G.L. Johnston, D.L. Smith, and D.A. Fidock. Malaria's missing number: Calculating the human component of R0 by a within-host mechanistic model of *Plasmodium falciparum* infection and transmission. *PLoS Comput Biol*, 9(4):e1003025, 2013.

[178] M. Julian, R. Alcaraz, and J.J. Rieta. Generalized Hurst Exponents as a Tool to Estimate Atrial Fibrillation Organization from the Surface ECG. *Computing in Cardiology*, 40:1199–1202, 2013.

[179] W. Kagaya, J. Gitaka, C.W. Chan, Kongere J., Z.M. Idris, C. Deng, and A. Kaneko. Malaria resurgence after significant reduction by mass drug administration on Ngodhe Island, Kenya. *Scientific Reports*, 9:19060, 2019.

[180] J.C. Kamgang and S.Y. Tchoumi. A model of the dynamic of transmission of malaria, integrating SEIRS, SEIS, SIRS and SIS organization in the host-population. *J. Appl. Anal. Comput.*, 5(4):688–703, 2015.

[181] S. Karl, D. Gurarie, P.A. Zimmerman, C.H. King, T.G. St.Pierre, and T.M.E. Davis. A sub-microscopic gametocyte reservoir can sustain malaria

transmission. *PLoS One*, 6(6):e20805, 2011.

[182] S. Karl, M.T. White, G.J. Milne, D. Gurarie, S.I. Hay, A.E. Barry, I. Felger, and I. Mueller. Spatial effects on the multiplicity of *Plasmodium falciparum* infections. *PLoS One*, 11(10):1–20, 2016.

[183] M. Kashiwada and S. Ohta. Modeling the Spatio-Temporal Distribution of the *Anopheles* Mosquito based on Life History and Surface Water Conditions. *Open Ecol. J.*, 3(1):29–40, 2010.

[184] C. Kaufmann and H. Briegel. Flight performance of the malaria vectors *Anopheles gambiae* and *Anopheles atroparvus*. *J. vector Ecol.*, 29(1): 140–153, 2004.

[185] M.J. Keeling and P. Rohani. An introduction to infectious disease modelling. Princeton University Press, 2008.

[186] W.O. Kermack and A.G. McKendrick. A Contribution to the Mathematical Theory of Epidemics. *Proc.Roy.Soc.Lond.*, A115:700–721, 1927.

[187] S.E. Kern, A.B. Tiono, M. Makanga, and et al. Community screening and treatment of asymptomatic carriers of Plasmodium falciparum with artemether-lumefantrine to reduce malaria disease burden: a modelling and simulation analysis. *Malar. J.*, 10:210, 2011.

[188] G.F. Killeen, F.E. McKenzie, B.D. Foy, C. Schieffelin, P.F. Billingsley, and J.C. Beier. A simplified model for predicting malaria entomologic inoculation rates based on entomologic and parasitologic parameters relevant to control. *Am. J. Trop. Med. Hyg.*, 62(5):535–544, 2000.

[189] G.F. Killeen, A. Seyoum, and B.G.J. Knols. Rationalizing historical successes of malaria control in Africa in terms of mosquito resource availabilty management. *Am. J. Trop. Med. Hyg.*, 71(2 SUPPL.):87–93, 2004.

[190] G.F. Killeen, N.J. Govella, D.W. Lwetoijera, and F.O. Okumu. Most outdoor malaria transmission by behaviourally-resistant *Anopheles arabiensis* is mediated by mosquitoes that have previously been inside houses. *Malar. J.*, 15(1):225, 2016.

[191] Y Kim, J.V. Ratnam, T. Doi, and et al. Malaria predictions based on seasonal climate forecasts in South Africa: A time series distributed lag nonlinear model. *Scientific Reports*, 9:17882, 2019.

[192] L. Kirichenko, T. Radivilova, and V. Bulakh. Generalized approach to Hurst exponent estimating by time series. *IAPGOS*, 8(1):28–31, 2018.

[193] D.J. Klein, M. Baym, and P. Eckhoff. The separatrix algorithm for synthesis and analysis of stochastic simulations with applications in disease modeling. *PLoS One*, 9(7), 2014.

[194] E.Y. Klein, D.L. Smith, M.F. Boni, and R. Laxminarayan. Clinically immune hosts as a refuge for drug-sensitive malaria parasites. *Malar. J.*, 7:

67, 2008.

[195] K.C. Kobylinski, M. Sylla, P.L. Chapman, M.D. Sarr, and B.D. Foy. Ivermectin mass drug administration to humans disrupts malaria parasite transmission in Senegalese villages. *Am. J. Trop. Med. Hyg.*, 85(1):3–5, 2011.

[196] K.C. Kobylinski, B.D. Foy, and J.H. Richardson. Ivermectin inhibits the sporogony of *Plasmodium falciparum* in *Anopheles gambiae*. *Malar. J.*, 11 (1):381, 2012.

[197] J.C. Koella. On the use of mathematical models of malaria transmission. *Acta Trop.*, 49(1):1–25, 1991.

[198] J.C Koella and R. Antia. Epidemiological models for the spread of anti-malarial resistance. *Malar. J.*, 2:3, 2003.

[199] E. Korenromp, G. Mahiané, M. Hamilton, C. Pretorius, R. Cibulskis, J. Lauer, T.A. Smith, and O.J.T. Briët. Malaria intervention scale-up in Africa: effectiveness predictions for health programme planning tools, based on dynamic transmission modelling. *Malar. J.*, 15(1):417, 2016.

[200] O. Koutou, B. Traoré, and B. Sangaré. Mathematical model of malaria transmission dynamics with distributed delay and a wide class of nonlinear incidence rates. *Cogent Math. Stat.*, 5(1564531):1–25, 2018.

[201] A. Kuehn and G. Pradel. The coming-out of malaria gametocytes. *J. Biomed. Biotechnol.*, 2010(976827):1–11, 2010.

[202] S. Kulesza and M. Belej. Descriptive analysis on nonstationarity of the time series on real estate market. *Journal of International Studies*, 8(2): 34–42, 2015.

[203] A. Kumar, H.K. Chaturvedi, A.K. Mohanty, S.K. Sharma, M.S. Malhotra, and A. Pandey. Surveillance based estimation of burden of malaria in India, 2015–2016. *Malar. J.*, 19:156, 2020.

[204] V. Kumar, A. Mangal, S. Panesar, G. Yadav, R. Talwar, D. Raut, and S. Singh. Forecasting malaria cases using climatic factors in Delhi, India: a time series analysis. *Malar. Res. Treat.*, page 482851, 2014.

[205] F. Kurth, M. Develoux, M. Mechain, and et al. Severe malaria in Europe: an 8-year multi-centre observational study. *Malar J*, 16:57, 2017.

[206] R. Lacroix, W.R. Mukabana, L.C. Gouagna, and J.C. Koella. Malaria infection increases attractiveness of humans to mosquitoes. *PLoS Biol.*, 3 (9):1590–1593, 2005.

[207] F. Lalubin, A. Delédevant, O. Glaizot, and P. Christe. Natural malaria infection reduces starvation resistance of nutritionally stressed mosquitoes. *Journal of Animal Ecology*, 83:850–857, 2014.

[208] J. Landier, D.M. Parker, A.M. Thu, K.M. Lwin, G. Delmas, and for the Malaria Elimination Task Force Group Nosten, F.H. Effect of generalised

access to early diagnosis and treatment and targeted mass drug administration on *Plasmodium falciparum* malaria in Eastern Myanmar: an observational study of a regional elimination programme. *Lancet*, 391: 1916–1926, 2018.

[209] E.D. Landoh, P. Tchamdja, B. Saka, K.S. Tint, S.N. Gitta, P. Wasswa, and J. Christiaan. Morbidity and mortality due to malaria in Est Mono district, Togo, from 2005 to 2010: a times series analysis. *Malar. J.*, 11:389, 2012.

[210] J.M. Lauderdale, C. Caminade, A.E. Heath, and et al. Towards seasonal forecasting of malaria in India. *Malar. J.*, 13(1):310, 2014.

[211] M.B. Laurens, P. Billingsley, A. Richman, and et al. Successful Human Infection with *P. falciparum* Using Three Aseptic *Anopheles stephensi* Mosquitoes: A New Model for Controlled Human Malaria Infection. *PLoS One*, 8(7), 2013.

[212] S. Lawpoolsri, E.Y. Klein, P. Singhasivanon, and et al. Optimally timing primaquine treatment to reduce *Plasmodium falciparum* transmission in low endemicity Thai-Myanmar border populations. *Malar. J.*, 8:159, 2009.

[213] A.J. Lawrance and N.T. Kottegoda. Stochastic Modelling of Riverflow Time Series. *J.R. Statist. Soc. A*, 140, Part 1:1, 1977.

[214] P. Layie, V.C. Kamla, J.C. Kamgang, and Y.E. Wono. Agent-based modeling of malaria control through mosquito aquatic habitats management in a traditional sub-Sahara grouping. *BMC Public Health*, 21: 487, 2021.

[215] P.V.V. Le, P. Kumar, M.O. Ruiz, C. Mbogo, and E.J. Muturi. Predicting the direct and indirect impacts of climate change on malaria in coastal Kenya. *PLoS One*, 14(2):1–18, 2019.

[216] A. Le Menach, F.E. McKenzie, A. Flahault, and D.L. Smith. The unexpected importance of mosquito oviposition behaviour for malaria: non-productive larval habitats can be sources for malaria transmission. *Malar. J.*, 4:23, 2005.

[217] P.W. Lee, C.T. Liu, H.S. Rampao, V.E. Rosario, and M.F. Shaio. Pre-elimination of malaria on the island of Príncipe. *Malar. J.*, 9:26, 2010.

[218] Z. Li, Y. Yang, N. Xiao, and et al. Malaria Imported from Ghana by Returning Gold Miners, China, 2013. *Emerg. Infect. Dis.*, 21(5):864–867, 2015.

[219] P. Liehl, P. Meireles, I.S. Albuquerque, M. Pinkevych, F. Baptista, M.M. Mota, M.P. Davenport, and M. Prudêncio. Innate Immunity Induced by *Plasmodium* Liver Infection Inhibits Malaria Reinfections. *Infection and Immunity*, 83(3):1172–1180, 2015.

[220] M.V.M. Lima and G.Z. Laporta. Evaluation of prediction models for the occurrence of malaria in the state of Amapá, Brazil, 1997-2016: an

ecological study. *Epidemiol.Serv.Saúde, Brasília*, 30:e2020080, 2021.

[221] J.T. Lin, C. Lon, M.D. Spring, and et al. Single dose primaquine to reduce gametocyte carriage and *Plasmodium falciparum* transmission in Cambodia: An open-label randomized trial. *PLoS One*, 12(6):e0168702, 2017.

[222] J. Liu, B. Yang, W.K. Cheung, and G. Yang. Malaria transmission modelling: a network perspective. *Infect. Dis. Poverty*, 1(1):11, 2012.

[223] W. Liu, Y. Li, G.H. Learn, and et al. Origin of the human malaria parasite *Plasmodium falciparum* in gorillas. *Nature*, 467(7314):420–425, 2010.

[224] A.L Lloyd and R.M. May. Spatial Heterogeneity in Epidemic Models. *J. Theor. Biol.*, 179(March 1995):1–11, 1996.

[225] A.L. Lloyd, S Valeika, and A. Cintrón-Arias. Infection Dynamics on Small-World Networks. *Physical Review E*, 64(6):1–26, 2005.

[226] D.E. Loy, W. Liu, Y. Li, G.H. Learn, L.J. Plenderleith, S.A. Sundararaman, P.M. Sharp, and Hahn B.H. Out of Africa: origins and evolution of the human malaria parasites *Plasmodium falciparum* and *Plasmodium vivax*. *International Journal for Parasitology*, 47:87–97, 2015.

[227] G. Lu, S. Zhou, O. Horstick, X. Wang, Y. Liu, and O. Müller. Malaria outbreaks in China (1990 – 2013): a systematic review. *Malar. J.*, 13:269, 2014.

[228] T.M. Lunde, D. Korecha, E. Loha, A. Sorteberg, and B. Lindtjørn. A dynamic model of some malaria-transmitting anopheline mosquitoes of the Afrotropical region. I. Model description and sensitivity analysis. *Malar. J.*, 12(1):28, 2013.

[229] K.E. Lyke, M. Laurens, M. Adams, and et al. *Plasmodium falciparum* malaria challenge by the bite of aseptic *Anopheles stephensi* mosquitoes: Results of a randomized infectivity trial. *PLoS One*, 5(10), 2010.

[230] G. Macdonald. The analysis of equilibrium in malaria. *Trop. Dis. Bull.*, 49: 813–829, 1952.

[231] G. Macdonald. . The epidemiology and control of malaria. Oxford University Press, London., 1957.

[232] G. Macdonald, C. B. Cuellar, and C. V. Foll. The dynamics of malaria. *Bull. World Health Organ.*, 38(5):743–755, 1968.

[233] A. Mahande, F. Mosha, J. Mahande, and E. Kweka. Feeding and resting behaviour of malaria vector, *Anopheles arabiensis* with reference to zooprophylaxis. *Malar. J.*, 6:100, 2007.

[234] N. Maire, S.D. Shillcutt, D.G. Walker, F. Tediosi, and T.A. Smith. Cost-Effectiveness of the Introduction of a Pre-Erythrocytic Malaria Vaccine into the Expanded Program on Immunization in Sub-Saharan Africa: Analysis of Uncertainties Using a Stochastic Individual-Based

Simulation Model of *Plasmodium falciparum* Malaria. *Value in Health*, 14: 1028–1038, 2011.

[235] A. Malede, K. Alemu, M. Aemero, S. Robele, and H. Kloos. Travel to farms in the lowlands and inadequate malaria information significantly predict malaria in villages around Lake Tana, northwest Ethiopia: A matched case-control study. *Malar. J.*, 17(1):290, 2018.

[236] malERA Consultative Group on Modeling. A research agenda for malaria eradication: modeling. *PLoS Med.*, 8(1), 2011.

[237] S. Mandal, R.R. Sarkar, and S. Sinha. Mathematical models of malaria – a review. *Malar. J.*, 10:202, 2011.

[238] B.B. Mandelbrot. The fractal geometry of nature. *W.H. Freeman Editors. San Francisco.*, 1982.

[239] B.B. Mandelbrot and J.W. Van Ness. Fractional Brownian motions, fractional noises and applications. *SIAM Rev.*, 10:422–437, 1968.

[240] B.B. Mandelbrot and J R. Wallis. Noah, Joseph and operational hydrology. *Water Resources Research.*, 4:909–918, 1968.

[241] P. Martens and L. Hall. Malaria on the move: Human population movement and malaria transmission. *Emerg. Infect. Dis.*, 6(2):103–109, 2000.

[242] W.J.M. Martens, L.W. Niessen, J. Rotmans, T.H. Jetten, and A.J. McMichael. Potential impact of global climate change on malaria risk. *Environ. Health Perspect.*, 103(5):458–464, 1995.

[243] N. Martin and C. Mailhes. About periodicity and signal to noise ratio - The strength of the autocorrelation function. *Conf. Cond. Monit. Mach. Fail. Prev. Technol. (CM MFPT 2010)*, 2010.

[244] E. Massad and F.A.B. Coutinho. Vectorial capacity, basic reproduction number, force of infection and all that: formal notation to complete and adjust their classical concepts and equations. *Mem Inst Oswaldo Cruz, Rio de Janeiro*, 107(4):564–567, 2012.

[245] E. Massad, R.H. Behrens, M.N. Burattini, and F.A.B. Coutinho. Modeling the risk of malaria for travelers to areas with stable malaria transmission. *Malar. J.*, 8:296, 2009.

[246] T. Mathevet, M. Lepiller, and A. Mangin. Application of time-series analyses to the hydrological functioning of an Alpine karstic system: the case of Bange-L'Eau-Morte. *Hydrology and Earth System Sciences Discussions, European Geosciences Union*, 8(6):1051–1064, 2004.

[247] C.M. Mbogo, J.M. Mwangangi, J. Nzovu, and et al. Spatial and Temporal Heterogeneity of *Anopheles* Mosquitoes and *Plasmodium falciparum* Transmission Along the Kenyan Coast. *Am. J. Trop. Med. Hyg.*, 68(6): 734–742, 2018.

[248] K.A.. McCarthy, E.A. Wenger, G.H. Huynh, and P.A. Eckhoff. Calibration of an intrahost malaria model and parameter ensemble evaluation of a pre-erythrocytic vaccine. *Malar. J.*, 14(1):6, 2015.

[249] F.E. McKenzie and W.H. Bossert. An integrated model of *Plasmodium falciparum* dynamics. *J. Theor. Biol.*, 232(3):411–426, 2005.

[250] A.M. Mendes, I.S. Albuquerque, M. Machado, J. Pissarra, P. Meireles, and M. Prudêncio. Inhibition of *Plasmodium* liver infection by ivermectin. *Antimicrob. Agents Chemother.*, 61(2):1–8, 2017.

[251] A.M. Mendes, M. Machado, N. Gonçalves-Rosa, and et al. A *Plasmodium berghei* sporozoite-based vaccination platform against human malaria. *npj Vaccines*, 3:33, 2018.

[252] N. Mideo, T. Day, and A.F. Read. Modelling malaria pathogenesis. *Cell. Microbiol.*, 10(10):1947–1955, 2008.

[253] V. Mironova, N. Shartova, A. Beljaev, M. Varentsov, and M. Grishchenko. Effects of climate change and heterogeneity of local climates on the development of malaria parasite (*Plasmodium vivax*) in Moscow megacity region. *Int. J. Environ. Res. Public Health*, 16(5):694, 2019.

[254] N. Moiroux, A.S. Bio-Bangana, A. Djenontin, F. Chandre, V. Corbel, and H. Guis. Modelling the risk of being bitten by malaria vectors in a vector control area in southern Benin, west Africa. *Parasit Vectors*, 6:71, 2013.

[255] L. Molineaux and G. Gramiccia. The Garki project. *WHO*, 1980.

[256] E. Montosi, S. Manzoni, A. Porporato, and A. Montanari. An ecohydrological model of malaria outbreaks. *Hydrol. Earth Syst. Sci.*, 16 (8):2759–2769, 2012.

[257] E.A. Mordecai, K.P. Paaijmans, L.R. Johnson, and et al. Optimal temperature for malaria transmission is dramatically lower than previously predicted. *Ecology letters*, 16(1):22–30, 2013.

[258] E. Mosnier, I. Dusfour, G. Lacour, and et al. Resurgence risk for malaria, and the characterization of a recent outbreak in an Amazonian border area between French Guiana and Brazil. *BMC Infectious Diseases*, 20(1):1–14, 2020.

[259] G. Muchena, B. Dube, R. Chikodzore, J. Pasipamire, S. Murugasampillay, and J. Mberikunashe. A review of progress towards sub-national malaria elimination in Matabeleland South Province, Zimbabwe (2011-2015): a qualitative study. *Malar. J.*, 17(1):146, 2018.

[260] A.O. Muhammed and P.E. Orukpe. Modified Mathematical Model for Malaria Control. *Int. J. Appl. Biomed. Eng.*, 7(1):1–10, 2014.

[261] W.R. Mukabana, W. Takken, G.F. Killeen, and B.G.J. Knols. Allomonal effect of breath contributes to differential attractiveness of humans. 8:1–8, 2004.

[262] C. Mukandavire, G. Musuka, G. Magombedze, and Z. Mukandavire. Malaria model with immigration of infectives and seasonal forcing in transmission. *Int. J. Appl. Math. Comput.*, 2(3):1–16, 2010.

[263] M. Mungai, G. Tegtmeier, M. Chamberland, and M. Parise. Transfusion-transmitted malaria in the United States from 1963 through 1999. *N Engl J Med*, 344(26):1973–1978, 2001.

[264] Kassena Nankana Municipality. Population Dynamics. `https://kassenanankanama.org/population.html`, 2010.

[265] D.J. Murray-Smith. Testing and validation of computer simulation models. In *Simulation Foundations, Methods and Applications*, 2015.

[266] M.I. Musa. Malaria Disease Distribution in Sudan Using Time Series ARIMA Model. *International Journal of Public Health Science*, 4(1):7–16, 2015.

[267] F.R. Muwanika, L.K. Atuhaire, and B. Ocaya. Prediction of Monthly Malaria Incidence in Uganda and its Implications for Preventive Interventions. *J. Med. Diagn. Meth.*, 6:2, 2017.

[268] R.O. Mwaiswelo, B. Ngasala, D. Msolo, E. Kweka, B.P. Mmbando, and A. Mårtensson. A single low dose of primaquine is safe and sufficient to reduce transmission of *Plasmodium falciparum* gametocytes regardless of cytochrome P450 2D6 enzyme activity in Bagamoyo district, Tanzania. *Malar. J.*, 21:84, 2022.

[269] J.A. Nájera. A critical review of the field application of a mathematical model of malaria eradication. *Bull. World Health Organ.*, 50(5):449–457, 1974.

[270] C.N. Ngonghala, S.Y. Del Valle, R. Zhao, and J. Mohammed-Awel. Quantifying the impact of decay in bed-net efficacy on malaria transmission. *J. Theor. Biol.*, 363:247–261, 2014.

[271] C.N. Ngonghala, J. Mohammed-Awel, R. Zhao, and O. Prosper. Interplay between insecticide-treated bed-nets and mosquito demography: Implications for malaria control. *J. Theor. Biol.*, 397:179–192, 2016.

[272] G.A. Ngwa. Modelling the Dynamics of Endemic Malaria in Growing Populations. *Discret. Contin. Dyn. Syst. - Ser. B*, 4(4):1173–1202, 2004.

[273] G.A. Ngwa and W.S. Shu. A mathematical model for endemic malaria with variable human and mosquito populations. *Math. Comput. Model.*, 32 (7-8):747–763, 2000.

[274] A. Noé, S.I. Zaman, M. Rahman, A.K. Saha, M.M. Aktaruzzaman, and R.J. Maude. Mapping the stability of malaria hotspots in Bangladesh from 2013 to 2016. *Malar. J.*, 17:259, 2018.

[275] F. Nyabadza. Modelling the role of prophylaxis in malaria prevention. *Int. J. Biol. Life Sci.*, 4(1):18–23, 2008.

[276] A.A. Obala, H.L. Kutima, H.D.N. Nyamogoba, A.W. Mwangi, C.J. Simiyu, G.N. Magak, B.O. Khwa-Otsyula, and J.H. Ouma. *Anopheles gambiae* and *Anopheles arabiensis* population densities and infectivity in Kopere village, Western Kenya. *J Infect Dev Ctries*, 6(8):637–643, 2012.

[277] B.A. Okech, L.C. Gouagna, E. Walczak, E.W. Kabiru, J.C. Beier, G. Yan, and J.I. Githure. The development of *Plasmodium falciparum* in experimentally infected *Anopheles gambiae* (Diptera: Culicidae) under ambient microhabitat temperature in western Kenya. *Acta Tropica*, 92: 99–108, 2004.

[278] B.A. Okech, I.K. Mwobobia, A. Kamau, and et al. Use of integrated malaria management reduces malaria in Kenya. *PLoS One*, 3(12):e4050, 2008.

[279] L.C. Okell, C.J. Drakeley, T. Bousema, C.J.M. Whitty, and A.C. Ghani. Modelling the Impact of Artemisinin Combination Therapy and Long-Acting Treatments on Malaria Transmission Intensity. *PLoS Med.*, 5 (11):e226, 2008.

[280] S. Olaniyi, K.O. Okosun, S.O. Adesanya, and R.S. Lebelo. Modelling malaria dynamics with partial immunity and protected travellers: optimal control and cost-effectiveness analysis. *Journal of Biological Dynamics*, 14 (1):90–115, 2020.

[281] S. Olaniyi, M. Mukamuri, K.O. Okosun, and O.A. Adepoju. Mathematical analysis of a social hierarchy-structured model for malaria transmission dynamics. *Results in Physics*, 34:104991, 2022.

[282] J.A. Omumbo, S.I. Hay, R.W. Snow, A.J. Tatem, and D.J. Rogers. Modelling malaria risk in East Africa at high-spatial resolution. *Tropical Medicine and International Health*, 10(6):557–566, 2005.

[283] S. Omura and A. Crump. Ivermectin and malaria control. *Malar. J.*, 16(1): 1–3, 2017.

[284] S.I. Onah, O.C. Collins, C. Okoye, and G.C.E. Mbah. Dynamics and control measures for malaria using a mathematical epidemiological model. *Electron. J. Math. Anal. Appl.*, 7(1):65–73, 2019.

[285] World Health Organization. *Global technical strategy for malaria 2016-2030.* 2015.

[286] World Health Organization. *World malaria report.* 2018.

[287] World Health Organization. *World malaria report.* 2019.

[288] World Health Organization. *World malaria report.* 2020.

[289] World Health Organization. *World malaria report.* 2021.

[290] A. Ostovar, A.A. Haghdoost, A. Rahimiforoushani, A. Raeisi, and R. Majdzadeh. Time series analysis of meteorological factors influencing Malaria in south eastern Iran. *J. Arthropod. Borne. Dis.*, 10(2):222–237,

2016.

[291] A.L. Ouédraogo, G.J.H. Bastiaens, A.B. Tiono, and et al. Efficacy and safety of the mosquitocidal drug ivermectin to prevent malaria transmission after treatment: A double-blind, randomized, clinical trial. *Clin. Infect. Dis.*, 60(3):357–365, 2015.

[292] A.L. Ouédraogo, P.A. Eckhoff, A.J.F. Luty, W. Roeffen, R.W. Sauerwein, T. Bousema, and E.A. Wenger. Modeling the impact of *Plasmodium falciparum* sexual stage immunity on the composition and dynamics of the human infectious reservoir for malaria in natural settings. *PLoS Pathog.*, 14(5):1–23, 2018.

[293] S. Ozawa, D.R. Evans, C.R. Higgins, S.K. Laing, and P. Awor. Development of an agent-based model to assess the impact of substandard and falsified anti-malarials: Uganda case study. *Malar. J.*, 18(1):1–14, 2019.

[294] F. Pagès, S. Houze, B. Kurtkowiak, E. Balleydier, F. Chieze, and L. Filleul. Status of imported malaria on Réunion Island in 2016. *Malar. J.*, 17:210, 2018.

[295] V. Pareto. Cours d'Economie Politique - I. 1896.

[296] V. Pareto. Cours-déconomie-politique - II. 1897.

[297] P.E. Parham and E. Michael. Modeling the effects of weather and climate change on malaria transmission. *Environ. Health Perspect.*, 118(5):620–626, 2010.

[298] D.M. Parker, S.T.T. Tun, L.J. White, and et al. Potential herd protection against *Plasmodium falciparum* infections conferred by mass antimalarial drug administrations. *eLife*, 8:e41023, 2019.

[299] R. Parveen, W. Song, B. Qiu, M.N. Bhatti, T. Hassan, and Z. Liu. Probabilistic Model-Based Malaria Disease Recognition System. *Complexity*, 6633806:1–11, 2021.

[300] C.L. Peatey, T.S. Skinner-Adams, A. Dixon, J.S. McCarthy, D.L. Gardiner, and K.R. Trenholme. Effect of Antimalarial Drugs on *Plasmodium falciparum* Gametocytes. *J. Infect. Dis.*, 200:1518–1521, 2009.

[301] P. Pemberton-Ross, N. Chitnis, E. Pothin, and T.A. Smith. A stochastic model for the probability of malaria extinction by mass drug administration. *Malar. J.*, 16(1):1–9, 2017.

[302] A.E. Permanasari, I. Hidayah, and I.A. Bustoni. SARIMA (Seasonal ARIMA) implementation on time series to forecast the number of Malaria incidence. *International Conference on Information Technology and Electrical Engineering (ICITEE)*, 2(2):203–207, 2013.

[303] N.M. Pham, W. Karlen, H. Beck, and E. Delamarche. Malaria and the 'last' parasite: how can technology help? *Malar. J.*, 17:260, 2018.

[304] V. Phillips, J. Njau, S. Li, and P. Kachur. Simulations show diagnostic

testing for malaria in young African children can be cost-saving or cost-effective. *Health Aff.*, 34(7):1196–1203, 2015.

[305] D.K. Pindolia, A.J. Garcia, Z. Huang, D.L. Smith, V.A. Alegana, A.M. Noor, R.W. Snow, and A.J. Tatem. The demographics of human and malaria movement and migration patterns in East Africa. *Malar. J.*, 12(1): 397, 2013.

[306] E. T. Piperaki and G. L. Daikos. Malaria in Europe: emerging threat or minor nuisance? *Clin. Microbiol. Infect.*, 22(6):487–493, 2016.

[307] F. Pizzitutti, W. Pan, B. Feingold, B. Zaitchik, C.A. Álvarez, and C. F. Mena. Out of the net: An agent-based model to study human movements influence on local-scale malaria transmission. *PLoS One*, 13(3), 2018.

[308] M. Pombi, M. Calzetta, W.M. Guelbeogo, and et al. Unexpectedly high *Plasmodium* sporozoite rate associated with low human blood index in *Anopheles coluzzii* from a LLIN-protected village in Burkina Faso. *Sci. Rep.*, 8(1):1–10, 2018.

[309] W. Pongtavornpinyo, S. Yeung, I.M. Hastings, A.M. Dondorp, N.P.J. Day, and N.J. White. Spread of anti-malarial drug resistance: mathematical model with implications for ACT drug policies. *Malar. J.*, 7:229, 2008.

[310] N. Protopopoff, M. Van Herp, P. Maes, T. Reid, D. Baza, U. D'Alessandro, W. Van Bortel, and M. Coosemans. Vector control in a malaria epidemic occurring within a complex emergency situation in Burundi: a case study. *Malar J.*, 6:93, 2007.

[311] M. Prudêncio, A. Rodriguez, and M.M. Mota. The silent path to thousands of merozoites: The *Plasmodium* liver stage. *Nature Reviews Microbiology*, 4:849–856, 2006.

[312] J. Raman, N. Morris, J. Frean, and et al. Reviewing South Africa's malaria elimination strategy (2012-2018): Progress, challenges and priorities. *Malar. J.*, 15(1):1–11, 2016.

[313] F. Rateb, B. Pavard, N. Bellamine-Bensaoud, J.J. Merelo, and M.G. Arenas. Modeling Malaria with Multi-Agent Systems. *Int. J. Intell. Inf. Technol.*, 1(2):17–27, 2005.

[314] T. Reiker, N. Chitnis, and T. Smith. Modelling reactive case detection strategies for interrupting transmission of *Plasmodium falciparum* malaria. *Malar. J.*, 18(1):259, 2019.

[315] R.C. Reiner, T.A. Perkins, C.M. Barker, and et al. A systematic review of mathematical models of mosquito-borne pathogen transmission: 1970–2010. *J R Soc Interface*, 10:20120921, 2013.

[316] F. Retief and L. Cilliers. The death of Alexander the Great. *Acta Theologica Supplementum*, 7:14–28, 2005.

[317] R. Ross. Some a Priori Pathometric Equations. *Br. Med. J.*, 1(2830):

546–547, 1915.

[318] S. Ruan, D. Xiao, and J.C. Beier. On the delayed Ross-Macdonald model for malaria transmission. *Bull. Math. Biol.*, 70(4):1098–1114, 2008.

[319] S. Sainz-Elipe, J.M. Latorre, R. Escosa, M. Masià, M.V. Fuentes, S. Mas-Coma, and M.D. Bargues. Malaria resurgence risk in southern Europe: Climate assessment in an historically endemic area of rice fields at the Mediterranean shore of Spain. *Malar. J.*, 9(1):1–16, 2010.

[320] W. Sama, G. Killeen, and T. Smith. Estimating the duration of *Plasmodium falciparum* infection from trials of indoor residual spraying. *Am. J. Trop. Med. Hyg.*, 70(6):625–634, 2004.

[321] S. Sande, M. Zimba, P. Chinwada, H.T. Masendu, J. Mberikunshe, and A. Makuwaza. A review of new challenges and prospects for malaria elimination in Mutare and Mutasa Districts, Zimbabwe. *Malar. J.*, 15(1): 1–9, 2016.

[322] G. Santamaria-Bonfil, C. Gershenson, and N. Fernández. A Package for Measuring emergence, Self-organization, and Complexity Based on Shannon entropy. *Frontiers in Robotics and AI*, 4:1–12, 2017.

[323] M. Santos-Vega, P.P. Martinez, K.G. Vaishnav, V. Kohli, V. Desai, M.J. Bouma, and M. Pascual. The neglected role of relative humidity in the interannual variability of urban malaria in Indian cities. *Nature communications*, 13:533, 2022.

[324] R.R. Sarkar and C. Chatterjee. Application of Different Time Series Models on Epidemiological Data - Comparison and Predictions for Malaria Prevalence. *SM J. Biometrics Biostat.*, 2(4):1022, 2017.

[325] A. Scherf, J.J. Lopez-Rubio, and L. Riviere. Antigenic Variation in *Plasmodium falciparum*. *Annu. Rev. Microbiol.*, 62:445–470, 2008.

[326] J. Sequeira, J. Louçã, A.M. Mendes, and P.G. Lind. Transition from endemic behavior to eradication of malaria due to combined drug therapies: an agent-model approach. *J. Theor. Biol.*, 484:110030, 2020.

[327] J. Sequeira, J. Louçã, A.M. Mendes, and P.G. Lind. A Model for Assessing the Quantitative Effects of Heterogeneous Affinity in Malaria Transmission along with Ivermectin Mass Administration. *Appl. Sci.*, 10(23):8696, 2020.

[328] J. Sequeira, J. Louçã, A. M. Mendes, and P. G. Lind. Using the Hurst Exponent and Entropy Measures to Predict Effective Transmissibility in Empirical Series of Malaria Incidence. *Appl. Sci.*, 12:496, 2022.

[329] L.P. Shah, N. Krishnamoorthy, T. Vijayakumar, and P. Basker. Risk of malaria transmission in stone quarry sites of Villupuram district in Tamil Nadu , India. *Int. J. Mosq. Res.*, 5(1):33–40, 2018.

[330] C.E. Shannon. A Mathematical Theory of Communication. *The Bell System Technical Journal*, 27:379–423, 623–656, 1948.

[331] V. Sharma, A. Kumar, L. Panat, G. Karajkhede, and A. Lele. Malaria Outbreak Prediction Model Using Machine Learning. *International Journal of Advanced Research in Computer Engineering and Technology (IJARCET)*, 4(12):4415–4419, 2015.

[332] A. Shcherbacheva, H. Haario, and G.F. Killeen. Modeling host-seeking behavior of African malaria vector mosquitoes in the presence of long-lasting insecticidal nets. *Math. Biosci.*, 295(October 2017):36–47, 2018.

[333] S. Shekalaghe, D. Mosha, A. Hamad, T.A. Mbaga, M. Mihayo, T. Bousema, C. Drakeley, and S. Abdulla. Optimal timing of primaquine to reduce *Plasmodium falciparum* gametocyte carriage when co-administered with artemether– lumefantrine. *Malar. J.*, 19:34, 2020.

[334] R.H. Shumway and D.S. Stoffer. *Time Series Analysis and Its Applications.* Springer, 2006.

[335] S.P. Silal, F. Little, K.I. Barnes, and L.J. White. Towards malaria elimination in Mpumalanga, South Africa: A metapopulation modeling approach. *Am. J. Trop. Med. Hyg.*, 91:278, 2014.

[336] M. Sinan, H. Ahmad, Z. Ahmad, J. Baili, S. Murtaza, M.A. Aiyashi, and T. Botmart. Fractional mathematical modeling of malaria disease with treatment & insecticides. *Results in Physics*, 34:105220, 2022.

[337] M.E. Sinka, M.J. Bangs, S. Manguin, and et al. The dominant *Anopheles* vectors of human malaria in Africa, Europe and the Middle East: occurrence data, distribution maps and bionomic précis. *Parasites & Vectors*, 3:117, 2010.

[338] D. Sinzinkayo, V. Baza, D. Gnanguenon, and C. Koepfli. The lead-up to epidemic transmission: malaria trends and control interventions in Burundi 2000 to 2019. *Malar J.*, 20:298, 2021.

[339] H.C. Slater, P.G.T. Walker, T. Bousema, L.C. Okell, and A.C. Ghani. The potential impact of adding ivermectin to a mass treatment intervention to reduce malaria transmission: A modelling study. *J. Infect. Dis.*, 210(12): 1972–1980, 2014.

[340] H.C. Slater, J.T. Griffin, A.C. Ghani, and L.C. Okell. Assessing the potential impact of artemisinin and partner drug resistance in sub-Saharan Africa. *Malar. J.*, 15(1):1–11, 2016.

[341] H.C. Slater, L.C. Okell, and A.C. Ghani. Mathematical Modelling to Guide Drug Development for Malaria Elimination. *Trends Parasitol.*, 33(3): 175–184, 2017.

[342] H.C. Slater, B.D. Foy, K. Kobylinski, and et al. . *Lancet Infectious Diseases*, 2020. URL `https://doi.org/10.1016/S1473-3099(19)30633-4`.

[343] D.L. Smith and F.E. McKenzie. Statics and dynamics of malaria infection in *Anopheles* mosquitoes. *Malar. J.*, 3:13, 2004.

[344] D.L. Smith, F.E. McKenzie, R.W. Snow, and S.I. Hay. Revisiting the basic reproductive number for malaria and its implications for malaria control. *PLoS Biol*, 5(3):e42, 2007.

[345] J.L. Smith, J. Auala, E. Haindongo, P. Uusiku, R. Gosling, I. Kleinschmidt, D. Mumbengegwi, and H.J.W. Sturrock. Malaria risk in young male travellers but local transmission persists: a case–control study in low transmission Namibia. *Malar. J.*, 16(1):70, 2017.

[346] N.R. Smith, J.M. Trauer, M. Gambhir, J.S. Richards, R.J. Maude, J.M. Keith, and J.A. Flegg. Agent-based models of malaria transmission: A systematic review. *Malar. J.*, 17(1):1–16, 2018.

[347] T. Smith and A. Schapira. Reproduction numbers in malaria and their implications. *Trends Parasitol.*, 28(1):3–8, 2012.

[348] T. Smith, N. Maire, A. Ross, and et al. Towards a comprehensive simulation model of malaria epidemiology and control. *Parasitology*, 135: 1507–1516, 2008.

[349] T.A. Smith. Estimation of heterogeneity in malaria transmission by stochastic modelling of apparent deviations from mass action kinetics. *Malar. J.*, 7:12, 2008.

[350] H.E. Stanley. Introduction to Phase Transitions and Critical Phenomena. Oxford University Press, 1971.

[351] D.H. Stapleton. Lessons of History? Anti-Malaria Strategies of the International Health Board and the Rockefeller Foundation from the 1920s to the Era of DDT. *Public Health Reports*, 119(2):206–215, 2004.

[352] G.H. Stresman, E. Giorgi, A. Baidjoe, and et al. Impact of metric and sample size on determining malaria hotspot boundaries. *Sci. Rep.*, 7 (March):1–8, 2017.

[353] E.M Stuckey, J.C. Stevenson, M.K. Cooke, and et al. Simulation of malaria epidemiology and control in the highlands of western Kenya. *Malar. J.*, 11 (1):357, 2012.

[354] S.A. Sundararaman, L.J. Plenderleith, W. Liu, and et al. Genomes of cryptic chimpanzee *Plasmodium* species reveal key evolutionary events leading to human malaria. *Nature Communications*, 7:11078, 2016.

[355] I. Sutanto, S. Suprijanto, A. Kosasih, and et al. The effect of primaquine on gametocyte development and clearance in the treatment of uncomplicated falciparum malaria with dihydroartemisinin- piperaquine in South Sumatra, Western Indonesia: An open-label, randomized, controlled trial. *Clin. Infect. Dis.*, 56(5):685–693, 2013.

[356] N.Y.N. Syams, H. Sumarno, and P. Sianturi. Analysis of SIS-SI Stochastic

Model with CTMC on the Spread of Malaria Disease. *J. Math. Fund. Sci.*, 53(2):166–181, 2021.

[357] M. Sylla, K.C. Kobylinski, M. Gray, P.L. Chapman, M.D. Sarr, J.L. Rasgon, and B.D. Foy. Mass drug administration of ivermectin in south-eastern Senegal reduces the survivorship of wild-caught, blood fed malaria vectors. *Malar. J.*, 9:365, 2010.

[358] A.J. Tatem, C.A. Guerra, C.W. Kabaria, A.M. Noor, and S.I. Hay. Human population, urban settlement patterns and their impact on *Plasmodium falciparum* malaria endemicity. *Malar. J.*, 7:1–17, 2008.

[359] A.M. Tompkins and V. Ermert. A regional-scale, high resolution dynamical malaria model that accounts for population density, climate and surface hydrology. *Malar. J.*, 12(1):65, 2013.

[360] L. Torres-Sorando and D.J. Rodriguez. Models of spatio-temporal dynamics in malaria. *Ecol. Modell.*, 104:231–240, 1997.

[361] B. Traoré, O. Koutou, and B. Sangaré. A global mathematical model of malaria transmission dynamics with structured mosquito population and temperature variations. *Nonlinear Analysis: Real World Applications*, 53: 103081, 2020.

[362] S. Tukwasibwe, P. Tumwebaze, M. Conrad, and et al. Drug resistance mediating *Plasmodium falciparum* polymorphisms and clinical presentations of parasitaemic children in Uganda. *Malar. J.*, 16:125, 2017.

[363] J. Tumwiine, J.Y.T. Mugisha, and L.S. Luboobi. On oscillatory pattern of malaria dynamics in a population with temporary immunity. *Computational and Mathematical Methods in Medicine*, 8(3):191–203, 2007.

[364] M.B. Tyrrell, K. Verdonck, S.H. Muela, and C. Gryseels. Defining micro-epidemiology for malaria elimination: systematic review and meta-analysis. *Malar. J.*, pages 1–20, 2017.

[365] L. Valderrama, S. Ayala, C. Reyes, and C.R. González. Modeling the Potential Distribution of the Malaria Vector *Anopheles (Ano.) pseudopunctipennis* Theobald (Diptera: Culicidae) in Arid Regions of Northern Chile. *Frontiers in Public Health*, 9:611152, 2021.

[366] A.F. Vallejo, N.L. Martínez, I.J. González, M. Arévalo-Herrera, and S. Herrera. Evaluation of the Loop Mediated Isothermal DNA Amplification (LAMP) Kit for Malaria Diagnosis in P. vivax Endemic Settings of Colombia. *PLoS Neglected Tropical Diseases*, 9(1):e3453, 2015.

[367] K.L. VanderWaal and V.O. Ezenwa. Heterogeneity in pathogen transmission: mechanisms and methodology. *Funct. Ecol.*, 30(10): 1606–1622, 2016.

[368] A.K. Verma, V. Kuppili, S.K. Srivastava, and J.S. Suri. A new backpropagation neural network classification model for prediction of

incidence of malaria. *Front Biosci*, 25(2):299–334, 2020.

[369] B.L. Verma, S.K. Ray, and R.N. Srivastava. A stochastic model of malaria transition rates from longitudinal data: considering the risk of "lost to follow-up". *Journal of Epidemiology and Community Health*, 37:153–156, 1983.

[370] V. Volterra. Variations and Fluctuations of the Number of Individuals in Animal Species living together. *ICES Journal of Marine Science*, 3(1): 3–51, 1928.

[371] E. Vynnycky and R.G. White. *An introduction to Infectious Disease Modelling*. Oxford University Press, 2010.

[372] P.G.T. Walker, J.T. Griffin, N.M. Ferguson, and A.C. Ghani. Estimating the most efficient allocation of interventions to achieve reductions in *Plasmodium falciparum* malaria burden and transmission in Africa: A modelling study. *Lancet Glob. Heal.*, 4(7):e474–e484, 2016.

[373] D.I. Wallace, B.S. Southworth, X. Shi, J.W. Chipman, and A.K. Githeko. A comparison of five malaria transmission models: benchmark tests and implications for disease control. *Malar. J.*, 13(1):268, 2014.

[374] D. Wanduku. Threshold conditions for a family of epidemic dynamic models for malaria with distributed delays in a non-random environment. *International Journal of Biomathematics*, 11(6):1850085, 2018.

[375] X. Wang, Y. Chen, M. Martcheva, and L. Rong. Asymptotic analysis of a vector-borne disease model with the age of infection. *Journal of Biological Dynamics*, 14(1):332–367, 2020.

[376] K. Wangdi, P. Singhasivanon, T. Silawan, S. Lawpoolsri, N.J. White, and J. Kaewkungwal. Development of temporal modelling for forecasting and prediction of malaria infections using time-series and ARIMAX analyses: a case study in endemic districts of Bhutan. *Malar. J.*, 9:251, 2010.

[377] O.J. Watson, H.C. Slater, R. Verity, J.B. Parr, M.K. Mwandagalirwa, A. Tshefu, S.R. Meshnick, and A.C. Ghani. Modelling the drivers of the spread of *Plasmodium falciparum* hrp2 gene deletions in sub-Saharan Africa. *Elife*, 6:1–24, 2017.

[378] J.L.A. Webb. Humanity's Burden: A Global History of Malaria. *International Journal for Parasitology*, 2015.

[379] D.J. Weiss, T.C.D. Lucas, M. Nguyen, and et al. Mapping the global prevalence, incidence, and mortality of *Plasmodium falciparum*, 2000–17: a spatial and temporal modelling study. *Lancet*, 394(10195):322–331, 2019.

[380] E.A. Wenger and P.A. Eckhof. A mathematical model of the impact of present and future malaria vaccines. *Malar. J.*, 12:126, 2013.

[381] L.J. White, R.J. Maude, W. Pongtavornpinyo, S. Saralamba, R. Aguas, T. Van Effelterre, N.P.J. Day, and N.J. White. The role of simple

mathematical models in malaria elimination strategy design. *Malar. J.*, 8 (1):212, 2009.

[382] N.J. White. *Malaria.* Manson's "Tropical Diseases" 21st Ed. W.B. Saunders, 2003.

[383] P. Winskill, P.G.T. Walker, J.T. Griffin, and A.C. Ghani. Modelling the cost-effectiveness of introducing the RTS,S malaria vaccine relative to scaling up other malaria interventions in sub-Saharan Africa. *BMJ Glob. Heal.*, 2(1):e000090, 2017.

[384] P. Witbooi, G. Abiodun, and M. Nsuami. A model of malaria population dynamics with migrants. *Mathematical Biosciences and Engineering*, 18(6): 7301–7317, 2021.

[385] M.L. Wong, J.W.K. Liew, W.K. Wong, and et al. Natural Wolbachia infection in field-collected Anopheles and other mosquito species from Malaysia. *Parasites & Vectors*, 13:414, 2020.

[386] M.E. Woolhouse, C. Dye, J.F. Etard, and et al. Heterogeneities in the transmission of infectious agents: implications for the design of control programs. *Proc. Natl. Acad. Sci. U. S. A.*, 94(1):338–42, 1997.

[387] World Health Organization. *Malaria entomology and vector control.* 2013.

[388] X. Xu, G. Zhou, Y. Wang, and et al. Microgeographic heterogeneity of border malaria during elimination phase, Yunnan Province, China, 2011-2013. *Emerg. Infect. Dis.*, 22(8):1363–1370, 2016.

[389] L. Yakob and G. Yan. Modeling the effects of integrating larval habitat source reduction and insecticide treated nets for malaria control. *PLoS One*, 4(9), 2009.

[390] T.K. Yamana, X. Qiu, and E.A.B. Eltahir. Hysteresis in simulations of malaria transmission. *Adv. Water Resour.*, 108:1–7, 2016.

[391] V. Yiga, H. Nampala, and J. Tumwiine. Analysis of the Model on the Effect of Seasonal Factors on Malaria Transmission Dynamics. *Journal of Applied Mathematics*, 8885558:1–19, 2020.

[392] S. Yu, J. Wang, X Luo, H. Zheng, L. Wang, X. Yang, and Y. Wang. Transmission-Blocking Strategies Against Malaria Parasites During Their Mosquito Stages. *Front. Cell. Infect. Microbiol.*, 12:820650, 2022.

[393] J.O. Yukich, C. Taylor, T.P. Eisele, and R. Reithinger. Travel history and malaria infection risk in a low-transmission setting in Ethiopia : a case control study. *Malar. J.*, 12(1):33, 2013.

[394] O.P. Zacarias and M. Andersson. Mapping malaria incidence distribution that accounts for environmental factors in Maputo Province - Mozambique. *Malar.J.*, 9(1):79, 2010.

[395] Y. Zhang, P. Bi, and J.E. Hiller. Meteorological variables and malaria in a Chinese temperate city: A twenty-year time-series data analysis. *Environ*

Int., 36(5):439–445, 2010.

[396] L. Zhu, G.C. Müller, J.M. Marshall, and et al. Is outdoor vector control needed for malaria elimination? An individual-based modelling study. *Malar. J.*, 16(1):266, 2017.

Part IV

APPENDICES

Appendix A

Markov transition matrix

A.1 Markov chain model

Here, we will present the mathematical formalism underlying the continuous Markov process used in our stochastic model.

The Markov process is of critical importance in defining a stochastic model that evolves in time, such as the one used by the computational algorithm of our model.

It consists in a probabilistic process regarding the transition between stochastic states as a result of a stochastic model evolution in time. The essence of a Markov process lies in the specific characteristic that the current model state only depends on the previous state from which the system evolved, without memory of any of the previous states. It relates to the property defined by equation A.1.

$$Prob.\{X_n = i_n \mid X_0 = i_0, ..., X_{n-1} = i_{n-1}\} = Prob.\{X_n = i_n \mid X_{n-1} = i_{n-1}\} \tag{A.1}$$

A.2 The Markov transition matrix P and generator matrix Q

In the present model, a discrete time Markov chain was applied in terms of a Markov transition matrix, and later on we will deduce the Taylor approximation to the process assuming the presence of a continuous-time Markov chain.

Based upon a irreducible continuous-time Markov transition matrix we obtain the generator matrix $Q = (q_{ij})$ with a stationary probability distribution π such as $Q\pi = 0$.

$$\lim_{n\to\infty} p_{ij}(t) = \pi_i = -\frac{1}{q_{ii}\mu_{ii}}, \qquad i, j = 1, 2, ..., N \tag{A.2}$$

The matrix of transition rates $Q = \{q_{ij}\}$ is known as the infinitesimal generator matrix. This matrix is important to define the forward and backward Kolmogorov equations, which supports the transition matrix $P(t)$ in terms of a differential equation.

The transition probabilities p_{ij} – equation A.2 – are used here to derive the transitions rates q_{ij} in which the generator matrix Q is based upon. These transition rates q_{ij} define the rate of change of the transition probabilities according to equation A.3,

$$q_{ij} = \lim_{\Delta t\to 0^+} \frac{p_{ij}(\Delta t) - p_{ij}(0)}{\Delta t} = \lim_{\Delta t\to 0^+} \frac{p_{ij}(\Delta t)}{\Delta t}, \qquad i \neq j \tag{A.3}$$

where we also define the transition rates q_{ii} according to equation A.4.

$$q_{ii} = \lim_{\Delta t\to 0^+} \frac{p_{ii}(\Delta t) - p_{ii}(0)}{\Delta t} = \lim_{\Delta t\to 0^+} \frac{p_{ii}(\Delta t) - 1}{\Delta t}, \qquad i \neq j \tag{A.4}$$

From the definition of the Transition Probability Matrix $P(t)$ and the Generator transition rates $Q(t)$ we may deduce the forward and backward Kolmogorov equations A.5 and A.6:

Forward Kolmogorov equation

$$\frac{dP(t)}{dt} = Q(t)P(t) \tag{A.5}$$

and

Backward Kolmogorov equation

$$\frac{dP(t)}{dt} = P(t)Q(t) \tag{A.6}$$

Where $P(0) = I$ and the unique solution is given by equations A.7 and A.8

$$P(t) = e^{Qt}P(0) = e^{Qt} \tag{A.7}$$

where $e^{Q}t$ is the matrix exponential

$$e^{Qt} = I + Qt + Q^2\frac{t^2}{2!} + Q^3\frac{t^3}{3!} + ... = \sum_{k=0}^{\infty} Q^k\frac{t^k}{k!} \tag{A.8}$$

A.3 The embedded Markov chain matrix T

In addition, the generator matrix Q is used to define a transition matrix for the embedded Markov chain T.

The matrix $T = (t_{ij})$ is the transition matrix of the embedded Markov chain of random states Y_n of a continuous-time Markov chain process of n jumps between states. The matrix components are given by equations A.9 and A.10.

$$t_{ii} = \begin{cases} 0, & \text{if} \quad q_{ii} \neq 0 \\ 1, & \text{if} \quad q_{ii} = 0 \end{cases} \tag{A.9}$$

$$t_{ij} = \begin{cases} \frac{q_{ij}}{\sum_{k=0,k\neq i}^{\infty} q_{ik}} = -\frac{q_{ij}}{q_{ii}}, & \text{if} \quad q_{ii} \neq 0 \\ 0, & \text{if} \quad q_{ii} = 0 \end{cases} \tag{A.10}$$

A.4 Mosquito bite algorithm

We will use a stochastic model with N_m mosquito and N_h fixed human populations.

The main algorithm results from a forced mosquito bite in a random human host that will take place daily and once in all mosquitoes. The time step was defined as a single day. This cycle will be repeated for the whole duration of the simulation. Depending on predicted probabilities from each bite several type of transitions may occur.

The number of infected mosquitoes will be defined as I_m. The number of infected human hosts is represented by I_h. Therefore, we will obtain susceptible populations groups with healthy mosquitoes (S_m) and healthy human hosts (S_h).

The baseline probability of a mosquito bite occurrence – R results from previous equations defining 5.5 and 5.6, and depends on several model parameters included in those equations.

$P_{(+)} = R.$

Thus, the failed mosquito bite probability is obtained from:

$P_{(-)} = 1 - R.$

After a successful bite $P_{(+)}$ with baseline conditions, the following 6 transitions may occur:

Mosquito transitions:

a) $M_{i,i+1}$: $M_i \longrightarrow M_i + 1$

b) $M_{i,i}$: $M_i \longrightarrow M_i$

c) $M_{i,i-1}$: $M_i \longrightarrow M_i - 1$

Human individual transitions:

d) $H_{i,i+1}$: $H_i \longrightarrow H_i + 1$

e) $H_{i,i}$: $H_i \longrightarrow H_i$

f) $H_{i,i-1}$: $H_i \longrightarrow H_i - 1$

A.4.1 Healthy mosquito bites healthy human individual

1. Event M_0H_0

The probability of the event M_0H_0 will be obtained from:

$$Prob.(M_0H_0) = \frac{(1 - M_i)}{N_m} \frac{(1 - H_i)}{N_h} \tag{A.11}$$

A healthy mosquito M_0 bites a healthy human host H_0. In this case there will be no infection status change (M_0H_0) – with two neutral transition events: $M_{i,i}$ and $H_{i,i}$.

This event will depend on the proportion of mosquito and human infected populations (m and h):

A.4.2 Healthy mosquito bites infected human individual

2. Event M_0H_i

The probability of event M_0H_i will be obtained from:

$$Prob.(M_0H_i) = \frac{(1 - M_i)}{N_m} \frac{(H_i)}{N_h} \; R \tag{A.12}$$

A healthy mosquito M_0 bites an infected human host H_i – with two possible transition events:

- $M_{i,i+1}$: Mosquito acquires infection (M_iH_i).

- $M_{i,i}$: Mosquito infection fails (M_0H_i).

The mosquito infection probability will depend on several random variables (probability of human host gametocytemia, human latency probability, or other random causes of mosquito infection failure) – Φ_m.

$$Prob.(M_iH_i \mid M_0H_i) = \frac{(1 - M_i)}{N_m} \frac{(H_i)}{N_h} \; R \; \Phi_m \tag{A.13}$$

Thus, the mosquito infection failure probability after an effective mosquito bite will be obtained from:

$$Prob.(M_0H_i \mid M_0H_i) = \frac{(1 - M_i)}{N_m} \frac{(H_i)}{N_h} \; R \; (1 - \Phi_m) \tag{A.14}$$

Φ_m and Φ_h are the result of equations 5.12 and 5.11.

A.4.3 Infected mosquito bites healthy human individual

3. Event M_iH_0

The probability of the event M_iH_0 will be obtained from:

$$Prob.(M_i H_0) = \frac{(M_i)}{N_m}\frac{(1-H_i)}{N_h}\ R \tag{A.15}$$

An infected mosquito M_i bites a healthy human host H_0 – with two possible events:

- $H_{i,i+1}$: Human host acquires infection ($M_i H_i$).

- $H_{i,i}$: Human host infection fails ($M_i H_0$).

The human host infection probability resulting from $M_i H_0$ will depend on several random variables (probability of human pre-erythrocytic immunity protection, mosquito latency probability, or other random causes of failed human infection) – Φh.

$$Prob.(M_i H_i \mid M_i H_0) = \frac{(M_i)}{N_m}\frac{(1-H_i)}{N_h}\ R\ \Phi_h \tag{A.16}$$

and human host failed infection probability after a successful bite will be obtained from:

$$Prob.(M_i H_0 \mid M_i H_0) = \frac{(M_i)}{N_m}\frac{(1-H_i)}{N_h}\ R\ (1-\Phi_h) \tag{A.17}$$

A.4.4 Infected mosquito bites infected human individual – Super-infection

4. Event $M_i H_i$

The probability of the event $M_i H_i$ will be obtained from:

$$Prob(M_i H_i) = \frac{(M_i)}{N_m}\frac{(H_i)}{N_h}\ R \tag{A.18}$$

An infected mosquito M_i bites an infected human host H_i – with no change in mosquito or human infection status $M_i H_i$. This event will correspond to a super-infection process. For every super-infection there will be a time reset in the disease duration counter, decreasing it by a proportion of the expected remaining time of the previous infection. This way, for every repeated super-infection, human infection healing time will be delayed in a proportional amount of remaining expected infection time.

Human host super-infection with disease time counter reset will result from $M_i H_i$ and depends on several random variables (probability of human immunity protection, human host disease duration, mosquito latency probability, or other random causes of failed human infection) – Φ_h.

$$p(M_iH_i \mid M_iH_i) = \frac{(M_i)}{N_m}\frac{(H_i)}{N_h}\ R\ \Phi_h \tag{A.19}$$

Thus, human host super-infection failed probability after successful bite (without disease time counter reset) will be obtained from:

$$p(M_iH_i \mid M_iH_i) = \frac{(M_i)}{N_m}\frac{(H_i)}{N_h}\ R\ (1-\Phi_h) \tag{A.20}$$

A.5 Markov transition probabilities matrix

In this section we will present the Markov transition probabilities of mosquito and human transmission, P_M and P_H respectively.

A.5.1 Mosquito transition probabilities matrix P_M

For clearer notation purposes, the following transition probabilities will be considered (see also equation 5.14):

$$p_{m+} = p_m = h\Phi_m \tag{A.21}$$

$$p_{m=} = 1 - p_m = 1 - h\Phi_m \tag{A.22}$$

$q_m =$ daily probability of mosquito death

$(1-q_m) =$ daily probability of mosquito survival.

a) $M_{i,i+1}$

$$p[(M_{i+1}, t+\Delta t) \mid (M_i, t)] = p(M_i, t)(1-q_m)\ p_{m+} \tag{A.23}$$

b) $M_{i,i}$

$$p[(M_i, t+\Delta t) \mid (M_i, t)] = p(M_i, t)[q_m p_{m+} + (1-q_m)\ p_{m=}] \tag{A.24}$$

c) $M_{i,i-1}$

$$p[(M_{i-1}, t+\Delta t) \mid (M_i, t)] = p(M_i, t)\ q_m\ p_{m=} \tag{A.25}$$

where p_{m+} is the probability of a healthy mosquito acquiring infection after biting an infectious human host, $p_{m=}$ is the probability of a healthy mosquito not

acquiring infection after biting an infectious human host, μ_m represents the daily probability of mosquito death, and $(1 - q_m)$ represents the daily probability of mosquito survival.

And we obtain the mosquito transition matrix P_M, where n represents the total number of mosquitoes:

$$P_M = \begin{bmatrix} M_{0,0} & M_{0,1} & 0 & 0 & 0 & 0 & 0 & 0 \\ M_{1,0} & M_{1,1} & M_{1,2} & 0 & 0 & 0 & 0 & 0 \\ 0 & M_{2,1} & M_{2,2} & M_{2,3} & 0 & 0 & 0 & 0 \\ 0 & ... & ... & ... & ... & ... & ... & 0 \\ 0 & ... & ... & M_{j,j-1} & M_{j,j} & M_{j,j+1} & ... & 0 \\ 0 & ... & ... & ... & ... & ... & ... & 0 \\ 0 & 0 & 0 & 0 & 0 & M_{n-1,n-2} & M_{n-1,n-1} & M_{n-1,n} \\ 0 & 0 & 0 & 0 & 0 & 0 & M_{n,n-1} & M_{n,n} \end{bmatrix} \tag{A.26}$$

A.5.2 Human transition probabilities matrix P_H

In obtaining the human transition matrix P_H the following transition probabilities will be considered (see also equation 5.13):

$$p_{h+} = p_h = m\Phi_h \tag{A.27}$$

$$p_{h=} = 1 - m\Phi_h \tag{A.28}$$

q_h = daily probability of human disease cure.

$(1 - q_h)$ = daily probability of human disease persistence.

d) $H_{j,j+1}$

$$p[(H_{j+1}, t + \Delta t) \mid (H_j, t)] = p(H_j, t)\ (1 - q_h)\ p_{h+} \tag{A.29}$$

e) $H_{j,j}$

$$p[(H_j, t + \Delta t) \mid (H_j, t)] = p(H_j, t)[q_h p_{h+} + (1 - q_h)\ p_{h=}] \tag{A.30}$$

f) $H_{j,j-1}$

$$p[(H_{j-1}, t + \Delta t) \mid (H_j, t)] = p(H_j, t) q_h\ p_{h=} \tag{A.31}$$

where p_{h+} is the probability of a healthy human host acquiring infection after an infectious mosquito bite, $p_{h=}$ is the probability of a healthy human host not acquiring infection after an infectious mosquito bite, q_h represents the daily probability of human disease cure, and $(1 - q_h)$ represents the daily probability of human disease persistence.

And we obtain the human transition matrix P_H, where k represents the total number of human individuals:

$$P_H = \begin{bmatrix} H_{0,0} & H_{0,1} & 0 & ... & ... & ... & ... & 0 \\ H_{1,0} & H_{1,1} & H_{1,2} & 0 & ... & ... & ... & 0 \\ 0 & H_{2,1} & H_{2,2} & H_{2,3} & 0 & 0 & 0 & 0 \\ 0 & ... & ... & ... & ... & ... & ... & 0 \\ 0 & ... & ... & H_{j,j-1} & H_{j,j} & H_{j,j+1} & ... & 0 \\ 0 & ... & ... & ... & ... & ... & ... & 0 \\ 0 & ... & ... & ... & ... & H_{k-1,k-2} & H_{k-1,k-1} & H_{k-1,k} \\ 0 & ... & ... & ... & ... & ... & H_{k,k-1} & H_{k,k} \end{bmatrix} \tag{A.32}$$

Thus, we obtain a pair of matrices, P_M and P_H:

$$P_H = \begin{bmatrix} ... & ... & ... \\ ... & p_{H_{i,j}} & ... \\ ... & ... & ... \end{bmatrix} \tag{A.33}$$

and

$$P_M = \begin{bmatrix} ... & ... & ... \\ ... & p_{M_{i,j}} & ... \\ ... & ... & ... \end{bmatrix} \tag{A.34}$$

Transition rates generator matrix Q_M and Q_H

From these results we may obtain the transition rates $q_{M_{i,j}}$ and $q_{H_{i,j}}$, corresponding to the infinitesimal generator matrix: Q_M and Q_H respectively, according to the following equations:

Mosquito

$$Q_M = \lim_{\Delta t \to 0^+} \frac{P_M - I}{\Delta t} \tag{A.35}$$

Human individual

$$Q_H = \lim_{\Delta t \to 0^+} \frac{P_H - I}{\Delta t} \tag{A.36}$$

g)$q_{M_{i,j}}$

where

$i = j$

$$q_{M_{i,i}} = \lim_{\Delta t \to 0^+} \frac{p_{M_{i,i}}(\Delta t) - 1}{\Delta t} \tag{A.37}$$

$i \neq j$

$$q_{M_{i,j}} = \lim_{\Delta t \to 0^+} \frac{p_{M_{i,j}}(\Delta t)}{\Delta t} \tag{A.38}$$

And we obtain the mosquito transition rates generator matrix Q_M, where n represents the total number of mosquitoes:

$$Q_M = \begin{bmatrix} q_{M_{0,0}} & q_{M_{0,1}} & \cdots & \cdots & \cdots & \cdots & \cdots & 0 \\ q_{M_{1,0}} & q_{M_{1,1}} & q_{M_{1,2}} & \cdots & \cdots & \cdots & \cdots & 0 \\ 0 & q_{M_{2,1}} & q_{M_{2,2}} & q_{M_{2,3}} & \cdots & \cdots & \cdots & 0 \\ 0 & \cdots & \cdots & \cdots & \cdots & \cdots & \cdots & 0 \\ 0 & \cdots & \cdots & q_{M_{i,i-1}} & q_{M_{i,i}} & q_{M_{i,i+1}} & \cdots & 0 \\ 0 & \cdots & \cdots & \cdots & \cdots & \cdots & \cdots & 0 \\ 0 & \cdots & \cdots & \cdots & \cdots & q_{M_{n-1,n-2}} & q_{M_{n-1,n-1}} & q_{M_{n-1,n}} \\ 0 & \cdots & \cdots & \cdots & \cdots & \cdots & q_{M_{n,n-1}} & q_{M_{n,n}} \end{bmatrix} \tag{A.39}$$

Finally we will obtain:

$$-\frac{q_{M_{i,j}}}{q_{M_{i,i}}} = \lim_{\Delta t \to 0^+} \frac{p_{M_{i,j}}(\Delta t)}{1 - p_{M_{i,i}}(\Delta t)} \tag{A.40}$$

h) $q_{H_{i,j}}$

where

$i = j$

$$q_{H_{i,i}} = \lim_{\Delta t \to 0^+} \frac{p_{H_{i,i}}(\Delta t) - 1}{\Delta t} \tag{A.41}$$

and

$i \neq j$

$$q_{H_{i,j}} = \lim_{\Delta t \to 0^+} \frac{p_{H_{i,j}}(\Delta t)}{\Delta t} \tag{A.42}$$

And we obtain the human transition rates generator matrix Q_H, where k represents the total number of human individuals:

$$Q_H = \begin{bmatrix} q_{H_{0,0}} & q_{H_{0,1}} & \dots & \dots & \dots & \dots & \dots & 0 \\ q_{H_{1,0}} & q_{H_{1,1}} & q_{H_{1,2}} & \dots & \dots & \dots & \dots & 0 \\ 0 & q_{H_{2,1}} & q_{H_{2,2}} & q_{H_{2,3}} & \dots & \dots & \dots & 0 \\ 0 & \dots & \dots & \dots & \dots & \dots & \dots & 0 \\ 0 & \dots & \dots & q_{H_{j,j-1}} & q_{H_{j,j}} & q_{H_{j,j+1}} & \dots & 0 \\ 0 & \dots & \dots & \dots & \dots & \dots & \dots & 0 \\ 0 & \dots & \dots & \dots & \dots & q_{H_{k-1,k-2}} & q_{H_{k-1,k-1}} & q_{H_{k-1,k}} \\ 0 & \dots & \dots & \dots & \dots & \dots & q_{H_{k,k-1}} & q_{H_{k,k}} \end{bmatrix} \tag{A.43}$$

Finally we will obtain:

$$-\frac{q_{H_{i,j}}}{q_{H_{i,i}}} = \lim_{\Delta t \to 0^+} \frac{p_{H_{i,j}}(\Delta t)}{1 - p_{H_{i,i}}(\Delta t)} \tag{A.44}$$

Markov relations between probability transition matrix P and transition matrix Q

In order to compute the stationary distribution of the Markov chain we will use the stationary probability row vectors π_M and π_H in the following equations:

Mosquito

$$\pi_M P_M(dt) = \pi_M \tag{A.45}$$

$$\pi_M (I + Q_M dt) = \pi_M \tag{A.46}$$

$$\pi_M Q_M = 0 \tag{A.47}$$

Human individual

$$\pi_H P_H(dt) = \pi_H \tag{A.48}$$

$$\pi_H (I + Q_H dt) = \pi_H \tag{A.49}$$

$$\pi_H Q_H = 0 \tag{A.50}$$

Assuming $P_M(0) = I$ and $P_H(0) = I$, the solution of these matrix differential

equations is obtained from the backward and forward Kolmogorov equations:

Kolmogorov matrix backward equation

$$\frac{dP_M(t)}{dt} = Q_M(t)P(t) \tag{A.51}$$

$$\frac{dP_H(t)}{dt} = Q_H(t)P(t) \tag{A.52}$$

and

Kolmogorov matrix forward equation

$$\frac{dP_M(t)}{dt} = P_M(t)Q_M(t) \tag{A.53}$$

$$\frac{dP_H(t)}{dt} = P_H(t)Q_H(t) \tag{A.54}$$

with the following solutions:

$$P_M(t) = e^{Q_M t} \tag{A.55}$$

$$P_H(t) = e^{Q_H t} \tag{A.56}$$

and in component form:

Mosquito

$$\frac{d}{dt}p_M(i,j,t) = \sum_{\delta=1}^{m} q_{M_{i\delta}} p_M(\delta,j,t) \tag{A.57}$$

where $i, j = 1, 2, ..., n$

and $n =$ total of mosquitoes

Human individual

$$\frac{d}{dt}p_H(i,j,t) = \sum_{\delta=1}^{h} q_{H_{i\delta}} p_H(\delta,j,t) \tag{A.58}$$

where $i, j = 1, 2, ..., k$

and $k =$ total of human individuals

Embedded Markov chain matrix T

We may then obtain the embedded Markov chain mosquito and human matrix, T_M and T_H respectively:

The embedded Markov chain is a discrete-time Markov process useful for classifying states in corresponding continuous-time Markov processes.

Mosquito

$$T_M = \begin{bmatrix} t_{M_{0,0}} & t_{M_{0,1}} & ... & ... & ... & ... & ... & 0 \\ t_{M_{1,0}} & t_{M_{1,1}} & t_{M_{1,2}} & ... & ... & ... & ... & 0 \\ 0 & t_{M_{2,1}} & t_{M_{2,2}} & t_{M_{2,3}} & ... & ... & ... & 0 \\ 0 & ... & ... & ... & ... & ... & ... & 0 \\ 0 & ... & ... & t_{M_{i,i-1}} & t_{M_{i,i}} & t_{M_{i,i+1}} & ... & 0 \\ 0 & ... & ... & ... & ... & ... & ... & 0 \\ 0 & ... & ... & ... & ... & t_{M_{n-1,n-2}} & t_{M_{n-1,n-1}} & t_{M_{n-1,n}} \\ 0 & ... & ... & ... & ... & ... & t_{M_{n,n-1}} & t_{M_{n,n}} \end{bmatrix} \tag{A.59}$$

and n = total of mosquitoes

when $q_{M_{i,i}} \neq 0$:

$$t_{M_{i,j}} = -\frac{q_{M_{i,j}}}{q_{M_{i,i}}} \tag{A.60}$$

and when $q_{M_{i,i}} = 0$:

$$t_{M_{i,j}} = 0 \tag{A.61}$$

where

$$-\frac{q_{M_{i,j}}}{q_{M_{i,i}}} = \lim_{\Delta t \to 0^+} \frac{p_{M_{i,j}}(\Delta t)}{1 - p_{M_{i,i}}(\Delta t)} \tag{A.62}$$

the embedded Markov chain human matrix T_H:

Human individual

$$T_H = \begin{bmatrix} t_{H_{0,0}} & t_{H_{0,1}} & 0 & ... & ... & ... & ... & 0 \\ t_{H_{1,0}} & t_{H_{1,1}} & t_{H_{1,2}} & ... & ... & ... & ... & 0 \\ 0 & t_{H_{2,1}} & t_{H_{2,2}} & t_{H_{2,3}} & ... & ... & ... & 0 \\ 0 & ... & ... & ... & ... & ... & ... & 0 \\ 0 & ... & t_{H_{i,i-1}} & t_{H_{i,i}} & t_{H_{i,i+1}} & ... & ... & 0 \\ 0 & ... & ... & ... & ... & ... & ... & 0 \\ 0 & ... & ... & ... & ... & t_{H_{k-1,k-2}} & t_{H_{k-1,k-1}} & t_{H_{k-1,k}} \\ 0 & ... & ... & ... & ... & ... & t_{H_{k,k-1}} & t_{H_{k,k}} \end{bmatrix} \tag{A.63}$$

and k = total of human individuals

when $q_{H_{j,j}} \neq 0$:

$$t_{H_{i,j}} = -\frac{q_{H_{i,j}}}{q_{H_{j,j}}} \tag{A.64}$$

and when $q_{H_{j,j}} = 0$:

$$t_{H_{i,j}} = 0 \tag{A.65}$$

where

$$-\frac{q_{H_{i,j}}}{q_{H_{j,j}}} = \lim_{\Delta t \to 0^+} \frac{p_{H_{i,j}}(\Delta t)}{1 - p_{H_{j,j}}(\Delta t)} \tag{A.66}$$

Appendix B

Stochastic master equation

B.1 Taylor approximation – one dimension

a) Probability of human transition (from susceptible to infected) – $u(h,t)$ – and mosquito transition (from susceptible to infected) – $v(m,t)$

We begin with

$$u(h,t+\triangle t) = P_h(1-q_h)u(h-\triangle h,t) + (1-[P_h(1-q_h) \\ +q_h(1-P_h)])u(h,t) + q_h(1-P_h)u(h+\triangle h,t) \tag{B.1}$$

Likewise, in a similar line of reasoning, we may also obtain the same equation for the mosquito case.

$$v(m,t+\triangle t) = P_m(1-q_m)v(m-\triangle m,t) + (1-[P_m(1-q_m) \\ +q_m(1-P_m)])v(m,t) + q_m(1-P_m)v(m+\triangle m,t) \tag{B.2}$$

where, as was determined before:

$h = \frac{H_i}{H}$ stands for human infection prevalence (from 0.0 – disease extinction – to 1.0 – full invasion),

$m = \frac{M_i}{M}$ [1] stands for mosquito infection prevalence (from 0.0 – disease extinction – to 1.0 – full invasion),

P_h results from equations 5.15 and 5.16,

P_m is obtained from equations 5.17 and 5.18,

[1] We assume $m = \frac{M_i}{M}$, and not the original mosquito density m described in D.L. Smith,2004 [343], replaced here by $\Delta_m = \frac{N_m}{N_h}$.

q_h has been defined in equation 5.1,
and q_m was previously described in equation 5.4.

Knowing that in the discrete case

$$\triangle h = 1 \tag{B.3}$$

$$\triangle m = 1 \tag{B.4}$$

and we will have
Human case:

$$\begin{aligned} u(h, t+\triangle t) = P_h(1-q_h)u(h-1,t) + (1-[P_h(1-q_h) \\ +q_h(1-P_h)])u(h,t) + q_h(1-P_h)u(h+1,t) \end{aligned} \tag{B.5}$$

Mosquito case:

$$\begin{aligned} v(m, t+\triangle t) = P_m(1-q_m)v(m-1,t) + (1-[P_m(1-q_m) \\ +q_m(1-P_m)])v(m,t) + q_m(1-P_m)v(m+1,t) \end{aligned} \tag{B.6}$$

We will then apply Taylor expansion to $u(h,t)$, and $v(m,t)$, obtaining:

Human case:

$$\begin{aligned} u(h, t+\triangle t) = P_h(1-q_h)[u(h,t) + \frac{\partial u}{\partial h}(-\triangle h) + \frac{\partial^2 u}{\partial h^2}\frac{(\triangle h)^2}{2} \\ +o([\triangle h]^3)] + q_h(1-P_h)[u(h,t) + \frac{\partial u}{\partial h}(\triangle h) + \frac{\partial^2 u}{\partial h^2} + \frac{(\triangle h)^2}{2} \\ +o([\triangle h]^3)] + (1-[P_h(1-q_h) + q_h(1-P_h)])u(h,t) \end{aligned} \tag{B.7}$$

and joining terms

$$\begin{aligned} u(h, t+\triangle t) = (P_h[1-q_h] + q_h[1-P_h] + 1 - [P_h(1-q_h) \\ +q_h(1-P_h)])u(h,t) + (q_h[1-P_h] - P_h[1-q_h])\frac{\partial u}{\partial h}(\triangle h) \\ +(P_h[1-q_h] + q_h[1-P_h])\frac{\partial^2 u}{\partial h^2}\frac{(\triangle h)^2}{2} \\ +(P_h[1-q_h] + q_h[1-P_h])o(\triangle h)^3) \end{aligned} \tag{B.8}$$

where we have

$$P_h[1-q_h]+q_h[1-P_h]+1-[P_h(1-q_h)+q_h(1-P_h)]=1 \tag{B.9}$$

and after simplification of the term of $u(h,t)$ we get:

$$u(h,t+\triangle t) = u(h,t) + (q_h[1-P_h] - P_h[1-q_h])\frac{\partial u}{\partial h}(\triangle h) \\ +(P_h[1-q_h] + q_h[1-P_h])\frac{\partial^2 u}{\partial h^2}\frac{(\triangle h)^2}{2} \\ +(P_h[1-q_h] + q_h[1-P_h])o(\triangle h)^3) \tag{B.10}$$

Mosquito case:

$$v(m,t+\triangle t) = P_m(1-q_m)[v(m,t) + \frac{\partial v}{\partial m}(-\triangle m) + \frac{\partial^2 v}{\partial m^2}\frac{(\triangle m)^2}{2} \\ +o([\triangle m]^3)] + q_m(1-P_m)[v(m,t) + \frac{\partial v}{\partial m}(\triangle m) + \frac{\partial^2 v}{\partial m^2}\frac{(\triangle m)^2}{2} \\ +o([\triangle m]^3)] + (1-[P_m(1-q_m) + q_m(1-P_m)])v(m,t) \tag{B.11}$$

and joining terms

$$v(m,t+\triangle t) = (P_m[1-q_m] + q_m[1-P_m] + 1 - [P_m(1-q_m) \\ +q_m(1-P_m)])v(m,t) + (q_m[1-P_m] - P_m[1-q_m])\frac{\partial v}{\partial m}(\triangle m) \\ +(P_m[1-q_m] + q_m[1-P_m])\frac{\partial^2 v}{\partial m^2}\frac{(\triangle m)^2}{2} \\ +(P_m[1-q_m] + q_m[1-P_m])o(\triangle m)^3) \tag{B.12}$$

where we have

$$P_m[1-q_m] + q_m[1-P_m] + 1 - [P_m(1-q_m) + q_m(1-P_m)] = 1 \tag{B.13}$$

and after simplification of the term of $v(m,t)$ we get

$$v(m,t+\triangle t) = v(m,t) + (q_m[1-P_m] - P_m[1-q_m])\frac{\partial v}{\partial m}(\triangle m) \\ +(P_m[1-q_m] + q_m[1-P_m])\frac{\partial^2 v}{\partial m^2}\frac{(\triangle m)^2}{2} \\ +(P_m[1-q_m] + q_m[1-P_m])o(\triangle m)^3) \tag{B.14}$$

We will then assume the following 3 conditions, for humans and mosquitoes:

i)

for humans:

$$\lim_{\triangle t,\triangle h\to 0}[q_h(1-P_h)-P_h(1-q_h)]\frac{\triangle h}{\triangle t}=-c_h \tag{B.15}$$

for mosquitoes:

$$\lim_{\triangle t,\triangle m\to 0}[q_m(1-P_m)-P_m(1-q_m)]\frac{\triangle m}{\triangle t}=-c_m \tag{B.16}$$

ii)

for humans:

$$\lim_{\triangle t,\triangle h\to 0}[P_h(1-q_h)+q_h(1-P_h)]\frac{(\triangle h)^2}{\triangle t}=D_h \tag{B.17}$$

for mosquitoes:

$$\lim_{\triangle t,\triangle m\to 0}[P_m(1-q_m)+q_m(1-P_m)]\frac{(\triangle m)^2}{\triangle t}=D_m \tag{B.18}$$

iii)

for humans:

$$\lim_{\triangle t,\triangle h\to 0}[P_m(1-q_m)+q_m(1-P_m)]\frac{o(\triangle h)^3}{\triangle t}=0 \tag{B.19}$$

for mosquitoes:

$$\lim_{\triangle t,\triangle m\to 0}[P_m(1-q_m)+q_m(1-P_m)]\frac{o(\triangle m)^3}{\triangle t}=0 \tag{B.20}$$

Human infection:

subtracting $u(h,t)$ from both sides of the human equation, and dividing by $\triangle t$ we will obtain a Fokker-Planck equation for humans, where $u(h,t)$ represents the probability density function of the stochastic variable human infection prevalence h.

$$\lim_{\triangle t \to 0} \frac{u(h,t+\triangle t) - u(h,t)}{\triangle t} = -c_h \frac{\partial u}{\partial h} + \frac{D_h}{2} \frac{\partial^2 u}{\partial h^2} \tag{B.21}$$

Mosquito infection:

subtracting $v(m,t)$ from both sides of the human equation, and dividing by $\triangle t$ we will also obtain a Fokker-Planck equation FPE for mosquitoes, where $v(m,t)$ represents the probability density function of the stochastic variable mosquito infection prevalence m.

$$\lim_{\triangle t \to 0} \frac{v(m,t+\triangle t) - v(m,t)}{\triangle t} = -c_m \frac{\partial v}{\partial m} + \frac{D_m}{2} \frac{\partial^2 v}{\partial m^2} \tag{B.22}$$

and

$$\frac{\partial u(h,t)}{\partial t} = -c_h \frac{\partial u}{\partial h} + \frac{D_h}{2} \frac{\partial^2 u}{\partial h^2} \tag{B.23}$$

$$\frac{\partial v(m,t)}{\partial t} = -c_m \frac{\partial v}{\partial m} + \frac{D_m}{2} \frac{\partial^2 v}{\partial m^2} \tag{B.24}$$

Where c_h, c_m stand for the human and mosquito drift coefficients, and D_h, D_m stand for the human and mosquito diffusion coefficients, respectively, in the final diffusion human and mosquito differential equations (Fokker-Planck equation, also known as forward Kolmogorov equation).

The non-linear term is included in the drift coefficient $c_{h,m}$, as $c_h(h,m)$ and $c_m(h,m)$ both depend on h and m.

From equations 5.13 and 5.14 we then have:

Humans:

$$\lim_{\triangle t,\triangle h\to 0}[q_h(1-P_h)-P_h(1-q_h)]\frac{\triangle h}{\triangle t}=\lim_{\triangle t,\triangle h\to 0}(q_h-P_h)\frac{\triangle h}{\triangle t} \tag{B.25}$$

$$\lim_{\triangle t,\triangle h\to 0}(q_h-P_h)\frac{\triangle h}{\triangle t}=-c_h(h,m) \tag{B.26}$$

$$\lim_{\triangle t,\triangle m\to 0}(q_h-m\Phi_h)\frac{\triangle h}{\triangle t}=-c_h(h,m) \tag{B.27}$$

Mosquitoes:

$$\lim_{\triangle t,\triangle h\to 0}[q_m(1-P_m)-P_m(1-q_m)]\frac{\triangle m}{\triangle t}=\lim_{\triangle t,\triangle m\to 0}(q_m-P_m)\frac{\triangle m}{\triangle t} \tag{B.28}$$

$$\lim_{\triangle t,\triangle m\to 0}(q_m-P_m)\frac{\triangle m}{\triangle t}=-c_m(h,m) \tag{B.29}$$

$$\lim_{\triangle t,\triangle m\to 0}(q_m-h\Phi_m)\frac{\triangle m}{\triangle t}=-c_m(h,m) \tag{B.30}$$

B.2 Taylor approximation – two dimensions

In order to derive the 2D Fokker-Planck equation we must consider using a two-dimensional Taylor approximation (for the one-dimensional Taylor approximation to the Fokker Planck equation, please consider checking the previous section in the current Appendix.)

Based upon the previous equations defining human and mosquito events probabilities (from equations 5.11 to 5.20), we begin by defining the combined h and m probabilities.

Knowing the simpler expressions for Φ_h and Φ_m we then may use:

$$\Phi_h = k_h w_m (1 - \nu) \tag{B.31}$$

and

$$\Phi_m = k_m w_h \tag{B.32}$$

resulting in:

$$p_h = m\Phi_h \tag{B.33}$$

and

$$p_m = h\Phi_m \tag{B.34}$$

From these equations, we use the simplified equations B.31 and B.32 (previously mentioned in the form of equations 5.11 and 5.12). We will then obtain the probabilities of effective global human-mosquito disease transmission, P_h and P_m in equations B.39 and B.40 (previously presented in the form of equations 5.19 and 5.20) :

For human individuals:

$$P_h = R\ p_h \tag{B.35}$$

and

$$P_h = R\ m\Phi_h \tag{B.36}$$

and for mosquitoes:

$$P_m = R\ p_m \tag{B.37}$$

and

$$P_m = R\ h\Phi_m \tag{B.38}$$

From this, functions P_m and P_h will also both depend on m and h, finally having:

$$P_h = P_h(h, m) \tag{B.39}$$

and

$$P_m = P_m(h, m) \tag{B.40}$$

As was shown before, we have evidence of non-linearity in the coupled system $H - M$, as the human probability p_h depends both on human (k_h and ν) and mosquito (m and w_m) parameters. Likewise, the mosquito probability p_m will depend both on mosquito (k_m) and human (h and w_h) parameters.
In this case, non-linearity will only depend on variables h and m, as the the remaining parameters will be constant parameters, nested inside Φ_h and Φ_m.

We may then obtain the probabilities of different events following a mosquito bite in a human individual:

Human probability:

$$P_{h_+} = P_h(1 - q_h) \tag{B.41}$$

$$P_{h_=} = (1 - [P_h(1 - q_h) + q_h(1 - P_h)]) \tag{B.42}$$

$$P_{h_-} = q_h(1 - P_h) \tag{B.43}$$

Mosquito probability:

$$P_{m_+} = P_m(1 - q_m) \tag{B.44}$$

$$P_{m_=} = (1 - [P_m(1 - q_m) + q_m(1 - P_m)]) \tag{B.45}$$

$$P_{m_-} = q_m(1 - P_m) \tag{B.46}$$

and we have for the combined human-mosquito probabilities:

$$P_{h_+,m_+} = P_{h_+} \cdot P_{m_+} \tag{B.47}$$

$$P_{h_+,m_=} = P_{h_+} \cdot P_{m_=} \tag{B.48}$$

$$P_{h_+,m_-} = P_{h_+} \cdot P_{m_-} \tag{B.49}$$

$$P_{h_=,m_+} = P_{h_=} \cdot P_{m_+} \tag{B.50}$$

$$P_{h_=,m_=} = P_{h_=} \cdot P_{m_=} \tag{B.51}$$

$$P_{h_=,m_-} = P_{h_=} \cdot P_{m_-} \tag{B.52}$$

$$P_{h_-,m_+} = P_{h_-} \cdot P_{m_+} \tag{B.53}$$

$$P_{h_-,m_=} = P_{h_-} \cdot P_{m_=} \tag{B.54}$$

$$P_{h_-,m_-} = P_{h_-} \cdot P_{m_-} \tag{B.55}$$

and we have

$$\begin{aligned} u(h,m,t+\triangle t) = P_{h_+,m_+}\cdot u(h-\triangle h, m-\triangle m, t) \\ +P_{h_+,m_=}\cdot u(h-\triangle h, m, t) + P_{h_+,m_-}\cdot u(h-\triangle h, m+\triangle m, t) \\ +P_{h_=,m_+}\cdot u(h, m-\triangle m, t) + P_{h_=,m_=}\cdot u(h,m,t) \\ +P_{h_=,m_-}\cdot u(h, m+\triangle m, t) + P_{h_-,m_+}\cdot u(h \\ +\triangle h, m-\triangle m, t) + P_{h_-,m_=}\cdot u(h+\triangle h, m, t) \\ +P_{h_-,m_-}\cdot u(h+\triangle h, m+\triangle m, t) \end{aligned} \tag{B.56}$$

From these equations defining the possible events probabilities it is possible to deduce the final 2D Fokker-Planck equation.

We start by assuming the following 9 equations:

$$\begin{aligned} u_{++} = u(h,m,t) + \frac{\partial u}{\partial h}(-\triangle h) + \frac{\partial u}{\partial m}(-\triangle m) + \frac{1}{2}[\frac{\partial^2 u}{\partial h^2}(-\triangle h)^2 \\ +\frac{\partial^2 u}{\partial m^2}(-\triangle m)^2 + 2\frac{\partial^2 u}{\partial h \partial m}([-\triangle h][-\triangle m]) + o([\triangle h \triangle m]^3)] \end{aligned} \tag{B.57}$$

$$u_{+=} = u(h,m,t) + \frac{\partial u}{\partial h}(-\triangle h) + \frac{1}{2}\frac{\partial^2 u}{\partial h^2}(-\triangle h)^2 + o([\triangle h]^3) \tag{B.58}$$

$$\begin{aligned} u_{+-} = u(h,m,t) + \frac{\partial u}{\partial h}(-\triangle h) + \frac{\partial u}{\partial m}(\triangle m) + \frac{1}{2}[\frac{\partial^2 u}{\partial h^2}(-\triangle h)^2 \\ +\frac{\partial^2 u}{\partial m^2}(-\triangle m)^2 + 2\frac{\partial^2 u}{\partial h \partial m}(\triangle h[-\triangle m])] + o([\triangle h \triangle m]^3) \end{aligned} \tag{B.59}$$

$$u_{=+} = u(h,m,t) + \frac{\partial u}{\partial m}(-\triangle m) + \frac{1}{2}\frac{\partial^2 u}{\partial m^2}(-\triangle m)^2 + o([\triangle m]^3)] \tag{B.60}$$

$$u_{==} = u(h, m, t) \tag{B.61}$$

$$u_{=-} = u(h, m, t) + \frac{\partial u}{\partial m}(\triangle m) + \frac{1}{2}\frac{\partial^2 u}{\partial m^2}(\triangle m)^2 + o([\triangle m]^3) \tag{B.62}$$

$$\begin{aligned} u_{-+} = u(h, m, t) + \frac{\partial u}{\partial h}(\triangle h) + \frac{\partial u}{\partial m}(-\triangle m) + \frac{1}{2}[\frac{\partial^2 u}{\partial h^2}(\triangle h)^2 \\ + \frac{\partial^2 u}{\partial m^2}(-\triangle m)^2 + 2\frac{\partial^2 u}{\partial h \partial m}(\triangle h[-\triangle m])] + o([\triangle h \triangle m]^3) \end{aligned} \tag{B.63}$$

$$u_{-=} = u(h, m, t) + \frac{\partial u}{\partial h}(\triangle h) + \frac{1}{2}\frac{\partial^2 u}{\partial h^2}(\triangle h)^2 + o([\triangle h]^3) \tag{B.64}$$

$$\begin{aligned} u_{--} = u(h, m, t) + \frac{\partial u}{\partial h}(\triangle h) + \frac{\partial u}{\partial m}(\triangle m) + \frac{1}{2}[\frac{\partial^2 u}{\partial h^2}(\triangle h)^2 \\ + \frac{\partial^2 u}{\partial m^2}(\triangle m)^2 + 2\frac{\partial^2 u}{\partial h \partial m}(\triangle h \triangle m)] + o([\triangle h \triangle m]^3) \end{aligned} \tag{B.65}$$

And we will then have the final 2D Fokker-Planck equation:

$$\begin{aligned} u(h, m, t + \triangle t) = P_{h_+, m_+} \cdot u_{++} + P_{h_+, m_=} \cdot u_{+=} + P_{h_+, m_-} \cdot u_{+-} \\ + P_{h_=, m_+} \cdot u_{=+} + P_{h_=, m_=} \cdot u_{==} + P_{h_=, m_-} \cdot u_{=-} \\ + P_{h_-, m_+} \cdot u_{-+} + P_{h_-, m_=} \cdot u_{-=} + P_{h_-, m_-} \cdot u_{--} \end{aligned} \tag{B.66}$$

We now apply the 2D Taylor expansion to $u(h, m, t)$ in the previous equation

$$u(h-\triangle h, m-\triangle m, t) = u(h, m, t) + \frac{\partial u}{\partial h}(-\triangle h) + \frac{\partial u}{\partial m}(-\triangle m) + \frac{1}{2}[\frac{\partial^2 u}{\partial h^2}(-\triangle h)^2 + \frac{\partial^2 u}{\partial m^2}(-\triangle m)^2 + 2\frac{\partial^2 u}{\partial h \partial m}([-\triangle h][-\triangle m])] + o([\triangle h \triangle m]^3) \tag{B.67}$$

and using $+\triangle m$ instead of $-\triangle m$ we will then have:

$$u(h-\triangle h, m+\triangle m, t) = u(h, m, t) + \frac{\partial u}{\partial h}(-\triangle h) + \frac{\partial u}{\partial m}(\triangle m) + \frac{1}{2}[\frac{\partial^2 u}{\partial h^2}(-\triangle h)^2 + \frac{\partial^2 u}{\partial m^2}(\triangle m)^2 + 2\frac{\partial^2 u}{\partial h \partial m}([-\triangle h]\triangle m)] + o([\triangle h \triangle m]^3) \tag{B.68}$$

while using $+\triangle h$ instead of $-\triangle h$, and $-\triangle m$ instead of $+\triangle m$, we will have:

$$u(h+\triangle h, m-\triangle m, t) = u(h, m, t) + \frac{\partial u}{\partial h}(\triangle h) + \frac{\partial u}{\partial m}(-\triangle m) + \frac{1}{2}[\frac{\partial^2 u}{\partial h^2}(\triangle h)^2 + \frac{\partial^2 u}{\partial m^2}(-\triangle m)^2 + 2\frac{\partial^2 u}{\partial h \partial m}(\triangle h[-\triangle m])] + o([\triangle h \triangle m]^3) \tag{B.69}$$

and using $+\triangle h$ instead of $-\triangle h$, and $+\triangle m$ instead of $-\triangle m$, we will have:

$$u(h+\triangle h, m+\triangle m, t) = u(h, m, t) + \frac{\partial u}{\partial h}(\triangle h) + \frac{\partial u}{\partial m}(\triangle m) + \frac{1}{2}[\frac{\partial^2 u}{\partial h^2}(\triangle h)^2 + \frac{\partial^2 u}{\partial m^2}(\triangle m)^2 + 2\frac{\partial^2 u}{\partial h \partial m}(\triangle h \triangle m)] + o([\triangle h \triangle m]^3) \tag{B.70}$$

where concerning u as a function of $h \pm \triangle h$, m, and t

$$u(h+\triangle h, m, t) = u(h, m, t) + \frac{\partial u}{\partial h}(\triangle h) + \frac{1}{2}\frac{\partial^2 u}{\partial h^2}(\triangle h)^2 + o([\triangle h]^3) \tag{B.71}$$

and

$$u(h-\triangle h,m,t)=u(h,m,t)+\frac{\partial u}{\partial h}(-\triangle h) \\ +\frac{1}{2}[\frac{\partial^2 u}{\partial h^2}(-\triangle h)^2+o([\triangle h]^3) \tag{B.72}$$

while concerning u as a function of h, $m\pm\triangle m$, and t

$$u(h,m+\triangle m,t)=u(h,m,t)+\frac{\partial u}{\partial m}(\triangle m) \\ +\frac{1}{2}\frac{\partial^2 u}{\partial m^2}(\triangle m)^2+o([\triangle m]^3) \tag{B.73}$$

and

$$u(h,m-\triangle m,t)=u(h,m,t)+\frac{\partial u}{\partial m}(-\triangle m) \\ +\frac{1}{2}\frac{\partial^2 u}{\partial m^2}(-\triangle m)^2+o([\triangle m]^3) \tag{B.74}$$

We now substitute the several versions of $u(h,m,t)$ in equation (B.67).

We begin by defining the following parameters:

For α:

$$\alpha=\sum_{i=(-;=;+)}\sum_{j=(-;=;+)}P_{h_i,m_j} \tag{B.75}$$

and explicitly

$$\alpha=P_{h_+,m_+}+P_{h_+,m_=}+P_{h_+,m_-}+P_{h_=,m_+}+P_{h_=,m_=}+P_{h_=,m_-} \\ +P_{h_-,m_+}+P_{h_-,m_=}+P_{h_-,m_-} \tag{B.76}$$

For β_h

$$\beta_h = [\sum_{i=(-;=;+)} P_{h_-,m_i}] - [\sum_{i=(-;=;+)} P_{h_+,m_i}] \tag{B.77}$$

and explicitly

$$\beta_h = [P_{h_-,m_+} + P_{h_-,m_=} + P_{h_-,m_-}] - [P_{h_+,m_+} + P_{h_+,m_=} + P_{h_+,m_-}] \tag{B.78}$$

For β_m

$$\beta_m = [\sum_{i=(-;=;+)} P_{h_i,m_-}] - [\sum_{i=(-;=;+)} P_{h_i,m_+}] \tag{B.79}$$

and explicitly

$$\beta_m = [P_{h_+,m_-} + P_{h_=,m_-} + P_{h_-,m_-}] - [P_{h_+,m_+} + P_{h_=,m_+} + P_{h_-,m_+}] \tag{B.80}$$

while obtaining γ_{hm}

$$\gamma_{hm} = [P_{h_+,m_+} + P_{h_-,m_-} - P_{h_-,m_+} + P_{h_+,m_-}] \tag{B.81}$$

We then assume that $\alpha = 1$, and we get modified versions for β_h, β_m and γ_{hm} in order to obtain a simplified version of equation B.67:

$$\alpha = 1 \tag{B.82}$$

$$\begin{aligned}\beta_h^* = \alpha - [P_{h_=,m_+} + P_{h_=,m_=} + P_{h_=,m_-}] \\ -2[P_{h_+,m_+} + P_{h_+,m_=} + P_{h_+,m_=}]\end{aligned} \tag{B.83}$$

$$\begin{aligned}\beta_m^* = \alpha - [P_{h_+,m_=} + P_{h_=,m_=} + P_{h_-,m_=}] \\ -2[P_{h_+,m_+} + P_{h_=,m_+} + P_{h_-,m_+}]\end{aligned} \tag{B.84}$$

$$\gamma^*_{hm} = \alpha - [P_{h_+,m_=} + P_{h_=,m_+} + P_{h_=,m_=} + P_{h_=,m_-} + P_{h_-,m_=}] \\ -2[P_{h_+,m_-} + P_{h_-,m_+}] \tag{B.85}$$

and finally we have

$$u(h-\triangle h, m-\triangle m, t) = u(h,m,t) + \beta^*_h[\frac{\partial u}{\partial h}(\triangle h) \\ +\frac{1}{2}\frac{\partial^2 u}{\partial h^2}(\triangle h)^2] + \beta^*_m[\frac{\partial u}{\partial m}(\triangle m) + \frac{1}{2}\frac{\partial^2 u}{\partial m^2}(\triangle m)^2] \\ +\gamma^*_{hm}[\frac{\partial^2 u}{\partial h \partial m}(\triangle h \triangle m)] + o([\triangle h, \triangle m]^3) \tag{B.86}$$

while dividing both terms by $\triangle t$ we obtain:

$$\lim_{\triangle t \to 0} \frac{u(h-\triangle h, m-\triangle m, t) - u(h,m,t)}{\triangle t} = \beta^*_h[\frac{\partial u}{\partial h}\frac{(\triangle h)}{\triangle t} \\ +\frac{1}{2}\frac{\partial^2 u}{\partial h^2}\frac{(\triangle h)^2}{\triangle t}] + \beta^*_m[\frac{\partial u}{\partial m}\frac{(\triangle m)}{\triangle t} + \frac{1}{2}\frac{\partial^2 u}{\partial m^2}\frac{(\triangle m)^2}{\triangle t}] \\ +\gamma^*_{hm}[\frac{\partial^2 u}{\partial h \partial m}\frac{(\triangle h \triangle m)}{\triangle t}] + o([\triangle h, \triangle m]^3) \tag{B.87}$$

and, like in the 1-D case, we assume:

$$\lim_{\triangle t \to 0} \beta^*_h \frac{(\triangle h)}{\triangle t} = c^*_h \tag{B.88}$$

$$\lim_{\triangle t \to 0} \beta^*_m \frac{(\triangle m)}{\triangle t} = c^*_m \tag{B.89}$$

$$\lim_{\triangle t \to 0} \beta^*_h \frac{(\triangle h)^2}{\triangle t} = D^*_{hh} \tag{B.90}$$

$$\lim_{\triangle t \to 0} \beta^*_m \frac{(\triangle m)^2}{\triangle t} = D^*_{mm} \tag{B.91}$$

$$\lim_{\triangle t \to 0} \gamma^*_{hm} \frac{(\triangle h \triangle m)}{\triangle t} = D^*_{hm} \tag{B.92}$$

finally obtaining the 2D Fokker-Planck equation:

$$\frac{\partial p(h,m,t)}{\partial t} = -c_h^* \frac{\partial p(h,m,t)}{\partial h} - c_m^* \frac{\partial p(h,m,t)}{\partial m} + \frac{1}{2} D_{hh}^* \frac{\partial^2 p(h,m,t)}{\partial h^2} + \frac{1}{2} D_{mm}^* \frac{\partial^2 p(h,m,t)}{\partial m^2} + D_{hm}^* \frac{\partial^2 p(h,m,t)}{\partial h \partial m} \tag{B.93}$$

B.3 Diffusion equation, master equation and Itô formulation

We are now in conditions to obtain the transition probabilities for the diffusion equation in differential form. Based upon the following previous equations (equations 5.11 to 5.14, 5.16 and 5.18), defining human and mosquito events probabilitiies, we define the combined h and m probabilities.

Knowing the simpler expressions for p_h and p_m we may then use:

$$\Phi_h = k_h w_m (1 - \nu) \tag{B.94}$$

and

$$\Phi_m = k_m w_h \tag{B.95}$$

resulting in:

$$p_h = m \Phi_h \tag{B.96}$$

and

$$p_m = h \Phi_m \tag{B.97}$$

From these equations, we use the simplified equations 5.13 and 5.14. We will then obtain the probabilities of effective global human-mosquito disease transmission, P_h and P_m:

For the human case:

$$P_h = R \; p_h \tag{B.98}$$

and for the mosquito case:

$$P_m = R \; h \Phi_m \tag{B.99}$$

From this, it is clear that functions P_m and P_h will also both depend on m

and h, finally having:

$$P_h = P_h(h, m) \tag{B.100}$$

and

$$P_m = P_m(h, m) \tag{B.101}$$

Finally, it is possible to define the final probabilities for all possible events:

3 equations:

-Human case:

$$P(h_{t+\triangle t} = h - \frac{1}{H}) = h(1 - P_h)q_h \triangle t \tag{B.102}$$

$$P(h_{t+\triangle t} = h) = [1 - ([1 - P_h]q_h + P_h[1 - q_h])]h \triangle t \tag{B.103}$$

$$P(h_{t+\triangle t} = h + \frac{1}{H}) = h(1 - q_h)P_h \triangle t \tag{B.104}$$

Mosquito case:

$$P(m_{t+\triangle t} = m - \frac{1}{M}) = m(1 - P_m)q_m \triangle t \tag{B.105}$$

$$P(m_{t+\triangle t} = m) = [1 - ([1 - P_m]q_m + P_m[1 - q_m])]m \triangle t \tag{B.106}$$

$$P(m_{t+\triangle t} = m + \frac{1}{M}) = m(1 - q_m)P_m \triangle t \tag{B.107}$$

The discrete increment of the process has a probability mass function in the following form:

-Human case:

$$P(\triangle h_t = -\frac{1}{H}) = h(1 - P_h)q_h \triangle t \tag{B.108}$$

$$P(\triangle h_t = 0) = (1 - [(1 - P_h)q_h + P_h(1 - q_h)])h \triangle t \tag{B.109}$$

$$P(\triangle h_t = \frac{1}{H}) = hP_h(1 - q_h) \triangle t \tag{B.110}$$

-Mosquito case:

$$P(\triangle m_t = -\frac{1}{M}) = m(1 - P_m)q_m\triangle t \tag{B.111}$$

$$P(\triangle m_t = 0) = (1 - [(1 - P_m)q_m + P_m(1 - q_m)])m\triangle t \tag{B.112}$$

$$P(\triangle m_t = \frac{1}{M}) = mP_m(1 - q_m)\triangle t \tag{B.113}$$

and we have

-Human case:

$$c_h = \langle\triangle h_t\rangle = [P_h(1 - q_h) - q_h(1 - P_h)]h\triangle t \tag{B.114}$$

$$c_h = \langle\triangle h_t\rangle = (P_h - q_h)h\triangle t \tag{B.115}$$

$$D_h = \sigma^2(\triangle h_t) = [P_h(1 - q_h) + q_h(1 - P_h)]h\triangle t \tag{B.116}$$

$$D_h = \sigma^2(\triangle h_t) = (P_h + q_h - 2P_hq_h)h\triangle t \tag{B.117}$$

-Mosquito case:

$$c_m = \langle\triangle m_t\rangle = [P_m(1 - q_m) - q_m(1 - P_m)]m\triangle t \tag{B.118}$$

$$c_m = \langle\triangle m_t\rangle = (P_m - q_m)m\triangle t \tag{B.119}$$

$$D_m = \sigma^2(\triangle m_t) = [P_m(1 - q_m) + q_m(1 - P_m)]m\triangle t \tag{B.120}$$

$$D_m = \sigma^2(\triangle m_t) = (P_m + q_m - 2P_mq_m)m\triangle t \tag{B.121}$$

Here, we will assume the more usual notation of Itô differential equation:

$$dX = A(X,t)\ dt + B(X,t)\ dW \tag{B.122}$$

with the corresponding human and mosquito equations:

- Human case:

$$dh = A_h\ dt + B_h\ dW \tag{B.123}$$

and

-Mosquito case:

$$dm = A_m\ dt + B_m\ dW \tag{B.124}$$

where:

$$A_h = c_h \tag{B.125}$$

$$A_m = c_m \tag{B.126}$$

and

$$B_h = \sqrt{D_h} \tag{B.127}$$

$$B_m = \sqrt{D_m} \tag{B.128}$$

According to the the one dimension diffusion differential equation ($\triangle t \to dt$), we will then have:

- Human case:

$$dh_t = A_h dt + B_h dW \tag{B.129}$$

$$A_h = [P_h(1-q_h) - q_h(1-P_h)]\ h \tag{B.130}$$

$$A_h = (P_h - q_h)\ h \tag{B.131}$$

$$A_h(h,m) = (m\Phi_h - q_h)\ h \tag{B.132}$$

$$B_h = \sqrt{[P_h(1-q_h) + q_h(1-P_h)]\ h} \tag{B.133}$$

$$B_h = \sqrt{(P_h + q_h - 2P_h q_h)\ h} \tag{B.134}$$

$$B_h(h,m) = \sqrt{(m\Phi_h + q_h - 2m\Phi_h q_h)\ h} \tag{B.135}$$

and we will have:

$$dh_t = [P_h(1-q_h) - q_h(1-P_h)]h\,dt + \sqrt{[P_h(1-q_h) + q_h(1-P_h)]\ h}\,dW \tag{B.136}$$

$$dh_t = (P_h - q_h)h\,dt + \sqrt{(P_h + q_h - 2P_h q_h)\ h}\,dW \tag{B.137}$$

$$dh_t = [m\Phi_h(1-q_h) - q_h(1-m\Phi_h)]h\,dt + \sqrt{[m\Phi_h(1-q_h) + q_h(1-m\Phi_h)]\ h}\,dW \tag{B.138}$$

$$dh_t = (m\Phi_h - q_h)h\,dt + \sqrt{(m\Phi_h + q_h - 2m\Phi_h q_h)\ h}\,dW \tag{B.139}$$

-Mosquito case:

$$dm_t = A_m dt + B_m dW \tag{B.140}$$

$$A_m = [P_m(1-q_m) - q_m(1-P_m)]\ m \tag{B.141}$$

$$A_m = (P_m - q_m)\ m \tag{B.142}$$

$$A_m(h,m) = (h\Phi_m - q_m)\ m \tag{B.143}$$

$$B_m = \sqrt{[P_m(1-q_m) + q_m(1-P_m)]\ m} \tag{B.144}$$

$$B_m = \sqrt{(P_m + q_m - 2P_m q_m)\ m} \tag{B.145}$$

$$B_m(h,m) = \sqrt{(h\Phi_m + q_m - 2h\Phi_m q_m)\ m} \tag{B.146}$$

and we will have:

$$dm_t = [P_m(1-q_m) - q_m(1-P_m)]m\,dt + \sqrt{[P_m(1-q_m) + q_m(1-P_m)]\ m}\,dW \tag{B.147}$$

$$dm_t = (P_m - q_m)m\,dt + \sqrt{(P_m + q_m - 2P_m q_m)\ m}\,dW \tag{B.148}$$

$$dm_t = [h\Phi_m(1-q_m) - q_m(1-h\Phi_m)]m\,dt + \sqrt{[h\Phi_m(1-q_m) + q_m(1-h\Phi_m)]\ m}\,dW \tag{B.149}$$

$$dm_t = (h\Phi_m - q_m)m\,dt + \sqrt{(h\Phi_m + q_m - 2h\Phi_m q_m)\ m}\,dW \tag{B.150}$$

and relating this result to original Fokker-Planck equations B.23 , B.24, and equations 5.13, 5.14, we will then obtain:

- Human case:

for the drift coefficient

$$c_h = [P_h(1-q_h) - q_h(1-P_h)]\ h \tag{B.151}$$

$$c_h = (P_h - q_h)\ h \tag{B.152}$$

$$c_h(h,m) = [m\Phi_h(1-q_h) - q_h(1-m\Phi_h)]\ h \tag{B.153}$$

$$c_h(h,m) = (m\Phi_h - q_h)\ h \tag{B.154}$$

and for the diffusion coefficient

$$D_h = [P_h(1-q_h) + q_h(1-P_h)]\ h \tag{B.155}$$

$$D_h = (P_h + q_h - 2P_h q_h)\ h \tag{B.156}$$

$$D_h(h,m) = (m\Phi_h + q_h - 2m\Phi_h q_h)\ h \tag{B.157}$$

$$\frac{\partial u(h,t)}{\partial t} = -\left[P_h(1-q_h) - q_h(1-P_h)\right]h\frac{\partial u}{\partial h} + \frac{\left[P_h(1-q_h) + q_h(1-P_h)\right]\ h}{2}\frac{\partial^2 u}{\partial h^2} \tag{B.158}$$

$$\frac{\partial u(h,t)}{\partial t} = -\left(P_h - q_h\right)h\frac{\partial u}{\partial h} + \frac{\left(P_h + q_h - 2P_h q_h\right)\ h}{2}\frac{\partial^2 u}{\partial h^2} \tag{B.159}$$

$$\frac{\partial u(h,m,t)}{\partial t} = -\left(m\Phi_h - q_h\right)h\frac{\partial u}{\partial h} + \frac{\left(m\Phi_h + q_h - 2m\Phi_h q_h\right)\ h}{2}\frac{\partial^2 u}{\partial h^2} \tag{B.160}$$

-Mosquito case:

for the drift coefficient

$$c_m = \left[P_m(1-q_m) - q_m(1-P_m)\right]\ m \tag{B.161}$$

$$c_m = \left(P_m - q_m\right)\ m \tag{B.162}$$

$$c_m(h,m) = \left[h\Phi_m(1-q_m) - q_m(1-h\Phi_m)\right]\ m \tag{B.163}$$

$$c_m(h,m) = \left(h\Phi_m - q_m\right)\ m \tag{B.164}$$

and for the diffusion coefficient

$$D_m = \left[P_m(1-q_m) + q_m(1-P_m)\right]\ m \tag{B.165}$$

$$D_m = \left(P_m + q_m - 2P_m q_m\right)\ m \tag{B.166}$$

$$D_m(h,m) = \left(h\Phi_m + q_m - 2h\Phi_m q_m\right)\ m \tag{B.167}$$

where we then have

$$\frac{\partial v(m,t)}{\partial t} = -[P_m(1-q_m) - q_m(1-P_m)]m\frac{\partial v}{\partial m} + \frac{[P_m(1-q_m) + q_m(1-P_m)]\ m}{2}\frac{\partial^2 v}{\partial m^2} \tag{B.168}$$

$$\frac{\partial v(m,t)}{\partial t} = -(P_m - q_m)m\frac{\partial v}{\partial m} + \frac{(P_m + q_m - 2P_m q_m)\ m}{2}\frac{\partial^2 v}{\partial m^2} \tag{B.169}$$

$$\frac{\partial v(h,m,t)}{\partial t} = -(h\Phi_m - q_m)m\frac{\partial v}{\partial m} + \frac{(h\Phi_m + q_m - 2h\Phi_m q_m)\ m}{2}\frac{\partial^2 v}{\partial m^2} \tag{B.170}$$

Appendix C

Initial conditions and outcome

C.1 Background

Chaotic dynamics is aperiodic, which means that the system will never return to the same state. In chaotic dynamics, different initial conditions will be exponentially amplified. Limited dynamics is also characteristic of chaotic behavior, where the variables defining the system states will vary in finite intervals. Thus, chaotic dynamics is aperiodic, limited and also deterministic. There are no random variables, no stochastic components in chaotic dynamics. Chaotic systems are unpredictable because of a sensitive dependence on initial conditions. It is possible to quantify sensitive dependence on initial conditions with Lyapunov exponents (see equation C.1). The Lyapunov exponent represents the average rate of separation along two different trajectories on an attractor with very close initial conditions, defined here as $\delta x_0 = |x_0 - x_0^{'}|$.

As an example, for a continuous system in a r-dimensional physical state space, there are as many Lyapunov exponents as there are space axes. If the dimension of phase space is 3, three Lyapunov exponents exist. To define a chaotic system, it is sufficient to determine if the maximum Lyapunov exponent is positive.

$$\lambda = \lim_{n\to\infty} \lim_{\delta x_0 \to 0} \frac{1}{n} \sum_{t=0}^{n-1} \log|f^{'}(x_t)| \tag{C.1}$$

, where $f^{'}(x_t)$ may represent the approximation to the derivative of $f(x_t)$ as in:

$$f^{'}(x_t) \approx \frac{f(x_t) - f(x_{t-1})}{x_t - x_{t-1}} \tag{C.2}$$

Malaria transmission could be described as a two-agents human-mosquito coupled dynamical system. However, several of its characteristics are responsible for random non-linear multi-dimensional behavior. Random factors influencing

mosquito survival, the presence of variation in time spent during the sporogony cycle, and human-to-mosquito efficiency transmission dependent upon random gametocytemia in the human host are several examples of additional stochastic complexity. Chaotic behavior in dynamical systems results from multi-dimensional non-linear deterministic models revealing positive Lyapunov exponents. Although chaotic behavior in dynamical systems may result from deterministic models, it could present many similarities with stochastic non-deterministic models. The sensitivity to initial conditions is a distinct feature of chaotic dynamical systems. However, dynamical models with stochastic behavior may reveal the presence of a periodic attractor with stable orbiting in the phase space.

C.2 Methods

The sensitivity to the initial conditions of a deterministic system is a consistent hallmark of chaotic behavior. As the present model is defined as a stochastic two-dimensional (human-mosquito) coupled oscillator system, it is expected that its behavior will reveal the presence of a well-behaved stable attractor with no evidence whatsoever of any unstable or chaotic trajectories.

Dynamical three-dimensional deterministic non-linear systems may assume chaotic behavior, with trajectory dependence on small different initial conditions. Although our dynamical non-linear stochastic system may have a dimension equal to 2 in the phase space (human and mosquito infection), its dynamics can be reduced to a single dimension by analyzing malaria incidence in the human group. Furthermore, with the inclusion of several independent parameters independently influencing human and mosquito behavior inside the computational model, it was considered adequate to define the degree of sensitivity to different initial conditions in the malaria incidence time evolution as representative of what could happen in the coupled human-mosquito system.

To determine the sensitivity of the present model, several simulations were obtained from different initial conditions of human and mosquito infection, based upon models with identical parameters. The time series obtained from these simulations were compared in relation to the average infection prevalence and distribution probability curves. Infection incidence was determined during a whole period of 30 years, according to the chosen metrics of predicted instant malaria annual incidence per 100 inhabitants.

Therefore, the system evolution in time was analyzed in a single model with identical global parameters: with full heterogeneity ($\frac{1}{\theta} = 4.0$), and moderate human-to-mosquito transmission efficiency ($w_h = 0.500$). With identical model parameters, two very different infection prevalence initial conditions were simulated: A full human and mosquito infection initial state ($Hi_0 = 1.0$ and $Mi_0 = 1.0$), compared to an initial state with a low human infection rate ($Hi_0 = 0.05$) and a residual mosquito infection rate ($Mi_0 = 0.01$). The evolution in time of these

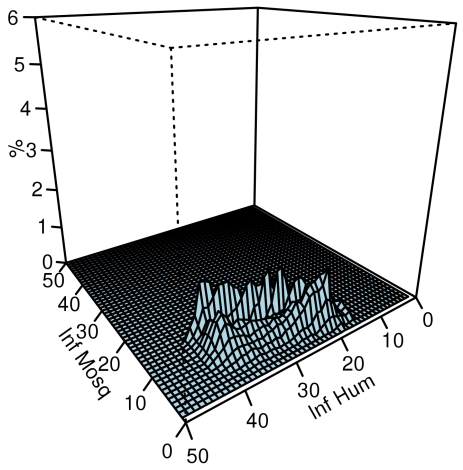

a)

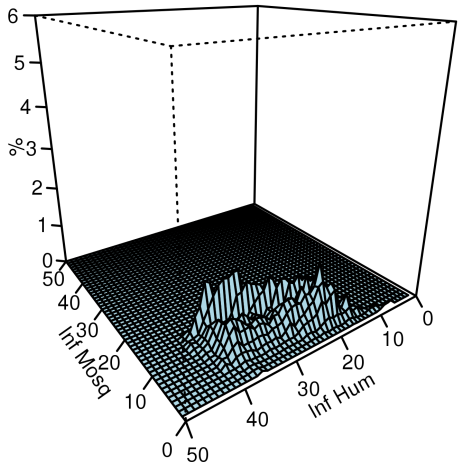

b)

Figure C.1: Two-dimensional human-mosquito probability density function with full heterogeneity ($\frac{1}{\theta} = 4.0$), and moderate human-to-mosquito transmission efficiency ($w_h = 0.500$), in different initial infection prevalence conditions: **(a)** Full human infection $Hi_0 = 1.0$ with full mosquito infection $Mi_0 = 1.00$, **(b)** Low human infection $Hi_0 = 0.05$ with residual mosquito infection $Mi_0 = 0.01$

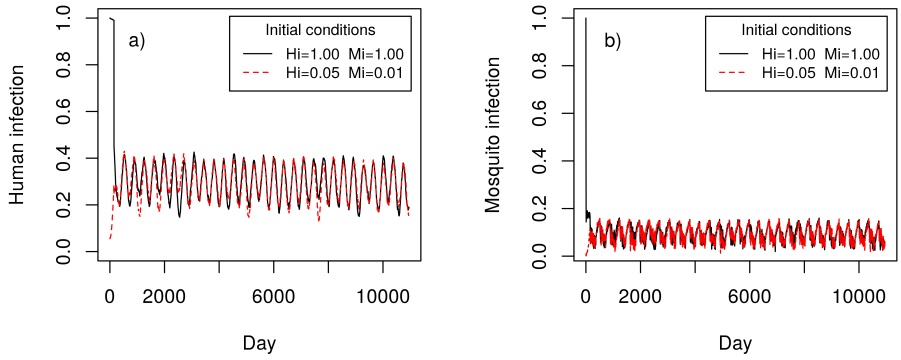

Figure C.2: Human and mosquito infection prevalence time series simulations, with full heterogeneity ($\frac{1}{\theta} = 4.0$), and moderate human-to-mosquito transmission efficiency ($w_h = 0.500$), in different infection prevalence initial conditions (Full human infection – $Hi_0 = 1.0$ and full mosquito infection – $Mi_0 = 1.0$ vs. Low human infection – $Hi_0 = 0.05$ and residual mosquito infection – $Mi_0 = 0.01$) : **(a)** Human infection, **(b)** Mosquito infection

different initial conditions was determined in terms of the similarity of human and mosquito infection prevalence time series (see figure C.1), malaria incidence cumulative distribution function (see figure C.2) and two-dimensional probability density function of human and mosquito infection prevalence (see figure C.3). The similarity between two different initial conditions was also compared by obtaining the Theil's inequality coefficient between time series with the same model parameters, but with different sets of initial conditions of human and mosquito infection prevalence – see table C.1.

Infection initial conditions		**Theil inequality**
Initial condition A	Initial condition B	U
$Hi_0 = 0.05/Mi_0 = 0.01$	$Hi_0 = 1.0/Mi_0 = 1.0$	0.178
$Hi_0 = 0.05/Mi_0 = 0.01$	$Hi_0 = 1.0/Mi_0 = 0.0$	0.129
$Hi_0 = 0.05/Mi_0 = 0.01$	$Hi_0 = 0.0/Mi_0 = 1.0$	0.165
$Hi_0 = 0.05/Mi_0 = 0.01$	$Hi_0 = 0.5/Mi_0 = 0.5$	0.142

Table C.1: Differences between malaria incidence time series at initial minimal human and mosquito infection prevalence ($Hi_0 = 0.05/Mi_0 = 0.01$ – condition A) against different initial levels of disease invasion (condition B), in a full heterogeneity scenario ($\frac{1}{\theta} = 4.0$) with moderate human-to-mosquito transmission efficiency ($w_h = 0.500$). Condition A was generally used as the standard initial condition in all other model simulations.

Infection initial conditions		**Lyapunov**
Initial condition A	Initial condition B	$\lambda_{Lyapunov}$
$Hi_0 = 0.05/Mi_0 = 0.01$	$Hi_0 = 1.0/Mi_0 = 1.0$	-3.964
$Hi_0 = 0.05/Mi_0 = 0.01$	$Hi_0 = 1.0/Mi_0 = 0.0$	-4.016
$Hi_0 = 0.05/Mi_0 = 0.01$	$Hi_0 = 0.0/Mi_0 = 1.0$	-3.978
$Hi_0 = 0.05/Mi_0 = 0.01$	$Hi_0 = 0.5/Mi_0 = 0.5$	-3.964

Table C.2: Negative values of Lyapunov exponent ($\lambda_{Lyapunov}$) at minimal human and mosquito infection prevalence ($Hi_0 = 0.05/Mi_0 = 0.01$ – condition A) against other different initial levels of disease invasion (condition B), in a full heterogeneity scenario ($\frac{1}{\theta} = 4.0$) with moderate human-to-mosquito transmission efficiency ($w_h = 0.500$).

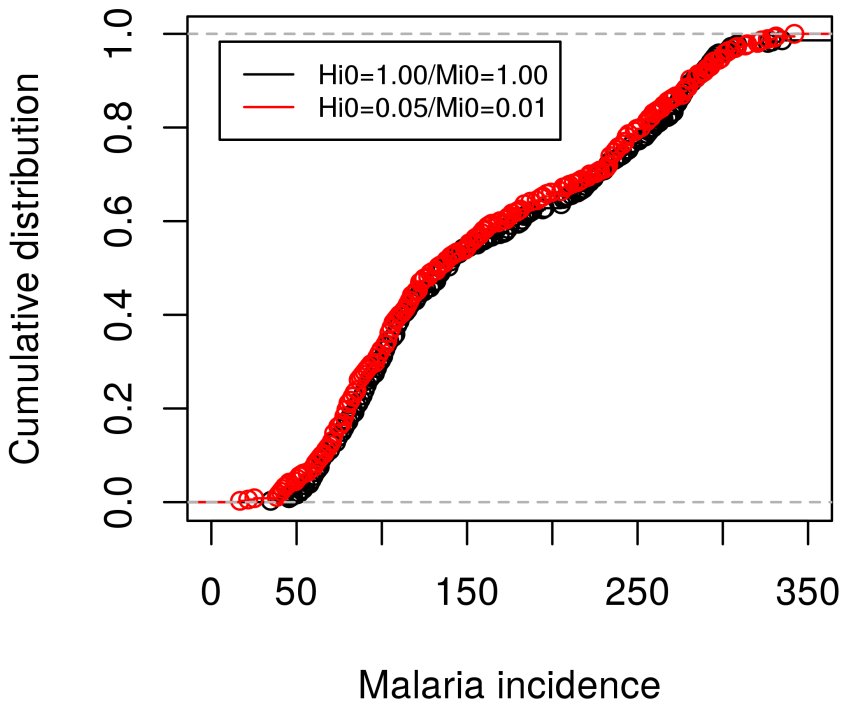

Figure C.3: Malaria incidence cumulative distribution function, with full heterogeneity ($\frac{1}{\theta} = 4.0$), and moderate human-to-mosquito transmission efficiency ($w_h = 0.500$), in different infection prevalence initial conditions: Disease invasion, with full human and mosquito infection ($Hi_0 = 1.0$ and $Mi_0 = 1.0$ – black) vs. mild human infection along with residual mosquito infection ($Hi_0 = 0.05$ and $Mi_0 = 0.01$ – red).

C.3 Results and discussion

In the presented figures (C.1, C.2, and C.3), no difference was found when comparing extreme cases of simulations with much different initial conditions (mild infection with $H_i = 0.05$ and $M_i = 0.01$ vs. full human-mosquito invasion with $H_i = 1.0$ and $M_i = 1.0$), suggesting that the present model is a two-dimensional stochastic process with a periodic, non-chaotic, non-deterministic behavior, in the presence of two negative Lyapunov exponents. Different types of initial conditions were also tested, with a very similar evolution of human and mosquito infection in time in all tested scenarios (see tables C.1 and C.2 for differences in Lyapunov exponent and Theil's inequality coefficient between different initial conditions).

When comparing simulations with identical global model parameters and different initial conditions, it was possible to determine the presence of a stable two-dimensional attractor in a coupled human-mosquito system, with nearly identical malaria human and mosquito infection prevalence time series (see figure C.1) , as well as very similar malaria incidence cumulative distribution function (see figure C.3), and very similar two-dimensional probability density function of human and mosquito infection prevalence (see figure C.1).

Also, by looking at differences in time series resulting from these different initial conditions, we may see very similar 2D probability density functions concerning the phase space of human and mosquito infection prevalence – see figure C.1.

Theil's inequality coefficient (here defined as U) has been useful in comparing the degree of dissimilarity between two time series. It should be close to 0 in the presence of two identical time series, and close to 1, in the case of two very different time series. In the case of significant similarity between two time series, Theil's U may range between 0.20 and 0.30 [265]. In the present case, Theil's U comparing time series with quite different initial conditions ($Hi_0 = 1.0$ and $Mi_0 = 1.0$ vs. $Hi_0 = 0.05$ and $Mi_0 = 0.01$) was significantly low (0.178), supporting the notion that both trajectories evolve identically as a stable stochastic attractor, with no evidence of chaotic dynamics. When comparing the initial condition generally used in most model simulations ($Hi_0 = 0.05$ and $Mi_0 = 0.01$) to other initial conditions, Theil's inequality coefficient was consistently low, with values in the range between 0.129 and 0.178, well below 0.30 – see table C.1.

Lyapunov exponent (here identified as $\lambda_{Lyapunov}$) has been widely used in trajectory analysis in chaotic systems. The estimation of trajectory divergence is based upon distance between different time series with small differences in initial conditions. When comparing the time series of two similar trajectories having small differences in initial conditions, we usually find positive Lyapunov exponents ($\lambda_{Lyapunov} > 0$) in deterministic non-linear chaotic systems. On the other

hand, in the presence of nonchaotic dynamics we may obtain negative values of $\lambda_{Lyapunov}$. In our case, when comparing different simulations with identical system parameters along with different initial conditions (initial conditions of human and mosquito infection prevalence), we find in all cases a significant negative value for the Lyapunov exponent – see table C.2.

We have analyzed the malaria human-mosquito dynamical system in terms of the impact of different initial conditions in epidemic outcome. In the present model, trajectories in phase space were shown to be stable, periodic, stochastic, and clearly insensitive to highly different initial conditions. This fact highlights the epidemic stability of the human-mosquito dynamical system, clearly independent of the initial conditions of infection prevalence in either compartment.

We have shown the process to be stochastic, periodic, non-chaotic, with trajectories independent of initial conditions of human and mosquito infection prevalence and evolving to epidemic stability at trajectories well distanced from phase transition. The implementation of effective strategies in lowering malaria transmission may achieve effective disease elimination in dynamical trajectories close to phase transition.

Appendix D

Malaria Box-Jenkins model

D.1 Time series background

Time series models have been widely used in economics, geophysics, biology and ecology. In particular, stock market analysis and hydrology planning have led to critical research in the field [6, 18, 31, 132, 166, 202, 213, 246]

The application of Fourier methods to random events have been useful in time series wave decomposition and spectrum analysis. From the study of stationarity, new theoretical concepts have emerged such as fractional regression (ARFIMA) and long-range dependence while the use of information entropy is somehow connected to other ideas such as the presence of long and short memory time series, self-organization, emergence and complexity [57, 129, 322]. The application of modern GARCH theory to the analysis of financial markets volatility is a promising research field [334].

Mathematical models based upon empirical time-series data have been used in forecasting, within reasonable confidence intervals, depending on the historical background of the random variable in question. A stochastic random variable may occur in the form of a random walk event presenting as gaussian white noise. Time series analysis may take place in two separate but connected domains: of time and frequency. Which form of analysis should be more suited will depend on the nature of the physical problem. Time series forecasting can be used in several forms of time domain analysis (ARIMA, Holt-Winters exponential smoothing and SARIMA). The frequency domain is sometimes used as an alternative in the presence of periodic behavior and spectral density, such as discrete Fourier transforms, non-parametric spectral estimation, signal extraction and filtering methods, single spectrum analysis, dynamical Fourier analysis and wavelets, among others. The more usual time domain approach will be in focus in the present Appendix [334].

D.2 Box-Jenkins theory in malaria modeling

Time series theory has been used extensively in malaria forecasting. A reliable time series model may antecipate predictions of future malaria epidemic behavior. In recent years, time series models have been developed with reasonable success to epidemiology and infectious disease research [2, 13, 21, 23, 40, 52, 96, 109, 122, 130, 141, 143, 144, 161, 163, 170, 204, 266, 290, 302, 324, 376].

A time series model may be stationary (time-independent) or non-stationary (time-dependent). Time evolution of the random variable may reveal a trend term (increasing or decreasing tendency of change in the average time-series value) with possible periodic cyclic behavior, a seasonality term (seasonal repetitive behavior with a more or less stable time frequency), and a random gaussian white noise term (with $\sigma^2 = 1$) defined here as Z_t – see equation D.1.

$$X_t = \sum_{i=1}^{p} \phi_{t-i} X_{t-i} + Z_t \tag{D.1}$$

Empirical time series of malaria incidence have been useful in monitoring disease transmission strength, and time series modeling has become more popular, based upon the concepts of autocorrelation, auto-regression, moving-average decomposition, and series differencing. Defining the presence of time series stationarity is usually an essential step in building a robust model [334]. The augmented Dickey-Fuller test may be useful for that purpose.

The Box-Jenkins time-series method was first described by Box and Jenkins in 1970 [46]. Since then, several different time series models have been implemented in malaria forecasting based upon this theory. To the best of our knowledge, the first consistent use of Box-Jenkins theory in malaria research was reported in Ethiopia (2002) by Abeku [2]. In 2007, Gomez-Elipe (hereafter referred to as Elipe,2007) used a time-series method in malaria modeling [147]. More recently, other authors have have looked more deeply into the possibility of forecasting malaria incidence with the help of different types of time-series models [21, 23, 40, 52, 96, 109, 122, 130, 141, 143, 144, 170, 204, 220, 266, 290, 302, 312, 321, 324, 376]

These different linear models have been useful in malaria forecasting. However, several random factors are a common source of data irregularity, and other important aspects of time series theory still need to be addressed in malaria prevention and forecasting.

In the present Appendix, malaria time series will be analyzed from a different perspective, involving simulations in different human-to-mosquito transmission efficiency w_h settings, based upon our malaria transmission agent-based stochastic model [326], while comparing results with empirical time series with different transmission patterns from world regions where malaria is still endemic [209, 278].

ARMA (autoregressive and moving average) and ARIMA (autoregressive, integrated, moving average) models have been consistently used in time series fore-

casting. Different linear models are usually well adapted to the study of stationary and non-stationary time series. ARMA models have proven reliable for forecasting in stationary time series. In the presence of non-stationary time series, the possibility of adding series differencing to a ARMA model, may be useful in building a robust ARIMA model.
Residual time-series analysis with the popular Box-Ljung method is acceptable in testing for model accuracy while obtaining more consistent forecast results. In the presence of seasonality, SARIMA (seasonal autorregressive integrated moving average) models are highly recommended. Other methods such as the exponential smoothing model (ETS) or the Holt-Winters forecasting (HW), may also be used in time-series forecasting [64, 334]. The importance of the autocorrelation function (ACF) in the presence of time series stationarity will be further discussed, in relation to ARIMA and SARIMA models. The autocorrelation function is related to the time series auto-covariance. The type of autocorrelation function decay and the partial autocorrelation function are both useful in anticipating the recommended ARIMA model to be used in forecasting [243].

The correlation of a time series stochastic variable with its previous values in the recent past is used in defining the type of model to be adopted. Time series stationarity evaluation is a necessary pre-requisite for the proper choice of autoregressive and moving average models. The type of ACF decay may also indicate the presence of a long or short memory stochastic process. ARIMA models are usually referred as short memory processes. In these cases, we may find a fast decay of the autocorrelation function (typically exponential) with growing time lags h. When ACF decay is slow (e.g. as in a power law) the process may be defined as a long memory one.

In the present chapter we use our stochastic agent-based model [326] in malaria epidemic simulations while analyzing the results in the context of the Box-Jenkins theory, with the help of dedicated ARIMA and SARIMA models, in different settings of malaria transmission. The impact of seasonality is not to be dismissed in malaria. As the present agent-based model includes a seasonal effect algorithm, differences between ARIMA and SARIMA models will be analyzed. Our objective will be to identify malaria transmission patterns at different human-to-mosquito transmission efficiency levels (w_h), as well as to link long-range dependence processes in malaria incidence time series to the occurrence of phase transition in close proximity to disease elimination. In chapter 11 we have already focused on the utility of time series in defining the memory nature of a stochastic process in phase transition by using Hurst exponent and Shannon entropy. A few examples of malaria empirical times series with different trends will be presented for comparative purposes.

D.3 Methods

Time series comparative analysis between model simulations were conducted at different levels of human-to-mosquito disease transmission efficiency, while comparing its results with real data empirical time series from African regions with different epidemic behavior. Our procedures consisted in the detection of diversity in patterns of disease transmission efficiency in Box-Jenkins time series comparative analysis while determining the proper type of auto-correlation function decay.

D.3.1 Malaria model simulation time series

Malaria transmission model simulations were conducted according to different intensities of human-to-mosquito transmission efficiency. Human-to-mosquito transmission was defined in terms of the percentual time of human disease duration having the presence of gametocytemia in the blood circulation – w_h. Six different scenarios were used for disease transmission model simulation – see table D.1.

Level	w_h	**Malaria transmission intensity**	**Malaria incidence*** (± **SE**)
1	0.420	Phase transition	7.7 (± 0.89)
2	0.453	Low	25.1 (± 0.96)
3	0.467	Intermediate/low	34.2 (± 0.82)
4	0.500	Intermediate	51.6 (± 0.94)
5	0.600	Intermediate/high	106.4 (± 0.94)
6	0.733	High	169.7 (± 0.64)

Table D.1: Human-to-mosquito disease transmission efficiency (w_h), disease transmission intensity levels and average malaria incidence (± SE) of ten simulations in all settings (* cases per 100 inhabitants-year)

Malaria incidence, per 100 inhabitants, per year, was defined as the metric of disease burden in the human population – see table D.8. This measure was defined as equivalent to what would be the expected average annual malaria incidence in 100 inhabitants along the whole year, if there were no changes in disease transmission. In empirical time series it represented an acceptable metrics for the assessment of malaria impact in human population during a period of one year.

In model simulations we used different levels of positive gametocytemia duration, corresponding to different disease transmission efficiencies. The highest transmission scenario (1 – High disease transmission) was defined by the presence of 110 days of positive gametocytemia during 150 days of expected disease duration ($w_h = 0.733$). Five other gametocytemia levels ranging from major transmission to phase transition close to disease extinction were analyzed. From our previously published model, intermediate phase transition was defined according to progressively lower gametocytemia levels of 90 days (2 – Intermediate/high transmission; $w_h = 0.600$), 75 days (3 – Intermediate transmission; $w_h = 0.500$, 70 days (4 – Intermediate/low transmission; $w_h = 0.467$, 68 days (5 – Low trans-

mission; $w_h = 0.453$), and 63 days (6 – Close to phase transition, where $\sim 50\%$ of all model simulations resulted in disease extinction during a time period of 30 years; $w_h = 0.420$) – see Table D.1. At all transmission levels, ten simulations were performed in identical initial conditions.

The results of these model simulations were compared with real data obtained from two empirical time series of malaria incidence in different world regions – see Table D.1.

D.3.2 Malaria empirical time series

From published literature, two empirical time series were considered adequate as an example for deeper comparative analysis – see table D.2. In these series, malaria monthly incidence is reported along different time periods. Two levels of disease transmission intensity according to human-to-mosquito transmission efficiency (w_h) are considered. These time series are presented in figures D.6 a) and b). These series were compared with those from our agent-based model simulation at different levels of disease transmission efficiency. Decreasing disease incidence vs. epidemic outcome are evaluated concerning a possible correlation between real data and model simulation time series.

Series	**Follow-up** (months)	**Region**	**Trend**	**Malaria incidence*** (± **SD**)
Okech,2008	96	Kenya	Decreasing	205.1 (± 169.8)
Landoh,2012	72	Togo	Increasing	24.4 (± 11.5)

Table D.2: Empirical time series with average malaria incidence (± SD) in diferent settings of malaria transmission (* cases per 100 inhabitants-year)

D.3.3 The auto-correlation function

Autocorrelation function (ACF) analysis was applied to our agent-based simulation model as well as to malaria empirical time series data, during long time intervals.

The dimensional nature of a long memory process presenting with a slow decay of its auto-correlation function, is commonly defined in terms of an increasing time lag.

The covariance $\gamma(h)$ of a time series X_t at time lag h may be obtained from:

$$\gamma(h) = \sum (X_{t+h} - \overline{X_t})(X_t - \overline{X_t}) \tag{D.2}$$

The ACF is represented here by $\rho(h)$ and expresses the degree of correlation of the co-variance of X_{t+h}, after a time lag h, with its co-variance at no time lag necessarily equivalent to the time series variance σ_X^2.

$$\rho(h) = \frac{\gamma(h)}{\gamma(0)} \tag{D.3}$$

The ACF results from dividing the time series covariance $\gamma(h)$ with a time lag h by its covariance with no time lag $\gamma(0)$ – as in equation D.3.

Several tests are effective in defining the presence of stationarity. Time series with a constant mean value in time (no trend) and a stabilized variance (constant volatility) are usually considered stationary. If necessary, special measures may be taken to assure stability in trend (time series differencing), seasonality (seasonal differencing), variance (logarithmic or square root transformation), and data normal distribution (Box-Cox transformation).

D.3.4 ARIMA and SARIMA modeling

Autoregressive and moving average models were defined according to the Box-Jenkins method (1970) [46].

In our case, a Box-Jenkins procedure was adopted in order to build an equivalent auto-regressive integrated moving average (ARIMA) model, as well as including seasonal modeling (SARIMA).

ARIMA model

In all simulations with variable gametocytemia duration an alternative ARIMA model was implemented according to the following equation:

$$\phi^p(B)\nabla^d X_t = \phi^p(B)(1-B)^d X_t = \theta^q(B)Z_t \tag{D.4}$$

where $\phi^p(B)$ is the autoregressive operator

$$\phi^p(B) = 1 - \phi_1 B - \phi_2 B^2 - \phi_3 B^3 - ... - \phi_p B^p \tag{D.5}$$

,

$\theta^q(B)$ is the moving average operator

$$\theta^q(B) = 1 + \theta_1 B + \theta_2 B^2 + \theta_3 B^3 + ... + \theta_q B^q \tag{D.6}$$

, the ∇ operator represents the first difference

$$\nabla X_t = X_t - X_{t-1} \tag{D.7}$$

, the B operator represents the backshift operator

$$B(X_t) = X_{t-1} \tag{D.8}$$

, d is the differencing level of ∇^d

$$\nabla^d X_t = (1-B)^d X_t \tag{D.9}$$

and Z_t represents a gaussian white noise time series

$$Z_t = N(0, \sigma^2) \tag{D.10}$$

SARIMA model

As our model included seasonality, a SARIMA model was tested with a period of 12 months – see tables D.3 and D.4.

The general SARIMA model was implemented according to:

$$\Phi^P(B^s)\phi^p(B)\nabla_s^D\nabla^d X_t = \Theta^Q(B^s)\theta^q(B)Z_t \tag{D.11}$$

where $\phi^p(B)$ is the ordinary autoregressive operator

$$\phi^p(B) = 1 - \phi_1 B - \phi_2 B^2 - \phi_3 B^3 - ... - \phi_p B^p \tag{D.12}$$

,

$\theta^q(B)$ is the ordinary moving average operator

$$\theta^q(B) = 1 + \theta_1 B + \theta_2 B^2 + \theta_3 B^3 + ... + \theta_q B^q \tag{D.13}$$

,$\Phi^P(B^s)$ is the seasonal autoregressive operator

$$\Phi^P(B^s) = 1 - \Phi_1 B^s - \Phi_2 B^{2s} - \Phi_3 B^{3s} - ... - \Phi_P B^{Ps} \tag{D.14}$$

,

$\Theta^Q(B^s)$ is the seasonal moving average operator

$$\Theta^Q(B^s) = 1 + \Theta_1 B^s + \Theta_2 B^{2s} + \Theta_3 B^3 + ... + \Theta_Q B^{Qs} \tag{D.15}$$

, the ordinary ∇ operator represents the once-difference operator

$$\nabla X_t = X_t - X_{t-1} \tag{D.16}$$

, d is the ordinary differencing level of ∇^d

$$\nabla^d X_t = (1 - B)^d X_t \tag{D.17}$$

, D is the differencing level of the seasonal ∇^D operator which represents the seasonal differencing operator

$$\nabla_s^D X_t = (1 - B^s)^D X_t \tag{D.18}$$

, the B operator represents the ordinary backshift operator

$$B(X_t) = X_{t-1} \tag{D.19}$$

,the seasonal backshift operator is given by

$$B^s(X_t) = X_{t-s} \tag{D.20}$$

and Z_t represents a gaussian white noise time series

$$Z_t = N(0, \sigma^2) \tag{D.21}$$

ARIMA and SARIMA linear models were also defined for empirical malaria time series. Initially, two time series with clear-cut opposite epidemic trends were selected for comparative analysis: Okech (2008) and Landoh (2012) [209, 278]. The Okech (2008) time series revealed a pattern consistent with an unstable epidemic state with decreasing trend from high levels of malaria incidence evolving to imminent disease elimination [278]. The other empirical time series (Landoh,2012) also revealed an unstable epidemic behavior, but this time with a non-stationary increasing trend and an average level of malaria incidence for african standards (between 10 and 50 malaria cases per 100 inhabitants-year) [209].

Special attention was devoted to the presence of a long memory time series process (long-range dependence), in which case the autocorrelation function was expected to decay with a longer time lag (h).

D.3.5 R packages

Auto-correlation function was estimated in all time series with the function *acf* from *stats* R package. Box-Jenkins ARIMA and SARIMA methodology, Hurst exponent estimation and non-linear time series analysis were implemented with different functions from the following time series dedicated R packages: *tseries, forecast, entropy,* and *pracma*. For time series stationarity analysis, we used the augmented Dickey-Fuller test, and the KPSS test according to the R implemented routine *adf.test*, and *kpss.test* both included in the package *tseries*. Aikake AICc optimization was implemented in defining the best ARIMA and SARIMA models.

D.4 Results

D.4.1 Disease transmission model

With the present model we analyzed the behavior of the human-mosquito coupled system, resulting from a complex interaction between the two compartments. Human-to-mosquito transmission efficiency (w_h) will depend on the sustained presence of gametocytemia in human blood circulation, as well as on the probability

of survival of infected mosquitoes beyond latency time. These aspects are critical in disease transmission. Our model simulations use gametocytemia as an independent variable influencing human-to-mosquito transmission. Different levels of gametocytemia intensity define different stages of disease transmission efficiency. Theoretical gametocytemia reduction is considered equivalent to effective treatment with gametocidal agents such as primaquine our methylene blue in a fraction of the human population .

Human-to-mosquito transmission efficiency was defined from our computational model [326]. Disease duration was assumed to be 150 days. Simulations used different levels of positive gametocytemia duration ranging from a phase transition before disease extinction (corresponding to 63 days of positive gametocytemia $w_h = 0.420$) to a high disease transmission efficiency (110 days of positive gametocytemia – $w_h = 0.733$) – see Table D.1.

Phase transition in the proximity of disease elimination correlated well with a malaria incidence in the proximity of 4 to 6 cases per 100 habitants during a one year interval [394].

D.4.2 Malaria model simulations

At first, we analyzed our time series data with the help of an ARIMA procedure (autoregressive integrated moving average) inspired upon the Box-Jenkins method. This simpler model does not include the seasonal variation expected from the rainy season in African regions. The absence of a seasonal effect significantly reduced the potential benefit of model predictions.

Seasonality was thus included within the setting of a more robust SARIMA model, while considering the need for stationarity in all time series as a prerequisite for proper model implementation.

Stochastic simulations were conducted with this human/mosquito infection model, at different levels of gametocytemia and human-to-mosquito transmission intensity, corresponding to a time period lasting for 30 years. Ten model simulations were conducted at every different level of transmission intensity (total of 60 simulations). In every disease level, one simulation was randomly selected for graphical display out of ten (see figures D.1 to D.4).

w_h	**ARIMA**	**Model** $\phi^p(B)(1-B)^d X_t = \theta^q(B) Z_t$
0.420	(4,1,5)	$(1 - \sum_{i=1}^{4} \phi_i B^i)(1-B)X_t = (1 + \sum_{i=1}^{5} \theta_i B^i) Z_t$
0.733	(5,0,1)	$(1 - \sum_{i=1}^{5} \phi_i B^i) X_t = (1 + \theta_1 B) Z_t$

Table D.3: Human-to-mosquito transmission efficiency (w_h) levels and ARIMA modeling

w_h	**0.420**	**0.733**
ARIMA	(4,1,5)	(5,0,1)
ϕ_1	0.0883	0.0157
ϕ_2	-0.4975	0.4182
ϕ_3	-0.2578	-0.0344
ϕ_4	0.1497	-0.1074
ϕ_5	–	-0.4306
θ_1	-0.6124	0.7244
θ_2	0.5240	–
θ_3	-0.1385	–
θ_4	-0.26653	–
θ_5	-0.3089	–
σ^2	18.87	2923
AICc	2083.09	3905.91

Table D.4: Gametocytemia transmission levels and coefficients of ARIMA models

ARIMA model

From simulations, the ARIMA more simple linear models were defined at every level of gametocytemia and disease transmission efficiency.

There were significant differences in the type of best ARIMA model between stochastic simulations at the same level of disease transmission intensity. As a rule, we analyzed the first tested simulation at every transmission level.

From a wide spectrum of disease transmission levels ($0.420 < w_h < 0.733$), two different levels of human-to-mosquito transmission (w_h) were selected at both extremes: A low transmission level ($w_h = 0.420$) close to phase transition, and a high transmission level ($w_h = 0.733$) – see Table D.3.

Close to phase transition at the lower transmission level (63 days gametocytemia duration; $w_h = 0.420$) the best ARIMA models was defined as a combination of auto-regressive ($p = 4$) and moving average ($q = 5$), with the need of time series differencing (once – $d = 1$).

At the higher transmission level (110 days gametocytemia duration; $w_h = 0.733$) we found the best model to be predominantly auto-regressive ($p = 5$) with a low order moving average ($q = 1$), and no need for time series differencing ($d = 0$).

The absence of seasonality was an important limitation of the ARIMA model. At high human-to-mosquito transmission levels ($w_h = 0.733$) the model was purely auto-regressive as there was no need for time series differencing due to the presence of stationarity. Likewise, the moving average component was also residual with only one component in the ARIMA model (5,0,1) – see tables D.3 and D.4.

SARIMA model

As our agent-based model included seasonality, a SARIMA model was additionally tested, with a 12 months period – see tables D.5 and D.6.

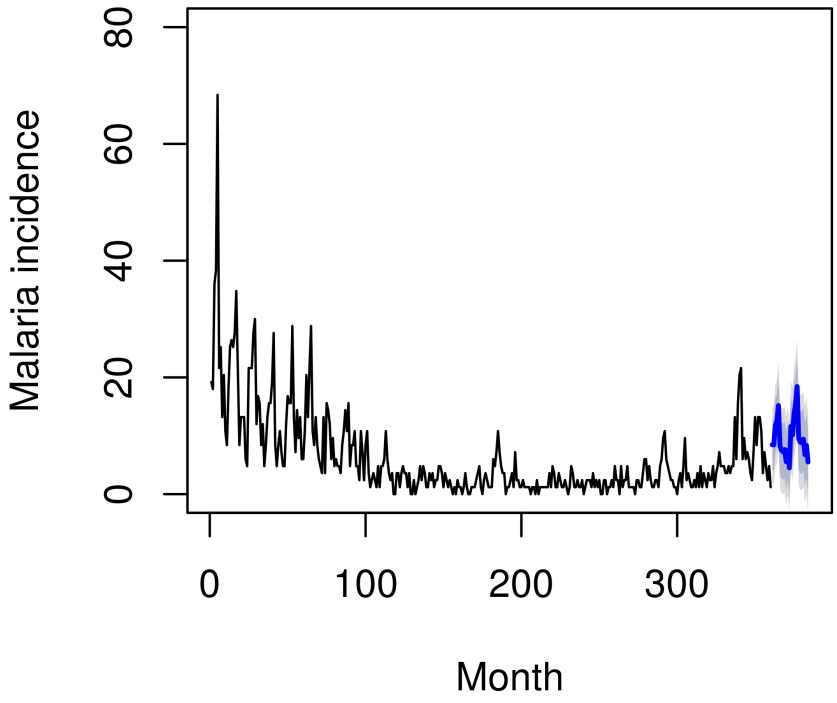

Figure D.1: Model simulation (black) and SARIMA model forecasting (blue) of model simulation at phase transition, with low human-to-mosquito transmission efficiency ($w_h = 0.420$)

w_h	**SARIMA** $(p,d,q) \times (P,D,Q)^s$	**Model** $\Phi^P(B^s)\phi^p(B)\nabla_s^D\nabla^d X_t = \alpha + \Theta^Q(B^s)\theta^q(B)Z_t$
0.420	$(2,1,2) \times (2,1,2)^{12}$	$\Phi^2(B^{12})\phi^2(B)\nabla_{12}^1\nabla^1 X_t = \alpha + \Theta^2(B^{12})\theta^2(B)Z_t$
0.733	$(2,1,1) \times (2,1,1)^{12}$	$\Phi^2(B^{12})\phi^2(B)\nabla_{12}^1\nabla^1 X_t = \alpha + \Theta^1(B^{12})\theta^1(B)Z_t$

Table D.5: H-to-M transmission efficiency (w_h) levels from model simulations and relation to SARIMA models (α = drift)

From present model simulations, SARIMA linear models were defined at every level of gametocytemia and disease transmission efficiency. There were small differences in the type of best SARIMA model between stochastic simulations at the same level of disease transmission intensity. Presented results were obtained from the first tested simulation at every transmission level.

Close to phase transition at the lower transmission level (63 days gametocytemia duration; $w_h = 0.420$) the most reliable SARIMA model was defined as

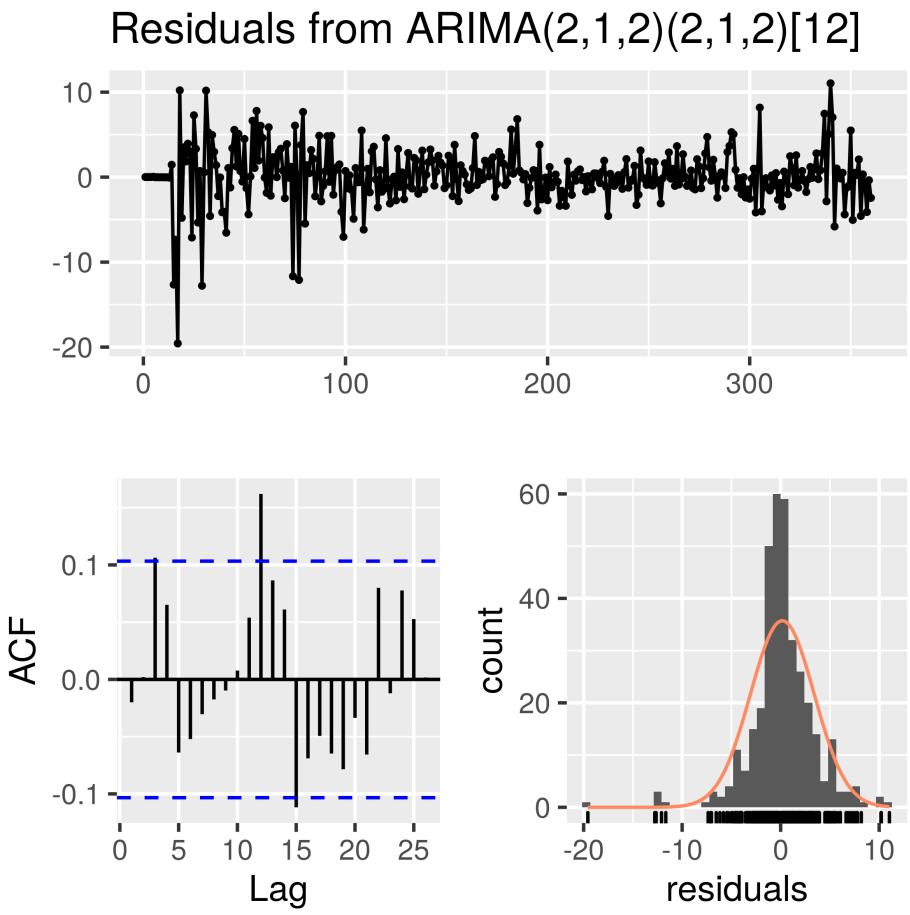

Figure D.2: Autocorrelation function and residuals of SARIMA forecasting of model simulation model at phase transition (2,1,2))×(2,1,2)^{12}, with low human-to-mosquito transmission efficiency ($w_h = 0.420$), with the implementation of *check-residuals* in the *R* package *forecast*

SARIMA		
w_h	**0.420**	**0.733**
$(p,d,q) \times (P,D,Q)^s$	$(2,1,2) \times (2,1,2)^{12}$	$(2,1,1) \times (2,1,1)^{12}$
ϕ_1	-0.3635	-0.3495
ϕ_2	0.3415	-0.2344
θ_1	-0.3455	-0.2997
θ_2	-0.5422	–
Φ_1	0.6564	-0.2221
Φ_2	-0.1574	-0.2273
Θ_1	-1.4685	-0.7408
Θ_2	0.7626	–
α (drift)	–	–
σ^2	10.89	1037
AICc	1849.32	3426.29

Table D.6: Different H-to-M transmission efficiency levels ($w_h = 0.420$ and $w_h = 0.733$), and coefficients of SARIMA models

$(2,1,2) \times (2,1,2)^{12}$, corresponding to a combination of auto-regressive ($p = 2$ and

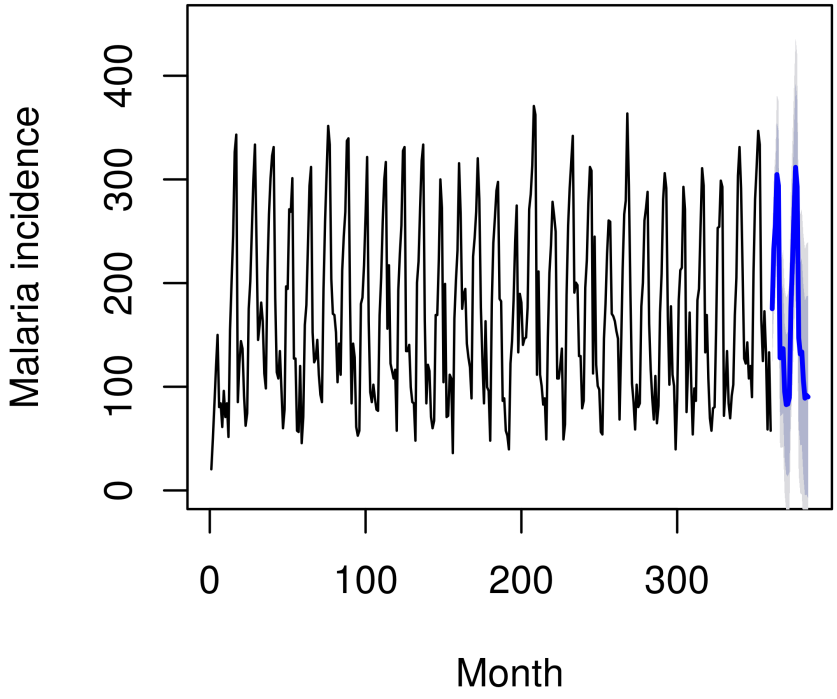

Figure D.3: Model simulation (black) and SARIMA model forecasting (blue) of model simulation at epidemics stability, with high human-to-mosquito transmission efficiency ($w_h = 0.733$)

$P = 2$) and moving average ($q = 2$ and $Q = 2$) procedures, with the need of time series differencing (once, $d = 1$ and $D = 1$) both in the non-seasonal and the 12-months seasonal model fraction.

At the higher transmission level (110 days gametocytemia duration; $w_h = 0.733$) the best SARIMA models was defined as $(2, 1, 1) \times (2, 1, 1)^{12}$, with a predominantly auto-regressive component ($p = 2$ and $P = 2$), and a lower order moving average ($q = 1$ and $Q = 1$), with the need for time series differencing (once, $d = 1$ and $D = 1$), both in the non-seasonal and the 12-months seasonal model fraction. In both cases, the best model was defined according to Akaike information criterion optimization.

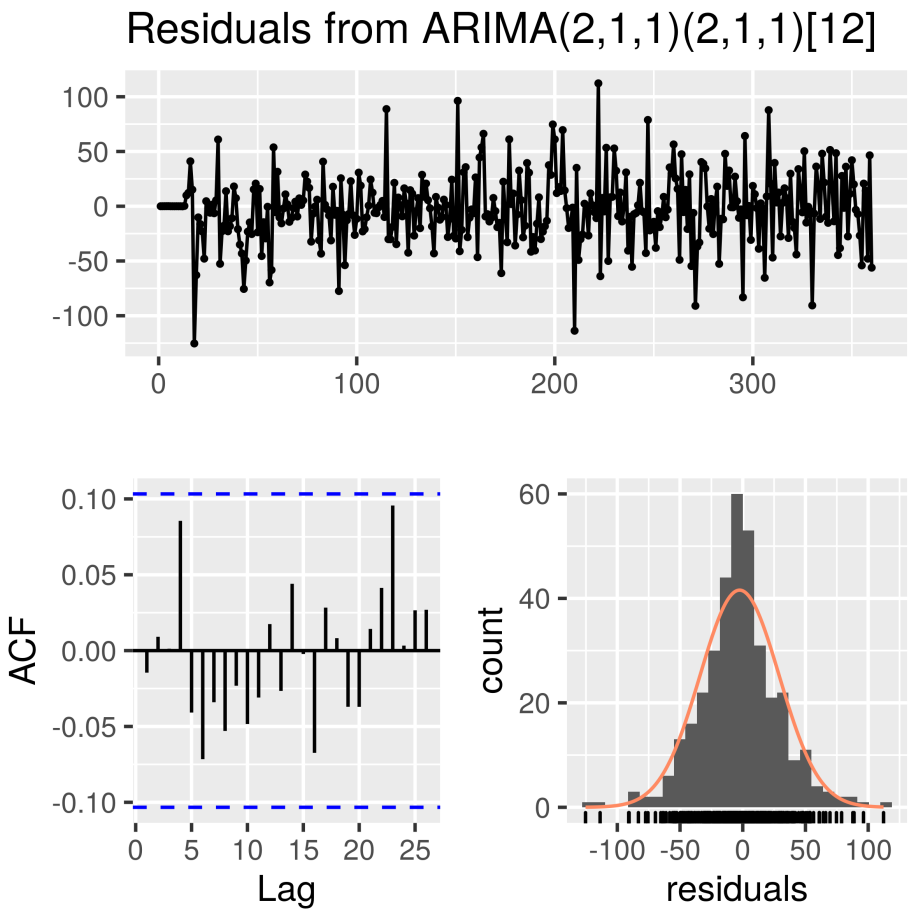

Figure D.4: Autocorrelation function and residuals of SARIMA forecasting of model simulation at epidemics stability $(2,1,1))\times(2,1,1)^{12}$, with high human-to-mosquito transmission efficiency ($w_h = 0.733$), with the implementation of *check-residuals* in the *R* package *forecast*

D.4.3 Typical malaria empirical time series with trend

The two presented model scenario simulations at extreme human-to-mosquito transmission conditions ($w_h = 0.420$ and $w_h = 0.733$) were compared to two typical empirical time series of malaria incidence in different geographical regions from West and East Africa (see Table D.2), with opposite disease transmission trends. They represent western and eastern Africa regions according to their apparent epidemic stability, seasonality and trend: West Africa (Togo) and East Africa (Kenya) – see Table D.2.

The ARIMA and SARIMA models of the two chosen typical empirical time series, Okech (2008) [278] and Landoh (2012) [209]), were obtained. Data is presented in tables D.7, D.8, D.9 and D.10.

Empirical time series from Okech (2008) reveal an initial high incidence in malaria incidence (close to 600 cases per 100 inhabitants per year) with a progressive decline along a time interval of a decade, towards disease elimination. On the contrary, in the case of Landoh (2012) we witness an initial low malaria incidence

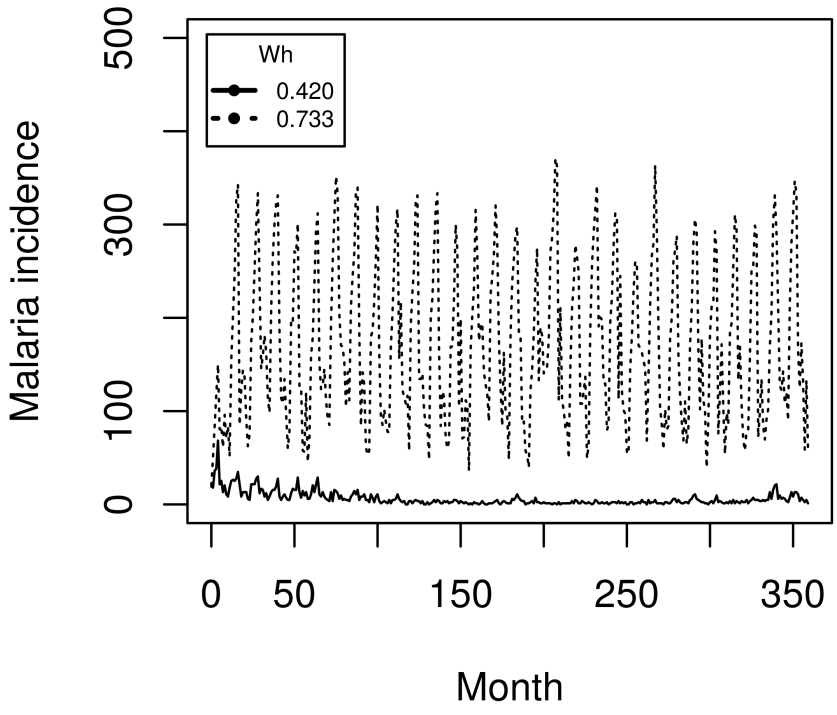

Figure D.5: Malaria incidence with different H-to-M transmission efficiencies: low transmission at phase transition ($w_h = 0.420$ – bold line) and high transmission epidemic stage ($w_h = 0.733$ – dotted line).

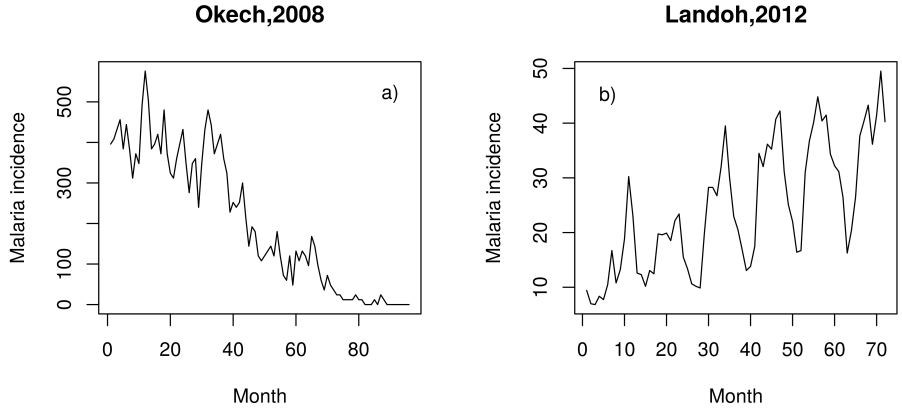

Figure D.6: **(a)** Major decline in malaria incidence in empirical time series from Okech (2008) [278]. **(b)** Moderate uprising malaria incidence in empirical series from Landoh (2012) [209].

(close to 10 cases per 100 inhabitants per year) with a five times steady increase along a period of 6 years. Both ARIMA series reveal a regression and moving

Empirical series	**ARIMA** (p,d,q)	**Model** $\phi^p(B)(1-B)^d X_t = \alpha + \theta^q(B)Z_t$
Okech (2008)	(0,1,2)	$(1-B)X_t = \alpha + (1 + \sum_{i=1}^{2} \theta_i B^i)Z_t$
Landoh (2012)	(0,1,1)	$(1-B)X_t = \alpha + (1 + \theta_1 B)Z_t$

Table D.7: ARIMA model in empirical data time series

average model with one time differencing (p,d,q) = (1,1,1).

Empirical series	**Okech (2008)**	**Landoh (2012)**
ARIMA model	(0,1,2)	(0,1,1)
θ_1	-0.2704	0.2102
θ_2	-0.3344	–
α (drift)	-4.5151	0.3940

Table D.8: ARIMA model in empirical data time series (* cases per 100 inhabitants-year)

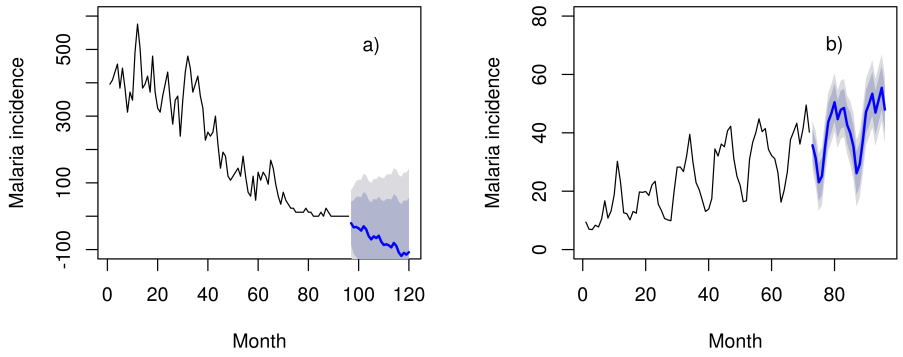

Figure D.7: **(a)** Empirical time series (black) and SARIMA model forecasting (blue) from Okech (2008) [278] empirical time series along with declining malaria incidence. SARIMA forecast predicts rapid disease elimination evolving towards negative values. **(b)** Empirical time series (black) and SARIMA model forecasting (blue) from Landoh (2012) [209] empirical time series along with a steady increase in malaria incidence. SARIMA forecast predicts a trend of progressive disease spreading.

In the case of the seasonal component, the regressive component of the SARIMA term vanishes in Okech (2008) model and we have (P,D,Q) = (0,1,1). On the contrary, the seasonal SARIMA model of Landoh (2012) is purely a regressive model with one time differencing, and we have (P,D,Q)=(1,1,0). SARIMA forecast of both empirical series is presented in figure D.7, while its equations and coefficients are available in tables D.9 and D.10.

T.Series	**SARIMA**	
	$(p,d,q)\times(P,D,Q)^s$	$\Phi^P(B^s)\phi^p(B)\nabla_s^D\nabla^d X_t = \Theta^Q(B^s)\theta^q(B)Z_t$
Okech	$(1,1,1)\times(0,1,1)^{12}$	$\Phi^0(B^{12})\phi^1(B)\nabla_{12}^1\nabla^1 X_t = \Theta^1(B^{12})\theta^1(B)Z_t$
Landoh	$(1,1,1)\times(1,1,0)^{12}$	$\Phi^1(B^{12})\phi^1(B)\nabla_{12}^1\nabla^1 X_t = \Theta^0(B^{12})\theta^1(B)Z_t$

Table D.9: SARIMA models of empirical time series from Okech (2008) [278] and Landoh (2012) [209]

SARIMA		
	Okech (2008)	**Landoh (2012)**
$(p,d,q)\times(P,D,Q)^s$	$(1,1,1)\times(0,1,1)^{12}$	$(1,1,1)\times(1,1,0)^{12}$
ϕ_1	0.6357	0.5306
θ_1	-0.8778	-1.000
Φ_1	–	-0.4894
Θ_1	-0.6522	–
σ^2	2518	17.49
$AICc$	900.8	351.15

Table D.10: Coefficients of SARIMA models of empirical time series from Okech (2008) [278] and Landoh (2012) [209]

D.4.4 Atypical malaria empirical time series

In this section four other empirical time series are also presented with atypical epidemic trends, as well as their respective SARIMA models after Akaike optimization. In all the cases, the model best fit was defined in the form of $\Phi^P(B^s)\phi^p(B)\nabla_s^D\nabla^d X_t = \Theta^Q(B^s)\theta^q(B)Z_t$, with $p=1$, $d=1$, $q=1$, $P=1$, $D=1$ and $Q=1$, resulting in $\Phi^1(B^{12})\phi^1(B)\nabla_{12}^1\nabla^1 X_t = \Theta^1(B^{12})\theta^1(B)Z_t$ – see table D.11 and figure D.8.

Elipe (2007)

In 2007, Gomez-Elipe defined a malaria prediction model based upon the results from a malaria empirical time series in Burundi [147]. The Karuzi province has a tropical climate with a 7-months rainy season starting in October followed by a dry season from May to September. The model pretended to predict malaria incidence from current rainfall, higher and lower atmospheric temperature, vegetation density and the preceding month malaria incidence. During the study time period there was a major epidemic outbreak during the first month of the rainy season (November,2000) probably related to increasing *Plasmodium* drug-resistance. Although the model revealed a satisfactory predictive power, it failed to predict the initial outbreak event – the prediction of 7.7 monthly malaria cases was much lower than the observed 41.6 cases per 100 inhabitants. This outbreak was tackled firmly by local health authorities with the help of IRS and ITN effective implementation, resulting in a massive decrease of new malaria cases in the following rainy season (5.9 observed malaria cases per 100 inhabitants in November, 2001, this time in line with the model prediction). This empirical series is a sound example of the power of adequate preventive measures in suppressing malaria transmission

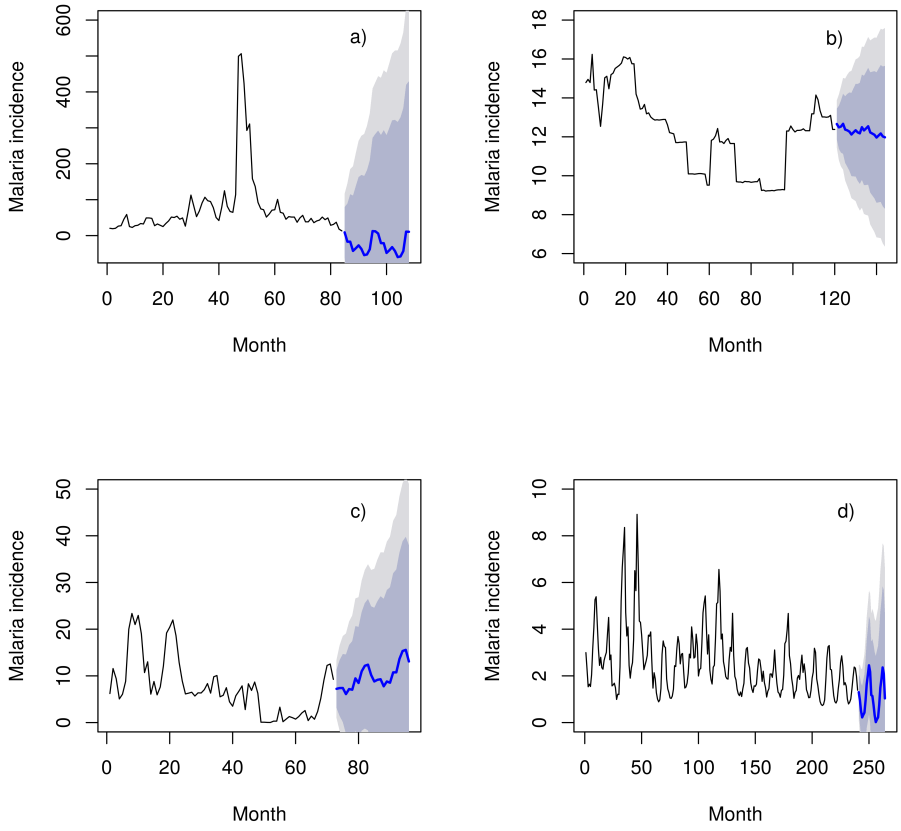

Figure D.8: Forecast from SARIMA models, optimized with the help of Akaike information criterion, and defined as $(1,1,1) \times (1,1,1)^{12}$
(a) Elipe (2007) [147] with malaria incidence revealing basal disease suppression broken down by a dramatic disease outbreak, rapidly put under control.
(b) Bedane (2016) [33] with different trends in malaria incidence revealing unstable epidemic behavior at average african malaria incidence levels.
(c) Alhassan (2017) [12] with an unstable trend at average african levels of malaria incidence levels.
(d) Lima (2021) [220] with a stable trend and a steady oscillation at lower levels of malaria incidence.

in the long term [310]. The SARIMA model based upon this empirical malaria time series forecasts imminent disease elimination in the short term, suggesting that the adopted measures of disease control were very effective – see figure D.8 a) and table D.11.

Bedane (2016)

The Kucha district in Ethiopia was used by Bedane (2016) as support data for the development of a predictive model based upon the Box-Jenkins approach [33]. In this case, an ARIMA model (3,1,1) was considered the best fit for forecasting of new malaria cases. However, no seasonality effect was considered in that model,

thus significantly reducing its predictive power. By using a more sophisticated Akaike optimized SARIMA model (1,1,1) we have included the proper seasonality effect, improving the predictive power of the initial model, and forecasting a future mild decreasing trend in malaria incidence – see figure D.8 b) and table D.11.

Alhassan (2017)

Alhassan presented a malaria forecasting model (2017) supported by malaria incidence data from Ghana, Kasena Nankana region [12]. The empirical time series covered the period from 2010 to 2015. A Box-Jenkins ARIMA model was used as the forecasting statistical tool. However, the proposed ARIMA model (1,0,1) revealed a low predictive power, as it did not include a seasonality effect. Therefore, we used a SARIMA Akaike optimized model based upon that malaria time series, suggesting a future increasing trend in malaria incidence in the months to follow – see figure D.8 c) and table D.11.

Lima (2021)

In 2021, Lima presented an extensive analysis comparing the predictive power of several statistical models concerning data obtained from malaria empirical time series in the state of Amapá, Brazil, from 1997 to 2016 [220]. Amapá is an important endemic malaria region in Brazil, with a predominant hot and very humid tropical, with average rainfall 3,300 mm annually. A large proportion of the state (73%) is covered by native vegetation. This time series included both *P.vivax* and *P.falciparum* malaria cases. Its results supported the notion that ARIMA could be used in the future for adequate malaria forecasting. However, the presence of an important climate seasonality strongly suggest the need for a SARIMA model. In this case after Akaike optimization we defined the proper SARIMA model as (1,1,1) x (1,1,1), predicting a stable low incidence malaria endemic seasonal pattern with stationary trend around 2 malaria cases per 100 inhabitants per year – see figure D.8 d) and table D.11. .

Empirical series	ϕ_1	θ_1	Φ_1	Θ_1	σ^2	$AICc$
Elipe (2007)	-0.0676	0.2099	0.0506	-0.9999	2590	791.68
Bedane (2016)	0.7597	-0.7769	-0.0683	-0.9666	0.3524	227.66
Alhassan (2017)	-0.9038	1.0000	-0.2602	-0.3752	9.968	320.11
Lima (2021)	-0.1613	-0.0037	0.1595	0.0629	0.3497	431.15

Table D.11: Coefficients related to SARIMA models of empirical time series with atypical trends from Elipe (2007) [147] , Bedane (2016) [33], Alhassan (2017) [12] and Lima (2021) [220]. In all cases we have a common SARIMA model $(1,1,1) \times (1,1,1)^{12}$, with different coefficients. Results were obtained from Akaike criterion optimization

D.5 Discussion

Overall, ARIMA and SARIMA models fared well as a consistent approach to malaria forecasting. In our model simulations, SARIMA models were more effective than ARIMA, as they included a seasonality coefficient in the standard model $(p, d, q) \times (P, D, Q)^s$. In all cases it was necessary to apply differentiation (one-time) to all the original simulation time series. In empirical time series with trend, the SARIMA model was simpler – see table D.10 –, resulting in a form without a regressive component in the seasonal term $(1, 1, 1) \times (0, 1, 1)^{12}$ from Okech (2008) empirical time series with decreasing trend, with only a minor difference from Landoh (2012) where the model was in the form with no moving average component in the seasonal term $(1, 1, 1) \times (1, 1, 0)^{12}$. In the four atypical empirical time series, Elipe (2007), Bedane (2016), Alhassan (2017) and Lima (2021), the SARIMA model forecasting was similar among all of them ($(1, 1, 1) \times (1, 1, 1)^{12}$), with only minor variations in the different coefficients. Still, the graphical forecasting was globally quite satisfactory in all empirical time series – see figures D.7 and D.8.

Index